NOTICE

The quality of this microform is heavily dependent upon the quality of the original thesis submitted for microfilming. Every effort has been made to ensure the highest quality of reproduction possible.

If pages are missing, contact the university which granted the degree.

Some pages may have indistinct print especially if the original pages were typed with a poor typewriter ribbon or if the university sent us an inferior photocopy.

Reproduction in full or in part of this microform is governed by the Canadian Copyright Act, R.S.C. 1970, c. C-30, and subsequent amendments.

AVIS

La qualité de cette microforme dépend grandement de la qualité de la thèse soumise au microfilmage. Nous avons tout fait pour assurer une qualité supérieure de reproduction.

S'il manque des pages, veuillez communiquer avec l'université qui a conféré le grade.

La qualité d'impression de certaines pages peut laisser à désirer, surtout si les pages originales ont été dactylographiées à l'aide d'un ruban usé ou si l'université nous a fait parvenir une photocopie de qualité inférieure.

La reproduction, même partielle, de cette microforme est soumise à la Loi canadienne sur le droit d'auteur, SRC 1970, c. C-30, et ses amendements subséquents.

SOLID-SUPERCRITICAL FLUID PHASE EQUILIBRIA OF BINARY AND TERNARY MIXTURES

by

DINGAN ZHANG

A Thesis
Presented to the University of Ottawa
in Fulfillment of the Thesis
Requirement for the Degree of
Doctor of Philosophy
in
Chemical Engineering

NOTICE

The quality of this microform is heavily dependent upon the quality of the original thesis submitted for microfilming. Every effort has been made to ensure the highest quality of reproduction possible.

If pages are missing, contact the university which granted the degree.

Some pages may have indistinct print especially if the original pages were typed with a poor typewriter ribbon or if the university sent us an inferior photocopy.

Reproduction in full or in part of this microform is governed by the Canadian Copyright Act, R.S.C. 1970, c. C-30, and subsequent amendments.

AVIS

La qualité de cette microforme dépend grandement de la qualité de la thèse soumise au microfilmage. Nous avons tout fait pour assurer une qualité supérieure de reproduction.

S'il manque des pages, veuillez communiquer avec l'université qui a conféré le grade.

La qualité d'impression de certaines pages peut laisser à désirer, surtout si les pages originales ont été dactylographiées à l'aide d'un ruban usé ou si l'université nous a fait parvenir une photocopie de qualité inférieure.

La reproduction, même partielle, de cette microforme est soumise à la Loi canadienne sur le droit d'auteur, SRC 1970, c. C-30, et ses amendements subséquents.

ISBN 0-315-60604-5

UNIVERSITÉ D'OTTAWA
UNIVERSITY OF OTTAWA

ACKNOWLEDGEMENT

I would like to express my sincere gratitude to the following people:

Professor Benjamin C.-Y. Lu, my research supervisor, for his guidance and advice through all phases of this work, without whose patience and encouragement this work could never be completed.

Dr. K. Ohgaki, Assistant Professor of Osaka University for his helpful suggestions in the early part of the experimental work. Ms. L. Wang, for her assistance with part of the measurements. Dr. W. Sheng, for his helpful advice on computation. Mr. G. Gasperetti, Mr. D. Lefebvre, Mr. L. Tremblay and Mr. A. Bonaldo for their technical assistance.

Dr. G.C. Benson who patiently read through the rough draft and provided helpful suggestions on the organization of this thesis.

Finally, my parents and wife whose love and support have led me to the final step of completing this work.

ABSTRACT

Experimental investigation of phase equilibria at supercritical fluid conditions was carried out for four binary mixtures and two ternary mixtures consisting of supercritical carbon dioxide and aromatic compounds (naphthalene, biphenyl, m-terphenyl and phenanthrene).

A new technique, the first freezing point method, was developed in this study to determine the pressure-temperature (P-T) projection of the solid-liquid-gas (S-L-G) three-phase coexistence curves for binary and ternary mixtures at supercritical fluid conditions. In addition, the equilibrium liquid compositions along the three-phase coexistence curves were also determined. A temperature minimum in the P-T projection of the three-phase coexistence curve was observed for each of the binary mixtures.

The liquid-gas (L=G) critical loci of two binary mixtures consisting of supercritical carbon dioxide and a solid (naphthalene or biphenyl) were determined. The bubble-point pressures along three isotherms as well as the solubilities of carbon dioxide in liquid naphthalene and biphenyl were also measured. By means of the intersection method, the upper critical end points (UCEP) were established to be 333.4 K, 25.9 MPa and 0.16 mole fraction of naphthalene for naphthalene-carbon dioxide mixture and 328.5 K, 48.5 MPa and 0.18 mole fraction of biphenyl for biphenyl-carbon dioxide mixture.

A "crossover region" was found in the study of isothermal solubilities of supercritical CO_2 in liquid biphenyl at a pressure of about 36 MPa. Below the crossover region pressure, an increase in temperature caused a decrease in solubility of carbon dioxide in the liquid phase, while above the crossover region pressure the opposite effect occurs. A rational explanation was given.

The P-T projection of the solid 1-solid 2-liquid-gas (S_1-S_2-L-G) four-phase coexistence curve of two ternary mixtures—naphthalene-biphenyl-carbon dioxide and naphthalene-phenanthrene-carbon dioxide—were determined. The results in-

dicate that the assumption of an unchanged eutectic composition of the solids with pressure may lead to a not negligible error in the measurements.

The freezing point depression of the solid under the pressure of a supercritical solvent and the solubility behavior in the vicinity of the lower critical end point (LCEP) and the UCEP were explored and discussed. The slopes of the depression curves at the triple points of the solids were predicted.

Two different approaches, based respectively on the compressed gas model (equation of state) and the expanded liquid model (activity coefficient model), were developed to describe the S-L-G three-phase equilibria and the solubilities of supercritical carbon dioxide in the melted solids. Using the Peng-Robinson equation of state with the modified correction factors, α, together with the composition-dependent mixing rules, the correlations of the experimental results were accomplished with satisfactory accuracy. The merits of these two approaches in the representation of the S-L-G three-phase equilibria were compared.

NOMENCLATURE

a, b	constants in equations of state
A, B	alternate forms for the above constants
C	critical point of pure substance
CP	critical point of mixture
C_p	heat capacity
d	density
f	fugacity
G	Gibbs energy
H	enthalpy
$\bar{H}$	partial molar enthalpy
ΔH_f	enthalpy of fusion
J	Jacobian determinant
k, l	binary interaction parameter
k	Henry's coefficient
L	liquid
LCEP	lower critical end point
M	triple point
p	upper critical end point
P	pressure
q	lower critical end point
R	gas constant
s	molar entropy
$\bar{s}$	partial molar entropy
S	solid

T	temperature
TLCEP	ternary lower critical end point
TUCEP	ternary upper critical end point
UCEP	upper critical end point
v	molar volume
$\bar{v}$	partial molar volume
V	volume, vapor
x	composition of liquid phase
y	composition of gas phase
z	compressibility factor

SUPERSCRIPTS

G	gas state
L	liquid state
S	solid state
sat	saturated state
o	reference state
*	ideal gas state

SUBSCRIPTS

c	critical property
f	state of fusion
i, j	refer to components
m	melting state
p	ternary upper critical end point
P	differentiation with respect to pressure

q	ternary lower critical end point
R	reduced state
T	differentiation with respect to temperature
y	differentiation with respect to composition

GREEK LETTERS

α	correction factor, a/a_c
γ	activity coefficient
Φ	fugacity coefficient
ρ	density
μ	chemical potential
ω	acentric factor

Contents

ABSTRACT iii

NOMENCLATURE v

LIST OF FIGURES xii

LIST OF TABLES xix

1 INTRODUCTION 1

1.1 Extraction with Supercritical Fluid 1

1.2 Development of Supercritical Fluid Extraction 4

1.3 Applications of Supercritical Fluid Extraction 6

1.4 Thesis Objectives 7

2 PHASE BEHAVIOR AT SUPERCRITICAL FLUID CONDITIONS INVOLVING SOLID PHASES 9

2.1 Phase Diagrams for Binary Mixtures 10

2.2 Phase Diagrams of Ternary Mixtures 17

3 CRITICAL REVIEW OF LITERATURE 22

3.1 Experimental Approach 22

3.1.1 Determination of Multiphase Equilibria 23

3.1.2 Determination of Liquid-Gas Critical Loci 24

3.1.3 Entrainer Effects on the Solubility of Solids and the Selectivity of Supercritical Solvents 26
3.2 Upper Critical End Point 27
3.3 Thermodynamic Modeling 31
3.3.1 Modeling of Solid-Liquid-Gas Equilibria 32
3.3.2 Modeling of Liquid-Gas Critical Loci 38
3.4 Conclusions Reached After Review 40

4 EXPERIMENTAL 42
4.1 Determination of Three-Phase Equilibria 42
4.1.1 First Freezing Point Method— Experimental Apparatus and Procedure I 42
4.1.2 Analysis of Liquid Phase Composition 45
4.1.3 Experimental Results I 46
4.1.4 First Freezing Point Method— Experimental Apparatus and Procedure II 54
4.1.5 Experimental Results II 57
4.2 Determination of Liquid-Gas Critical Loci 62
4.2.1 Experimental Apparatus and Procedure 62
4.2.2 Observation of Critical Opalescence 68
4.2.3 Experimental Results and Discussion 68
4.3 Determination of Upper Critical End Point 78
4.4 Determination of P-T Projection of Four-Phase Equilibria 80
4.4.1 Experimental Apparatus and Procedure 85
4.4.2 Experimental Results 87
4.5 Analysis of Liquid Phase Composition of the Solid-Liquid-Gas Equilibria for Ternary Mixtures 95
4.6 Materials 101

5 MODELING OF SOLID-SUPERCRITICAL FLUID PHASE EQUILIBRIA 105

5.1 A Modified Peng-Robinson Equation of State for Multiphase Equilibrium Calculation 105

5.1.1 The Three Phase S-L-G Equilibria For Binary Mixtures . . . 109

5.1.2 The Four Phase S_1-S_2-L-G Equilibria For Ternary Mixtures . 114

5.2 A Combination of Activity-Coefficient Model and Equation-of-State Model for Solid-Liquid-Gas Equilibrium Calculation 122

5.3 Comparison of the Two Approaches Used in the Representation of S-L-G Equilibria 124

5.4 Correlation of Solubility Data of Supercritical CO_2 in Liquid Naphthalene and Biphenyl 128

5.5 Some Comments on the Correlation of Liquid-Gas Critical Loci . . . 129

6 DISCUSSION OF RESULTS 135

6.1 The Merits of the First Freezing Point Method 135

6.2 Freezing Point Depression Under the Pressure of a Supercritical Fluid 139

6.2.1 Pressure Effects on the Freezing Point Depression of Solid . . 140

6.2.2 Effect of the Melting Point of Aromatic Compound on the Freezing Point Depression 142

6.2.3 The Slope of the S-L-G Curve at the Triple Point of Solid . . 143

6.3 Phase Behavior in the Vicinity of the Critical End Points 146

6.3.1 Inflection Point of the Solid-Fluid Equilibrium Line at the Critical End Points 146

6.3.2 The Solubility Phenomena Near the Critical End Points . . . 148

7 CONCLUSIONS 153

8 RECOMMENDATIONS FOR FUTURE STUDIES 156

BIBLIOGRAPHY 158

APPENDIX 173

A Calibration of the Supercritical Fluid Chromatograph (SFC) 173

B Calibration of Pressure Transducers 180

C Calibration of Quartz Thermometer and Thermocouples 184

D Determination of the P-n_{CO_2} Relationship in the Sample Loop for P-T-x Measurement 188

E Computer Programs for the Calculation of the S-L-G Three-Phase Equilibria 190

F Computer Program for the Calculation of the Solubility of Supercritical CO_2 in the Liquid Phase of the Aromatic Compound 209

List of Figures

1.1 Variation of Reduced Density of a Pure Substance in the Region of Interest for Supercritical Fluid Extraction. 3

2.1 Phase Diagram of Type I: L=G Critical Curve Runs Continuously Between Two Critical Points of Pure Components. M, Triple point; C_1, C_2, Critical points; - - -, L=G critical loci; -.-.-, S-L-G three-phase coexistence curve. 12

2.2 Phase Diagram of Type IIa: The S-L-G Curve in P-T Projection Has a Negative Slope. M, Triple point; C_1, C_2, Critical points; p, Upper critical end point; q, Lower critical end point; - - -, L=G critical loci; -.-.-, S-L-G three-phase coexistence curve. 14

2.3 Phase Diagram of Type IIb: The S-L-G Curve in P-T Projection Has a Temperature Minimum. M, Triple point; C_1, C_2, Critical points; p, Upper critical end point; q, Lower critical end point; - - -, L=G critical loci; -.-.-, S-L-G three-phase coexistence curve. 15

2.4 Phase Diagram of Type IIc: The S-L-G Curve in P-T Projection Has a Positive Slope. M, Triple point; C_1, C_2, Critical points; p, Upper critical end point; q, Lower critical end point; - - -, L=G critical loci; -.-.-, S-L-G three-phase coexistence curve. 16

2.5 Pressure-Temperature Projection of Ternary Mixture Naphthalene-Hexachloroethane-Ethylene. p, Ternary upper critical end point; q, Ternary lower critical end point [72]. 18

2.6 Three Types of Phase Behavior of Ternary Mixtures Consisting of Two Solids and One SCF. p, Ternary upper critical end point; q, Ternary lower critical end point; △, Triple points of pure solids; ◇, Quadruple point of solid mixture. 20

3.1 Isothermal Solubility of Naphthalene in Supercritical Ethylene [75]. . 29

3.2 Comparison of the Calculated Results using PR Equation with the Experimental Results for the Biphenyl-CO_2 System. ×, Experimental Data; -.-.-, Calculated Results [99]. 36

3.3 Representation of S-L-G line and L=G Critical Loci with the PR Equation and the SL Equation for the Naphthalene-Xenon System. o, Experimental S-L-G Line; •, Experimental L=G Critical Loci; —, Calculated by PR Equation; - - - - -, Calculated by SL Equation [100]. 37

4.1 Schematic Diagram of Apparatus for Measurement of Three-Phase Coexistence Curve. **A** - High pressure view cell; **B** - Pressure transducer; **C** - Pressure gauge; **D** - Solid container; **E** - Hand pump; **F** - Syringe; **G** - Solid sampler; **H** - Pressure gauge; **I** - Sample cylinder; **J** - Water bath; **a, b** - Three-way valves; 1-15 - Valves. 44

4.2 Pressure-Temperature Projection of the S-L-G Curve for the Naphthalene(1)-Carbon Dioxide(2) System. 49

4.3 Pressure-Temperature Projection of the S-L-G Curve for the Biphenyl (1)-Carbon Dioxide(2) System. 50

4.4 Location of "Liquid Island" Determined from the P-T-x Values of S-L-G Curve and Solubility Values of 332.15 K Isotherm for the Naphthalene(1)-Carbon Dioxide(2) System. 52

4.5 T-x Values along the S-L-G Curve for the Naphthalene(1)-Carbon Dioxide(2) System. Solid Line is Calculated in Terms of Liquid Activity Coefficient. 53
4.6 Schematic Diagram of Apparatus. **A** - Dual window equilibrium cell; **B** - Magnetic pump; **C** - Variable-speed motor; **D** - Temperature indicator; **E** - Pressure transducer; **F** - Pressure gauge; **G** - Pressure intensifier; **H** - Liquid carbon dioxide cylinder; **I** - Syringe; **J** - Air bath; **K** - Solid sampler; **L** - Sample cylinder; **M** - Water bath; **N** - Pressure gauge; **O** - Vacuum gauge; **P** - Vacuum pump; **a, b** - Three way valves; 1 to 10- Valves. 55
4.7 Pressure-Temperature Projection of the S-L-G Three-Phase Curve for the m-Terphenyl(1)-Carbon Dioxide(2) System. •, Normal Freezing Point of m-Terphenyl. 60
4.8 Pressure-Temperature Projection of the S-L-G Three-Phase Curve for the Phenanthrene(1)-Carbon Dioxide(2) System. •, Normal Freezing Point of Phenanthrene. 61
4.9 Experimental T-x Values of the Three-Phase (S-L-G) Coexistence Curve for Four Binary Mixtures. 64
4.10 Pressure-Temperature Projections of the S-L-G Curves for Four Binary Mixtures. 65
4.11 Experimental P-x Values of the Three-Phase (S-L-G) Coexistence Curve for Four Binary Mixtures. 66
4.12 A Photograph of the Content in the Equilibrium Cell Before the Critical-mixture Point Was Reached. Liquid and Gas Phases Existed in the Cell. 69
4.13 A Photograph of the Content in the Equilibrium Cell at the Critical-mixture Point. The Critical Opalescence Was Observed. 70

4.14 A Photograph of the Content in the Equilibrium Cell Above the Critical-mixture Point. Only One Supercritical Fluid Existed in the Cell. 71
4.15 Solubility of CO_2 in Liquid Naphthalene at 373.2 K. • Data of Barrick [77]; ○ This Work. 73
4.16 Solubility of CO_2 in Liquid Naphthalene at 348.2 K, 343.2 K and 338.2 K. ● Critical-mixture Point at 348.2 K; ■ Critical-mixture Point at 343.2 K; ▲ Critical-mixture Point at 338.2 K. 76
4.17 Solubility of CO_2 in Liquid Biphenyl at 343.2 K, 338.2 K and 333.2 K. ●, Critical-mixture Point at 343.2 K; ■, Critical-mixture Point at 338.2 K; ▲, Critical-mixture Point at 333.2 K. 77
4.18 Determination of the UCEP Temperature and Pressure for the Naphthalene-Carbon Dioxide and Biphenyl-Carbon Dioxide Systems by Means of the Intersection Method. • Estimated Values of the UCEP. 79
4.19 Experimental T-x Diagram of the S-L-G Curve and L=G Critical Loci for the System Naphthalene-CO_2 for Determination of the UCEP Composition. • Estimated Value of the UCEP. 81
4.20 Experimental T-x Diagram of the S-L-G Curve and L=G Critical Loci for the System Biphenyl-CO_2 for Determination of the UCEP Composition. • Estimated Value of the UCEP. 82
4.21 Pressure-Temperature Projection of Multiphase Coexistence Curves for the System Naphthalene(1)-Biphenyl(2)-CO_2(3). • Four-Phase (S_1-S_2-L-G) Equilibria, this work; □ Four-Phase (S_1-S_2-L-G) Equilibria, by White and Lira [121]. ○ Three-Phase (S-L-G) Equilibria with Initial Loading x_1=0.455; × Three-Phase (S-L-G) Equilibria with Initial Loading x_1=0.470. 91

4.22 Pressure-Temperature Projection of Multiphase Coexistence Curves for the System Naphthalene(1)-Phenanthrene(2)-CO_2(3). • Four-Phase (S_1-S_2-L-G) Equilibria, this work; □ Four-Phase (S_1-S_2-L-G) Equilibria, by White and Lira [121]. o Three-Phase (S-L-G) Equilibria with Initial Loading x_1=0.560; × Three-Phase (S-L-G) Equilibria with Initial Loading x_1=0.580. 92

4.23 Pressure-Temperature Projection of Multiphase Coexistence Curves for Mixtures Containing Naphthalene(S_1), Biphenyl(S_2), and CO_2. . 93

4.24 Pressure-Temperature Projection of Multiphase Coexistence Curves for Mixtures Containing Naphthalene(S_1), Phenanthrene(S_2), and CO_2. 94

4.25 Schematic Diagram of the Supercritical Fluid Chromatograph. **A** - Liquid CO_2 Cylinder; **B** - Filter; **C** - Cooling Bath; **D** - High Pressure Pump; **E** - Flow Transducer; **F** - Mixing Chamber; **G** - Six-way Valve; **H** - Analytical Column; **I** - Pressure Transducers; **J** - Column Oven; **K** - VW Detector; **L** - Back Pressure Regulator. . . 97

4.26 Selectivities of Supercritical CO_2 in Liquid State for the Systems Naphthalene-Biphenyl-CO_2 and Naphthalene-Phenanthrene-CO_2. . . 102

5.1 Flow Diagram of Computation Procedure Used for Determining the S-L-G Equilibria for Binary Mixtures. 111

5.2 Comparison of Calculated and Experimental Results of P-T Values of S-L-G Equilibria for the Naphthalene-CO_2 Mixture. 112

5.3 Comparison of Calculated and Experimental Results of P-x Values of S-L-G Equilibria for the Naphthalene-CO_2 Mixture. 113

5.4 Comparison of Calculated and Experimental Results of P-T Values of S-L-G Equilibria for the Biphenyl-CO_2 Mixture. 115

5.5 Comparison of Calculated and Experimental Results of P-x Values of S-L-G Equilibria for the Biphenyl-CO_2 Mixture. 116

5.6 Comparison of Calculated and Experimental Results of P-T Values of S-L-G Equilibria for the Phenanthrene-CO_2 Mixture. 117
5.7 Comparison of Calculated and Experimental Results of P-x Values of S-L-G Equilibria for the Phenanthrene-CO_2 Mixture. 118
5.8 Flow Diagram of Computation Procedure Used for Determining the S_1-S_2-L-G Equilibria for Ternary Mixtures. 121
5.9 Comparison of Calculated and Experimental Results of P-T Projection of S_1-S_2-L-G Equilibria for Naphthalene-Biphenyl-CO_2 Mixture. 123
5.10 Comparison of Calculated and Experimental Results of P-T Values of S-L-G Equilibria for Two Binary Mixtures, Naphthalene-CO_2 and Biphenyl-CO_2 Using the Activity-Coefficient Model. 125
5.11 Comparison of Calculated and Experimental Results of P-x Values of S-L-G Equilibria for Two Binary Mixtures, Naphthalene-CO_2 and Biphenyl-CO_2 Using the Activity-Coefficient Model. 126
5.12 Comparison of Calculated Results of the Solubility Data for the Biphenyl-CO_2 Mixture. (a): Results with SGR Mixing Rule; (b): Results with AS Mixing Rule. 131
5.13 Experimental P-T-x Values of S-L-G Equilibria and L=G Critical Loci for the Naphthalene-CO_2 Mixture. 133
5.14 Experimental P-T-x Values of S-L-G Equilibria and L=G Critical Loci for the Biphenyl-CO_2 Mixture. 134

6.1 Pressure-Temperature Values of the S-L-G Equilibria Determined by the "First Melting Point" Method for the Binary Mixtures Naphthalene-CO_2 and Biphenyl-CO_2 [84,66]. 136
6.2 Pressure-Temperature Values of the S-L-G Equilibria Determined by the "First Freezing Point" Method for the Binary Mixtures Naphthalene-CO_2 and Biphenyl-CO_2. 137
6.3 Partial Molar Volume of Naphthalene in Supercritical Ethylene [140]. 150

B.1 Calibration Curve of Pressure Transducer for Model AB/HP Serial No. A06342. 181
B.2 Calibration Curves of Pressure Transducer for Model AB/HP Serial No. 13429. 182
B.3 Calibration Curves of Pressure Transducer for Model SA Serial No. 13585. 183

C.1 Calibration Curves I of the Thermocouples in the Air Bath. 186
C.2 Calibration Curves II of the Thermocouples in the Air Bath. 187

List of Tables

3.1 Experimental Results of LCEPs for Some Binary Mixtures [83]. . . . 28

4.1 Experimental Pressure-Temperature-Liquid Composition Values of the Three-Phase (S-L-G) Coexistence Curve for the System Naphthalene (1)-Carbon Dioxide(2). 47

4.2 Experimental Pressure-Temperature-Liquid Composition Values of the Three-Phase (S-L-G) Coexistence Curve for the System Biphenyl(1)-Carbon Dioxide(2). 48

4.3 Experimental Pressure-Temperature-Liquid Composition Values of the Three-Phase (S-L-G) Coexistence Curve for the System m-Terphenyl (1)-Carbon Dioxide(2). 58

4.4 Experimental Pressure-Temperature-Liquid Composition Values of the Three-Phase (S-L-G) Coexistence Curve for the System Phenanthrene (1)-Carbon Dioxide(2). 59

4.5 Additional Measurement of Pressure-Temperature- Liquid Composition Values of the Three-Phase (S-L-G) Coexistence Curve for the System Biphenyl(1)-Carbon Dioxide(2). 63

4.6 Solubility of Carbon Dioxide(2) in Naphthalene(1) at 348.2 K, 343.2 K and 338.2 K. 74

4.7 Solubility of Carbon Dioxide(2) in Biphenyl(1) at 343.2 K, 338.2 K and 333.2 K. 75

4.8 Comparison of the Binary LCEP and UCEP for the System Naphthalene-Ethylene and the Ternary LCEP and UCEP for the System Naphthalene-Hexachloroethane-Ethylene with the Critical Temperature and Pressure of Ethylene [75,72]. 84

4.9 Pressure-Temperature Values of the Four-Phase (S_1-S_2-L-G) Coexistence Curve for Two Ternary Systems, Naphthalene(1)- Biphenyl(2)-CO_2 and Naphthalene(1)-Phenanthrene(2)-CO_2. 89

4:10 Pressure-Temperature Values of the Three-Phase (S-L-G) Equilibria for Two Ternary Systems Starting with Different Solid Loadings. . . 90

4.11 SFC Settings for Analysis of the System Naphthalene-Biphenyl. . . . 99

4.12 SFC Settings for Analysis of the System Naphthalene-Phenanthrene. 100

4.13 Physical Properties of the Materials Used in This Study [131]. 103

5.1 Values of Interaction Parameters Used in the Correlation of the S-L-G Three-Phase Equilibria for the Binary Mixtures, Naphthalene-CO_2, Biphenyl-CO_2 and Phenanthrene-CO_2. 119

5.2 Correlation of the Solubility Data for Two Binary Mixtures, Naphthalene-CO_2 and Biphenyl-CO_2. 130

A.1 Calibration Results of Naphthalene for the Naphthalene-Biphenyl-CO_2 System. 175

A.2 Calibration Results of Biphenyl for the Naphthalene-Biphenyl-CO_2 System. 176

A.3 Calibration Results of Naphthalene for the Naphthalene-Phenanthrene-CO_2 System. 177

A.4 Calibration Results of Phenanthrene for the Naphthalene-Phenanthrene-CO_2 System. 178

A.5 The Values of Intercepts, Slopes and Linear Correlation Coefficients (LCC) for Two Ternary Systems. 179

C.1 Calibration Results of the Quartz Thermometer. 185

D.1 Determination of P-n_{CO_2} Relationship in the Sample Loop for the P-T-x Measurement. 189

Chapter 1

INTRODUCTION

Supercritical fluid extraction (SFE), developed two decades ago, is a new separation technique in chemical engineering. Due to rising energy costs, pollution concerns and some expected shifts in chemical manufacturing patterns, supercritical processes have received wide attention for many applications in the chemical, energy, food and pharmaceutical industries.

1.1 Extraction with Supercritical Fluid

At a temperature and pressure above its critical point, a gas, referred to as a supercritical fluid (SCF), exhibits a greatly enhanced and selective solubility effect towards solids and liquids. Besides, a SCF has certain desirable transportation properties which make it an excellent solvent. While the density and therefore the solvent power of a SCF is comparable to that of a liquid, its diffusion coefficient and viscosity are near to those of a gas. As a consequence, a rather large diffusion coefficient is found, that is favorable for mass transfer. Since the SCF is also soluble in the liquid phase, viscosities and surface tensions are decreased and diffusion coefficients increased in the equilibrium liquid phase. Most of the characteristics that the SCF possesses, such as high solvent power, large diffusion coefficients and low viscosity, are favorable to fluid extraction.

The basic concept of the SFE process is to exploit this unusual behavior by contacting a mixture which is either in a solid or liquid state with a SCF, such as carbon dioxide, ethylene, ethane, propane, etc. The density of the extracted mixture is then reduced, by either pressure reduction or heating, causing the solvent and extracts to separate. As suggested by virtually all authors in their review papers [1-6], the solvent power of a SCF can be related in a first approximation to the solvent density in the critical region. This statement as well as the operating features of SFE processes can be rationalized by considering the density behavior of a pure substance. Figure 1.1 shows the reduced density-reduced pressure diagram for carbon dioxide at various reduced temperatures in the vicinity of the critical point. For practical considerations, the SCF region of interest is defined at conditions bounded along the isotherms T_r=1.0 to T_r=1.2 and P_r above 1.0. In this region the SCF is highly compressible. The reduced density of the solvent, ρ_r, can change from a liquidlike density to a gaslike density. The isotherms run rather vertical which means that a slight change in pressure will result in a considerable change of density, hence the change of the solvent power. On the other hand, in a certain range of pressures (e.g., $1.0 < P_r < 2.0$), an increase of temperature at constant pressure will reduce greatly the density of the solvent.

Extraction with supercritical fluids combines, to a certain extent, the characteristics of distillation and liquid extraction. The term "destraction" has therefore been proposed by Zosel [7] for this method of separation. However, because an auxiliary material is needed for the separation, it counts rather more as an extraction procedure. In brief, this new method is characterized by the following features:

1) Phenomena of distillation and extraction are utilized simultaneously in the SFE process, i.e., the difference in volatility of materials and selective affinity between molecules both play a role. For example, olefins are taken up into the supercritical ethylene in the order of their increasing boiling points; and caffeine and aroma are selectively extracted by supercritical carbon dioxide.

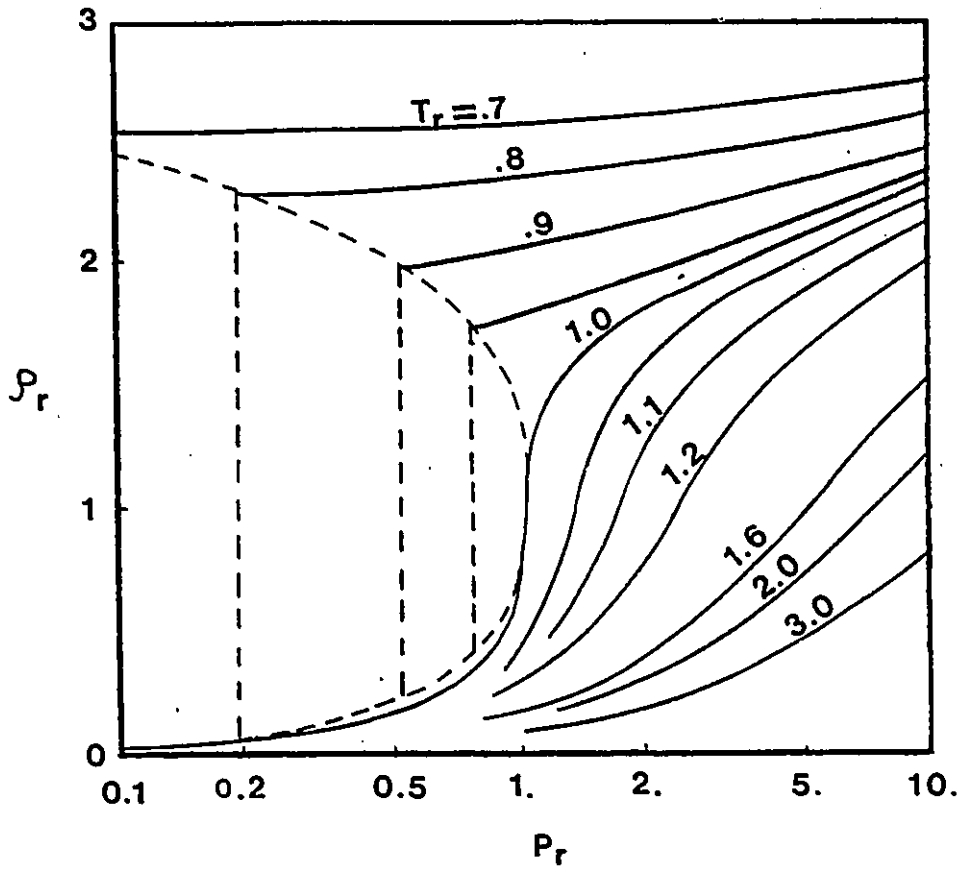

Figure 1.1: Variation of Reduced Density of a Pure Substance in the Region of Interest for Supercritical Fluid Extraction.

2) The unique feature of SFE process is that the loading power of a SCF depends on its density, which can be controlled simply by altering pressure or temperature.

3) Separation of the dissolved substances from the solvent can be accomplished either by reducing the pressure or by raising the temperature. Energy demand is less for SCF than for liquid extraction where solvent distillation is required. For the recycle of the gas, only recompression is needed.

4) High-boiling-point materials can be greatly and sometimes even selectively dissolved by SCF to form a supercritical phase. Since a SFE process does not have to be operated at high temperature, this technique is particularly suitable for the separation of heat labile substances.

The major disadvantage of SFE is considerable capital cost required for working under high pressure. As a result, SFE is only an alternative when distillation or liquid extraction have marked weaknesses or shortcomings.

SFE is a separation method based on thermodynamics, predominantly on the phase equilibrium of mixtures at supercritical fluid conditions. Whereas many research activities have been dedicated to the study of properties of pure compounds at high pressure, the thermodynamics of mixtures at supercritical fluid conditions is still in a developing state.

1.2 Development of Supercritical Fluid Extraction

Historically, in the field of chemical engineering, interest in SCF was initially related to the observation, noted by Hannay and Hogarth [8,9] over one hundred years ago, that such fluids were excellent solvents for non-volatile substances in the same manner as normal liquids. In 1896, Villard [10] published a review of supercritical fluid solubility phenomena, in which he reported the observation that the interaction

of a high-pressure gas with a solid hydrocarbon would result in the lowering of the normal melting point of the pure solid. In 1915, Prins [11] measured the solubility of naphthalene in supercritical ethane and carbon dioxide. He determined solid-liquid-gas three-phase curves and critical end points for naphthalene in both gases.

The first suggestion of using dense gas as an auxiliary for separation of high molecular mixtures is to be found in the U.S. patent in 1936 [12]. It was also known half century ago that hydrocarbons were entrained in highly compressed natural gas during the recovery of petroleum [13]. Purely academic studies on well-defined binary systems (including one supercritical component) started in the 1940's [14-16]. At the end of the fifties, Zhuze [17] suggested a procedure for fractionating crude oil and extracting earth waxes with the aid of a gas under supercritical conditions. It appears, however, that no chemical engineering applications were seriously considered until the 1970s. The considerable experimental problem associated with investigation in the region of the critical state was the prime obstacle which hindered intensive research at the early stage in this domain.

In early 1970, Zosel [18] developed a process, decaffeinating green coffee beans with supercritical carbon dioxide, which was soon commercialized in West Germany. Since then, SFE as a separation process has received greater attention in energy and chemical as well as in food and pharmaceutical industries. Reviews, patents and extensive research works have been found widely in the literature (e.g., [1-6]).

The motivation for the development of SFE technology as a viable separation technique is a consequence of the following factors:

1) The energy costs for carrying out a separation by distillation or by liquid extraction have increased ten-fold during the last decade, and preliminary evaluations [5] have shown that in many cases SFE with lower energy requirements can be employed as an alternative process.

2) Due to the increased pollution problems, such as acid rain, stringent legislation was made by the government agencies for the use of common industrial

solvents, such as halogenated hydrocarbons. Nontoxic, environmentally acceptable supercritical solvents such as carbon dioxide are considered as ideal industrial solvents.

3) In the food and pharmaceutical industries, more and more traditional extraction processes with organic solvents are being abandoned for human health reasons. The potential applications of SFE technique with non-corrosive and harmless solvents are very attractive in these fields.

1.3 Applications of Supercritical Fluid Extraction

In the last ten years, much of the interest in the application of SFE has been focused on the energy, food and chemical industries.

In energy-related areas, SFE has considerable potential since it does not involve solvent loss or energy consumption in large quantities, nor the decomposition of heat-labile substances as occurs during distillation or liquid extraction in the solvent recovery. These areas include deasphalting of heavy petroleum (e.g., the so called ROSE process) [19], coal processing [20-23], extraction of bitumen from tar sand and oil shale [24] and tertiary oil recovery [25].

As mentioned above, the main advantage of SFE is its selective extraction of low volatility substances by the suitable choice of pressure and temperature. Many examples of this type of application arise in the field of natural products, especially in the food industry. The widely cited examples are the decaffeination of coffee [18,26,27], the oil extraction from seeds and foods [28,29,30], the extraction of flavor, aromas and drugs [31,32,33] and the extraction of hops and nicotine [34-37].

Many examples of SFE applied in the field of chemical engineering have been described, including the separation of azeotropes [38,39], desalination of sea water [40], regeneration of activated carbon [41,42], fractionation of polymers [43],

separation of isomers [44,45], treatment of waste water [46,47], etc.

In addition to chemical processing, it should also be noted that the principles associated with SFE can be exploited as an analytical tool and for physico-chemical property measurements. The primary application in this area is the supercritical fluid chromatography (SFC). Using a SCF as a mobile phase, the new chromatography technique can be employed especially for the separation of substances with a very low volatility through a pressure programming [48,49]. Some physico-chemical properties can be derived from SFC experiment, such as the capacity ratio and the diffusivity [50,51].

SCFs are also important as reaction media, e.g., the synthesis of polyethylene [52,53], and the isomerization of C_4- C_{12} n-paraffins in supercritical CO_2, HBr or HCl [54].

1.4 Thesis Objectives

There currently exists a lack of experimental data of mixtures, especially multicomponent mixtures, at supercritical fluid conditions and of fundamentally based thermodynamic models which accurately predict phase behavior at critical and supercritical regions. Without this necessary background, SFE process design and economic evaluation is extremely difficult, if not impossible. The experimental work on the phase equilibria of supercritical mixtures is very demanding because the high-pressure technique is involved. Simple and reliable experimental method for the determination of the multiphase equilibria of binary and ternary systems is needed.

The objectives of this study can be divided into three parts: experimental investigation, thermodynamic modeling and theoretical exploration of the freezing point depression of the solid and solubility behavior in the vicinity of the critical end points.

In experimental investigation, the high-pressure phase equilibria of highly asymmetric systems, involving one supercritical component and one or two solid components, are to be measured over a wide range of pressures up to 50 MPa. In order to have quick and reliable measurements and to obtain more information of multiphase equilibria for binary and ternary mixtures, a new experimental technique is to be developed. The liquid-gas critical loci of the same binary mixtures are also to be determined in an attempt to establish the upper critical end points (UCEP) by means of an intersection method.

The systems investigated consist of carbon dioxide as supercritical solvent and aromatic compounds, naphthalene, biphenyl, m-terphenyl and phenanthrene as slightly volatile components. The choice of carbon dioxide as a supercritical solvent in this study is based on the fact that it is the most popular and important solvent used in SFE processes and has favorable critical conditions. In addition, it is cheap and available in large quantities, and is neither flammable nor explosive. It is also non-toxic, noncorrosive, and harmless to the environment and human body. The aromatic compounds chosen in this study are comprised of two and three benzene rings. They are relatively well defined, and their physical properties useful for phase equilibrium modeling are available in the literature. Besides, the author chose these compounds with an intent of providing some insight into how different positions and structures of benzene rings would affect the phase behavior of binary and ternary mixtures of this type at supercritical fluid conditions.

The freezing point depression of the solids under the pressure of a SCF and the solubility behavior in the vicinity of both critical end points are to be explored and discussed.

Thermodynamic modeling will follow two different approaches to representing the solid-liquid-gas three-phase equilibria. The aim of this study is to describe experimentally and theoretically the phase behavior of mixtures at supercritical fluid conditions, especially in the vicinity of the upper critical end point.

Chapter 2

PHASE BEHAVIOR AT SUPERCRITICAL FLUID CONDITIONS INVOLVING SOLID PHASES

Among the many applications mentioned in the previous section, very few can be considered commercially viable. The high equipment cost is one of the reasons for the reluctant acceptance of SFE by industry. The more fundamental problem, as pointed out by Basta and McQueen [55], is that too little is known about the thermodynamics of supercritical mixtures. The exploitation of the SFE technology depends on our understanding of the phase behavior of mixtures in the critical region.

Supercritical fluid mixtures have very complex phase behavior, especially when more than two components are involved. While phase diagrams for binary fluid mixtures are classified into six categories and have been studied in some detail (e.g., [56-62]), phase equilibria involving solids at supercritical fluid conditions have not been well studied. Since the Gibbs phase rule specifies a maximum of three

independent variables for a two-component system, the phase behavior for binary mixture can be completely described by three-dimensional phase diagrams with the most convenient variables being pressure, temperature and the mole fraction of one of the components (P-T-x) as their coordinates. Important features included in such P-T-x diagrams are:

1) liquid-gas, solid-gas and solid-liquid equilibrium lines for both pure components;

2) liquid-liquid and liquid-gas critical lines;

3) solid-liquid-gas and liquid-liquid-gas three-phase equilibrium lines.

Each of these equilibrium lines has only one degree of freedom according to the Gibbs phase rule.

One convenient way to present information in P-T-x diagrams is to use P-T projections and P-x diagrams. The enhanced solubilities in SCF and the influence of critical phenomena on solubility behavior can be examined conveniently using these diagrams. The classifications of the different types of phase behavior may be identified in P-T projections by the shapes and the number of critical lines, the existence or absence of three-phase lines and the manner in which the critical lines connect with the pure component critical points and the three-phase lines.

In this section, the phase behavior of binary and ternary systems where a fluid is in equilibrium with one or two solid phases is summarized.

2.1 Phase Diagrams for Binary Mixtures

A binary mixture consisting of a low volatility solid and a supercritical solvent (SCF) is usually a system in which the critical temperature of the pure components are far apart. In many such systems, the critical temperature of the solvent lies below the triple point of the solute, and there is no common range of temperature in which both pure components are in the liquid state.

The phase diagrams of this class of binary system can be classified into two

types. Type I, as shown in Figure 2.1, has the simplest pressure-temperature (P-T) projection curve. The liquid-gas critical mixture curve runs continuously between the critical points, C_1 (relatively low-volatile component) and C_2 (supercritical solvent). M is the triple point of the component 1. MN and ME represent the melting curve and the sublimating curve for pure component 1, respectively. Under high pressure, the melting curve bends toward the lower temperatures due to the increase of solubility of component 2 in component 1. This phenomenon is the so called freezing point depression. The freezing point depression curve depicted by MF in Figure 2.1a represents the solid-liquid-gas (S-L-G) three-phase equilibrium. The three-dimensional pressure-temperature-composition (P-T-x) diagrams as well as three isothermal pressure-composition (P-x) diagrams are also presented in Figure 2.1.

Both components of a type I mixture do not differ appreciably in molecular sizes, shape, structure or critical conditions. The critical temperature of the light component is not far apart from the melting temperature of the heavy component. Binary systems like sodium chloride-water [63] and carbon dioxide-methane [64] exhibit phase behavior of this type.

In this discussion emphasis is placed on the second class of mixtures, in which the critical loci and the S-L-G curves are not continuous. Phase diagram of Type II (see figures 2.2-2.4) usually occurs for mixtures whose components are not chemically similar and differ considerably in size, shape, polarity and critical properties. As pressure is elevated, the solid-liquid-gas (S-L-G) curve eventually intersects the liquid-gas critical loci at two locations: the upper-critical-end-point (UCEP) and the lower-critical-end-point (LCEP). The lower-temperature branch of the S-L-G curve intersects the critical mixture curve at the LCEP while the higher-temperature branch of the S-L-G curve begins at the triple point temperature of the solid and ends at the UCEP, the intersection of the critical mixture curve and the S-L-G curve. Between the two branches of the S-L-G curves, solid-fluid equilibrium exists

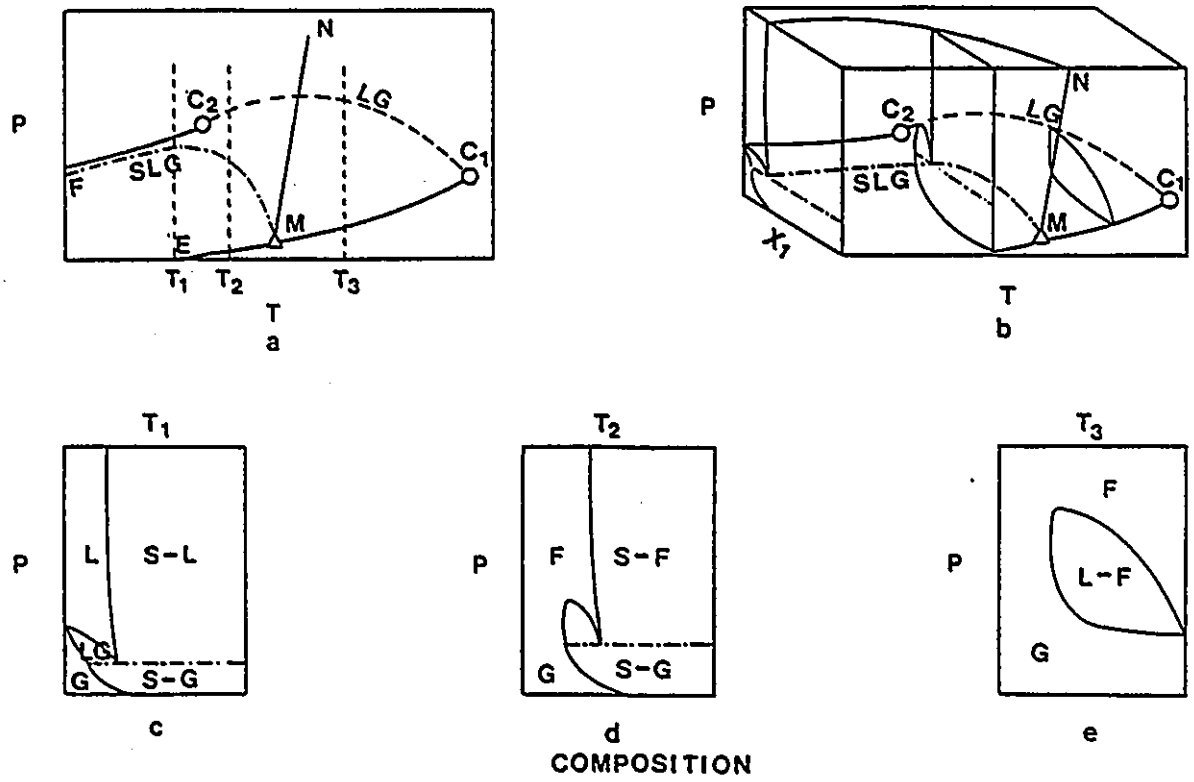

Figure 2.1: Phase Diagram of Type I: L=G Critical Curve Runs Continuously Between Two Critical Points of Pure Components. M, Triple point; C_1, C_2, Critical points; - - -, L=G critical loci; -.-.-, S-L-G three-phase coexistence curve.

at all pressures. It is this region where the SFE process would take place.

Phase diagrams for Type II mixtures may be further classified into three categories according to the shape of the higher-temperature branch of the S-L-G curve, as shown in Figures 2.2-2.4. Pressure-temperature-composition diagrams and pressure-composition diagrams as well as pressure-temperature projections are presented in these figures.

The first kind of phase diagram is shown in Figure 2.2, in which the S-L-G curve in P-T projection tilts towards the lower temperature and has a negative slope. Many binary mixtures reported in the literature have this type of phase behavior. The following substances with ethylene as supercritical fluid belong to this group [15,65]: naphthalene, biphenyl, n-octacosane, n-hexatriacontane, p-dibromobenzene, p-iodochlorobenezene, 1,3,5-trichlorobenzene, anthracene, anthraquinone, hexaethylbenzene, stilbene, m-dinitrobenzene and hexachloroethane.

Figure 2.3 presents the second type of phase diagram, in which the S-L-G curve has a temperature minimum in P-T projection. At $T=T_2$, the three-phase curve is intersected twice at P_a and P_b as shown in Figure 2.3d. At pressures below the first three-phase pressure, P_b, there exists a solid-gas equilibrium. At pressures above the second three-phase pressure, P_a, a solid-fluid equilibrium exists. Between P_a and P_b, different phase equilibria or phase states are possible depending on the composition of the mixture: liquid-vapor equilibrium, solid-liquid equilibrium and single liquid phase. The latter is referred to as a liquid island. The solid line on the left in Figure 2.3d shows that the solubility of the heavy component in the SCF changes with the pressure. The location of the liquid island indicates that the solubility of the solid and that of the gas in the liquid phase both are high.

Figure 2.3e shows the phase behavior at constant temperature $T=T_{UCEP}$. As the pressure approaches the UCEP pressure, where the SCF is highly compressible, the solubility of the solid in the fluid phase increases dramatically, as depicted by a horizontal inflection. At the UCEP, the derivative $\left(\frac{\partial P}{\partial y}\right)_{T_{UCEP}} = 0$. If the pressure is

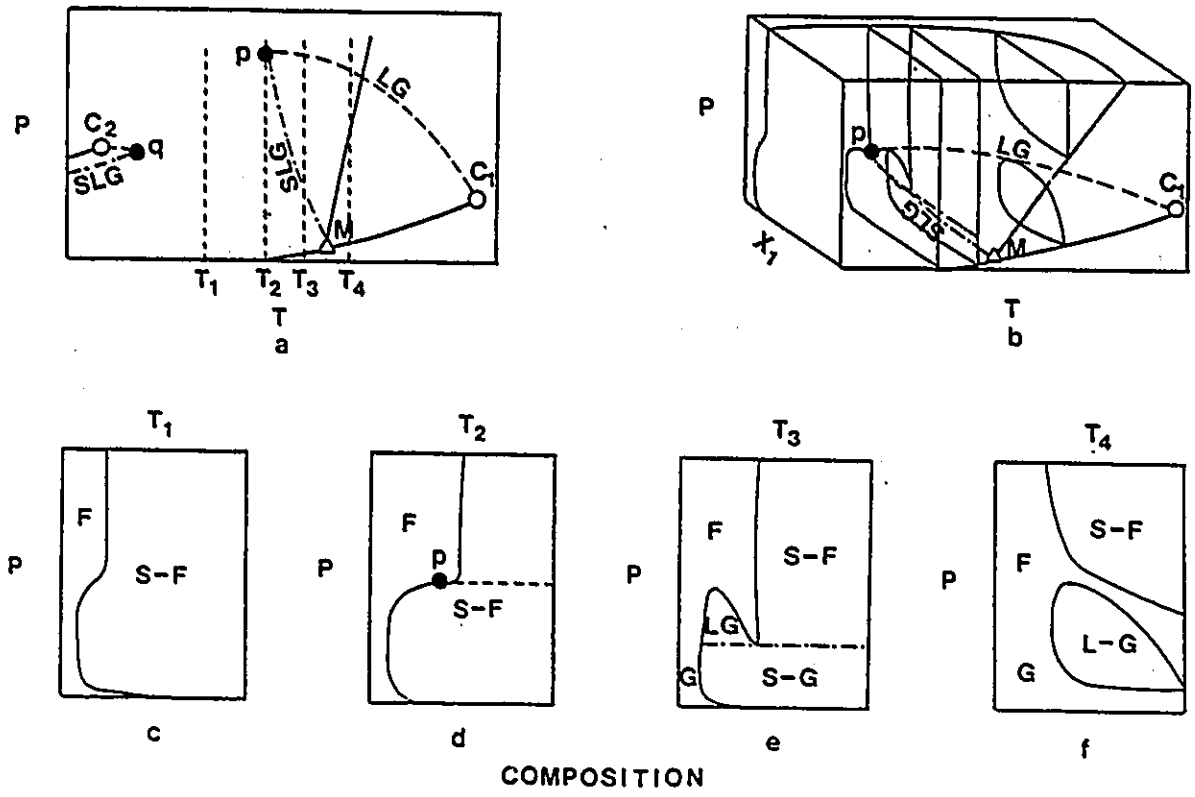

Figure 2.2: Phase Diagram of Type IIa: The S-L-G Curve in P-T Projection Has a Negative Slope. M, Triple point; C_1, C_2, Critical points; p, Upper critical end point; q, Lower critical end point; - - -, L=G critical loci; -.-.-, S-L-G three-phase coexistence curve.

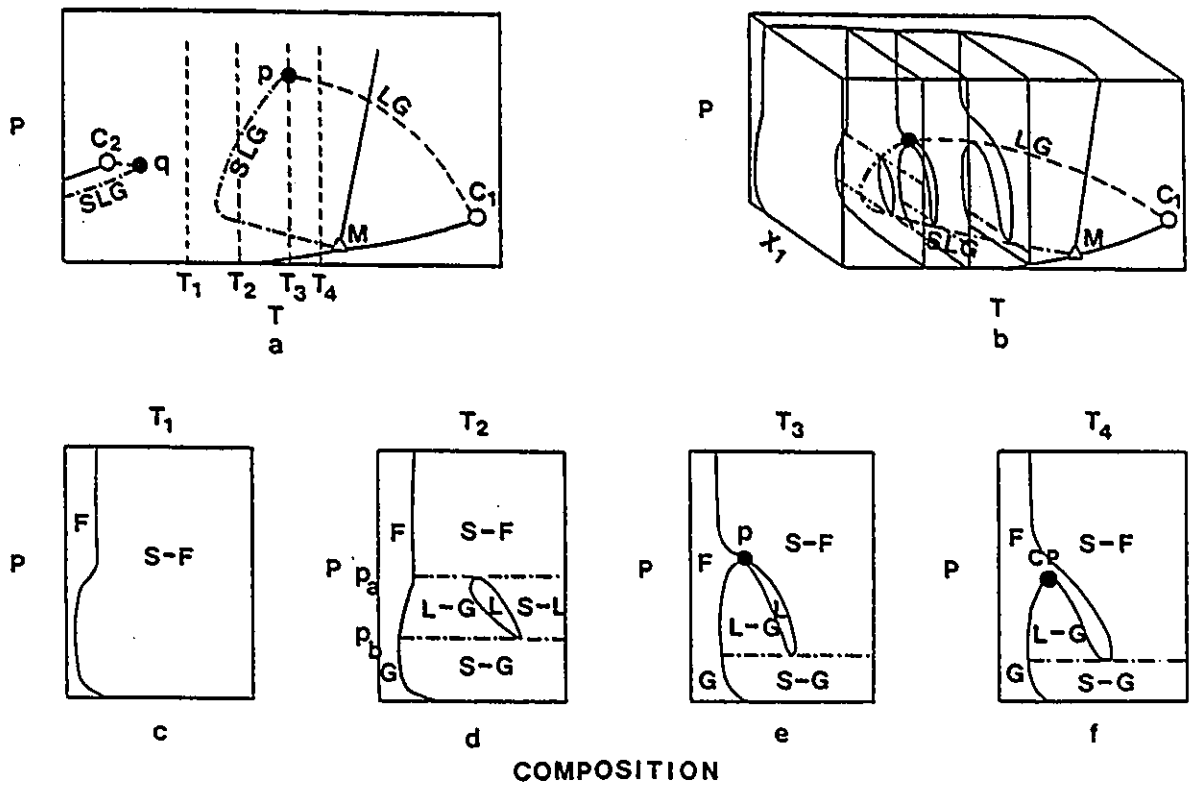

Figure 2.3: Phase Diagram of Type IIb: The S-L-G Curve in P-T Projection Has a Temperature Minimum. M, Triple point; C_1, C_2, Critical points; p, Upper critical end point; q, Lower critical end point; - - -, L=G critical loci; -.-.-, S-L-G three-phase coexistence curve.

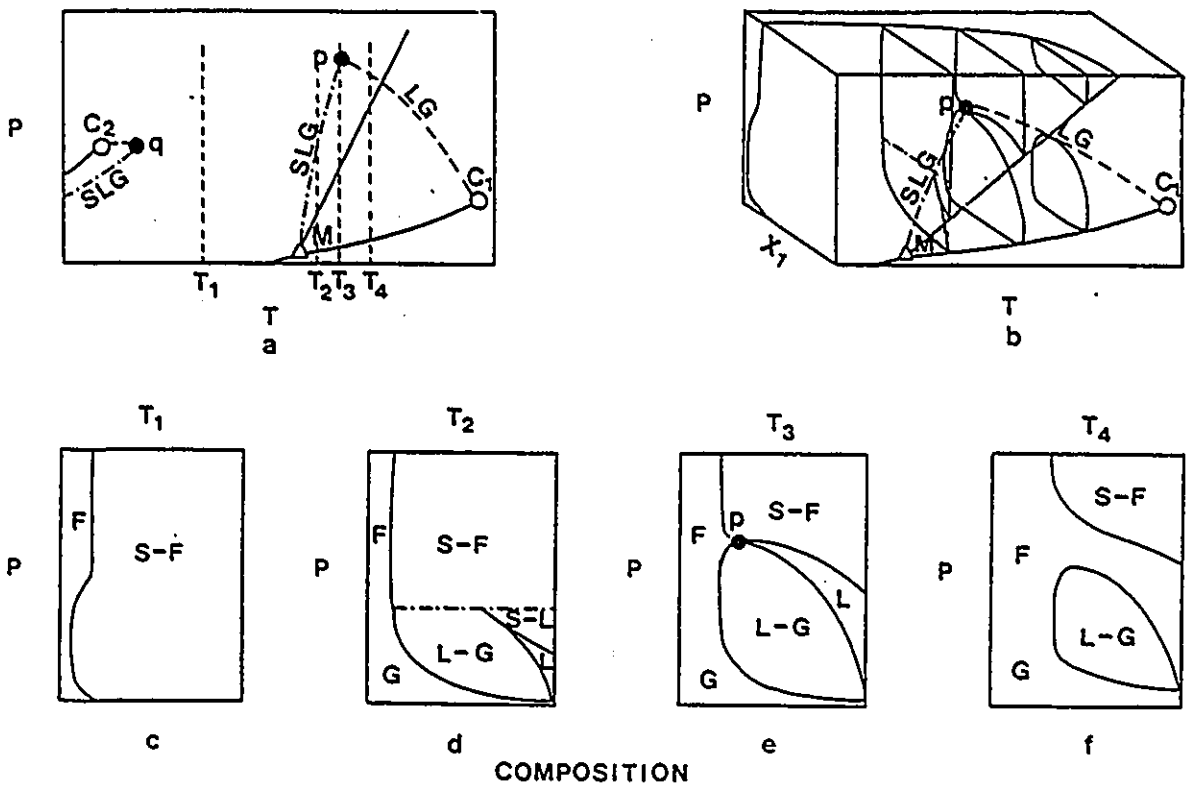

Figure 2.4: Phase Diagram of Type IIc: The S-L-G Curve in P-T Projection Has a Positive Slope. M, Triple point; C_1, C_2, Critical points; p, Upper critical end point; q, Lower critical end point; - - -, L=G critical loci; -.-.-, S-L-G three-phase coexistence curve.

increased further more, the solubility quickly reaches a limiting value. The closer the temperature is to the UCEP temperature, the more significant will be the solubility enhancement at the UCEP pressure.

It is interesting to note in Figure 2.3f that the shape of solid-fluid curve near the UCEP reflects the effect of the liquid-gas critical point, CP. Examples of this type of phase behavior were found in systems naphthalene-CO_2 [66,67,68], biphenyl-CO_2 [66,67,68], n-octacosane-CO_2 [66,69], m-terphenyl-CO_2 [79] and phenanthrene-CO_2 [119].

In Figure 2.4, the temperature of the UCEP is higher than the triple point temperature of component 1. The three-phase (S-L-G) curve (M-p) bends towards the higher temperature as the pressure increases, and has a positive slope. Examples of this type reported in the literature are found in gas mixtures at cryogenic conditions such as hydrogen-carbon dioxide [70] and neon-argon [71].

2.2 Phase Diagrams of Ternary Mixtures

The separation of a binary solid mixture utilizing a SCF is frequently encountered in a SFE process. In spite of their practical usefulness, experimental investigation of phase equilibria for ternary mixtures consisting of a SCF and two nonvolatile solids is rather limited.

Van Gunst et al. [72] described the phase behavior of the naphthalene-hexachloroethane-ethylene system using a P-T diagram which is shown in Figure 2.5. The S_1-S_2-L-G four-phase curve and the so called ternary critical-end-point curves, S_1-L=G and S_2-L=G are found in the P-T diagram. The latter two curves represent the ternary critical loci, along which the fluid phases are saturated with one of the solids. In the diagram, the four-phase curve intersects the critical-end-point curves and gives rise to two invariant ternary critical-end-points: one ternary upper critical end point, p and one ternary lower critical end point, q.

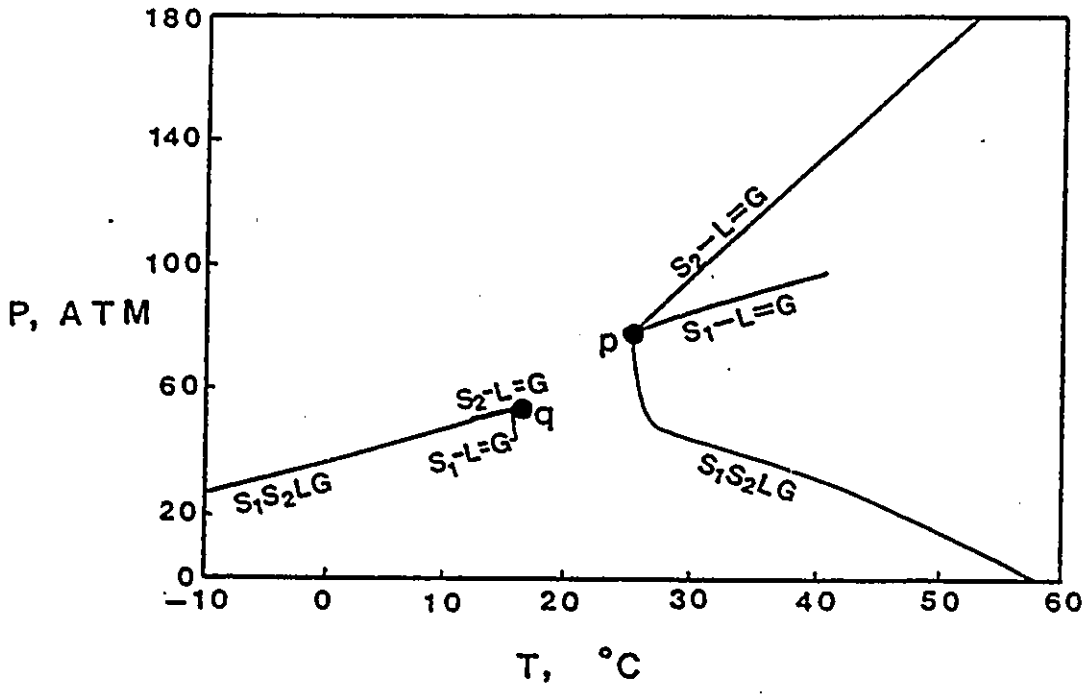

Figure 2.5: Pressure-Temperature Projection of Ternary Mixture Naphthalene-Hexachloroethane-Ethylene. p, Ternary upper critical end point; q, Ternary lower critical end point [72].

Koningsveld and Diepen [73] suggested that three main types of such ternary mixtures can be distinguished according to the extent of the existence of binary and ternary critical end points:

Type I: Systems without ternary upper or lower critical end points (TUCEP or TLCEP), but with binary critical end points (UCEP/LCEP) of the SCF and one of the solids (Figure 2.6a).

Type II: Systems without TUCEP and TLCEP but with UCEP and LCEP formed by the SCF with both of the solids (Figure 2.6b).

Type III: Systems with UCEP and LCEP, and TUCEP and TLCEP (Figure 2.6c).

In Figure 2.6a-c, the triple points of pure solids and the quadruple point of the solid mixture are designated by Δ , $\diamond$, respectively. It should be noted that the above classification is based on the fact that a binary system of two solids has an eutectic temperature in the melting diagram, i.e., both solids have different crystalline structures and do not form a solid mixture.

Koningsveld and co-workers [73,74] described qualitatively the phase behavior of the solid 1-solid 2-SCF ternary systems. Figure 2.6c shows the most probable situation when the solubilities of the solids in the SCF are both small. At any temperature which is between the TLCEP, T_q, and TUCEP, T_p, there are two solid phases in equilibrium with a fluid phase at any pressure. The two four-phase (S_1-S_2-L-G) curves, one ends at the TLCEP and the other at the TUCEP, form the boundaries for SFE operations. A dramatic solubility enhancement of solid in SCF is achieved in the vicinity of the TUCEP, p. It should be mentioned that S_1-S_2-L-G curves reported in the literature are limited to very few systems [72,79].

Besides the separation of the solid mixture, the phase behavior of the ternary systems is of importance for the study of entrainer effects. Kurnik and Reid [80] reported the experimental results for the binary solid mixture consisting of naphthalene, phenanthrene, benzoic acid, 2,3-dimethyl-naphthalene and 2,6-dimethyl-

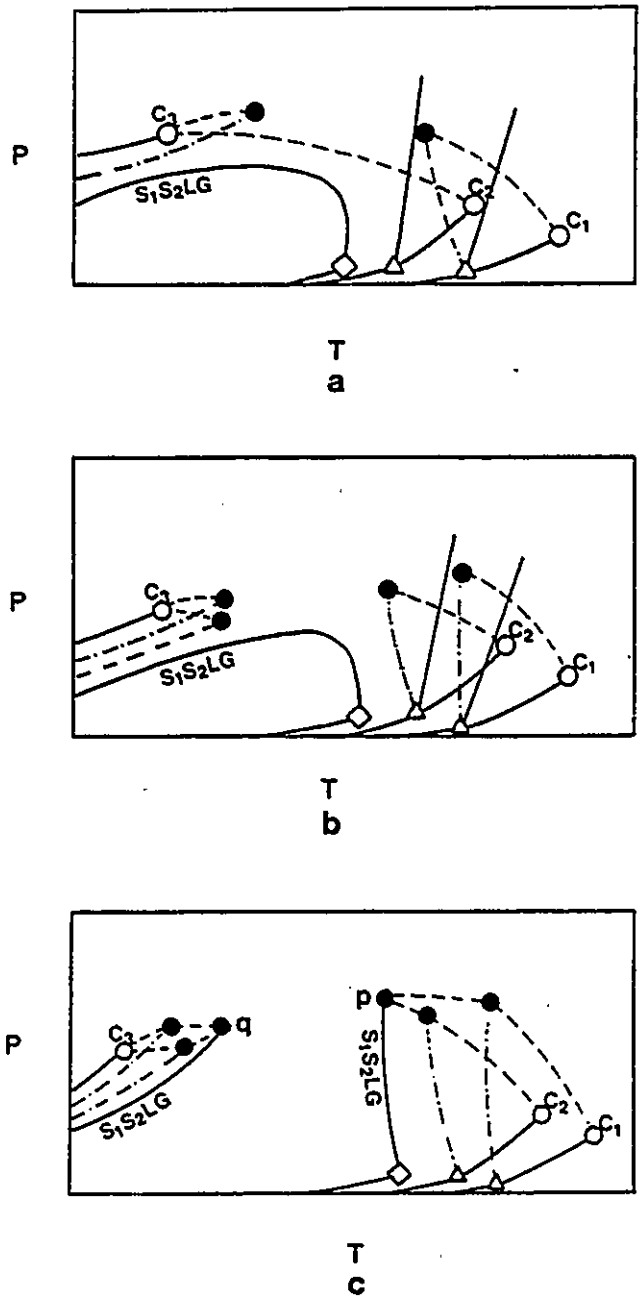

Figure 2.6: Three Types of Phase Behavior of Ternary Mixtures Consisting of Two Solids and One SCF. p, Ternary upper critical end point; q, Ternary lower critical end point; Δ, Triple points of pure solids; $\diamond$, Quadruple point of solid mixture.

naphthalene in supercritical CO_2 and ethylene. They found that for a binary solid mixture, the presence of one of the solid components enhances the solubility of the other solid component in the SCF phase. The former is referred to as an "entrainer" or a co-solvent. For example, Kurnik and Reid [80] showed that under the same operating conditions, the presence of naphthalene can enhance the solubility of phenanthrene as much as 300%.

Chapter 3

CRITICAL REVIEW OF LITERATURE

A critical review of the literature is given in this chapter with emphasis on experimental approaches and thermodynamic modeling for the determinations of the multiphase equilibria and of the liquid-gas critical loci for locating the upper critical end point where the great solubility enhancement is achieved. Some conclusions are reached after the review.

3.1 Experimental Approach

In order to have a better theoretical understanding of the phase behavior of the mixtures at supercritical fluid conditions, the recent research has been focused on the systematic experimental studies of the well-defined systems.

The experimental studies of the phase behavior of the supercritical mixtures include:

1. the measurement of the solubilities of heavy components (solids or liquids) in the supercritical solvents;

2. the determination of the phase boundaries suitable for the SFE process (such as the L_1-L_2-G or S-L-G three-phase curve and the S_1-S_2-L-G four-phase

curve), and the L=L and L=G critical loci helpful for locating the upper critical solution point and upper critical end point; and

3. the study on the entrainer effect in order to modify the solubility and the selectivity of the supercritical solvents.

In this section, the experimental determinations of the solid-liquid-gas three-phase coexistence curve and the liquid-gas critical loci as well as the study on the entrainer effect are critically reviewed. Both experimental determinations are highly demanding since high pressure technique is involved and the solidification of the heavy component presents significant problems when the deposit of the solid blocks the tubing of the experimental apparatus.

3.1.1 Determination of Multiphase Equilibria

The experimental study of the multi-phase equilibria (i.e., the determination of S-L-G three-phase curves for binary mixtures or that of the S_1-S_2-L-G four-phase curves for ternary mixtures) is of importance for the following reasons:

1) The characteristics of the 3-/4- phase curve in the P-T projection and the way these curves connect with the critical loci are usually the basis of phase-diagram classification for binary or ternary mixtures;

2) It is essential to determine multiphase coexistence curves for establishing the phase boundaries suitable for SFE operation;

3) The multiphase coexistence curve is useful in the UCEP determination with the aid of liquid-vapor critical loci.

Different techniques have been described in the literature for determining the S-L-G curve, or the freezing-point depression of a solid component in the presence of a supercritical fluid. As far as pressure-temperature-liquid composition (P-T-x) measurements are concerned, very few systems have been investigated.

In one approach, referred to as the static solubility measurement, the compressed gas is metered into a view cell after a known amount of solid has been

loaded. The P-T projection of the S-L-G curve is deduced from the intersections of constant-composition solid-gas (S-G or S-F) and liquid-gas (L-G) equilibrium curves. The isopleths of S-G (or S-F) equilibrium are determined by slowly heating the mixture at constant pressure until the solid phase disappears. The isopleths of L-G equilibrium are measured by slowly increasing the pressure at constant temperature until the vapor phase disappears into the liquid phase or the liquid phase disappears into the vapor phase, depending on whether the composition of the prepared mixture is greater or smaller than the composition of the mixture at the UCEP.

Van Welie and Diepen [81,82] studied the solubility of naphthalene in supercritical ethylene and that of naphthalene in supercritical ethane, and deduced the P-T projections of the three phase S-L-G coexistence curves from the intersections of constant-composition S-G and L-G equilibrium curves.

The advantage of this approach is that the compositions of both liquid and vapor phases on the three-phase curve are obtained, but the process is tedious and time consuming.

In another approach [11,65,66], the P-T projection of the three-phase curve was determined by slowly increasing the temperature of an initial solid-gas condition at constant pressure until the solid begins to melt, and the temperature and pressure were taken to be the three-phase temperature and pressure. This is the so called "first melting point" method.

This approach provides a simple and quick determination of the P-T projection. However, the compositions of the equilibrium phases along the S-L-V curve are not determined.

3.1.2 Determination of Liquid-Gas Critical Loci

It is well known that in the vicinity of the critical point, the density of the fluid fluctuates violently with slight changes in pressures or temperature. The fluctuation

in density over a distance comparable with wavelength of the visible light gives rise to the strong scattering of light, which is the so called critical opalescence, a striking visual property of the critical state. In addition, the slight change in temperature or pressure near the critical point also causes a dramatic change in the amount of SCF phase or liquid phase in the equilibrium cell.

As early as over a hundred years ago, Andrew [85] and van der Waals [86] described both experimentally and theoretically the physical phenomena at or near the critical point of a substance. However, their unambiguous description of the now well-known critical phenomena, especially the idea of the existence of a state of continuity through the supercritical region, was hard to accept by many researchers at the beginning. The slow acceptance can be attributed to the experimental difficulties encountered in the critical region where the requirement for a high pressure and/or high temperature technique made precise measurements very difficult.

The experimental determination of the liquid-gas critical loci for binary mixtures is reviewed by Hicks [87] and Young [88]. The commonly used technique is the static method, in which the temperature and pressure are adjusted while agitating the system in an open-ended or sealed tube until the appearance or disappearance of the meniscus of the mixture is observed. If the composition of the mixture is close enough to that of the critical point, the intense scattering critical phenomena will be detected. In many investigations (for example, [89-92]), the critical properties have been determined as parts of a more general study of the gas-liquid equilibria.

Liphard and Schneider [93] used a high pressure view cell to measure the liquid-gas and liquid-liquid critical loci for binary systems consisting of subcritical CO_2 and hydrocarbons over a wide range of pressures up to 100 MPa. The critical loci were determined when the phase transition from one phase to two phases in the cell was observed. The accuracy of the measurements on the temperature and that on pressure were reported to be ± 0.1 K and ± 0.2 MPa, respectively.

Thies and Paulaitis [94,95] recently used a flow technique to determine the

liquid-gas equilibria and the critical properties of binary mixtures. In their measurements, two components, each as a compressed liquid, were delivered by separate high-pressure feed pumps to a preheater where a mixture was formed. The mixture passed through a 1.5 m-long tubing located in an air bath, and then entered into a view cell where the liquid and gas phases were separated. By opening two micrometering valves, samples of both phases were taken, and analyzed with a gas chromatograph utilizing a flame ionization detector. When the systems measured also involved solid components, such as naphthalene and 1-naphthol, the pumping problem was solved by dissolving the solid in a known amount of methanol which was the second component of the mixtures investigated. The solution was then compressed and delivered into the apparatus.

We are not aware of any measurements of the liquid-gas critical loci of a binary system consisting of one solid and one SCF in the open literature.

3.1.3 Entrainer Effects on the Solubility of Solids and the Selectivity of Supercritical Solvents

As mentioned in Section 2.2, the solubility of a low-volatility solute in a supercritical solvent will be enhanced by adding a small amount of the component referred to as an "entrainer". The use of an entrainer not only increases the solvent power but also improves the selectivity of the supercritical solvent when extracting a mixture. The volatility of the entrainer should be between that of the supercritical solvent and that of the extracted solute. The entrainer is usually added to the supercritical fluid at a concentration less than 15 mole% [143]. In the process of decaffeination of coffee bean, for example, water is used as the entrainer [18,26,27]. The addition of a certain amount of water improves greatly the solubility of caffeine in supercritical CO_2, and makes this SFE process commercially feasible. Benzene, methylene chloride, carbon tetrachloride hexane, acetone, methanol, ethanol, toluene and cyclohexane have also been studied as potential entrainers in supercritical solvents [144,145].

Entrainers are not confined to the conventional liquid solvents. Naphthalene dissolved in a supercritical fluid could be used as an entrainer if a component of lower volatility, such as phenanthrene or benzoic acid, were being extracted [80].

Schmitt and Reid [143] measured the solubility of phenanthrene and that of benzoic acid in supercritical CO_2 and ethane using four organic solvents as the entrainers. Based on their results, these authors suggest that it was the amount of entrainer and not the specific choice of entrainer that caused the solubility of the solid in the supercritical solvent to increase.

3.2 Upper Critical End Point

The previous reports for the naphthalene-ethylene system [16,75,76] show that although the solubility increases quickly near LCEP, the overall loading of naphthalene in supercritical ethylene is rather low. Besides, the lower critical end point usually occurs very close to the critical point of the pure SCF for most of the binary systems reported in the literature. Table 3.1 gives the experimental results of the LCEP for some binary mixtures. As can be noticed from this table, the temperature and pressure of the LCEP of each of the mixtures are very close to the critical temperature and pressure of the respective pure solvent. Therefore, to locate the LCEP is of less importance to both SFE operations and theoretical studies.

Diepen and Scheffer [75] measured the isothermal solubilities of naphthalene in ethylene over a wide range of pressures. As shown in Figure 3.1, the solubilities at temperatures ranging from 12 to 45°C do not change much with the increases in pressure. However, the 50°C isotherm in the P-x diagram is very sensitive to the slight change of pressure from 170 to 180 atm (~17 to 18 MPa). This region happens to be in the vicinity of the UCEP of the mixture. The UCEP temperature and the pressure of the naphthalene ethylene system, as reported by Van Gunst et al. [65], are 52°C and 174 atm (17.6 MPa), respectively. With further increase of the pres-

Table 3.1: Experimental Results of LCEPs for Some Binary Mixtures [83].

System	Pure Comp. 2		LCEP	
Comp. 2-Comp. 1	T_c, K	P_c, MPa	T_c, K	P_c, MPa
CO_2-octacosane	304.3	7.38	305.4	7.36
ethane-naphthalene	305.5	4.88	310.0	5.22
ethylene-naphthalene	282.4	5.04	283.9	5.19
ethylene-biphenel			284.4	5.17
ethylene-anthracene			282.6	5.12
ethylene-octacosane			282.7	5.06
ethylene-hexaethylbenzene			284.8	5.29
ethylene-hexamethylbenzene			283.0	5.11
ethylene-stilbene			282.7	5.11
ethylene-dinitrobenzene			282.5	5.09
ethylene-hexachloroethane			285.6	5.07
ethylene-1,3,5,-trichlorobenzene			286.3	5.34
ethylene-p-chlorobromobenzene			286.6	5.38
ethylene-p-chloroiodobenzene			285.2	5.26
ethylene-p-dibromobenzene			283.8	5.14
ethylene-hexatriacontane			282.8	5.06
ethylene-benzophenone			283.1	5.09

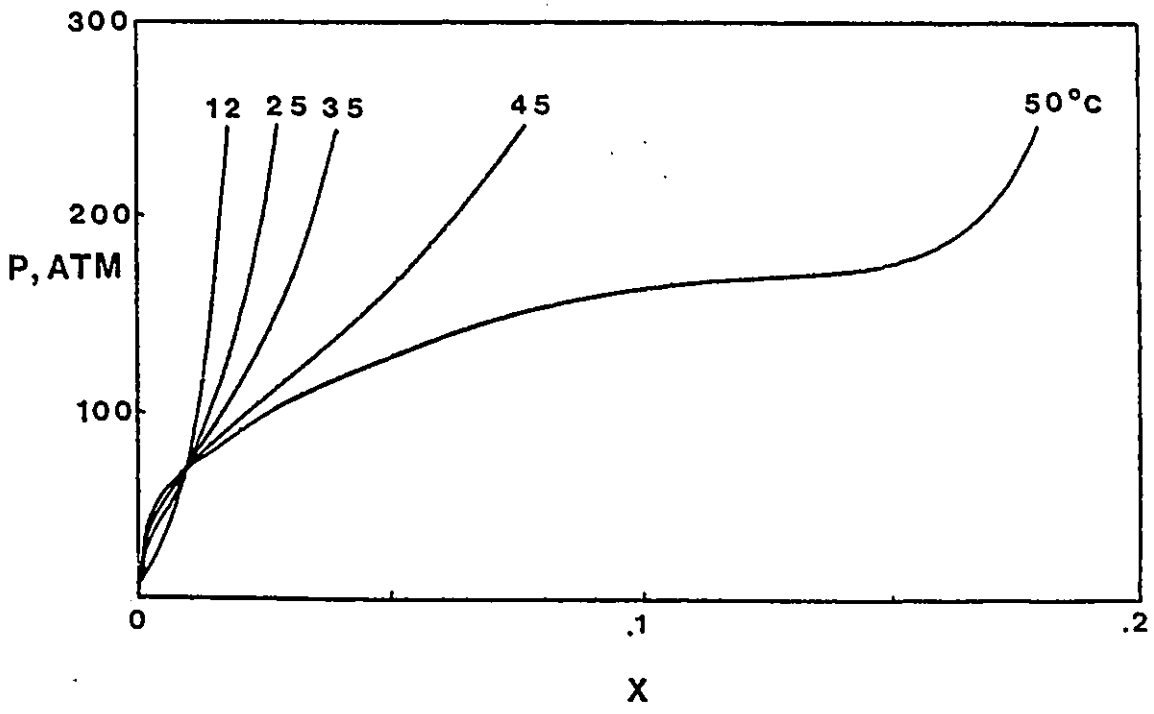

Figure 3.1: Isothermal Solubility of Naphthalene in Supercritical Ethylene [75].

sure, the solubility remains almost unchanged. The great solubility enhancement is achieved near the UCEP. The solubility of naphthalene in the supercritical phase is as high as 15 mole%, i.e., 45 wt%. From the viewpoint of phase equilibrium, the advantages of carrying out the SFE operation near the UCEP, that is the region near the mixture critical loci in the presence of solid, are obvious.

The solubility enhancement achieved near the UCEP is depicted in Figure 2.2. At T_1, which is lower than the UCEP temperature, the solubility of the heavy component in SCF is small at any pressure (see Figure 2.2c). However, when the temperature approaches the UCEP temperature, the solubility increases dramatically if the pressure is raised to the UCEP pressure. At the UCEP, the liquid-gas critical locus meets the solid-liquid-gas curve. The fluid-solid equilibrium curve must be tangent to the horizontal solid-liquid-gas curve in the P-x diagram. Hence, it makes a sharp bend towards the right, i.e., $\left(\frac{\partial P}{\partial y}\right)_T = 0$ (see Figure 2.2d). A quite appreciable amount of solid will dissolve into the SCF. Similar effects were obtained with the variation of temperature. Namely, $\left(\frac{\partial T}{\partial y}\right)_P$ is small in the vicinity of the UCEP pressure and $\left(\frac{\partial T}{\partial y}\right)_P = 0$ at the UCEP. It is this sensitivity of the solubility with small changes in pressure or temperature in the vicinity of the UCEP that provides the opportunity for SFE processes. A thermodynamic analysis of this behavior will be demonstrated in Section 6.3.

Since the location of UCEP plays an important role in choosing the operating conditions for SFE processes, the study of phase behavior near the UCEP is of great significance both theoretically and practically. The UCEP can be experimentally determined or estimated.

McHugh and Paulaitis [67] measured the isothermal solubilities of naphthalene and biphenyl in supercritical carbon dioxide over a range of pressure from 8 to 50 MPa. They estimated the UCEP for naphthalene and biphenyl in supercritical carbon dioxide based on the characteristics of the P-y curves. In this method, valuable information about the solubility of solids in SCF is obtained. However,

the UCEP temperature and pressure as well as composition can only be estimated rather approximately.

McHugh and Yogan [66] determined the UCEP for several binary mixtures to be the pressure and temperature at which critical opalescence is observed along the solid-liquid-gas curve for a very slight change in either pressure or temperature. There is a disadvantage in using this method. Since there is only one degree of freedom in the solid-liquid-gas equilibrium for a binary mixture, the critical opalescence at the UCEP can hardly be observed along the solid-liquid-gas curve unless the composition of the loading components is very close to the composition of the UCEP, which is usually unknown.

The UCEP can be accurately determined from the intersection of the solid-liquid-gas coexistence curve with the liquid-gas critical loci of mixture. Using this intersection method, Van Gunst et al. [65] determined the pressure and temperature values of the UCEP for the system naphthalene-ethylene. Van Welie and Diepen [81,82] deduced also the composition of the UCEP for the same system.

3.3 Thermodynamic Modeling

Since the experimental determination of high-pressure phase equilibria is very difficult and costly to perform, it would be of great advantage to extend and complement the experimental data using thermodynamic models. Besides, thermodynamic models are also necessary tools for supercritical-fluid process design and economic evaluation.

However, there currently exists a lack of fundamentally based thermodynamic models for describing phase behavior of supercritical systems. The major reasons for this are the lack of knowledge about supercritical fluid behavior and the interactions of the molecules between the SCF and the heavy component, which significantly differ in size, shape, polarity and critical properties.

There are two approaches to modelling the phase equilibria of supercritical

systems: the compressed gas model approach and the expanded liquid model approach. In the former, the SCF is treated as a "compressed gas", and equations of state, as well as the principle of corresponding states and the lattice-gas models can then be used to calculate the fugacity coefficients of components in the supercritical fluid phase. In the latter, the SCF is treated as an "expanded liquid", and therefore, liquid theories, such as the quasi-lattice model or the regular solution model can be applied for calculating the activity coefficients of the components in the supercritical fluid phase.

While some improvements in the representation of solid solubilities in the SCF, i.e., in the description of the S-F equilibrium, have been achieved, the application of thermodynamic models to the representation of P-T-x along S-L-G coexistence curves and L=G critical loci requires further development. In the following section, the attention will be focussed on the representations of the S-L-G three-phase equilibria and the L=G critical loci.

3.3.1 Modeling of Solid-Liquid-Gas Equilibria

For any system that is at solid-liquid-gas three-phase equilibrium, the following conditions must be satisfied for all components in the mixture:

$$P^S = P^L = P^G \tag{3.1}$$

$$T^S = T^L = T^G \tag{3.2}$$

$$\mu_i^S = \mu_i^L = \mu_i^G \tag{3.3}$$

where μ_i is the chemical potential of the component i. For a binary mixture at a specified temperature and a specified pressure, the equilibrium conditions (3.3) may be written in terms of the fugacities of the solid-forming component 1 as

$$f_1^L = f_1^G \tag{3.4}$$

$$f_1^S = f_1^G \tag{3.5}$$

It is understood that the fugacities of the supercritical fluid, component 2, must follow the equation:

$$f_2^L = f_2^G \tag{3.6}$$

The solid phase is normally assumed to be a pure solid. Therefore, f_1^S is a function of temperature and pressure while the fugacities f_1^L, f_1^G, f_2^L and f_2^G are functions of temperature, pressure and composition. Using a compressed gas model, the fugacities of both gas and liquid phase can be written:

$$f_i^G = P y_i \Phi_i^G \tag{3.7}$$

$$f_i^L = P x_i \Phi_i^L \tag{3.8}$$

The fugacity coefficients of components in the fluid phases, Φ_i^G and Φ_i^L, can be calculated by applying a suitable equation of state in accord with the following rigorous thermodynamic equation:

$$\ln \frac{f_i}{x_i P} = \int_V^\infty \left[\frac{1}{RT} \left(\frac{\partial P}{\partial n_i} \right)_{T,V,n_j} - \frac{1}{V} \right] dV - \ln z \tag{3.9}$$

The fugacity of the solid component can be written as

$$f_1^S = f_1^{oS} x_1 \gamma_1^S \int_{P^o}^P \left(\frac{v_1^S}{RT} \right) dP \tag{3.10}$$

Since it is quite safe to assume that the solid is pure, i.e., the supercritical solvent does not dissolve in it, x_1=1 and γ_1^S=1, Eq.(3.10) can be simplified by further neglecting the pressure dependency of the molar volume of solid and taking the saturated pressure, P^{sat} as the reference pressure:

$$\begin{aligned} f_1^S &= f_1^{sat} exp \frac{v_1^S (P - P_1^{sat})}{RT} \\ &= P_1^{sat} \Phi_1^{sat} exp \frac{v_1^S (P - P_1^{sat})}{RT} \end{aligned} \tag{3.11}$$

Equation (3.11) simply states that the fugacity of solid component 1 at pressure P equals the fugacity of pure solid 1 at its vapor pressure multiplied by a Poynting correction factor.

As they are simple in forms and easy to extend to mixtures once a certain mixing rules are employed, the cubic equation of state of the van der Waals type, such as the Soave-Redlich-Kwong (SRK) [96] and the Peng-Robinson (PR) [97], are often used to calculate the fugacity coefficients These equations are based on the van der Waals theory and possess usually terms for attraction and repulsion [86].

The SRK and PR equations-of-state are

$$P = \frac{RT}{(v-b)} - \frac{a}{v(v+b)} \tag{3.12}$$

and

$$P = \frac{RT}{(v-b)} - \frac{a}{v(v+b)+b(v-b)} \tag{3.13}$$

respectively. Using the conventional mixing rules:

$$\begin{aligned} a &= \sum_i \sum_j x_i x_j a_{ij} \\ a_{ij} &= (a_i a_j)^{1/2}(1-k_{ij}) \\ b &= \sum_i x_i b_i \end{aligned} \tag{3.14}$$

Equation (3.9) can be rewritten as

$$\ln \Phi_i = -\ln(z-B) + \frac{b_i}{b}(z-1) - \frac{A}{B}\left(\frac{a_i'}{a} - \frac{b_i}{b}\right)\ln\left(1+\frac{B}{z}\right) \tag{3.15}$$

for the SRK equation, and

$$\ln \Phi_i = -\ln(z-B) + \frac{b_i}{b}(z-1) - \frac{A}{2.828B}\left(\frac{a_i'}{a} - \frac{b_i}{b}\right)\ln\left(\frac{z+2.414B}{z-0.414B}\right) \tag{3.16}$$

for the PR equation, where

$$A = aP/(RT)^2, \qquad B = bP/RT \tag{3.17}$$

$$a_i' = 2\sum_j x_j a_{ji} \tag{3.18}$$

Using their equation of state, Peng and Robinson [98] calculated the three-phase solid-liquid-gas equilibria of the binary mixture carbon dioxide-methane. A

good agreement between the calculated results and the experimental data was achieved for this not so highly asymmetric system as it was defined in the previous section.

Paulaitis et al. [99] calculated the P-T projection of the S-L-G equilibrium line for the biphenyl-CO_2 system utilizing the PR equation of state with one adjustable parameter. The agreement of the calculated results with the experimental data is only semi-quantitative (see Figure 3.2).

McHugh et al. [100] recently fitted the S-L-G line for the naphthalene-xenon system using the PR and the Sanchez-Lacombe (SL) equations. The latter equation is a lattice-gas equation which includes both a van der Waals attractive term and a lattice-gas repulsive term. Their work shows that the quantitative presentation of three-phase S-L-G line with either equation is not adequate (see Fig. 3.3).

Van der Haegen et al. [101] recently applied the mean-field lattice-gas model to the S-L-G three-phase equilibria in the system naphthalene-ethylene. While a fair agreement between the calculated and the experimental data in the lower pressure range was achieved, the model failed to represent the three-phase equilibria in the higher pressure range.

Another approach to correlating S-L-G three-phase equilibria is to calculate the fugacities of the components in the gas and liquid phases using different methods, i.e., using equation of state for calculating the gas-phase fugacities and using a solution model in terms of the activity coefficient for the liquid-phase fugacities. With this approach, while the fugacities of both components in the gas phase remain the same as equation (3.7), the fugacity of component 1 in the liquid phase can be expressed by

$$f_1^L = x_1 \gamma_1 f_1^{oL} exp\left[\frac{\bar{v}_1^L (P - P^o)}{RT}\right] \tag{3.19}$$

and the fugacity of component 1 in the solid phase by

$$f_1^S = f_1^{oS} exp\left[\frac{v_1^S (P - P^o)}{RT}\right] \tag{3.20}$$

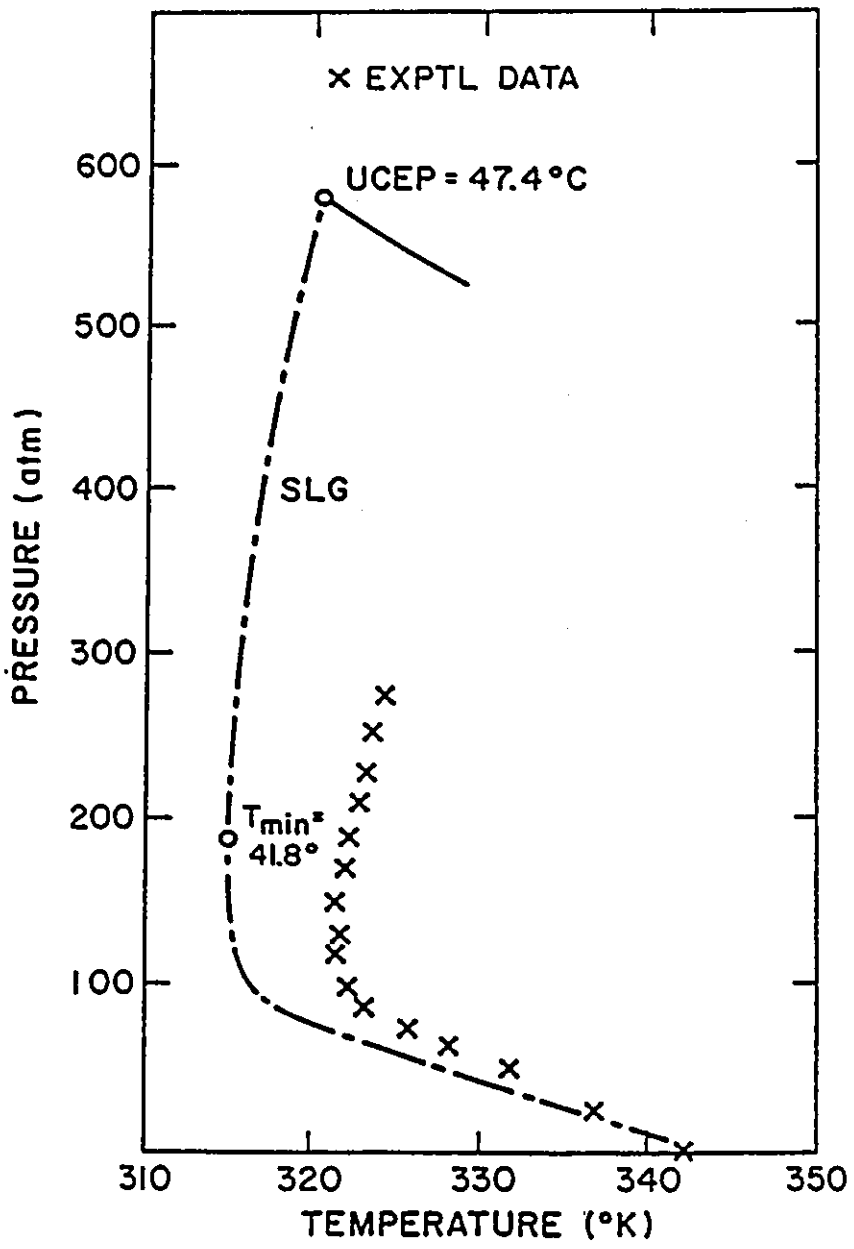

Figure 3.2: Comparison of the Calculated Results using PR Equation with the Experimental Results for the Biphenyl-CO_2 System. ×, Experimental Data; -.-.-, Calculated Results [99].

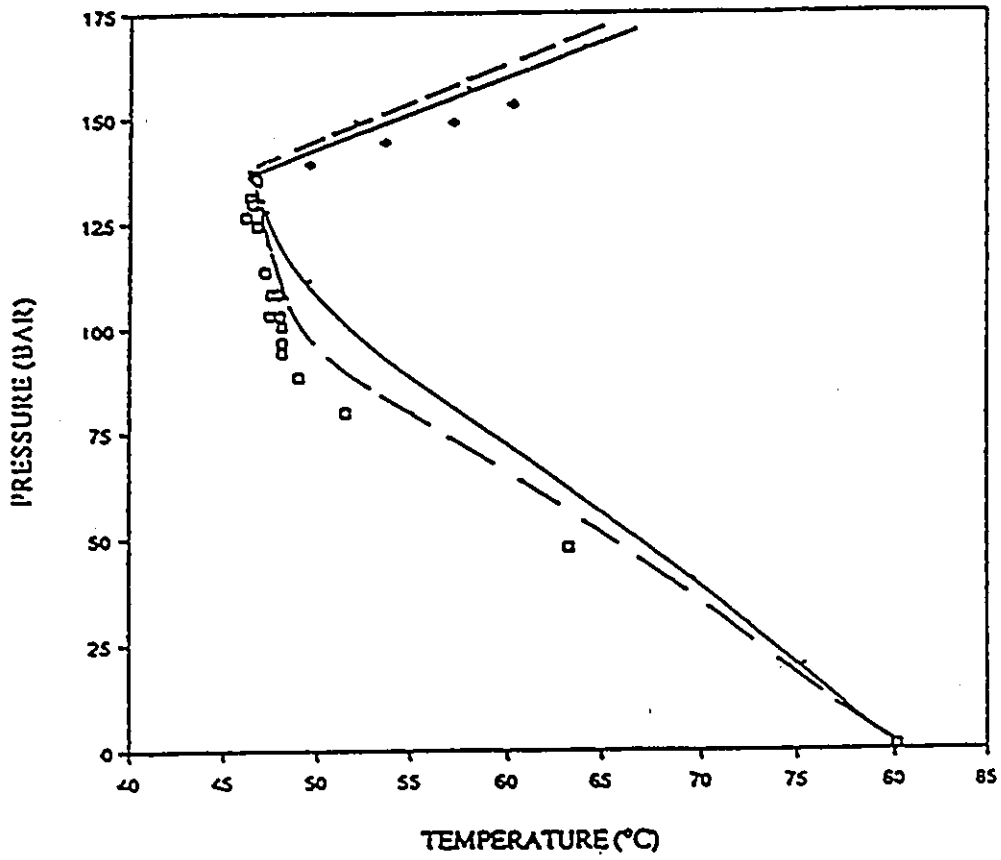

Figure 3.3: Representation of S-L-G line and L=G Critical Loci with the PR Equation and the SL Equation for the Naphthalene-Xenon System. o, Experimental S-L-G Line; •, Experimental L=G Critical Loci; —, Calculated by PR Equation; — — —, Calculated by SL Equation [100].

where P° is a reference pressure and $f_1^{\circ L}$ and $f_1^{\circ S}$ are hypothetical fugacities of pure liquid 1 and solid 1 at the system temperature and at the reference pressure P°. The partial molar volume of component 1 in the liquid, $\bar{v}_1^L$, and the molar volume of solid, v_1^S, are assumed to be independent of pressure.

If one chooses the reference pressure as the system pressure for $f_1^{\circ L}$, $f_1^{\circ S}$ and γ_1, and equates equations (3.19) and (3.20), the following expression is obtained,

$$x_1\gamma_1 = \frac{f_1^{\circ S}}{f_1^{\circ L}} \qquad (3.21)$$

The ratio of standard state fugacities at the system pressure can be expressed by the following thermodynamic equation [138]:

$$-\ln\frac{f_1^{\circ S}}{f_1^{\circ L}} = \left(\frac{\Delta H_f - T_m\,\Delta C_p}{R}\right)\left(\frac{1}{T}-\frac{1}{T_m}\right) + \frac{\Delta C_p}{R}\ln\frac{T_m}{T} + \int_0^p \left(\frac{\Delta v_1}{RT}\right) dp \quad (3.22)$$

where T_m is the normal melting point of solid 1, ΔH_f is the enthalpy of fusion, $\Delta C_p \equiv C_{p1}^L - C_{p1}^S$ and $\Delta v_1 \equiv v_1^L - v_1^S$. C_{p1}^L and C_{p1}^S are the heat capacities of component 1 in the liquid and the solid states, respectively.

Lemert and Johnston [103] recently used the above approach to correlate the S-L-G equilibria for the systems naphthalene-ethane, biphenyl-ethane, naphthalene-ethylene, biphenyl-ethylene, naphthalene-CO_2 and biphenyl-CO_2. While using one adjustable parameter in the equation of state for calculating the gas-phase fugacity, they used the regular solution model [102] to calculate the activity coefficient. The calculated temperatures on the S-L-G line agreed closely with the experimental data, though the correlation of the liquid compositions along the line seemed unsatisfactory in the higher pressure region.

3.3.2 Modeling of Liquid-Gas Critical Loci

The basis for calculation of critical loci of mixtures is the theory of thermodynamic stability. The critical point corresponds to an incipient separation into different phases, whether liquid-gas, liquid-liquid, or other phases. The mathematical ex-

pressions for the critical point were first stated by Gibbs in 1876 [104] and developed by Prigogine and Defay [105] later. The rigorous thermodynamic definition of the critical state of an n-component mixture involves two matrixes with their determinants equal to zero. These two determinants can be simply expressed by two Jacobians:

$$J_1 = \frac{\partial(\mu_1, \mu_2, ..., \mu_{n-1})}{\partial(x_1, x_2, ..., x_{n-1})} \tag{3.23}$$

$$J_2 = \frac{\partial(J_1, \mu_2, ..., \mu_{n-1})}{\partial(x_1, x_2, ..., x_{n-1})} \tag{3.24}$$

For a binary mixture, these determinants simplify to [105]:

$$\left(\frac{\partial \mu_1}{\partial x_2}\right)_{T,P} = 0 \tag{3.25}$$

$$\left(\frac{\partial^2 \mu_1}{\partial x_2^2}\right)_{T,P} = 0 \tag{3.26}$$

where the chemical potential μ_1 is related to the fugacity at constant temperature by

$$d\mu_1 = RTd\ln f_1 \tag{3.27}$$

Therefore, the critical conditions (3.25) and (3.26) can be written in terms of fugacity:

$$\left(\frac{\partial \ln f_1}{\partial x_2}\right)_{T,P} = 0 \tag{3.28}$$

$$\left(\frac{\partial^2 \ln f_1}{\partial x_2^2}\right)_{T,P} = 0 \tag{3.29}$$

By introducing the equations of state and their mixing rules into Eqs.(3.28) and (3.29), and solving them simultaneously, any two of the three variables, critical temperature, T_c, critical density, ρ_c and critical composition, x_c, could be obtained once the third one is fixed. The critical pressure, P_c can be calculated by introducing the values of the T_c, and ρ_c, into Eqs.(3.12) or (3.13).

Much work has been done to study the correlation and prediction of binary liquid-gas critical loci in the last two decades. A great deal of effort has been spent

in developing the calculation procedure using equations of state. Several workers, for example, used Redlich-Kwong [106], SRK [107,108], PR [109], Bennedict-Webb-Rubin [110] and Teja-Patel [111] to calculate the critical lines of binary fluid mixtures.

Mainwaring et al. [112,113] recently employed the Deiters' semi-empirical three-parameter equation [114-116] to predict the critical properties of binary mixtures and concluded that the equation has no advantage over the much simpler Guggenheim's "hard sphere + attractive term" equation of state [117].

Some efforts were made to improve the ability of equation of state to locate the critical point by adding a "nonclassical" contribution to the attractive term in the "classical" van der Waals-type equation of state. However, as pointed out by Chou and Prausnitz [118], "for mixtures, the nonclassical contribution has only a small effect on the calculated coexistence curve".

Very few studies reported in the literature deal with the calculations of liquid-gas critical loci for highly asymmetric binary systems which consist of one solid and one SCF. McHugh et al. [100] recently correlated the critical-mixture curve of naphthalene-xenon using the PR and the SL equations each with two mixture parameters. The agreement between calculated and experimental work was not very satisfactory (see Fig. 3.3).

3.4 Conclusions Reached After Review

From the above review, the following conclusions are obtained:

1) Due to the experimental difficulties, the investigation of phase behavior at supercritical fluid conditions for highly asymmetric mixtures, especially ternary mixtures are very limited in the literature. The meager experimental data resource for phase equilibria of supercritical systems needs to be extended significantly.

2) While the LCEP usually occurs very close to the critical point of the pure SCF for most binary mixtures, the experimental and theoretical study of phase

behavior near the UCEP, where the great solubility enhancement is achieved, is of great importance.

3) A simple technique for quick and reliable measurements of the solid-liquid-gas three-phase curve and the liquid-gas critical loci for highly asymmetrical binary mixture needs to be developed. Obtaining the compositions of the equilibrium phases along both curves is very important in attempting to establish accurate thermodynamic models.

4) The intersection method provides a more accurate and quicker determination of the UCEP than the estimation method based on the solubility measurements and should be adopted in this study.

5) Since the separation of a binary solid mixture utilizing a SCF is usually the most practical problem encountered in a SFE process, the experimental investigations of ternary mixtures consisting of one supercritical component and two solid components are especially needed. A different technique is required to determine the equilibrium liquid composition as well as the P-T projection of the solid 1-solid 2-liquid-gas four-phase curve.

6) Fundamentally based thermodynamic models for predicting the UCEP are needed. Simple cubic equations of state and/or solution models for representing S-L-G and S_1-S_2-L-G equilibria and L=G critical loci deserve further investigation.

7) The freezing point depression of a solid under the pressure of a supercritical fluid, and the phase behavior of a solid-supercritical fluid in the vicinity of both critical end points, the LCEP and the UCEP, need to be explored and discussed theoretically.

Chapter 4

EXPERIMENTAL

In this study, two sets of experiments were designed and the experimental apparatus was set up to determine the phase boundaries suitable for the SFE process and to establish the UCEP of binary mixtures. In the first set of experiments, the pressure-temperature-liquid compositions (P-T-x) of the solid-liquid-gas three-phase coexistence curves of highly asymmetric binary mixtures of supercritical CO_2 and an aromatic compound (naphthalene, biphenyl, m-terphenyl and phenanthrene) were determined. In the second set of experiments, the liquid-gas critical loci in the P-T-x space of the same systems were determined.

Moreover, an effort was also made to determine the solid 1-solid 2-liquid-gas four-phase coexistence curves for ternary mixtures of supercritical CO_2 and aromatic solid mixtures (naphthalene and biphenyl, naphthalene and phenanthrene).

4.1 Determination of Three-Phase Equilibria

4.1.1 First Freezing Point Method— Experimental Apparatus and Procedure I

For the measurement of the S-L-G three-phase curves, a new technique called the "first freezing point" method has been developed in this study. The P-T projection

of the S-L-G curve could be quickly determined by observing the initial appearance of the solid phase. In addition, the composition of the liquid phase along the S-L-G curve was determined.

In the early experimental determinations of the S-L-G three-phase coexistence curve, the apparatus consisted of five major sections: a pressurizing system, a temperature-controlled water bath, a high-pressure view cell equipped with a magnetic stirrer, a solid charging system and a liquid composition analysis system. A schematic diagram of the apparatus is shown in Figure 4.1.

A 20 cc. Jerguson high pressure gauge (max. 35.0 MPa) was used as the view cell. The system pressure was measured using a calibrated pressure transducer (Data Instrument, model SA, max. 69.0 MPa) located very close to the view cell. The accuracy of the pressure measurements was estimated to be $\pm$ 0.05 MPa. A two-layer stainless steel water bath, insulated with foam, was used to maintain the temperature of the view cell. Polypropylene balls (Enromatics, dia. 20 mm) was used to keep water from evaporating and to cut down the heat loss. The bath temperature was maintained to within $\pm$ 0.01 K of the set point using a precision temperature controller (model 250, Bayley Instrument Co.). The bath was equipped with a high speed stirrer and two heaters. The bath temperature was measured using a calibrated quartz thermometer (Hewlett-Packard, model 2801 A). The sensor of the quartz thermometer was located at the outside wall of the view cell. The accuracy of the temperature measurement was estimated to be $\pm$ 0.05 K.

In the pressurizing system, liquid carbon dioxide from a supply cylinder was pressurized by an air-operated automatic boost pump (max. 69.0 MPa, Futurecraft Corp). A hand loader type pressure regulator was adjusted to a desired outlet pressure and the boost pump operated automatically until reaching the adjusted setting.

In the solid charging system, the solid was melted in a container by a heating tape and then was displaced into the view cell by a hand pump (Ruska Instrument

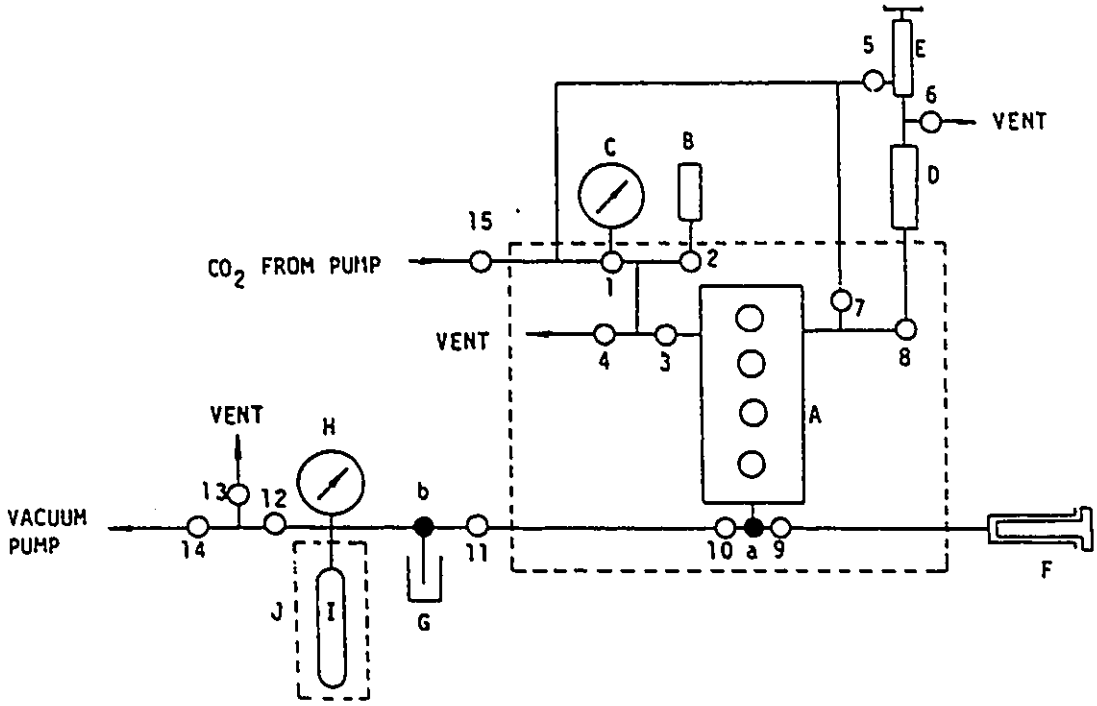

Figure 4.1: Schematic Diagram of Apparatus for Measurement of Three-Phase Coexistence Curve. **A** - High pressure view cell; **B** - Pressure transducer; **C** - Pressure gauge; **D** - Solid container; **E** - Hand pump; **F** - Syringe; **G** - Solid sampler; **H** - Pressure gauge; **I** - Sample cylinder; **J** - Water bath; **a, b** - Three-way valves; 1-15 - Valves.

Corp).

Before the desired amount of solid was charged into the view cell A from the solid container D, the cell and the container were purged with CO_2 (or other SCF solvent) three or four times. After the cell was charged, the pressure in the cell was then brought to the desired level. All experiments started with such a solid-gas condition. The temperature of the water bath, hence the temperature of the cell, was increased slowly until the solid phase completely disappeared. The liquid and the gas phases were agitated by a magnetic stirrer for about one hour. Thereafter, the temperature was decreased slowly so that the first appearance of the solid phase could be observed precisely with a cathetometer. The temperature and pressure of the S-L-G point obtained from the "first freezing point" were recorded. The solid was then melted and frozen again to obtain a second measurement of the "first freezing point". In general the difference between the two temperature measurements was within 0.1 K.

4.1.2 Analysis of Liquid Phase Composition

The composition of the liquid phase at the three-phase condition was sampled immediately after the second measurement of the freezing point through the three-way valve a and using the space between valves 9 and 10 as the sampling loop (see Fig. 4.1). The tubing leading to this sampling tube as well as the sample cylinder I was evacuated prior to the sampling. The small amount of the saturated liquid phase immediately crystallized in the sampling loop. The gas CO_2 was then expanded into the sample cylinder I by opening valve 10 and then valve 11. The volume of the sample cylinder as well as the volume of the tubing leading to it from the sampling tube were calibrated before the measurements. Hence the amount of CO_2 could be determined from the known volume of the sample system calibrated previously and the pressure measured by a pressure gauge. The amount of solid remaining in the sampling loop was collected, using acetone injected from the syringe F into the

solid sampler G through the three-way valve b. After drying, the solid was weighed using a microbalance. The accuracy of the weighing was ± 0.0001 g.

The P-T-x measurements of the three-phase coexistence curve started from the low pressure end. After each sampling, the reduced liquid volume in the cell was replaced by the increased amount of carbon dioxide dissolved in the liquid under a higher pressure. The liquid level in the cell could then be maintained approximately constant during the whole run.

4.1.3 Experimental Results I

The experimental P-T-x values of the three-phase curve for the binary mixtures, naphthalene-carbon dioxide and biphenyl-carbon dioxide are listed in Tables 4.1 and 4.2. The P-T projections of the S-L-G curves for the two systems are shown in Figures 4.2 and 4.3. In these figures, the experimental values of McHugh et al. [84,66] and the values obtained from the P-T curves reported by Prins [11] are also included for comparison.

The values obtained in this work using the "first freezing point" method are more consistent than those values determined by the "first melting point" method reported by McHugh et al. The merits of the first freezing point method will be discussed in Section 6.1.

When operating at low pressure, the liquid phase solidified soon after the first appearance of a few observable crystals in the view cell. At high pressure, but before the "first freezing point" was reached, very tiny bubbles in the liquid phase were observed. At first, these tiny bubbles looked like fine powdery particles to the observer. However, these tiny bubbles would disappear immediately by a very slight increase of pressure. The "first freezing point " was only recorded after the appearance of crystallized solid was observed.

With the additional information on the isothermal solubility of the solid in the SCF, the experimental values reported in Table 4.1 and 4.2 can be used to

Table 4.1: Experimental Pressure-Temperature-Liquid Composition Values of the Three-Phase (S-L-G) Coexistence Curve for the System Naphthalene (1)-Carbon Dioxide(2).

P/MPa	T/K	x_1	P/MPa	T/K	x_1
2.19	348.27	-	12.46	332.40	-
3.07	346.44	0.870	13.64	331.95	0.451
4.74	343.87	0.815	14.26	331.98	-
6.17	341.27	0.745	16.00	332.05	0.425
7.90	338.12	-	17.08	332.30	0.403
8.40	337.71	0.668	17.59	332.34	-
9.42	335.83	0.630	19.56	332.46	0.343
10.19	334.46	-	21.02	332.65	-
10.68	333.97	0.568	21.92	332.83	-
11.54	332.99	-	22.89	333.14	0.319
12.16	332.66	0.499	24.25	333.18	0.290

Table 4.2: Experimental Pressure-Temperature-Liquid Composition Values of the Three-Phase (S-L-G) Coexistence Curve for the System Fiphenyl(1)-Çarbon Dioxide(2).

P/MPa	T/K	x_1	P/MPa	T/K	x_1
2.25	338.11	-	10.48	321.85	0.517
2.88	335.70	0.875	11.02	321.61	-
3.48	334.19	0.842	12.10	321.67	0.488
4.52	332.02	0.805	12.42	321.57	0.495
5.69	329.61	0.744	14.34	321.78	0.458
6.72	327.56	-	15.89	321.87	0.453
7.26	326.48	0.660	19.38	322.46	0.431
8.18	324.53	0.608	22.48	322.98	0.410
8.79	323.79	-	25.59	323.73	0.383
9.34	322.84	0.558	29.74	324.81	0.349
10.42	321.97	0.514	33.97	325.85	0.318

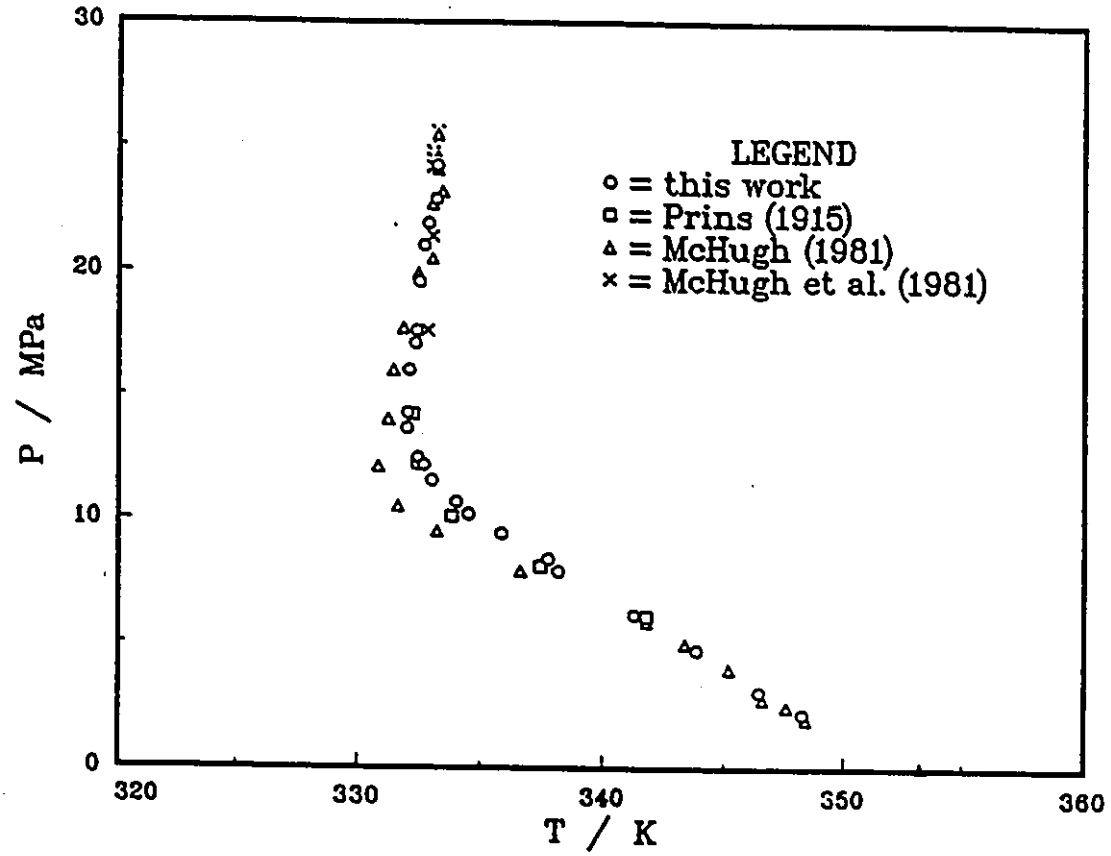

Figure 4.2: Pressure-Temperature Projection of the S-L-G Curve for the Naphthalene(1)-Carbon Dioxide(2) System.

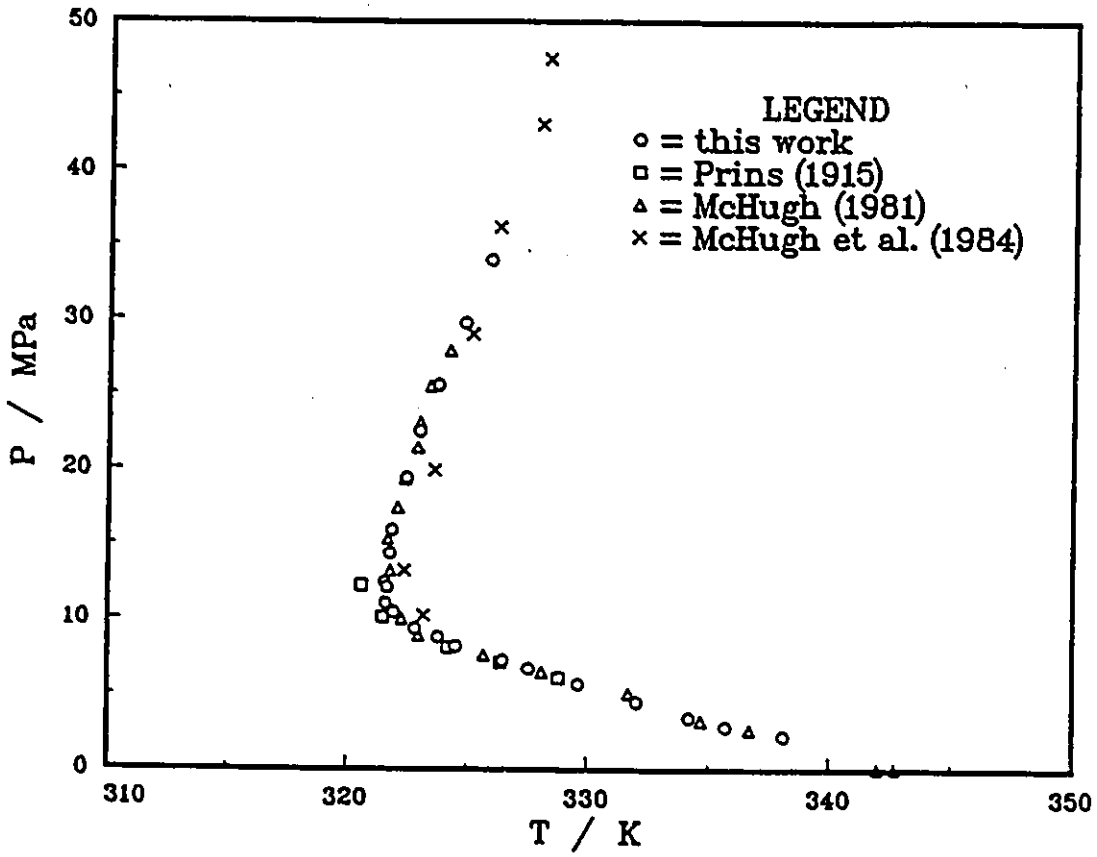

Figure 4.3: Pressure-Temperature Projection of the S-L-G Curve for the Biphenyl(1)-Carbon Dioxide(2) System.

determine the location of the "liquid island". The solubility values of naphthalene in carbon dioxide at 332.15 K [120] are plotted in Figure 4.4. At this temperature, the S-L-G curve is intersected at two pressures, 12.7 and 17.0 MPa (Figure 4.2). The solubility curve intersects the two pressures of the S-L-G curve and thus yields the mole fraction y_1 of naphthalene in carbon dioxide on the S-L-G curve. Between these two pressures, A solid-liquid region, a liquid-vapor region or a single liquid phase exists, depending on the concentration. From a T-x plot (shown in Figure 4.5) using the data of Table 4.1, the liquid concentrations x_1 of naphthalene at these two pressures are estimated to be 0.435 and 0.380 mole fractions. These two concentrations are the limiting values of the "liquid island" as shown in figure 4.4.

An effort was made to correlate the x_1 values in terms of the liquid activity coefficient γ. Following the approach of Prausnitz [60] and neglecting the difference between the heat capacities of the solid and liquid of component 1 (naphthalene or biphenyl) from the triple point temperature to the operating temperature. γ_1 x_1 can be approximately expressed by

$$\ln \gamma_1 x_1 = -(\Delta H_f/R)(1/T - 1/T_m) \tag{4.1}$$

where ΔH_f is the heat of fusion, and T_m is the melting temperature. The van Laar Equations,

$$\ln \gamma_1 = A_{12}/(1 + x_1 A_{12}/x_2 A_{21})^2 \tag{4.2}$$

$$\ln \gamma_2 = A_{21}/(1 + x_2 A_{21}/x_1 A_{12})^2 \tag{4.3}$$

were used for correlating the γ_1 values. The best fitted values were A_{12}= 3.132 and A_{21}= 1.400 for the system naphthalene-carbon dioxide, and A_{12}= 7.067 and A_{21}= 1.673 for the system biphenyl-carbon dioxide. These values were obtained by minimizing the sum of the squares of the differences between experimental and calculated γ_1 values. These van Laar constants can be used for estimating the limiting x_1 values of the liquid island shown in Figure 4.4. A comparison of the

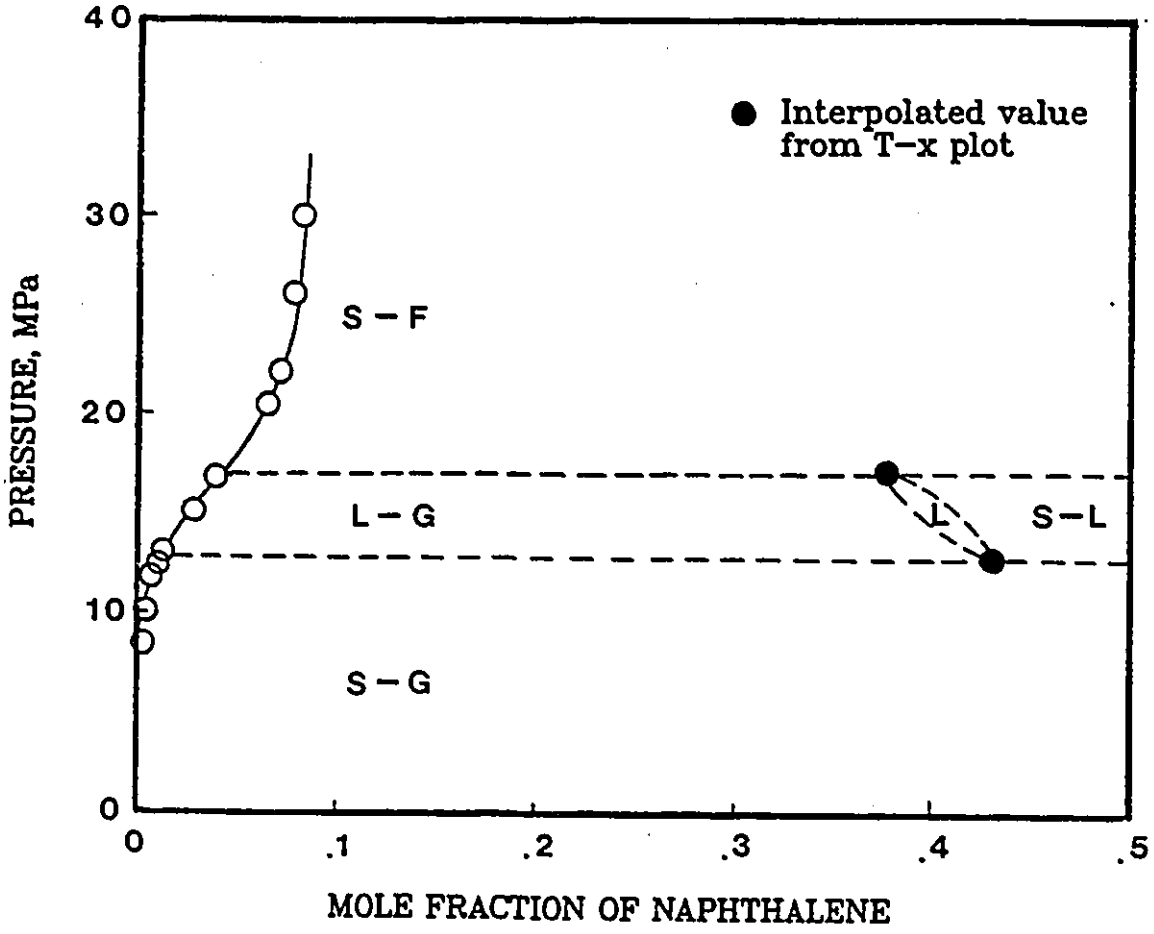

Figure 4.4: Location of "Liquid Island" Determined from the P-T-x Values of S-L-G Curve and Solubility Values of 332.15 K Isotherm for the Naphthalene(1)-Carbon Dioxide(2) System.

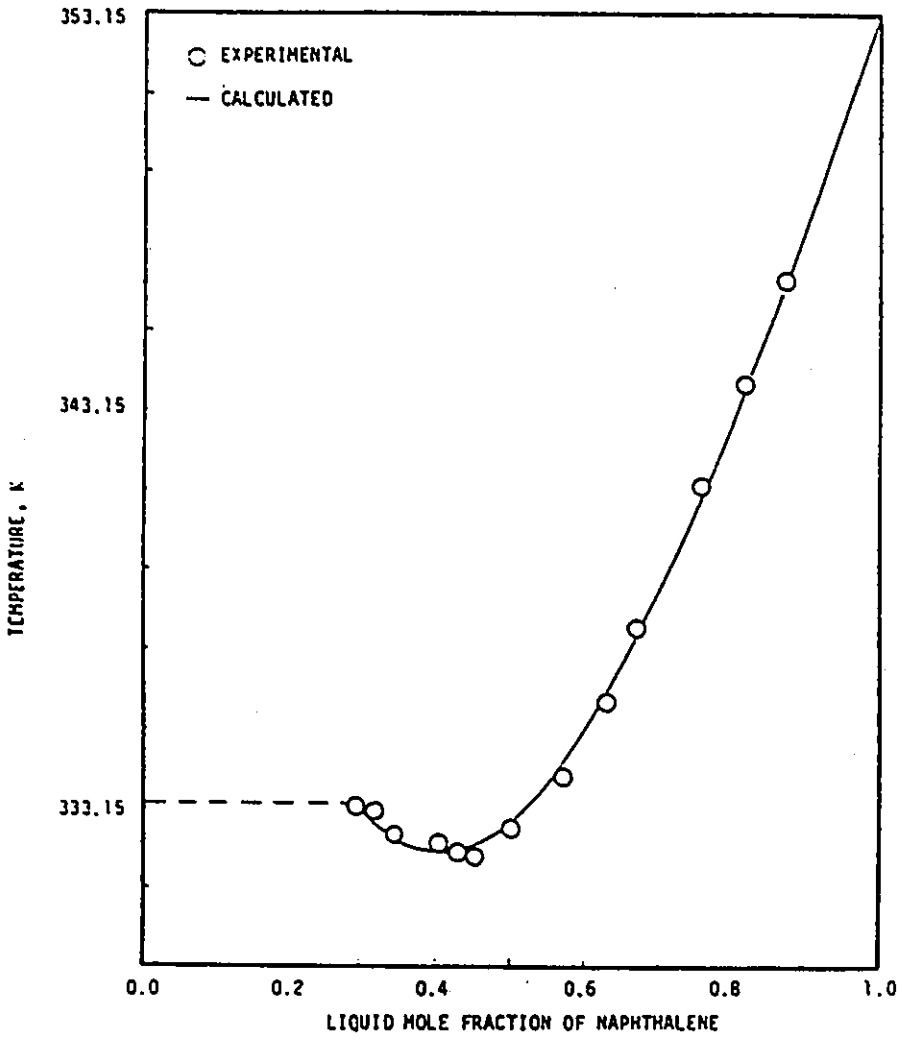

Figure 4.5: T-x Values along the S-L-G Curve for the Naphthalene(1)-Carbon Dioxide(2) System. Solid Line is Calculated in Terms of Liquid Activity Coefficient.

calculated and experimental x_1 values for the system naphthalene-carbon dioxide is shown in Figure 4.5.

4.1.4 First Freezing Point Method— Experimental Apparatus and Procedure II

During the course of this study, further modifications were made to improve the performance of the first freezing point technique in the extension of the experimental determination of the S-L-G three-phase curve. A high-pressure Ruska Dual-Window PVT cell was used to replace the pressure-gauge view cell. Instead of the water bath and the magnetic stirrer, a temperature-controlled air bath and a magnetic pump were employed. The reasons for the improvement are as follows:

1) The maximum working pressure of the pressure-gauge view cell was 35 MPa, which was not high enough for our further investigation;

2) The pressure gauge used as a view cell became rusty in the water bath, and the dirty water made the observation of the first appearance of the solid difficult;

3) The agitation of the mixture by a magnetic stirrer moving vertically required a long period of time. Often the stirrer became jammed inside the cell as a result of inadequate space;

4) There existed a small dead volume at the bottom of the cell.

A new experimental set up was made to reduce both the dead space of the equilibrium cell encountered previously and the time required for the mixture in the cell to reach equilibrium. This was achieved by means of a magnetic pump which recirculated the mixture in the cell when it was in the fluid state. A temperature-controlled air bath, instead of a water bath, was used to improve the visibility of the contents in the equilibrium cell.

A schematic diagram of the apparatus is shown in Figure 4.6. A high-pressure PVT cell (Ruska, Model 2329-801-60900 with a cell volume of 40 cm^3; max. 69.0 MPa) was used as the equilibrium cell A. This cell has two windows mounted

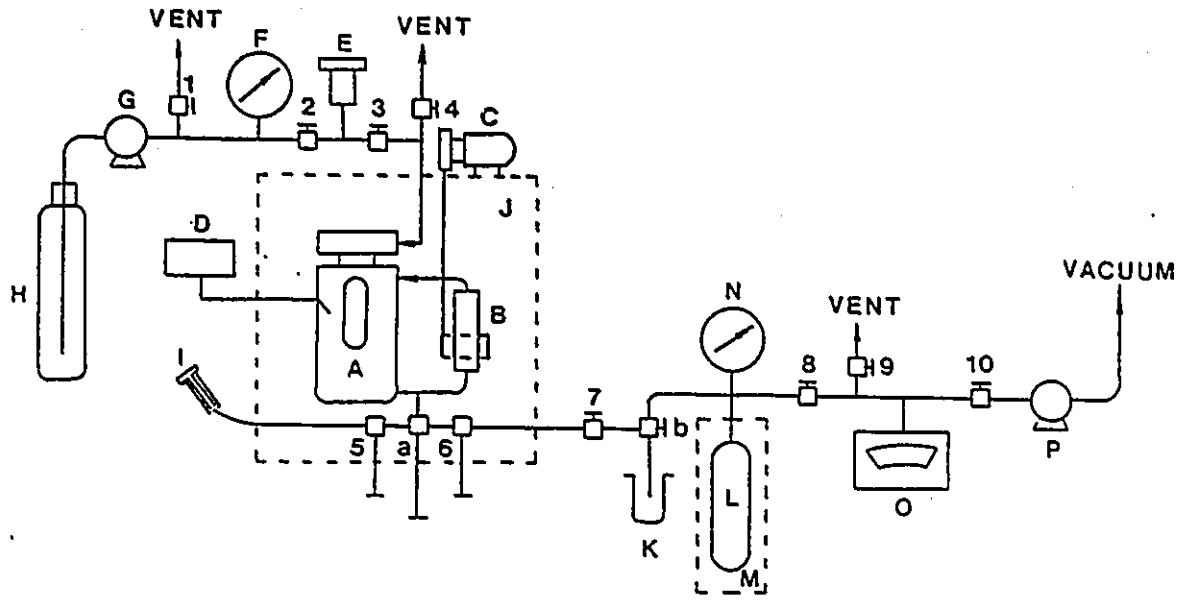

Figure 4.6: Schematic Diagram of Apparatus. A - Dual window equilibrium cell; B - Magnetic pump; C - Variable-speed motor; D - Temperature indicator; E - Pressure transducer; F - Pressure gauge; G - Pressure intensifier; H - Liquid carbon dioxide cylinder; I - Syringe; J - Air bath; K - Solid sampler; L - Sample cylinder; M - Water bath; N - Pressure gauge; O - Vacuum gauge; P - Vacuum pump; a, b - Three way valves; 1 to 10- Valves.

opposite to each other to allow see-through visibility. Exposed window surface is approximately 2.5 inch long and 0.25 inch wide. By placing a light behind one window, it was easy to discern liquid-gas interface level. The cell was kept in an air bath J (Ruska, Model 2320-801-16800 equipped with a LFE temperature controller). The temperature of the bath could be maintained to within ± 0.05 K of the set point. A pressure transducer E (Data Instrument, Model AB/HP; max 69.0 MPa) was used to measure the pressure. A magnetic pump B (Ruska, Model 2330-802, max. 82.8 MPa) was installed in the air bath for recirculating the mixture in A. An air operated automatic pressure intensifier G (Futurecraft, max. 69.0 MPa) was used in the pressurizing section of the apparatus to pressurize liquid carbon dioxide from a supply cylinder.

The operation procedure was only slightly different from that described in Section 4.1.1. (also see [68]). Briefly, the equilibrium cell was purged with CO_2 after the solid was loaded. The temperature of the air bath was raised until the solid phase inside the cell disappeared. Liquid CO_2 was compressed by the pressure intensifier and introduced to and vaporized in the cell until the pressure in the cell was brought to the desired level. The mixture in the cell was then recirculated by means of the magnetic pump. The temperature of the air bath was then slowly reduced at a rate of about 0.02 K per minute. The temperature of the cell was reduced at approximately the same rate as monitored by means of thermocouples installed inside the wall of the cell at two locations. The first appearance of the solid phase could be observed precisely through the window of the cell by means of a mirror system. The temperature and pressure of the first appearance were recorded and a liquid sample was immediately taken for analysis. It should be mentioned that after the first appearance of the solid in the cell, the liquid phase soon solidified completely. For the preparation of the next measurement, the temperature of the cell was first increased to melt the solid, the system pressure was subsequently raised to a desired value, then with the mixture in the cell being recirculated by

the magnetic pump, the temperature of the cell was again slowly reduced to reach the first freezing temperature for the new point on the P-T projection. For all systems, measurements started from the low pressure end. The accuracies of the temperature and pressure measurements were estimated to be ±0.1 K and ±0.05 MPa, respectively.

The CO_2 content in the liquid sample was determined by means of the same procedure reported earlier. Briefly, the space between valves 5 and 6 was used as the sampling tube. Upon sampling, the dissolved solid immediately crystallized in the tube. CO_2 was then expanded into the cylinder L by opening valves 6 and then 7. The volume of the cylinder and that of the tubing leading to it from the sampling tube were calibrated. Hence the amount of CO_2 could be determined.

The amount of solid remained in the sampling tube was collected, using acetone injected from the syringe I. A microbalance was used to determine the amount of the solid after the evaporation of acetone. The accuracy of the weighing was ±0.0001 g.

To verify the new experimental set up, the S-L-G three-phase equilibria were determined for the systems naphthalene-ethylene and biphenyl-ethylene [137]. The results agreed well with those in the literature [75,65,81,66].

4.1.5 Experimental Results II

The experimental P-T-x values for another two binary mixtures, m-terphenyl-carbon dioxide and phenanthrene-carbon dioxide are reported in Tables 4.3 and 4.4. The P-T projection of the S-L-G curves for the two systems are shown in Figures 4.7 and 4.8. For the binary mixture phenanthrene-carbon dioxide, the experimental results reported recently by White and Lira [121] are also presented in Figure 4.8 for comparison. The pressure range in their determination of the S-L-G three-phase equilibria was below 9 MPa and the equilibrium compositions along the three-phase curve were not determined. Discussion will be given in Section 6.1.

Table 4.3: Experimental Pressure-Temperature-Liquid Composition Values of the Three-Phase (S-L-G) Coexistence Curve for the System m-Terphenyl (1)-Carbon Dioxide(2).

P/MPa	T/K	x_1	P/MPa	T/K	x_1
5.25	350.0	0.771	17.30	341.4	0.536
6.97	348.6	-	18.91	341.8	0.528
8.70	345.8	0.688	20.08	342.1	0.517
10.56	343.9	0.676	21.74	342.4	0.504
12.02	341.9	0.621	22.31	342.7	-
13.49	341.5	0.602	23.24	343.1	0.516
13.96	341.4	0.582	24.77	343.2	0.502
15.48	341.4	0.544	27.32	343.2	0.513
16.72	341.3	-	28.90	343.3	0.506
17.03	341.4	-			

Table 4.4: Experimental Pressure-Temperature-Liquid Composition Values of the Three-Phase (S-L-G) Coexistence Curve for the System Phenanthrene (1)-Carbon Dioxide(2).

P/MPa	T/K	x_1	P/MPa	T/K	x_1
3.81	364.6	0.861	14.10	354.0	0.680
5.30	362.4	-	14.67	353.7	0.674
5.47	362.0	0.825	15.87	353.4	0.654
6.39	360.5	0.812	17.18	353.3	0.651
7.23	359.4	0.795	17.70	353.5	0.646
8.50	357.8	0.750	18.49	353.6	0.629
9.83	356.4	0.736	19.76	354.3	0.628
11.12	355.4	0.722	20.84	354.3	0.621
11.23	355.4	-	21.72	354.3	-
12.19	355.0	0.710	21.83	354.2	0.604
12.65	354.7	0.708	23.19	354.3	0.614
13.50	354.4	0.697	24.14	354.4	0.611

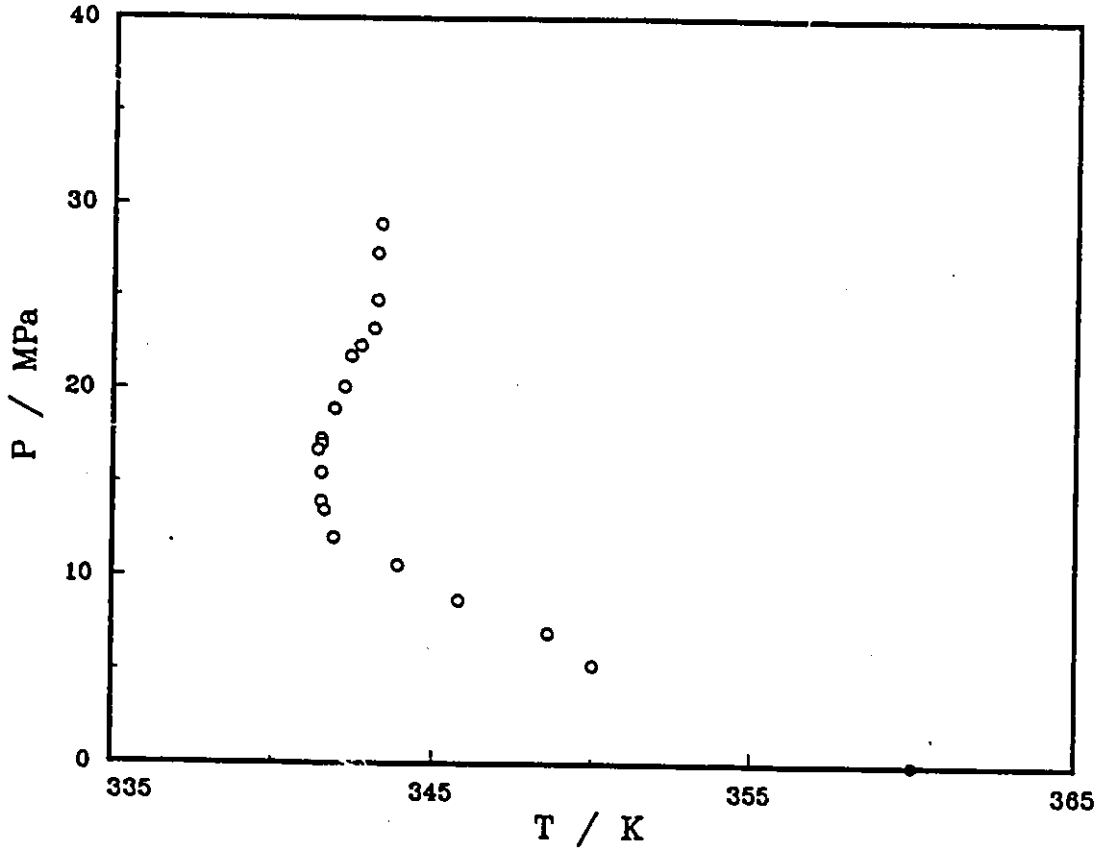

Figure 4.7: Pressure-Temperature Projection of the S-L-G Three-Phase Curve for the m-Terphenyl(1)-Carbon Dioxide(2) System. •, Normal Freezing Point of m-Terphenyl.

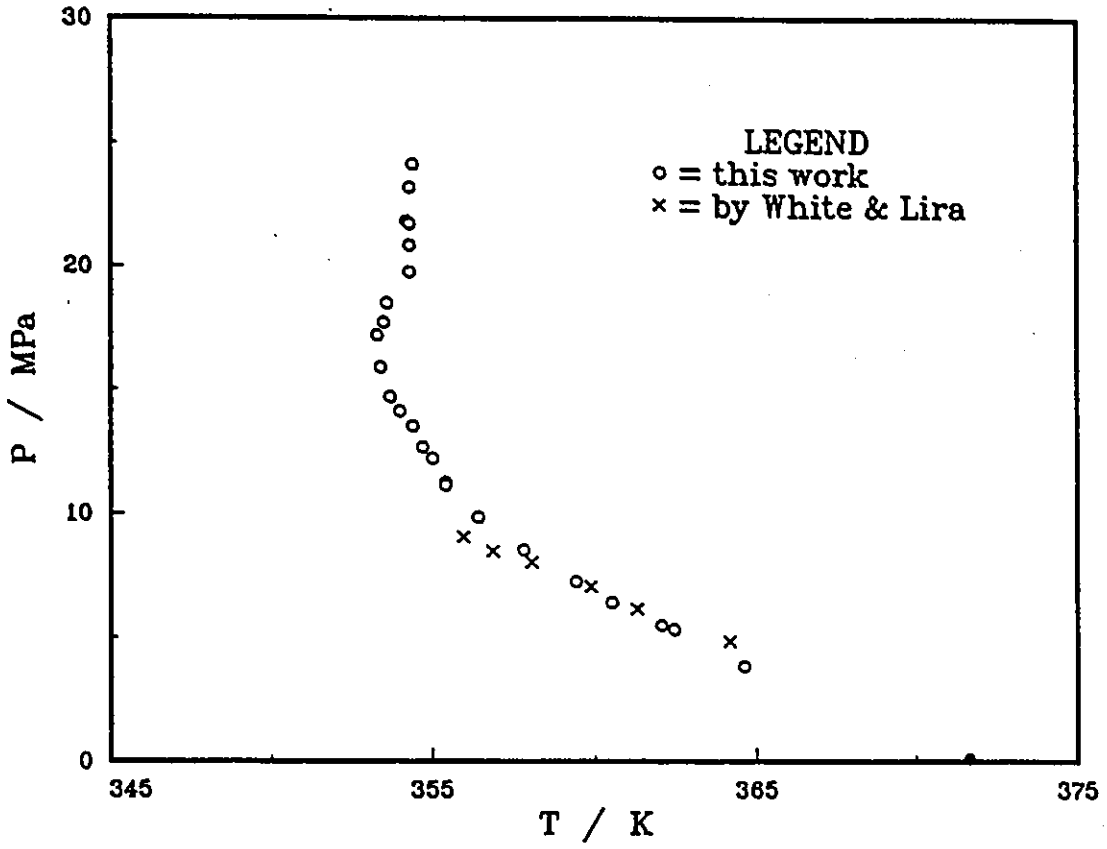

Figure 4.8: Pressure-Temperature Projection of the S-L-G Three-Phase Curve for the Phenanthrene(1)-Carbon Dioxide(2) System. •, Normal Freezing Point of Phenanthrene.

We are not aware of any experimental data for the binary mixture of m-terphenyl-carbon dioxide.

The additional measurements of the S-L-G three-phase equilibria for the binary mixture biphenyl-carbon dioxide were made under higher pressures than those in the earlier part of this study where the working-pressure limit of the equilibrium cell was lower. The results are presented in Table 4.5.

A temperature minimum was observed for each of the four binary systems, as shown in the T-x diagram (see Figure 4.9) as well as the P-T projections of the three-phase coexistence curves (see Figure 4.10).

The liquid compositions of the S-L-G curves obtained in this study provide the important information for studying the freezing point depression of a solid under the pressure of a supercritical fluid, and for establishing fundamentally based thermodynamic models describing the solid-supercritical fluid phase equilibria.

The pressure effect on the solubilities of supercritical carbon dioxide in the equilibrium liquid phase can be illustrated by the P-x diagram of the S-L-G curves (see Figure 4.11). At low pressure (below 10 MPa), the solubilities of CO_2 in liquid phase increase rapidly, as depicted by the low values of the slopes of the solubility curves in Figure 4.11. At high pressure, the solubility curves tend to become vertical, indicating a slowdown in the rate of absorption of CO_2 in the liquid phase with further increase of the pressure. In the cases of m-terphenyl- CO_2 and phenanthrene-CO_2 mixtures, where the solubility of CO_2 in the liquid phase is low, the solubilities of CO_2 quickly reach limiting values.

4.2 Determination of Liquid-Gas Critical Loci

4.2.1 Experimental Apparatus and Procedure

The apparatus used in the first freezing point method, as shown in Figure 4.6, was employed in this study to determine the liquid-gas critical loci for the naphthalene-

Table 4.5: Additional Measurement of Pressure-Temperature- Liquid Composition Values of the Three-Phase (S-L-G) Coexistence Curve for the System Biphenyl(1)-Carbon Dioxide(2).

P/MPa	T/K	x_1
40.58	327.5	0.276
45.63	328.3	0.239

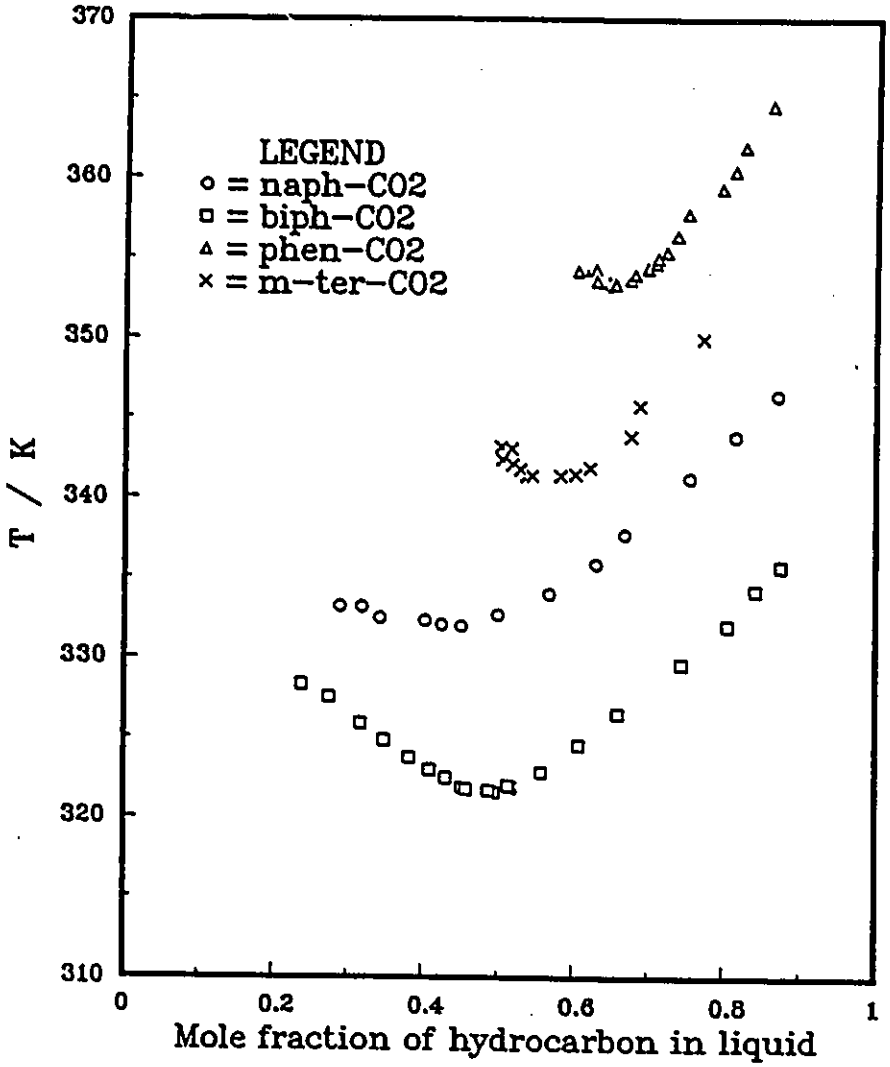

Figure 4.9: Experimental T-x Values of the Three-Phase (S-L-G) Coexistence Curve for Four Binary Mixtures.

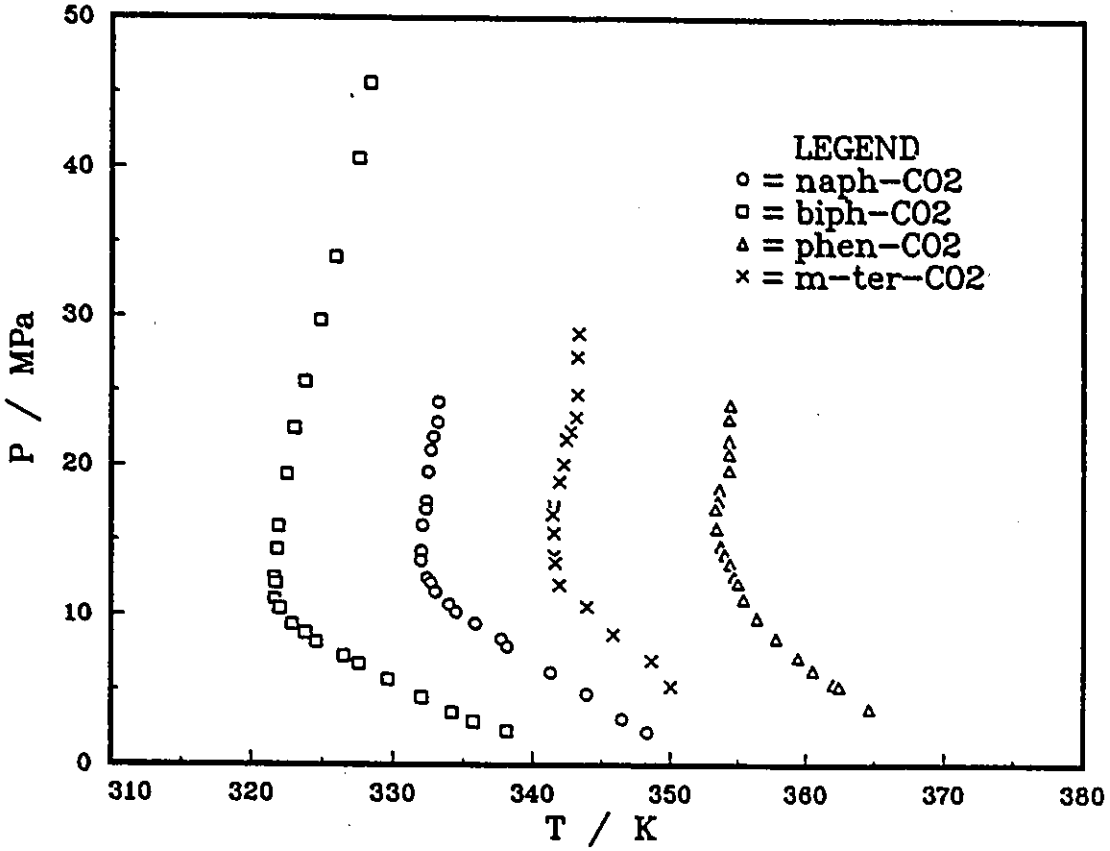

Figure 4.10: Pressure-Temperature Projections of the S-L-G Curves for Four Binary Mixtures.

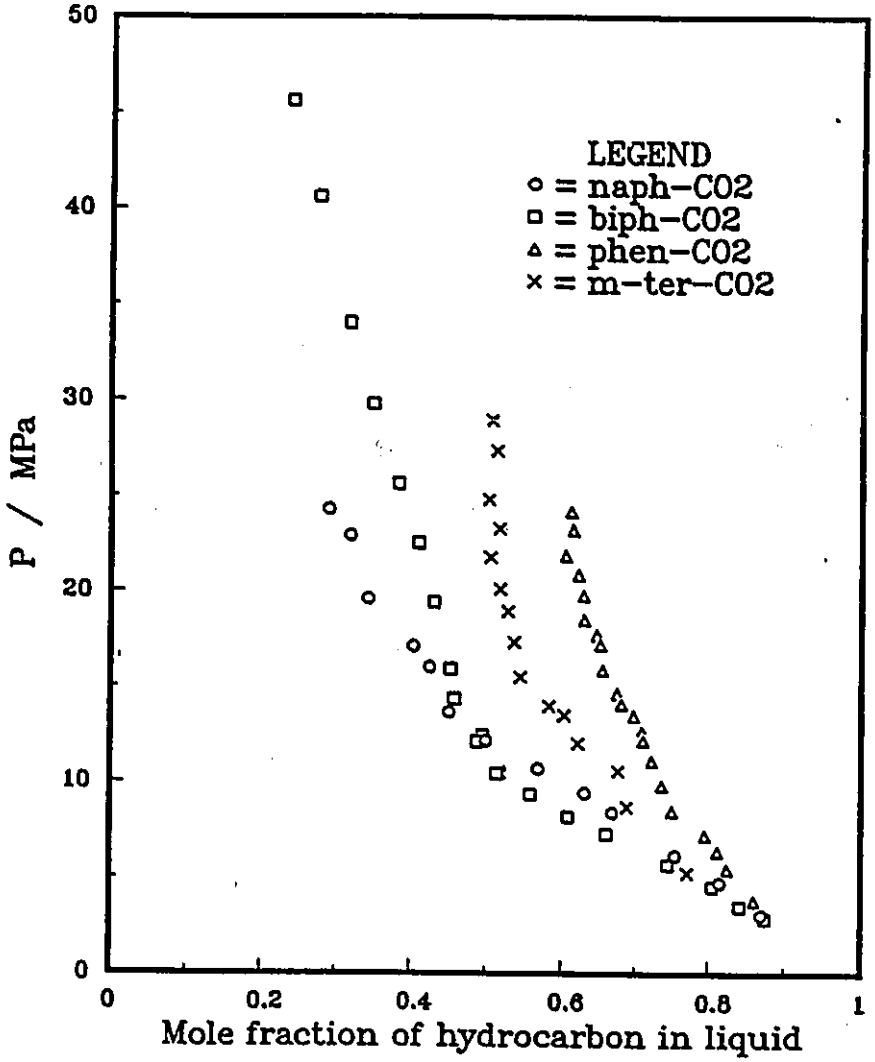

Figure 4.11: Experimental P-x Values of the Three-Phase (S-L-G) Coexistence Curve for Four Binary Mixtures.

carbon dioxide and biphenyl-carbon dioxide systems. In the determination, the bubble point pressure along the several isotherms as well as the solubility of carbon dioxide in liquid naphthalene and biphenyl were also measured. The description of the procedure for the bubble-point as well as the liquid-gas critical loci measurements is as follows:

1) The equilibrium cell **A** as well as the magnetic pump **B** were purged with carbon dioxide before the naphthalene or biphenyl was charged. This was done to avoid air being trapped in cell **A** and magnetic pump **B** by the loading solid.

2) The solid was charged through the top of the cell by opening the head cap. The cell **A** was purged again with carbon dioxide three or four times.

3) The temperature of the air bath was raised until the solid in the cell was melted completely. The temperature of the bath could be adjusted to within ±0.05 K of the desired temperature. The temperature of the cell and that of the magnetic pump were monitored by three thermocouples.

4) Liquid carbon dioxide was compressed by the pressure intensifier **G**, introduced to and vaporized in the cell until the pressure in the cell was brought to an appropriate level. The accuracy of the pressure measurement was estimated to be ±0.05 MPa.

5) The liquid mixture in the cell was recirculated by means of the magnetic pump **B**. The equilibrium condition was reached when there was no more change of the system pressure at the desired temperature.

6) Sampling of the liquid phase was made 30 minutes after the equilibrium pressure was reached. The accuracy of the liquid composition determination was estimated to be ±0.005 mole fraction.

For each isotherm, the experiment was carried out until the liquid-gas critical point was reached.

4.2.2 Observation of Critical Opalescence

The critical opalescence was observed clearly for two binary mixtures of supercritical carbon dioxide with aromatic compounds, naphthalene and biphenyl. At the critical point, the meniscus between the liquid and gas phases disappeared, the mixture in the cell turned scarlet and the critical opalescence reached its maximum intensity. When the pressure of the system was further increased above the critical point, the scarlet color disappeared and only one phase existed in the cell.

Figures 4.12-4.14 are the photographs of the content in the equilibrium cell, taken before, during and after the critical-mixture point was reached.

When the critical point was approached, the pressure of the system was increased very slowly at the rate of about 0.03 MPa per minute by opening slightly the shutoff valve 2.

After the critical opalescence was observed, the system pressure was decreased slowly by opening valve 4 until the liquid and gas phase reappeared in the cell. The observations of the critical opalescence were repeated several times. The accuracy of the pressure measurement of the critical-mixture point was estimated to be ± 0.05 MPa.

In this study, the critical loci of two binary mixtures were determined as part of a more general study of the solubility of supercritical carbon dioxide in liquid naphthalene and biphenyl, as the latter information is of importance in the processing of petroleum products, coal liquification and enhanced oil recovery. One can, however, make a quick and direct determination of the liquid-gas critical loci following the procedure outlined above.

4.2.3 Experimental Results and Discussion

To check the experimental technique used in this study, the solubility of supercritical carbon dioxide in liquid naphthalene at 373.2 K previously measured by Barrick et

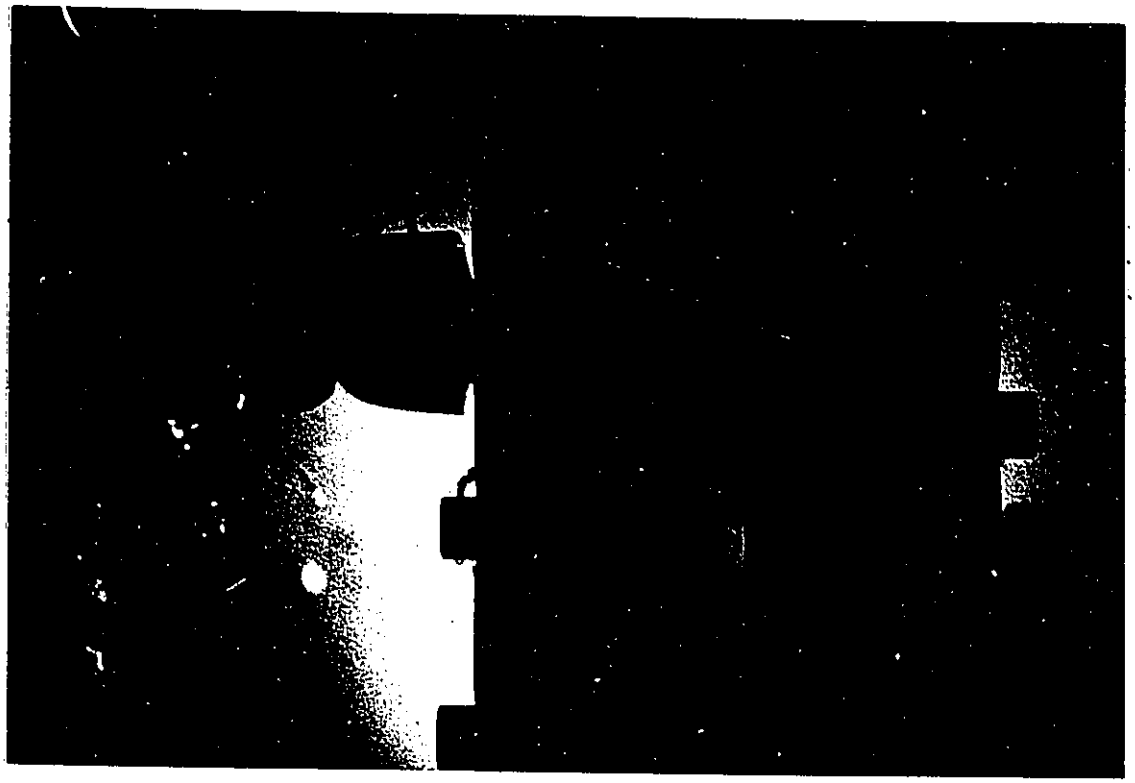

Figure 4.12: A Photograph of the Content in the Equilibrium Cell Before the Critical-mixture Point Was Reached. Liquid and Gas Phases Existed in the Cell.

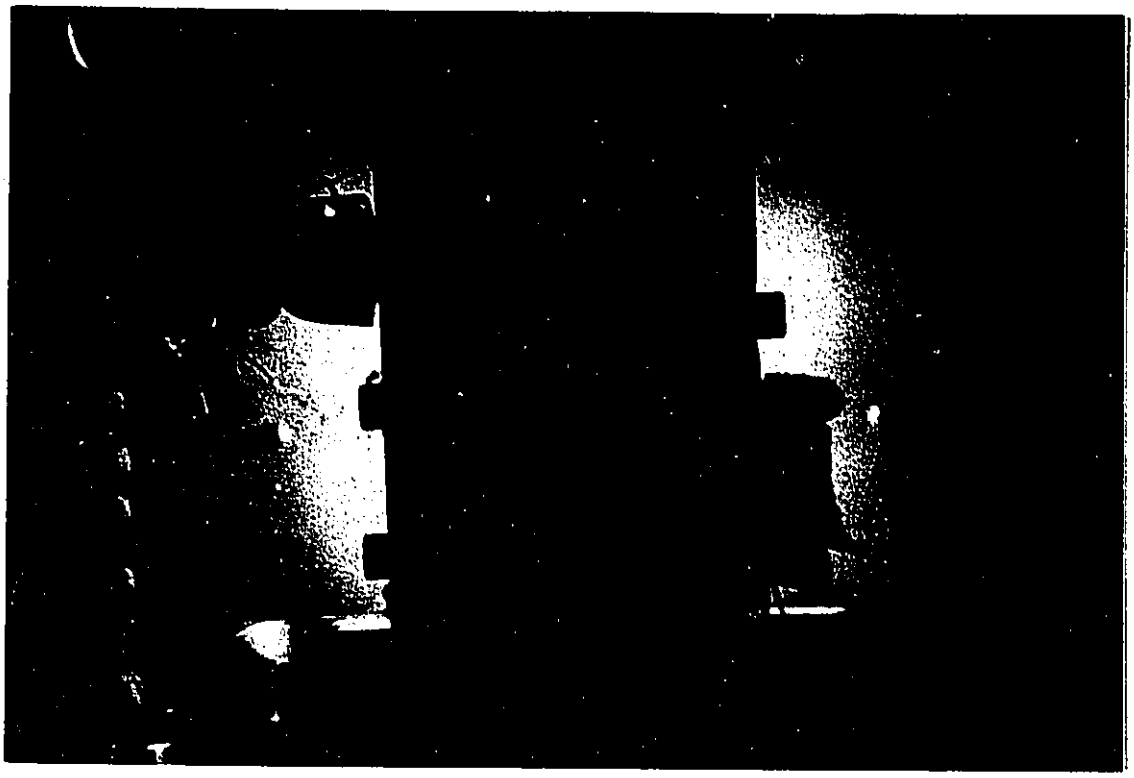

Figure 4.13: A Photograph of the Content in the Equilibrium Cell at the Critical-mixture Point. The Critical Opalescence Was Observed.

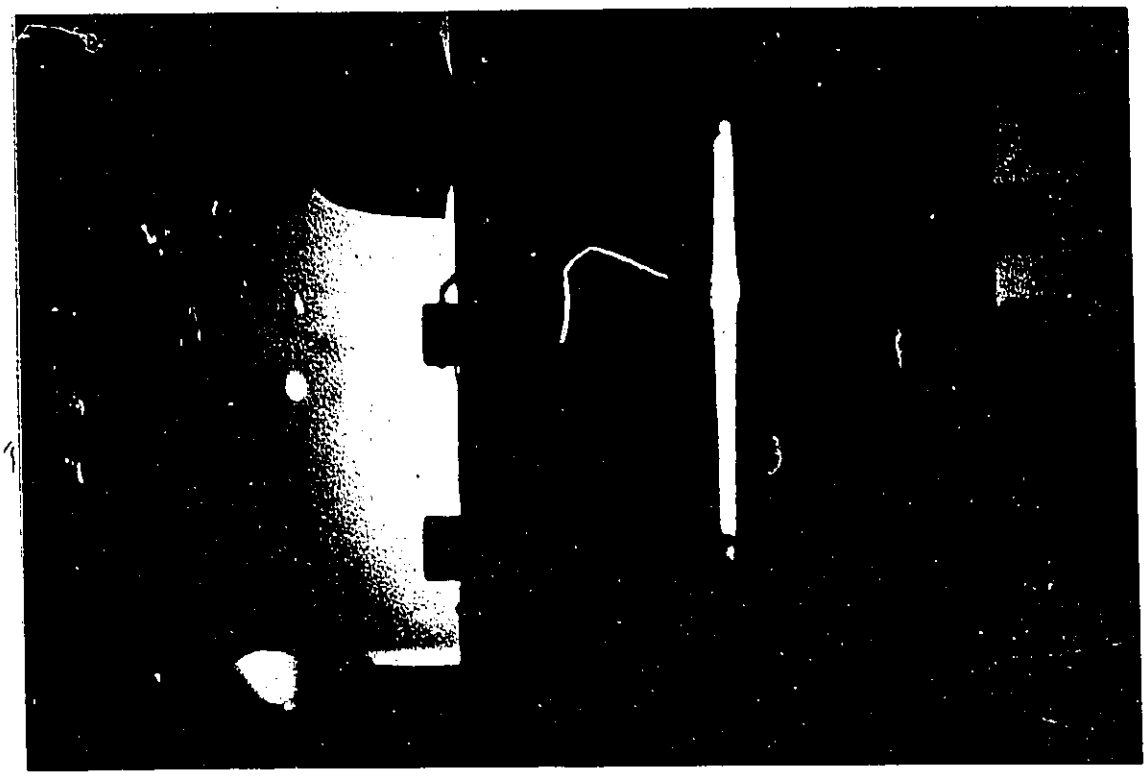

Figure 4.14: A Photograph of the Content in the Equilibrium Cell Above the Critical-mixture Point. Only One Supercritical Fluid Existed in the Cell.

al. [77] was reproduced.

Barrick et al. employed the same technique as described previously by Anderson et al. [78]. In their measurements, a magnetically stirred cell was used as an equilibrium cell. Mercury was injected to vary the volume of the cell in an attempt to determine the amount of solvent and solute charged into the cell. Shown in Figure 4.15 is a comparison of the results obtained from this study with the data of Barrick et al. [77]. In the low pressure range (below 10 MPa), where the solubility of carbon dioxide is almost a linear function of the system pressure, the results obtained in this study agreed well with those of Barrick et al., indicating that this technique yields reliable results for the solubility measurements.

The experimentally determined P-T-x values at three temperatures for the naphthalene-carbon dioxide and biphenyl-carbon dioxide systems are reported in Tables 4.6 and 4.7, respectively. The P-x isotherms at 348.2 K, 343.2 K and 338.2 K for the naphthalene-carbon dioxide system and the P-x isotherms at 343.2 K, 338.2 K and 333.2 K for the biphenyl-carbon dioxide system are presented in Figures 4.16 and 4.17, respectively.

For the biphenyl-carbon dioxide system, there exists a "crossover region", around which the three isotherms converge. Below the crossover region pressure (about 36 MPa), an increase in temperature caused a decrease in solubility of carbon dioxide in the liquid phase, while above the crossover region pressure the opposite effect occurs. This phenomenon is unusual as it does not occur in the normal conditions where the pressure is low. The explanation for this phenomenon is that at pressures above the crossover region, due to the high density of the gas phase, or supercritical fluid phase, the "escape" of the lighter component from the liquid phase into the gas phase is much less sensitive to the increased temperature than at lower pressures.

The same explanation holds also for the naphthalene-carbon dioxide system where no "crossover region" exists, because the critical-mixture loci appear at a

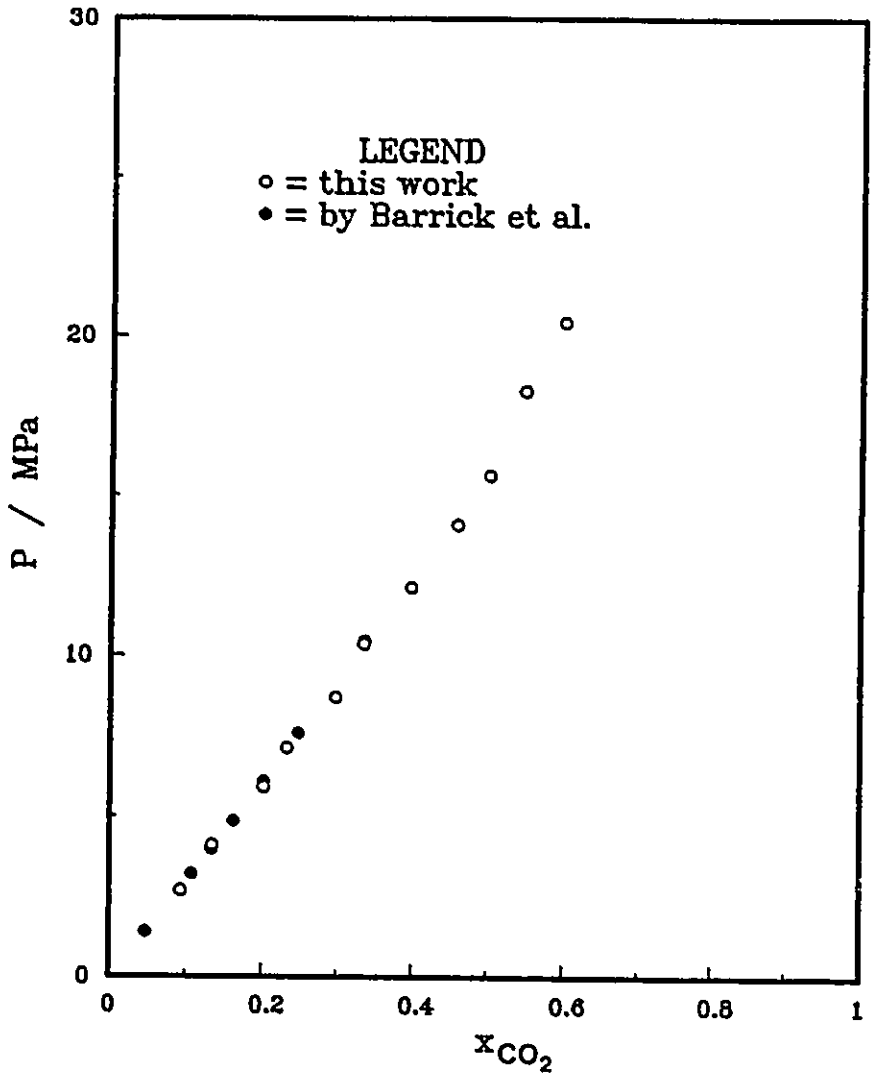

Figure 4.15: Solubility of CO_2 in Liquid Naphthalene at 373.2 K. • Data of Barrick [77]; o This Work.

Table 4.6: Solubility of Carbon Dioxide(2) in Naphthalene(1) at 348.2 K, 343.2 K and 338.2 K.

T/K	x_2	P/MPa	x_2	P/MPa	x_2	P/MPa
348.2	0.185	4.12	0.535	14.08	0.711	24.25
	0.245	5.77	0.574	15.95	0.726	24.99
	0.299	7.39	0.576	16.00	0.741	24.46
	0.359	8.86	0.605	18.01	0.754	25.96
	0.424	10.41	0.635	20.05	0.787	26.26(c.p.)
	0.425	10.46	0.667	22.11		
	0.495	12.66	0.708	24.17		
343.2	0.311	6.43	0.609	15.58	0.733	24.26
	0.312	6.46	0.638	17.62	0.773	25.74
	0.411	8.99	0.657	19.39	0.804	26.20(c.p.)
	0.507	11.28	0.658	19.44		
	0.571	13.51	0.708	22.55		
338.2	0.483	10.12	0.666	16.18	0.763	24.01
	0.544	11.48	0.700	18.45	0.781	25.30
	0.590	12.94	0.711	20.06	0.822	26.10(c.p.)
	0.630	14.50	0.745	22.40		

Table 4.7: Solubility of Carbon Dioxide(2) in Biphenyl(1) at 343.2 K, 338.2 K and 333.2 K.

T/K	x_2	P/MPa	x_2	P/MPa	x_2	P/MPa
343.2	0.246	5.41	0.535	18.15	0.685	33.32
	0.289	6.54	0.566	20.92	0.715	36.06
	0.330	7.96	0.573	21.69	0.739	38.29
	0.393	9.94	0.607	24.86	0.756	39.05
	0.402	10.16	0.628	26.93	0.760	39.18
	0.457	12.10	0.639	28.02	0.792	40.81(c.p.)
	0.505	15.47	0.658	30.37		
	0.521	16.71	0.661	30.59		
338.2	0.297	6.06	0.593	20.90	0.728	38.36
	0.361	8.00	0.620	24.06	0.751	40.48
	0.384	8.48	0.653	26.94	0.752	40.60
	0.463	10.94	0.668	30.31	0.777	42.40
	0.532	15.47	0.690	33.27	0.800	43.64(c.p.)
	0.554	17.66	0.703	36.07		
333.2	0.385	7.74	0.602	19.96	0.739	42.00
	0.388	7.75	0.633	23.30	0.758	43.26
	0.480	10.39	0.677	30.01	0.789	45.16
	0.537	13.49	0.719	35.61	0.807	46.32(c.p.)
	0.571	16.54	0.721	37.46		

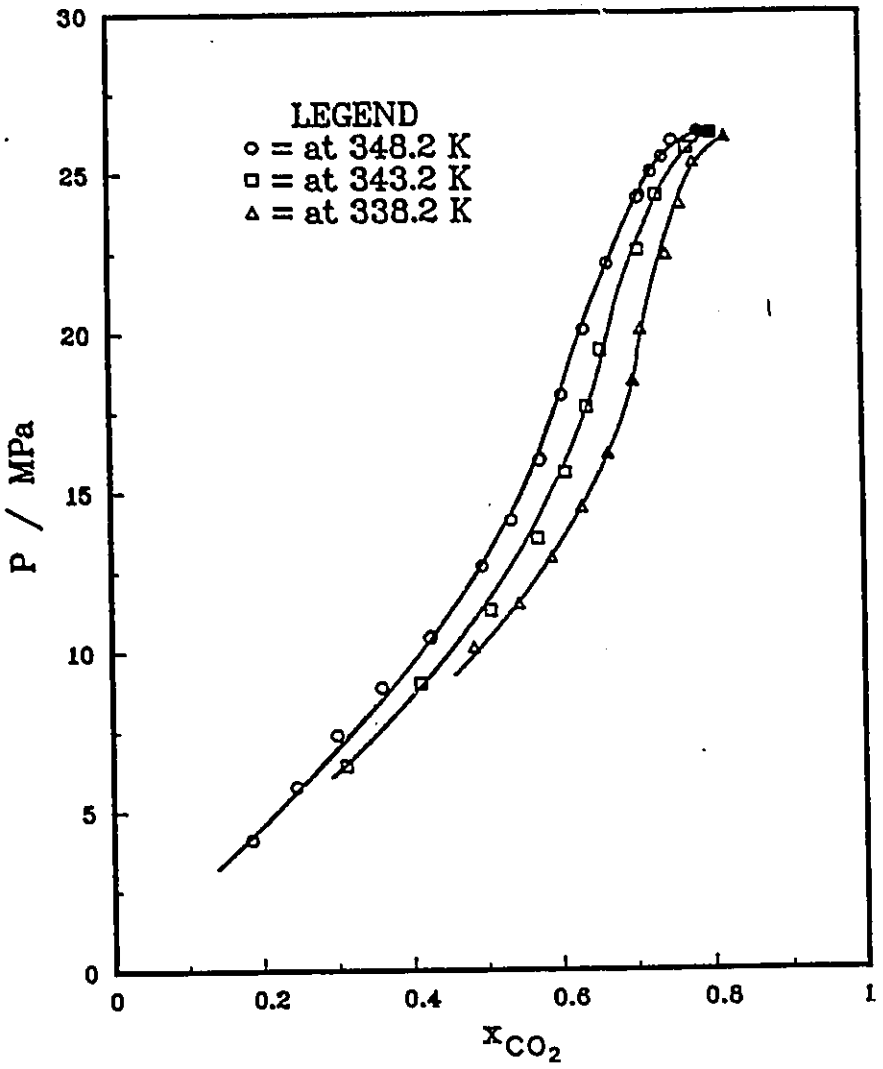

Figure 4.16: Solubility of CO_2 in Liquid Naphthalene at 348.2 K, 343.2 K and 338.2 K. ● Critical-mixture Point at 348.2 K; ■ Critical-mixture Point at 343.2 K; ▲ Critical-mixture Point at 338.2 K.

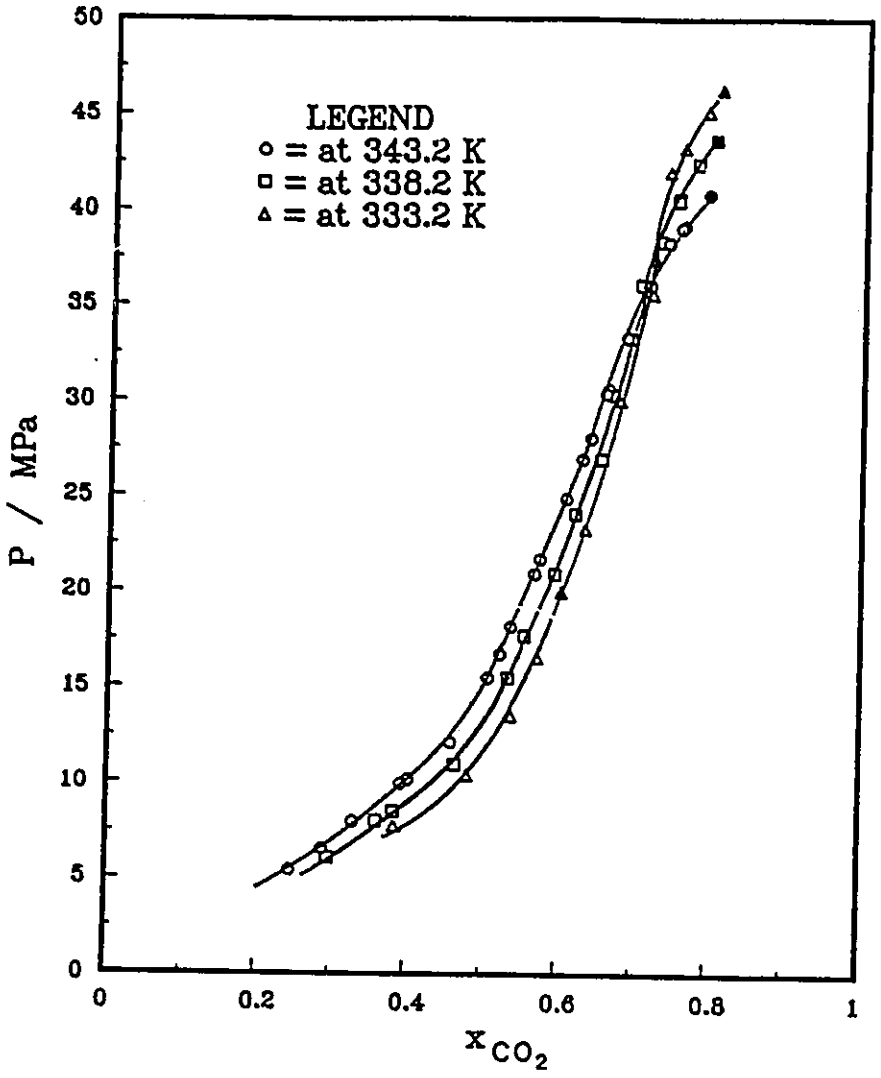

Figure 4.17: Solubility of CO_2 in Liquid Biphenyl at 343.2 K, 338.2 K and 333.2 K. ●, Critical-mixture Point at 343.2 K; ■, Critical-mixture Point at 338.2 K; ▲, Critical-mixture Point at 333.2 K.

relatively lower pressure (about 26 MPa) region, i.e., at relatively lower densities of the supercritical fluid.

Attempts at measuring the critical-mixture loci in the vicinity of the UCEP for both m-terphenyl-CO_2 and phenanthrene-CO_2 systems proved fruitless since the critical opalescence was not observed in the temperature range from 350 K to 370 K and at pressures up to 52 MPa.

4.3 Determination of Upper Critical End Point

The experimental UCEP of the binary mixtures, naphthalene-CO_2 and biphenyl-CO_2 were determined in this study from the intersection of the solid-liquid-gas coexistence curve with the liquid-gas critical loci of the mixture. The pressure-temperature projection of the L=G critical loci and the S-L-G curve for the naphthalene-carbon dioxide and the biphenyl-carbon dioxide systems are presented in Figure 4.18.

The temperature and pressure of the UCEP for the system naphthalene-carbon dioxide were established to be 333.3 $\pm$0.1 K and 25.9 $\pm$0.1 MPa, respectively. McHugh and Paulaitis [67] estimated the UCEP to be 336.2 K and 24.3 MPa based on the characteristics of the P-y isotherms. McHugh and Yogen [66] also reported a UCEP of 333.3 K and 25.6 MPa by noting the critical opalescence at the end of the solid-liquid-gas curve. Lemert and Johnston [103] recently estimated the UCEP to be 333.3 K and 26.3 MPa by locating the intersection of the S-L-G line with the critical-mixture curve, although the data of the critical curve were not reported.

The temperature and pressure of the UCEP for biphenyl-carbon dioxide were determined to be 328.5 $\pm$0.1 K and 48.6 $\pm$0.1 MPa, respectively. The corresponding values reported in the literature are 329.2 K and 46.6 MPa [67], and 328.3 K and 47.5 MPa [66].

Although the estimated values for these two binary mixtures obtained from

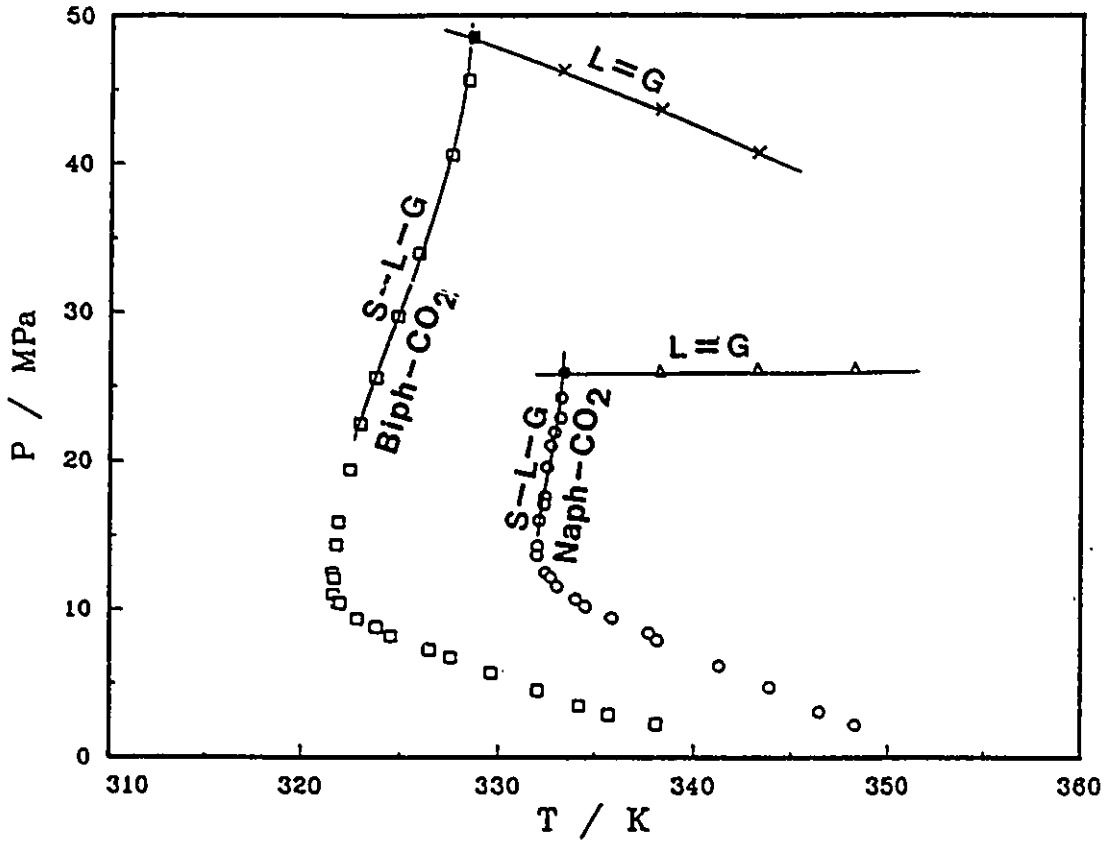

Figure 4.18: Determination of the UCEP Temperature and Pressure for the Naphthalene-Carbon Dioxide and Biphenyl-Carbon Dioxide Systems by Means of the Intersection Method. • Estimated Values of the UCEP.

the other two approaches appear to be close enough for engineering approximations, the temperature and pressure values of the UCEP obtained from the intersection method are more reliable.

The compositions of the UCEP for the systems naphthalene-CO_2 and biphenyl-CO_2 can also be determined by means of the intersection method from the T-x diagrams of the UCEP temperature determined from Figure 4.18 and the L=G critical loci (Figures 4.19 and 4.20). The estimated composition values of the UCEP are ~0.16 mole fraction of naphthalene for the system naphthalene-CO_2, which agrees with the estimation reported by McHugh and Paulaitis [67], and ~0.18 mole fraction of biphenyl for the system biphenyl-CO_2. We are not aware of any comparable experimental data in the literature for the latter system.

4.4 Determination of P-T Projection of Four-Phase Equilibria

The solid 1-solid 2-liquid-gas four-phase equilibria of ternary systems have also been investigated in this study. Such ternary systems each consists of one supercritical component and two solids. While there are a few data available for binary mixtures, data for multicomponent mixtures are scarce. It appears that the only one reference available in the literature dealing with the determination of S_1-S_2-L-G four-phase coexistence curves is that reported by van Gunst et al. [72] for the ternary system ethylene-naphthalene-hexachloroethane. However, only pressure-temperature measurements were made.

The systems investigated in this work were naphthalene-biphenyl-CO_2 and naphthalene-phenanthrene-CO_2. For these systems, the critical temperature of CO_2 is lower than the eutectic temperatures of the solids at atmospheric pressure, which are 312.2 K for the system naphthalene-biphenyl and 325.0 K for the system naphthalene-phenanthrene, respectively [122]. There is no temperature range

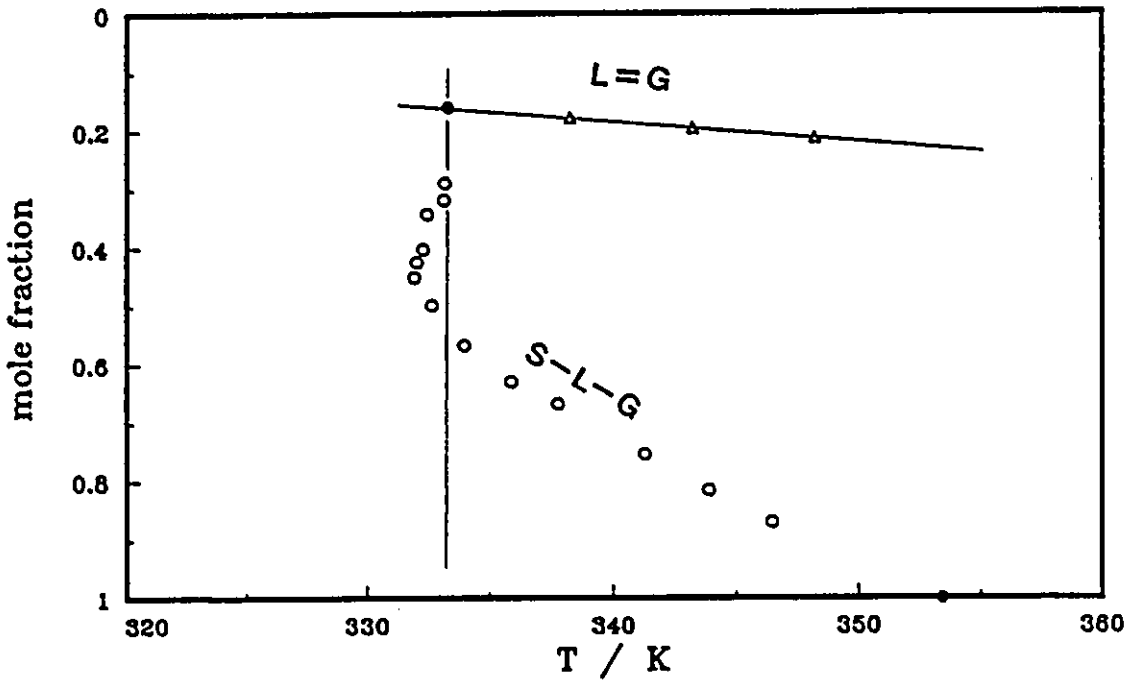

Figure 4.19: Experimental T-x Diagram of the S-L-G Curve and L=G Critical Loci for the System Naphthalene-CO_2 for Determination of the UCEP Composition. • Estimated Value of the UCEP.

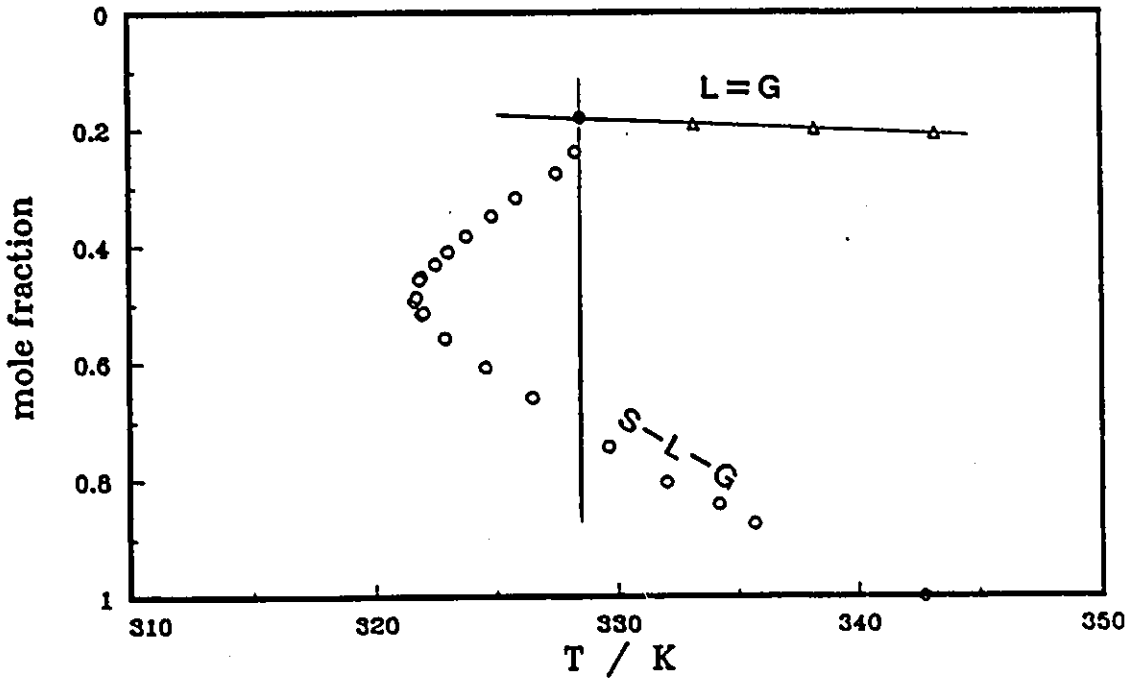

Figure 4.20: Experimental T-x Diagram of the S-L-G Curve and L=G Critical Loci for the System Biphenyl-CO_2 for Determination of the UCEP Composition. • Estimated Value of the UCEP.

in which CO_2 and the solids are all in the liquid state. The eutectic compositions at atmospheric pressure are 0.4496 mole fraction of naphthalene for the system naphthalene-biphenyl and 0.5626 mole fraction of naphthalene for the system naphthalene-phenanthrene, respectively [122]. There are two four-phase (solid 1-solid 2-liquid-gas, S_1-S_2-L-G) coexistence curves for both mixtures, starting from the quadruple points and ending at the ternary upper-critical-end-point UCEP and the ternary lower-critical-end-point LCEP, respectively. These two coexistence curves form the boundaries of the temperature and pressure conditions for SFE operations. Between these two curves, there are two solids in equilibrium with a supercritical solvent at all given pressure.

It appears from the limited data found in the literature that the ternary LCEP is also very close to the critical temperature and pressure of the pure supercritical fluid. Table 4.8 gives the comparison of the binary LCEP and UCEP for the system naphthalene-ethylene and the ternary LCEP and UCEP for the system naphthalene-hexachloroethane-ethylene as well as the critical temperature and pressure of ethylene. The temperature and pressure of the ternary LCEP of the naphthalene-hexachloroethane-ethylene mixture are close to the critical temperature and pressure of pure ethylene. For the same reason as for binary mixtures, only the four-phase S_1-S_2-L-G coexistence curve below the ternary UCEP is determined in this study.

Van Gunst et al. [72] measured the P-T projection of the S_1-S_2-L-G equilibria for the ternary system using a Cailletet apparatus with a glass capillary filled with mercury at the bottom. The four-phase line was determined by the first melting point. The details of the experimental procedure were not given.

The previously described apparatus was used to determine the pressure (P)-temperature (T) projection of one of the S_1-S_2-L-G curves, the curve below the ternary UCEP for both systems. The "first freezing point" method was extended to the determination of the P-T projection of the three-phase, solids-liquid-gas

Table 4.8: Comparison of the Binary LCEP and UCEP for the System Naphthalene-Ethylene and the Ternary LCEP and UCEP for the System Naphthalene-Hexachloroethane-Ethylene with the Critical Temperature and Pressure of Ethylene [75,72].

System	Critical Point of C_2H_4		LCEP		UCEP	
	T_c, K	P_c, MPa	T_c, K	P_c, MPa	T_c, K	P_c, MPa
naphthalene-C_2H_4	282.4	5.04	283.9	5.19	325.3	17.63
naphthalene-hexachloroethane-C_2H_4	282.4	5.04	288.5	5.58	298.7	8.77

coexistence curves for the two ternary mixtures. The P-T traces of the three-phase curves vary depending on the different ratios of the two loading solids. Only when the mixture of the solids is at its eutectic composition will both solids melt or crystallize simultaneously. In addition, an attempt was made to determine the liquid compositions (x) along the three-phase coexistence curves. While the amounts of CO_2 dissolved in the liquid phase were determined by the same procedure reported in Section 4.1.2, the solid contents of the liquid samples were determined by means of a Hewlett-Packard Supercritical Fluid Chromatograph.

The four-phase equilibria of the ternary mixtures were determined by further cooling the system after the "first freezing point" was observed until the whole contents of the equilibrium cell were completely crystallized.

By the time this work was finished, we came across the report by White and Lira [121], in which the S_1-S_2-L-G four-phase equilibria of the same two ternary systems were obtained using a different technique. In their measurements, a solid mixture of its eutectic composition at atmospheric condition was prepared before being charged into a capillary tube and a view cell. The first melting was identified with the four-phase equilibrium point. It was assumed that the eutectic composition of the binary solids did not change with pressure. The effect of the third component, supercritical carbon dioxide, on the eutectic composition, and hence on the eutectic temperature, was neglected.

The present determination of the solid 1-solid 2-liquid-gas equilibria avoids the above approximations. The eutectic temperature of the binary solids in the presence of supercritical CO_2 is the freezing point temperature of the four-phase (S_1-S_2-L-G) coexistence curve.

4.4.1 Experimental Apparatus and Procedure

The experimental set up for the determination of the four-phase equilibrium was virtually the same as that which was used for the measurements of the three-phase

(S-L-G) equilibria of the binary mixtures, except that a cooling system was employed when the system temperature was at below $\sim$ 300 K. The cooling system consisted of a heat sink of aqueous antifreeze solution and a 10 meter-long copper coil immersed in it. Air compressed to about 0.6 MPa was passed through the copper coil and into the air bath to cool the system. The temperature of the bath was maintained to within $\pm$0.05 K of the set point by a LFE temperature controller inside the air bath.

The minimum freezing point of a binary mixture of solids at atmospheric conditions occurs at its eutectic composition. A couple of solid mixtures very close to this composition were prepared for each ternary system. The solid mixture was then melted and well mixed by stirring with a glass rod before being charged into the equilibrium cell previously purged with CO_2. After the solid mixture was loaded, the cell was purged again with CO_2. The temperature of the air bath was raised to keep the mixture in the liquid state. Liquid CO_2 was compressed by the pressure intensifier and introduced into the cell and vaporized until the pressure in the cell was brought to the desired level. The mixture in the cell was then recirculated by means of the magnetic pump. The temperature of the air bath was slowly reduced at a rate of about 0.02 K per minute using an LFE temperature controller and was traced by a recorder.

The first appearance of the solid in the cell represented the three-phase, solids-liquid-gas equilibrium at a fixed ratio of the two loading solid components. After the "first melting point" was observed, the temperature of the air bath was reduced at an even slower rate. It should be mentioned that at lower pressures, the whole liquid phase would solidify soon after the first freezing point was observed. At higher pressures, however, the crystallization of the liquid phase took a longer time than it did in the lower pressure region, indicating that the pressure did have an effect on the eutectic composition of the binary solid mixture, and hence on the freezing point depression of the four-phase (S_1-S_2-L-G) coexistence curve. The

closer the composition of the loading solid mixture to its eutectic composition at the elevated pressure, the less time it took from the first freezing point of the three-phase equilibria to the freezing point of the four-phase equilibria. For the measurement of the next point, the temperature of the cell was first increased to melt the solids, the system pressure was subsequently raised to a desired value, then with the mixture in the cell being recirculated by the magnetic pump, the temperature of the cell was again slowly reduced to reach a new point on the P-T projection. For all runs, measurements started from the low pressure end. For ternary systems, measurements started from the high pressure end are not recommended. Since the solubility of the solids in supercritical CO_2 is quite high, releasing some of the gas phase could change the composition of the mixture in the cell and could also cause blockage of the inlet and outlet lines due to deposits of the solids. The accuracy of the temperature and pressure measurements of the four-phase equilibria are estimated to be ± 0.1 K in the lower pressure region and ± 0.2~0.3 K in the higher pressure region, and ± 0.05 MPa, respectively.

4.4.2 Experimental Results

In order to study the effect of pressure on eutectic composition of the binary solids, two solid mixtures with compositions very close to the eutectic compositions at atmospheric condition were prepared for the determination of the four-phase (S_1-S_2-L-G) equilibria of each ternary system. The initial loading-solid compositions were 0.455 and 0.470 mole fraction of naphthalene for the naphthalene-biphenyl-CO_2 system and 0.560 and 0.580 mole fraction of naphthalene for the naphthalene-phenanthrene-CO_2 system. Both solid-liquid-gas three-phase equilibria and solid 1-solid 2-liquid-gas four-phase equilibria were determined. The P-T values along the three-phase and four-phase coexistence curves for the two ternary systems are reported in Tables 4.9-4.10. The P-T projections of these multiphase equilibrium curves are shown in Figures 4.21 and 4.22. The four-phase equilibrium data reported

by White and Lira [121] are also presented in these figures for comparison.

For the ternary system naphthalene(1)-biphenyl(2)-CO_2(3), the values obtained in this work are in good agreement with those of White and Lira. The three-phase coexistence curve with initial loading x_1=0.455 is much closer to the four-phase coexistence curve than that of the curve with initial loading x_1=0.470. This indicates that the initial loading composition x_1=0.455 is closer to the eutectic composition of the binary solid mixture at the elevated pressures.

The temperature difference between the first freezing point, the three-phase coexistence curve, and the minimum freezing point, the four-phase coexistence curve, is smaller at lower pressure and becomes larger when the pressure is increased. It appears that the pressure and the presence of supercritical CO_2 do effect the eutectic composition of the binary solid mixture.

For the ternary system naphthalene(1)-phenanthrene(2)-CO_2(3), there are 1~2 K differences in temperature between the values obtained in this work and those by White and Lira [121]. It seems that the assumption that the eutectic composition does not change with pressure does not hold in this case. An example of pressure effect on the eutectic composition and temperature was given for the benzene-urethane system by Walas [123]. Besides, the presence of supercritical carbon dioxide could also have an effect on the eutectic composition of the binary solid mixture.

To illustrate the extent of freezing point depression, P-T projections of the S_1-S_2-L-G curves of these two ternary mixtures together with the S-L-G curves for their constituent solid-CO_2 binary mixtures are depicted in Figures 4.23 and 4.24. The presence of a second solid increased the freezing point depression significantly, regardless of whether its triple point is higher or lower than that of the first solid.

When the pressure was increased above ~ 2 MPa, the depression temperature of the four-phase coexistence curve of the ternary mixture naphthalene-biphenyl-CO_2 was below the critical point of pure carbon dioxide. So the working pressure

Table 4.9: Pressure-Temperature Values of the Four-Phase (S_1-S_2-L-G) Coexistence Curve for Two Ternary Systems, Naphthalene(1)- Biphenyl(2)-CO_2 and Naphthalene(1)-Phenanthrene(2)-CO_2.

naph(1)-biph(2)-CO_2(3)		naph(1)-phen(2)-CO_2(3)	
P/MPa	T/K	P/MPa	T/K
1.03	308.7	1.16	318.7
2.15	304.7	2.94	315.4
3.04	302.2	4.21	313.0
4.09	299.4	5.55	310.7
5.10	297.6	6.89	308.6
6.00	295.7	7.90	307.3
		9.30	305.8

Table 4.10: Pressure-Temperature Values of the Three-Phase (S-L-G) Equilibria for Two Ternary Systems Starting with Different Solid Loadings.

naphthalene(1)-biphenyl(2)-CO_2				naphthalene(1)-phenanthrene(2)-CO_2			
$x_1 = 0.455$		$x_1 = 0.470$		$x_1 = 0.560$		$x_1 = 0.580$	
P/MPa	T/K	P/MPa	T/K	P/MPa	T/K	P/MPa	T/K
1.03	309.1	1.07	310.3	1.62	319.0	2.20	318 1
2.15	305.6	2.16	307.4	2.87	315.9	4.29	314.0
3.03	303.2	3.15	304.6	4.16	313.7	6.49	310.6
4.08	300.3	4.21	302.3	5.55	311.6	8.64	308.2
5.09	298.7	5.11	299.8	6.88	309.3	9.66	307.5
5.99	296.7	5.98	298.2	8.16	308.0		

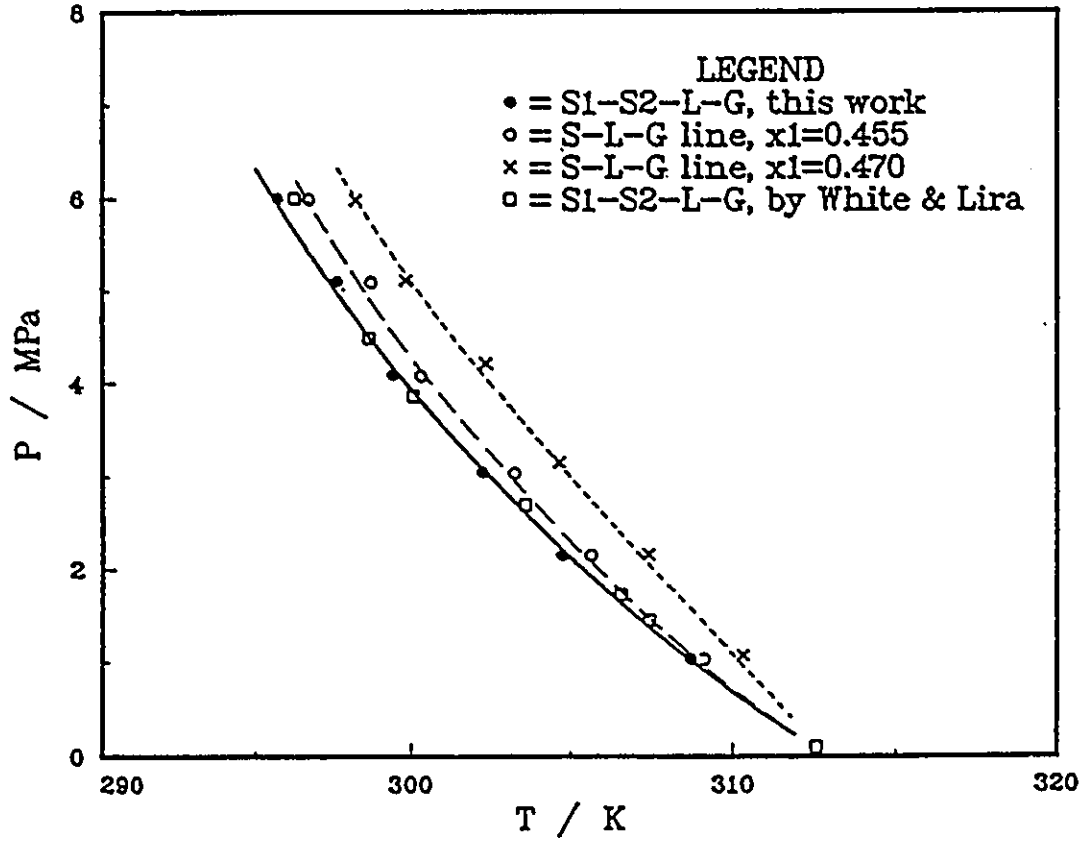

Figure 4.21: Pressure-Temperature Projection of Multiphase Coexistence Curves for the System Naphthalene(1)-Biphenyl(2)-CO_2(3). • Four-Phase (S_1-S_2-L-G) Equilibria, this work; □ Four-Phase (S_1-S_2-L-G) Equilibria, by White and Lira [121]. o Three-Phase (S-L-G) Equilibria with Initial Loading x_1=0.455; × Three-Phase (S-L-G) Equilibria with Initial Loading x_1=0.470.

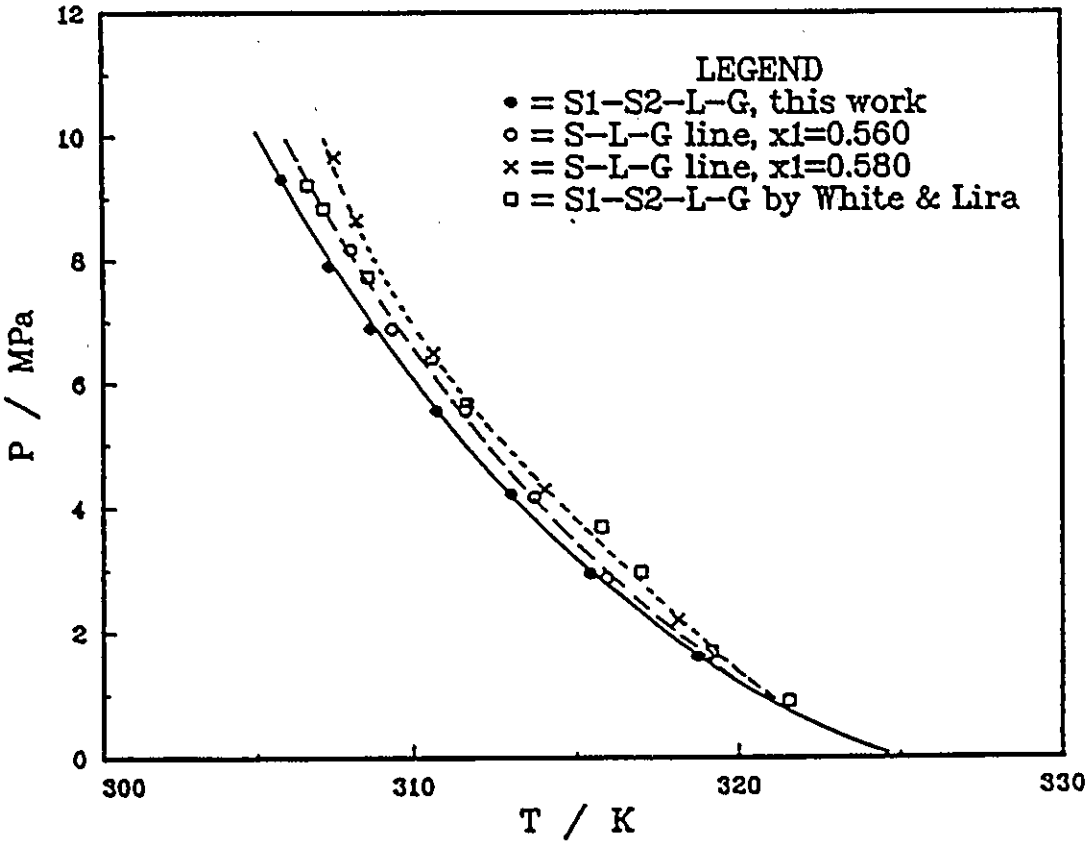

Figure 4.22: Pressure-Temperature Projection of Multiphase Coexistence Curves for the System Naphthalene(1)-Phenanthrene(2)-CO_2(3). • Four-Phase (S_1-S_2-L-G) Equilibria, this work; □ Four-Phase (S_1-S_2-L-G) Equilibria, by White and Lira [121]. o Three-Phase (S-L-G) Equilibria with Initial Loading x_1=0.560; × Three-Phase (S-L-G) Equilibria with Initial Loading x_1=0.580.

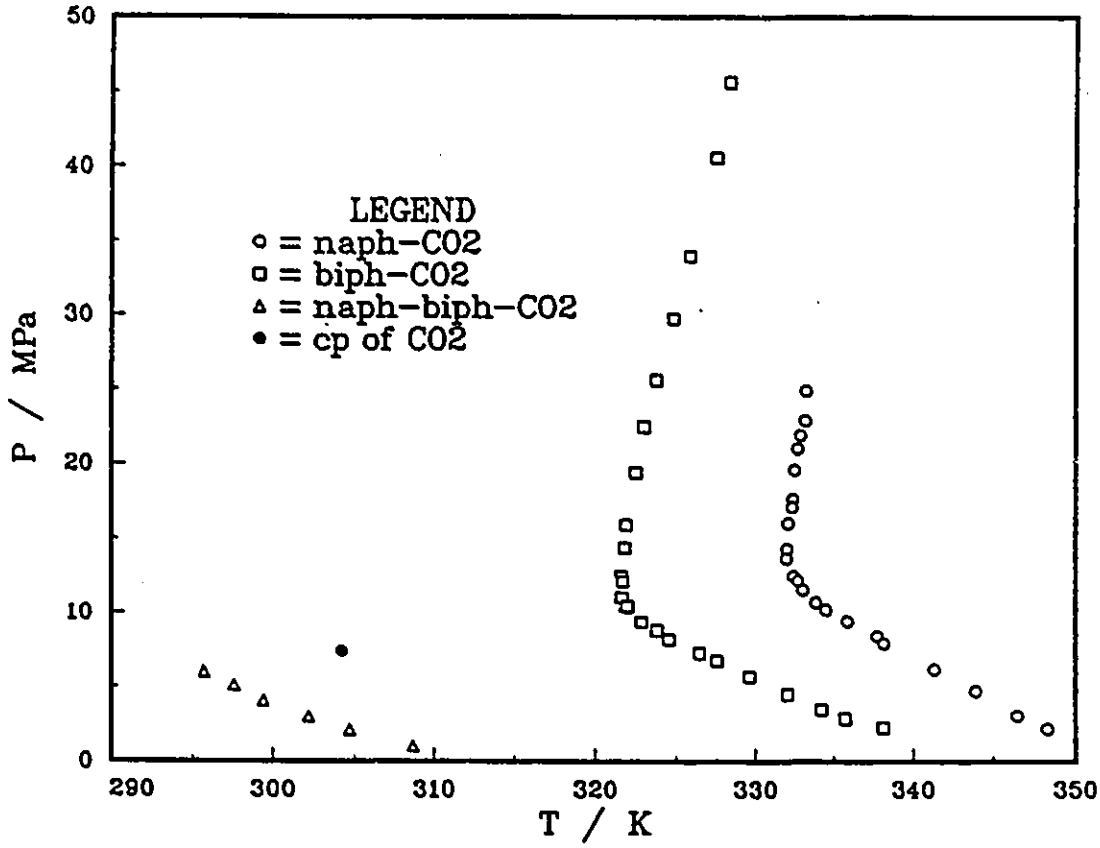

Figure 4.23: Pressure-Temperature Projection of Multiphase Coexistence Curves for Mixtures Containing Naphthalene(S_1), Biphenyl(S_2), and CO_2.

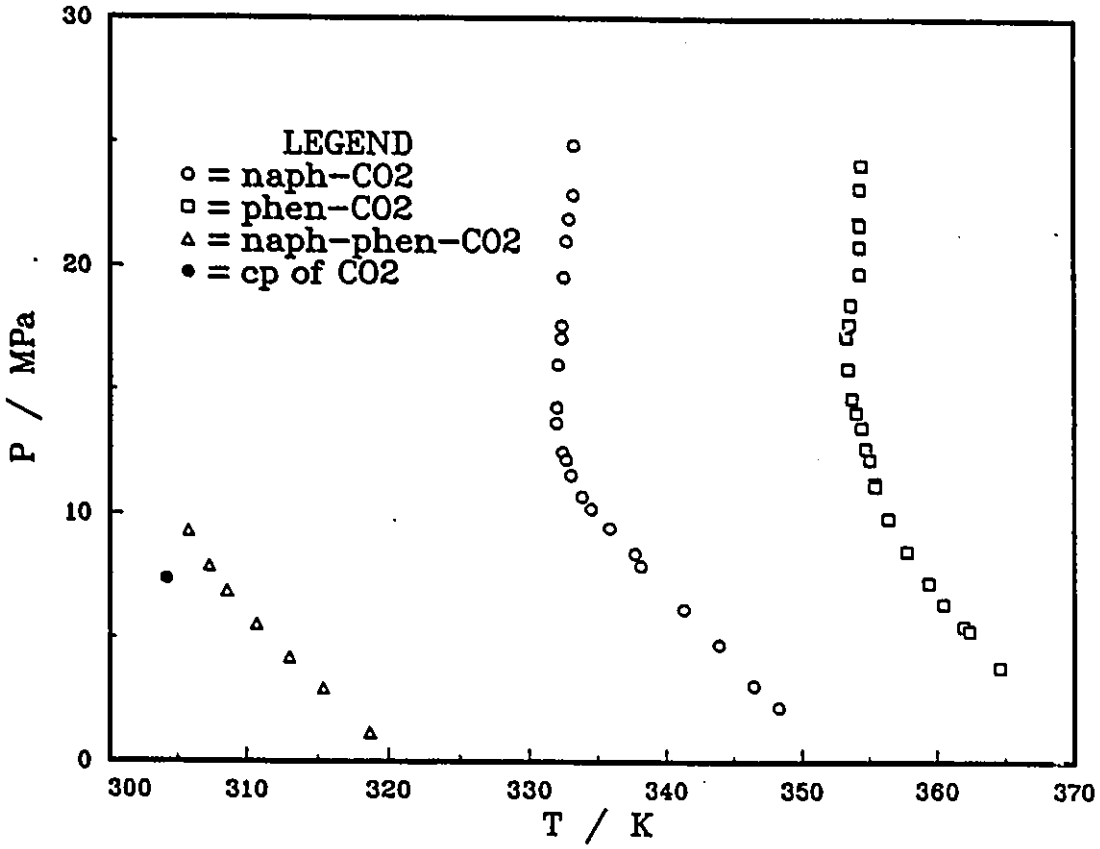

Figure 4.24: Pressure-Temperature Projection of Multiphase Coexistence Curves for Mixtures Containing Naphthalene(S_1), Phenanthrene(S_2), and CO_2.

of this system could not go beyond the vapor pressure of carbon dioxide at that depression temperature. The characteristics of the ternary upper-critical-end-point were not observed for this ternary system under the experimental conditions.

For the ternary system naphthalene(1)-phenanthrene(2)-CO_2(3) the temperature depression curve would run into the subcritical region of carbon dioxide when the pressure was increased over $\sim$ 10 MPa. The characteristics of the ternary upper-critical-end-point were not observed when the pressure was further increased while the temperature was kept either under or above the critical point of pure carbon dioxide.

The two ternary systems investigated in this study have phase diagrams of the type in Figure 2.6b since the ternary UCEP does not exist.

4.5 Analysis of Liquid Phase Composition of the Solid-Liquid-Gas Equilibria for Ternary Mixtures

One of the disadvantages of the supercritical fluid extraction process is that the loading of the solutes in the gas phase, or the supercritical fluid phase, is low. Besides, the selectivity of the pure supercritical solvents is usually not very high. Many studies have focused on the solubility enhancements in the supercritical fluids produced by adding a third component, referred to as an "entrainer", or a "co-solvent" [80,122,124-128].

In addition to making separations by enhanced extraction in the gas phase, where the solids and supercritical fluid are in equilibrium, operating in the liquid-gas region might be of interest, because the loading power and the selectivity of the solvent in the liquid state are relatively high. However, due to difficulties in operating a three-phase process, either solid-liquid-gas or liquid-liquid-gas, com-

mercial processes using supercritical extraction for liquid mixture separation are not available at present.

For the above reason, the composition analysis of the equilibrium liquid phase for the multicomponent mixtures is of importance.

An attempt was made in this study to develop the chromatographic conditions for liquid phase composition analysis of the three-phase equilibria for ternary mixtures.

After a first appearance of the solid phase, a first freezing point of the ternary mixture was observed, a liquid sample was immediately taken for analysis. The CO_2 content in the liquid sample was determined by means of the same procedure reported in Section 4.1.4. The amount of solids remained in the sampling tube was collected using acetone injected from a syringe. A Hewlett-Packard Supercritical Fluid Chromatograph (SFC) (Model 1082 B) was employed for determination of the solid content in the liquid sample. Supercritical carbon dioxide was used as the mobile phase.

A schematic diagram of the SFC is shown in Figure 4.25. Liquid carbon dioxide from a cylinder **A** equipped with a dip tube was filtered by a filter **B** of 2 micron frit and was cooled to below $\sim$ 260 K by a Neslab RTE-24 refrigerated recirculating bath **C**. The cooling bath was used to increase the pumping efficiency of the two high pressure chromatograph pumps **D**. The chromatograph pumps were of the reciprocating diaphragm type. They operated at a constant volumetric flow rate which was measured by means of flow transducers **E**. The system pressure was controlled by a back pressure regulator **L** at the outlet of the flow system of the chromatograph. The pressure was measured by two pressure transducers **I** (Instruments model SA 0-50000 psia) in conjunction with a Sonotek model 4100-K-O-B-O indicator at inlet and outlet of the column. After leaving the pump, one of the fluid streams was preheated in the column oven **J** and then mixed with the other stream in a chamber **F**.

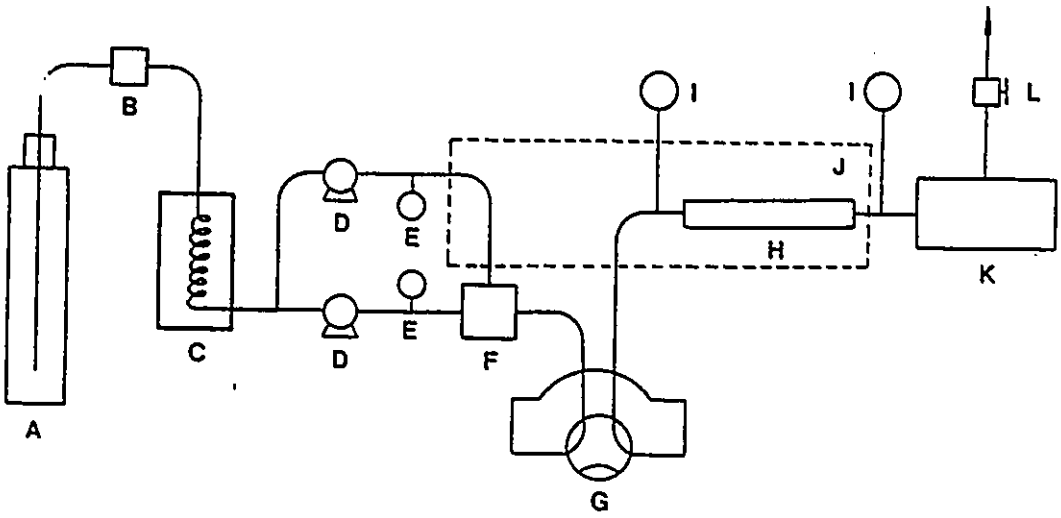

Figure 4.25: Schematic Diagram of the Supercritical Fluid Chromatograph. A - Liquid CO_2 Cylinder; B - Filter; C - Cooling Bath; D - High Pressure Pump; E - Flow Transducer; F - Mixing Chamber; G - Six-way Valve; H - Analytical Column; I - Pressure Transducers; J - Column Oven; K - VW Detector; L - Back Pressure Regulator.

Injected samples (solids + acetone) were conveyed by CO_2 through a manually operated Rheodyne 7125 syringe-loading six-way valve G into the chromatographic column H, which was 200 mm in length and 4.6 mm in diameter, packed with Hypersil ODS 5 μm particles.

The separated components eluting from the column passed through a variable-wavelength ultraviolet-absorbance detector K, where the intensity of light of the wavelength of the particular component is compared with that of a reference wavelength. The signal from the detector is integrated using a built-in integrator. In the determination, o-terphenyl was used as the internal standard for it has a proper residence time which makes a clear separation of its peak area from that of the detected components. (See Appendix A for the calibration of the supercritical fluid chromatograph).

The desired operation conditions of the chromatograph for analysis of the two ternary mixtures were found by adjusting the following operating parameters.

1. The flow rate of the mobile phase, which can be varied from 0 to 10.00 ml/min. in 0.01 ml/min. increments.

2. The pressure of the column, which can be adjusted by the back-pressure regulator L up to 700 bar with 1 bar increments.

3. The temperature of the oven, which may be set from 303 K to 373 K in 1 K steps.

4. The reference wavelength, which must be set at least 60 nm difference from the detected wavelength.

Except for pressure, all the other parameters are adjusted and controlled by a remote terminal. The SFC settings for analysis of the two ternary mixtures are reported in Tables 4.11 and 4.12.

It takes about 2 minutes to complete one sample analysis. A gas chromatograph with a flame ionization detector requires 6-8 minutes to complete the same analysis. Besides, the oven temperature of the SFC is only a little higher than the

Table 4.11: SFC Settings for Analysis of the System Naphthalene-Biphenyl.

FLOW	2.00 ml/min.
%B	50.0
COLUMN PRESSURE	92 bar
MAX PRESSURE	400 bar
MIN PRESSURE	0 bar
OVEN TEMPERATURE	35°C
VW SGNL	
WAVE LENGTH (S:R)	254 : 430 nm
CHART SPEED	1.00 cm/min.
ZERO	10.0%
ATTENUATION 2 ↑	12
AREA REJECTED	10000 area counts
SLOPE SENSITIVITY	0.0

Table 4.12: SFC Settings for Analysis of the System Naphthalene-Phenanthrene.

FLOW	2.00 ml/min.
%B	50.0
COLUMN PRESSURE	96 bar
MAX PRESSURE	400 bar
MIN PRESSURE	0 bar
OVEN TEMPERATURE	35°C
VW SGNL	
WAVE LENGTH (S:R)	264 : 430 nm
CHART SPEED	1.00 cm/min.
ZERO	10.0%
ATTENUATION 2 ↑	12
AREA REJECTED	10000 area counts
SLOPE SENSITIVITY	0.0

critical temperature of carbon dioxide, 304 K, while in a gas chromatograph the oven temperature must be set as high as 500~600 K.

Solid mixtures with various compositions were prepared for the analysis of the liquid phase compositions of the two ternary mixtures at their first-freezing-point conditions. The solid content of each sample was about 0.3 gram, which was very small comparing with the total loading of the solid mixture (about 75 grams).

A plot of selectivities of supercritical CO_2 ($x_{naphthalene}$ / $x_{biphenyl}$ and $x_{naphthalene}$ / $x_{phenanthrene}$) for both mixtures at various pressures of the three-phase S-L-G equilibrium conditions is shown in Figure 4.26. In both cases, the high selectivity of supercritical CO_2 is in favor of naphthalene. The ratio of the two solid compositions in the liquid phase remains essentially constant with pressure increases. This is not a good situation for the design of a continuous separation process using a supercritical fluid extraction technique, since the solid mixture extracted under high pressure will be expected to deposited at low pressure. It would be better if the selectivity were a strong function of pressure. It seems from the Figure 4.26 that an entrainer, or co-solvent is needed to make a separation of such solid mixtures in the SFE process using supercritical carbon dioxide as a solvent.

4.6 Materials

In the experimental measurements, naphthalene (Fisher, Scintanalyzed grade), biphenyl (Aldrich, 99%), m-terphenyl (Fisher, Scintanalyzed grade), o-terphenyl (Aldrich, 99%), phenanthrene (Aldrich, 98+%) and CO_2 (Air Product and Chemical 99.9%) were used as supplied. Acetone, used as a liquid solvent, was obtained from Canlab and had a purity exceeding 99.9%.

Physical properties of the materials used throughout this study are summarized in Table 4.13.

The vapor pressure of the solids are given by the Antoine equation $\log(P) =$

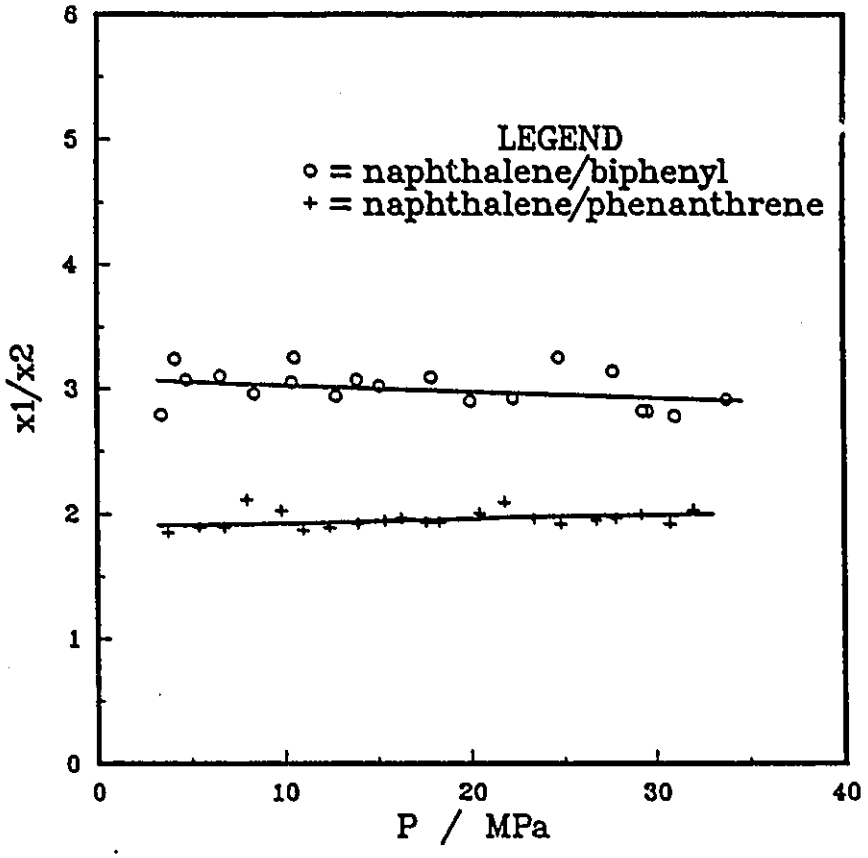

Figure 4.26: Selectivities of Supercritical CO_2 in Liquid State for the Systems Naphthalene-Biphenyl-CO_2 and Naphthalene-Phenanthrene-CO_2.

Table 4.13: Physical Properties of the Materials Used in This Study [131].

component	formula	structure	T_c, K	P_c, bar	ω	supplier, purity
naphthalene	$C_{10}H_8$	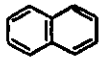	748.4	40.5	0.302	Fisher, Scintanalyzed
biphenyl	$C_{12}H_{10}$	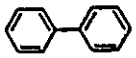	789.0	38.5	0.372	Aldrich, 99%
phenanthrene	$C_{14}H_{10}$	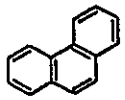	873.2	33.0	0.540	Aldrich, 98 +%
m-terphenyl	$C_{18}H_{14}$	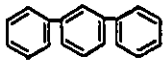	924.8	35.06	0.449	Fisher, Scintanalyzed
o-terphenyl	$C_{18}H_{14}$	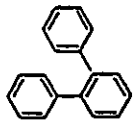	891.0	39.0	0.431	Aldrich, 98%
carbon dioxide	CO_2		304.1	73.8	0.239	Air Product & Chemical, 99.9%

				Antoine Coefficients		
component	T_m, K	$v_S, cm^3/mole$	$\Delta H_f, kJ/mole$	A	B	C
naphthalene	353.5	111.9[d]	19.30[a]	7.2144	2926.6	−35.8[a]
biphenyl	342.4	131.0[a]	18.60[d]	9.4068	4262.0	0[a]
phenanthrene	373.7	167.6[a]	16.45[b]	6.3175	2963.85	−71.11[c]
m-terphenyl	360.0					

a, [129]; b, [132]; c, [135]; d, [133].

A - B/(T + C) where P is the vapor pressure in bar and T is the temperature in K. The coefficients for naphthalene and biphenyl are from Ziger and Eckert [129], while the coefficients for phenanthrene are correlated from the experimental results by Bradley and Cleasby [134].

Chapter 5

MODELING OF SOLID-SUPERCRITICAL FLUID PHASE EQUILIBRIA

Two different approaches, the equation-of-state approach and a approach based on the combination of an activity-coefficient model and an equation-of-state model, were used to correlate the S-L-G equilibria for binary mixtures and the S_1-S_2-L-G equilibria for ternary mixtures. The merits of these two approaches are compared. Besides, the Peng-Robinson equation of state with three different mixing rules was used to correlate the solubility data of supercritical carbon dioxide in the melted naphthalene and biphenyl. The ability of the models to represent the solubility data is also discussed.

5.1 A Modified Peng-Robinson Equation of State for Multiphase Equilibrium Calculation

According to the Gibbs phase rule, there is only one degree of freedom available for S-L-G equilibria of binary mixtures and for S_1-S_2-L-G equilibria of ternary mixtures.

For a ternary mixture at four-phase equilibrium, the equilibrium conditions

$$f_i^L = f_i^G, \qquad i = 1,2,3 \tag{5.1}$$

$$f_i^S = f_i^G, \qquad i = 1,2 \tag{5.2}$$

coupled with the mass balances for both the liquid and the gas phases

$$x_1 + x_2 + x_3 = 1 \tag{5.3}$$

$$y_1 + y_2 + y_3 = 1 \tag{5.4}$$

are sufficient to calculate the values of seven of the eight variables, which are the temperature T, the pressure P, and the liquid and gas compositions x_i and y_i, providing the value of one of these variables is given. In the above equations, the subscripts 1 and 2 refer to the solid components, and the subscript 3 represents the supercritical carbon dioxide. The superscripts S, L and G represent the solid, the liquid and the gas phases, respectively.

For the type of the phase behavior investigated in this study, the P-T projections of the multiphase coexistence curves are monotropic functions of pressure, but not of temperature. The change of the pressure is significant within a short range of the temperature. Therefore, it is convenient to choose pressure as a fixed parameter. In our calculations, the pressure was chosen as a fixed parameter to find the iterative solution of Eqs.(5.1-5.4). The following assumptions were made throughout the iterative calculation:

1. the molar volumes v_i^S of the solids are constant;

2. supercritical CO_2 is insoluble in the solids;

3. the saturated vapor pressures of the solids are so low that the fugacity coefficients Φ_i^{sat} at the saturated temperature equal unity.

The fugacity of the pure solid component can therefore be written as

$$f_i^S = P_i^{sat} exp \frac{v_i^S (P - P_i^{sat})}{RT}, \qquad i = 1,2 \tag{5.5}$$

Eqs.(5.1) and (5.2) become

$$y_i\Phi_i^G = x_i\Phi_i^L, \qquad i = 1,2,3 \tag{5.6}$$

$$y_i\Phi_i^G P = P_i^{sat} exp\frac{v_i^S(P - P_i^{sat})}{RT}, \qquad i = 1,2 \tag{5.7}$$

The fugacities of the components in both the gas and the liquid phases can be calculated from suitable equations of state. The Peng-Robinson equation of state Eq.(3.13) is one of the most popular two-parameter equations of state. It uses a van der Waals type repulsive term and a modified attractive term. While the attractive parameter a_i for each component is shown to be temperature-dependent, the repulsive parameter b_i remains a constant which is related only to the critical temperature and pressure of each component:

$$a_i = a_{c_i}\alpha_i = 0.45724\frac{R^2T_{c_i}^2}{P_{c_i}}\alpha_i \tag{5.8}$$

$$b_i = b_{c_i} = 0.07780\frac{RT_{c_i}}{P_{c_i}} \tag{5.9}$$

In the development of the Peng-Robinson equation, the correction factor α_i was treated as a dimensionless function of the reduced temperature T_R and the acentric factor ω_i of the component. This factor equals unity at the critical temperature. The vapor pressure data, from normal boiling point to critical point, of several normal hydrocarbons were used to determine a functional form for α_i. It took the same form as that obtained by Soave [96] for the SRK equation:

$$\alpha_i^{1/2} = 1 + m_i(1 - T_R^{1/2}) \tag{5.10}$$

where the substance-dependent constants m_i were correlated against the acentric factors:

$$m_i = 0.37464 + 1.54226\omega_i - 0.26992\omega_i^2 \qquad 0 \le \omega_i \le 0.49 \tag{5.11}$$

$$m_i = 0.37964 + 1.48503\omega_i - 0.16442\omega_i^2 + 0.01667\omega_i^3 \qquad 0.2 \le \omega_i \le 2.0 \tag{5.12}$$

In the case of this study, the operating temperature range is above the critical point of carbon dioxide, and is far below the normal boiling points of the aromatic compounds. Accordingly, the quantities α of the Peng-Robinson equation are modified to take the following forms:

$$\alpha^{1/2} = 1 + C_1(1 - T_R^{1/2}) + C_2(1 - T_R) + C_3(1 - T_R^2) \tag{5.13}$$

for the aromatic compounds and

$$\alpha_{CO_2} = e^{C_4(1-T_R)} \tag{5.14}$$

for the supercritical carbon dioxide. The constants C_i in the equations are determined from the vapor pressure data for the proper temperature range for each component individually. The resulting equations are

$$\alpha_{naph}^{1/2} = 1 + 1.1254(1 - T_R^{1/2}) - 0.1792(1 - T_R) - 2.3589 * 10^{-3}(1 - T_R^2) \tag{5.15}$$

$$\alpha_{biph}^{1/2} = 1 - 13.0576(1 - T_R^{1/2}) + 16.1356(1 - T_R) - 5.3678(1 - T_R^2) \tag{5.16}$$

$$\alpha_{phen}^{1/2} = 1 + 4.2726(1 - T_R^{1/2}) - 2.0976(1 - T_R) + 4.7387 * 10^{-2}(1 - T_R^2) \tag{5.17}$$

$$\alpha_{CO_2} = e^{0.5856(1-T_R)} \tag{5.18}$$

There is no vapor pressure data for pure m-terphenyl in the literature, and the P-T-x values of the S-L-G three-phase equilibria for mixtures involving m-terphenyl were not correlated.

The conventional mixing rule Eq.(3.14), and the mixing rules proposed by Adachi-Sugie (AS) [141] and Schwartzentruber et al. (SGR) [142] were used to calculate the fugacity coefficients.

The difference between the latter two mixing rules is in the expression for a_{ij}:

$$a_{ij} = (a_i a_j)^{1/2}(1 - k_{ij} - l_{ij}X_{ij}) \tag{5.19}$$

For the AS mixing rule,

$$X_{ij} = x_i - x_j \tag{5.20}$$

and $l_{ij} = -l_{ji}$. For the SGR mixing rule,

$$X_{ij} = \frac{m_{ij}x_i - m_{ji}x_j}{m_{ij}x_i + m_{ji}x_j} \tag{5.21}$$

$l_{ij} = -l_{ji}$ and $m_{ij} = 1 - m_{ji}$. For binary mixtures, the SGR mixing rule will reduce to the AS mixing rule when m_{ij}=0.5.

For the AS and the SGR mixing rules, a_i' in Eq.(3.16) is defined for binary mixtures by

$$a_i' = 2\left[x_i a_i + x_j a_{ij} - 2x_i x_j^2 (a_i a_j)^{1/2} l_{ij} K_{ij}\right], \qquad i,j = 1,2, \qquad i \neq j \tag{5.22}$$

with $K_{ij} = 1$ for the AS mixing rule, and

$$K_{ij} = \frac{m_{ij}m_{ji}}{(m_{ij}x_i + m_{ji}x_j)^2} \tag{5.23}$$

for the SGR mixing rule.

5.1.1 The Three Phase S-L-G Equilibria For Binary Mixtures

The iterative calculation of the three phase S-L-G equilibria for binary mixtures was started by assuming a value for the temperature. The fugacity of the solid at the specified pressure and temperature was calculated according to Eq.(5.5). A liquid-gas equilibrium flash calculation was then performed at the specified conditions using assumed compositions. The fugacity coefficients of each component in both liquid and gas phases were calculated according to Eqs.(3.16-3.18). Liquid-gas equilibrium constant K_i ($=y_i/x_i$) was then obtained either from the ratio of the fugacity coefficients as a calculated value, or from the ratio of the assumed compositions as an assumed value. Comparison of the two values of the equilibrium constants was made at this stage to check if the assumed compositions were close enough to the calculated ones. If so, comparison of the fugacity of the solid phase with that of the solid compound in the gas phase was made to check if the assumed temperature was right.

A quasi-Newton method was used to find the minimum of the object function FOB:

$$FOB = \sum_j \left[\left(\frac{T_j^{cal} - T_j^{exp}}{T_j^{exp}} \right)^2 + \left(\frac{x_j^{cal} - x_j^{exp}}{x_j^{exp}} \right)^2 \right] \tag{5.24}$$

A flow diagram illustrating the algorithm used to compute the S-L-G equilibria for binary mixtures is shown in Figure 5.1.

Using the proposed procedure with the literature values summarized in Table 4.17 for the densities and vapor pressures of the solids, the S-L-G three-phase equilibria have been calculated for the binary mixtures of naphthalene-CO_2, biphenyl-CO_2 and phenanthrene-CO_2.

The interaction parameters k_{ij} in the van der Waals conventional mixing rule (vdW-1), k_{ij} and l_{ij} in the AS mixing rule and k_{ij}, l_{ij} and m_{ij} in the SGR mixing rule have been found from the fit of the P-T-x values of the S-L-G equilibria for the three binary systems using both the PR equation and the PR equation with the modified correction factor α (PRM). A good agreement was obtained between the experimental data and the calculated results for the naphthalene-carbon dioxide mixture using the PRM equation of state with the AS mixing rule where the parameters k_{ij}=0.127 and l_{ij}=0.025. The calculated temperatures on the S-L-G curve agree with the experimental data to within 0.6 K on the average, while the calculated liquid compositions agree with experimental values to within 0.02 mole fraction on the average. The results are shown in Figures 5.2 and 5.3. The PRM equation with the AS mixing rule made a small improvement in representing the P-T-x values of the S-L-G equilibria than the PR equation with the AS mixing rule in which the parameters k_{ij}=0.117 and l_{ij}=0.017. The PRM equation with vdW-1 mixing rule (k_{ij}=0.105) did not succeed in representing the P-T projection of the S-L-G equilibria. The results are also shown in Figures 5.2 and 5.3 for comparison.

Using the same procedure, the modeling of the P-T-x values of the S-L-G equilibria for the biphenyl-CO_2 and phenanthrene-CO_2 binaries was not as satisfactory as that for the naphthalene-CO_2 mixture. As shown in Figures 5.4-5.7, the good

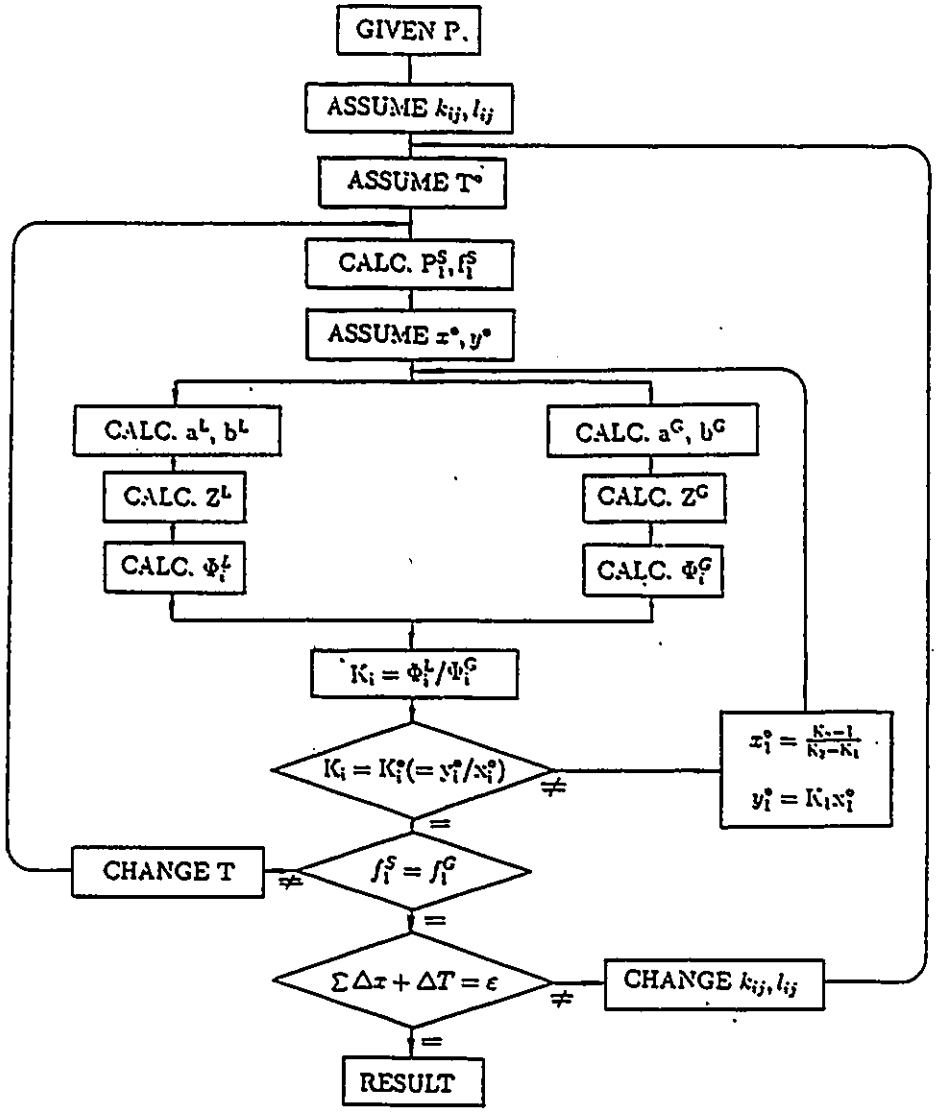

Figure 5.1: Flow Diagram of Computation Procedure Used for Determining the S-L-G Equilibria for Binary Mixtures.

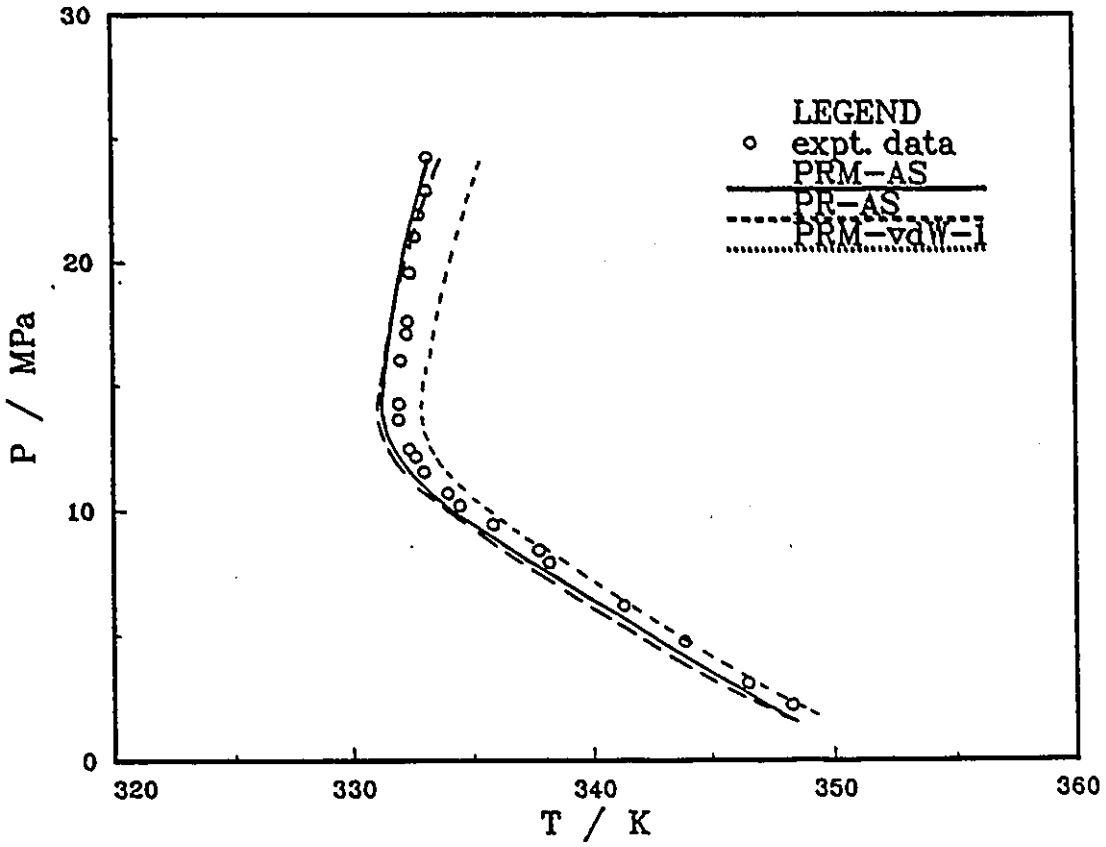

Figure 5.2: Comparison of Calculated and Experimental Results of P-T Values of S-L-G Equilibria for the Naphthalene-CO_2 Mixture.

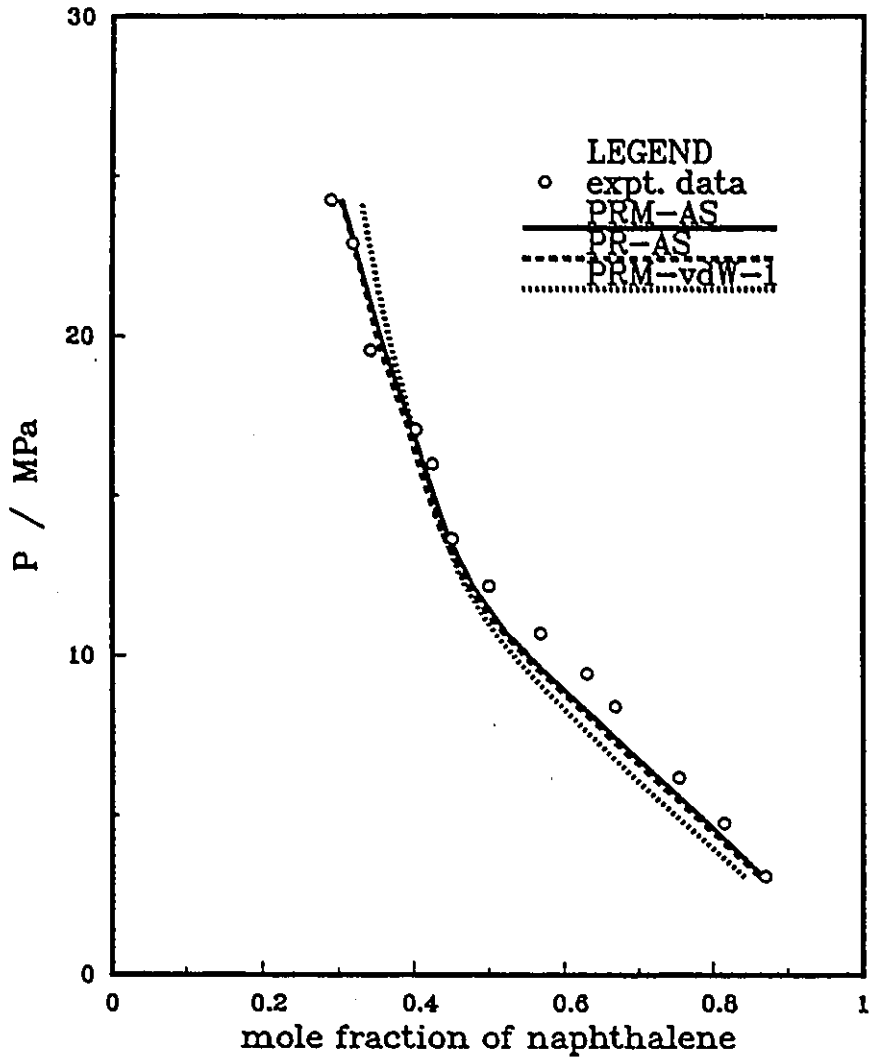

Figure 5.3: Comparison of Calculated and Experimental Results of P-x Values of S-L-G Equilibria for the Naphthalene-CO_2 Mixture.

agreement between the experimental data and the calculated results in either the P-T projection or the P-x diagram of the S-L-G equilibria was obtained at the cost of failure in representing either the liquid compositions of the S-L-G equilibria (in the case of the phenanthrene-CO_2 mixture), or the temperature of the S-L-G equilibria (in the case of the biphenyl-CO_2 mixture). In both cases, the PRM equation with the SGR mixing rule does a better job in representing the P-T-x values of the S-L-G equilibria than the PRM equation with either the AS mixing or the vdW-1 mixing rule. The obtained interaction parameters in the calculation of the S-L-G three-Phase equilibria are summarized in Table 5.1.

In some cases, the PR equation with the original correction factor α failed to reach convergence in the calculation of the S-L-G equilibria. This indicates that the modification of the quantity α is of importance. For the systems biphenyl-CO_2 and phenanthrene-CO_2, the PRM equation with three different mixing rules were used to calculate the S-L-G three-phase equilibria. The results are also shown in figures 5.4-5.7 for comparison.

The calculated results of the S-L-G equilibria for the biphenyl-CO_2 and phenanthrene-CO_2 mixtures are not as satisfactory as those for the naphthalene-CO_2 mixture. It is understandable since biphenyl and phenanthrene differ more significantly from carbon dioxide than naphthalene does in the molecular size, the vapor pressure and the critical conditions, making the first two binary systems more asymmetric than the naphthalene-CO_2 system.

5.1.2 The Four Phase S_1-S_2-L-G Equilibria For Ternary Mixtures

The above calculation for binary mixtures was extended to correlate the S_1-S_2-L-G four-phase equilibria of the ternary mixtures of naphthalene(1)-biphenyl(2)-CO_2 and naphthalene(1)-phenanthrene(2)-CO_2. Both systems were experimentally investigated in this study. According to the Gibbs phase rule, there is only one degree

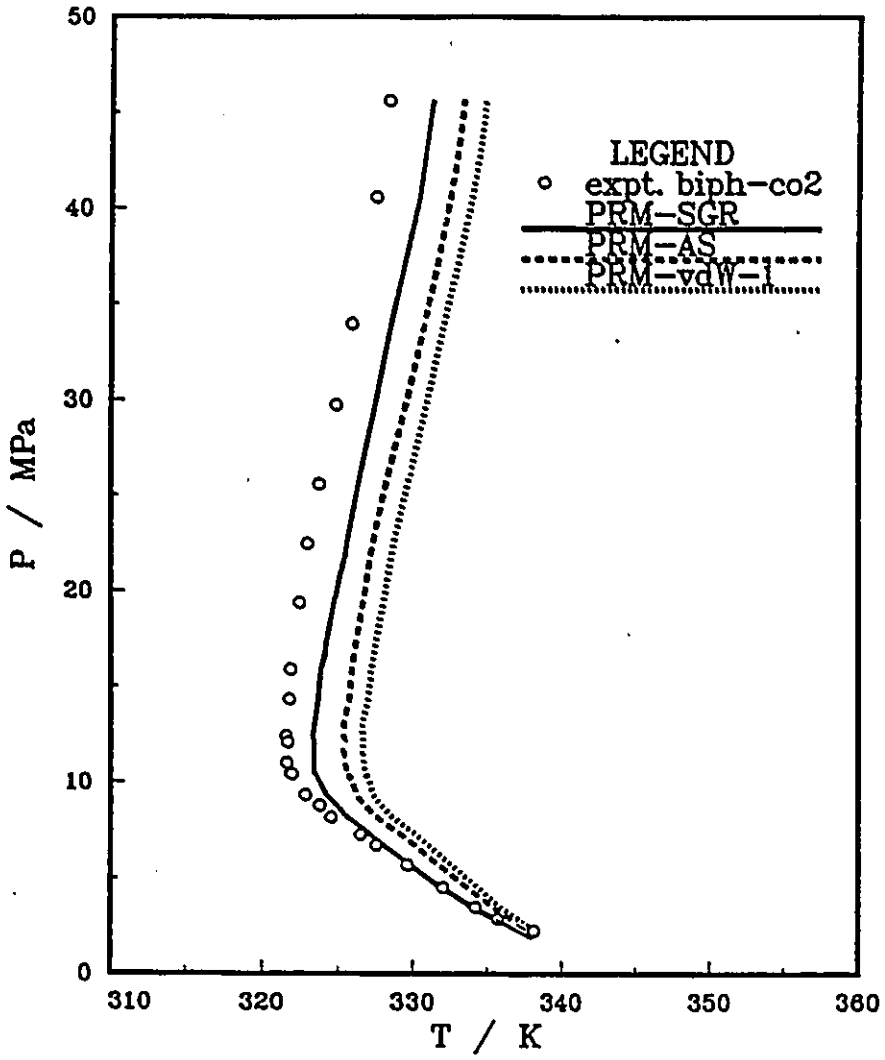

Figure 5.4: Comparison of Calculated and Experimental Results of P-T Values of S-L-G Equilibria for the Biphenyl-CO_2 Mixture.

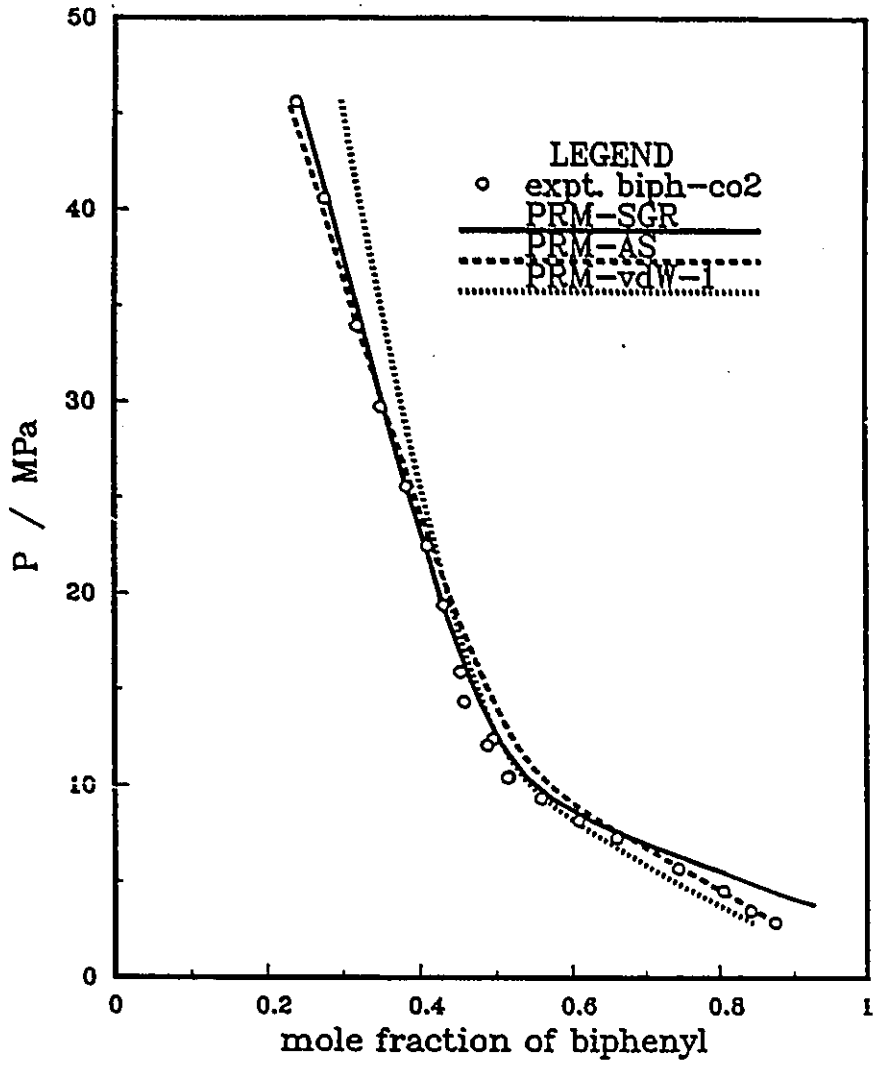

Figure 5.5: Comparison of Calculated and Experimental Results of P-x Values of S-L-G Equilibria for the Biphenyl-CO_2 Mixture.

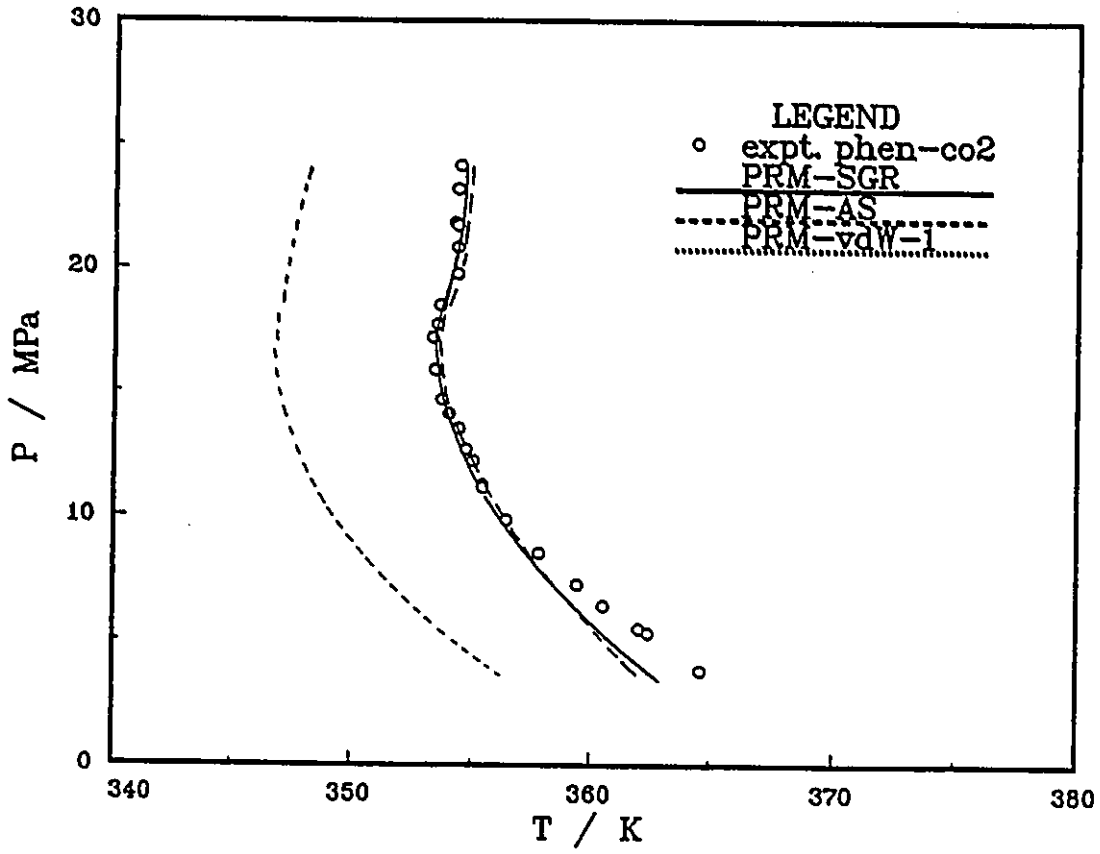

Figure 5.6: Comparison of Calculated and Experimental Results of P-T Values of S-L-G Equilibria for the Phenanthrene-CO_2 Mixture.

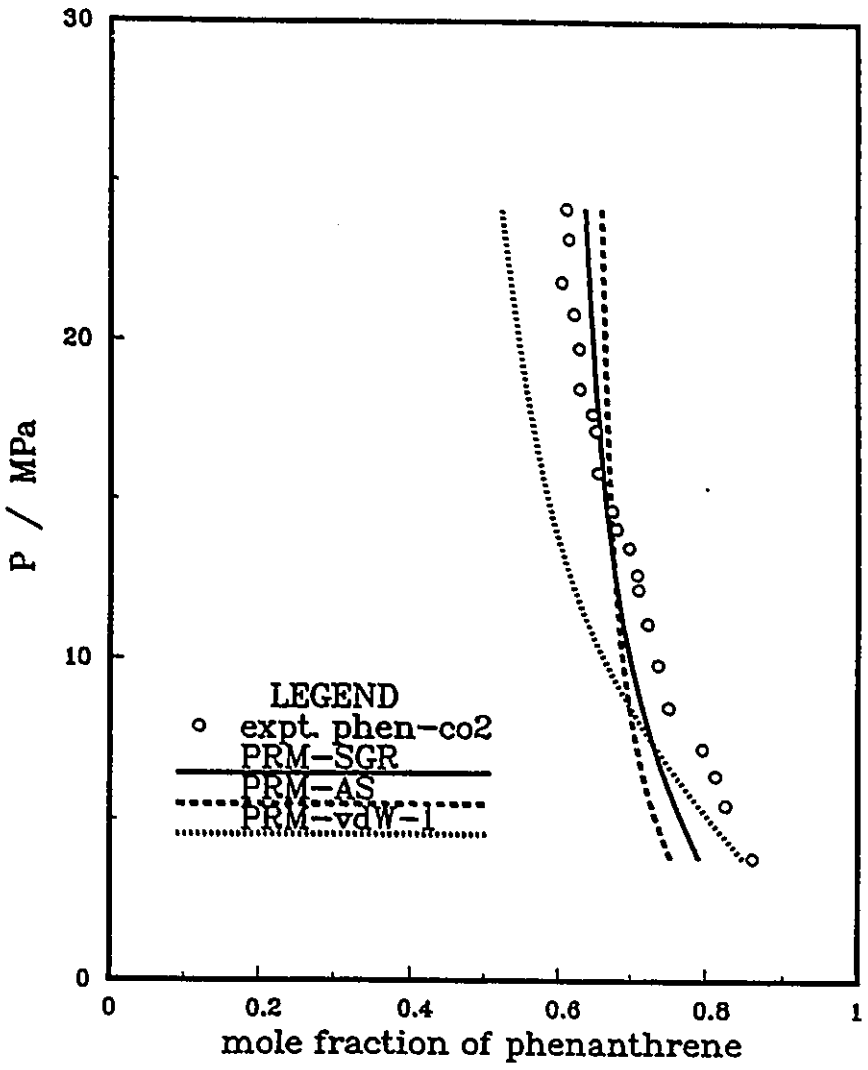

Figure 5.7: Comparison of Calculated and Experimental Results of P-x Values of S-L-G Equilibria for the Phenanthrene-CO_2 Mixture.

Table 5.1: Values of Interaction Parameters Used in the Correlation of the S-L-G Three-Phase Equilibria for the Binary Mixtures, Naphthalene-CO_2, Biphenyl-CO_2 and Phenanthrene-CO_2.

data point	equation	mixing rule	parameter k_{ij}	parameter l_{ij}	parameter m_{ij}
		Naphthalene-CO_2			
13	PRM	vdW-1	0.1051	-	-
	PR	AS	0.1170	0.0172	-
	PRM	AS	0.1270	0.0250	-
		Biphenyl-CO_2			
20	PRM	vdW-1	0.0962	-	-
		AS	0.1203	0.0316	-
		SGR	0.3029	0.2007	0.1407
		Phenanthrene-CO_2			
21	PRM	vdW-1	0.1309	-	-
		AS	0.0832	-0.5969	-
		SGR	-0.5060	-0.7140	0.1240

of freedom along the four-phase coexistence curve. Either temperature or pressure can be chosen as a fixed parameter in solving Eqs.(5.1-5.4). In this study, the iterative calculation of the four-phase equilibria was started with the pressure fixed. The fugacity of solid 1 and that of solid 2 at specified pressure and temperature, f_1^S and f_2^S, were both calculated using Eq.(5.5). With the assumed compositions for both the liquid and the gas phases, x_1°, x_2°, y_1° and y_2°, the fugacity coefficients of the heavy components, Φ_1^L, Φ_2^L, Φ_i^G and Φ_i^G, were calculated using Eqs.(3.16-3.18). The new composition values of the liquid and gas phases were determined from

$$x_i P \Phi_i^L = f_i^S \qquad i = 1,2 \tag{5.25}$$

$$y_i P \Phi_i^L = f_i^S \qquad i = 1,2 \tag{5.26}$$

Comparison of the composition values for both the liquid and the gas phases was then made to check if the assumed compositions were close enough to the calculated ones. In the next step, comparison of the liquid fugacity with the gas fugacity for the light component was made to check if the assumed temperature was right. The quasi-Newton method was used to find the minimum of the object function

$$FOB = \sum \left(\frac{T_j^{cal} - T_j^{exp}}{T_j^{exp}} \right)^2 \tag{5.27}$$

A flow diagram illustrating the algorithm used to calculate the S_1-S_2-L-G four-phase equilibria for ternary mixtures is shown in Figure 5.8.

The S_1-S_2-L-G four-phase equilibria have been calculated for the two ternary mixtures using the PRM equation with the vdW-1 mixing rule. The values of both k_{ij} and l_{ij} were obtained from the calculation of the S-L-G three-phase equilibria for the three binary mixtures, naphthalene-CO_2, biphenyl-CO_2 and phenanthrene-CO_2, respectively. The interaction parameter for the binary of two heavy components, k_{12}, was found from the fit of the P-T values of the S_1-S_2-L-G equilibria.

The calculated temperatures on the S_1-S_2-L-G curve for the naphthalene-biphenyl-CO_2 system agree with the experimental data to within 0.5°C on average

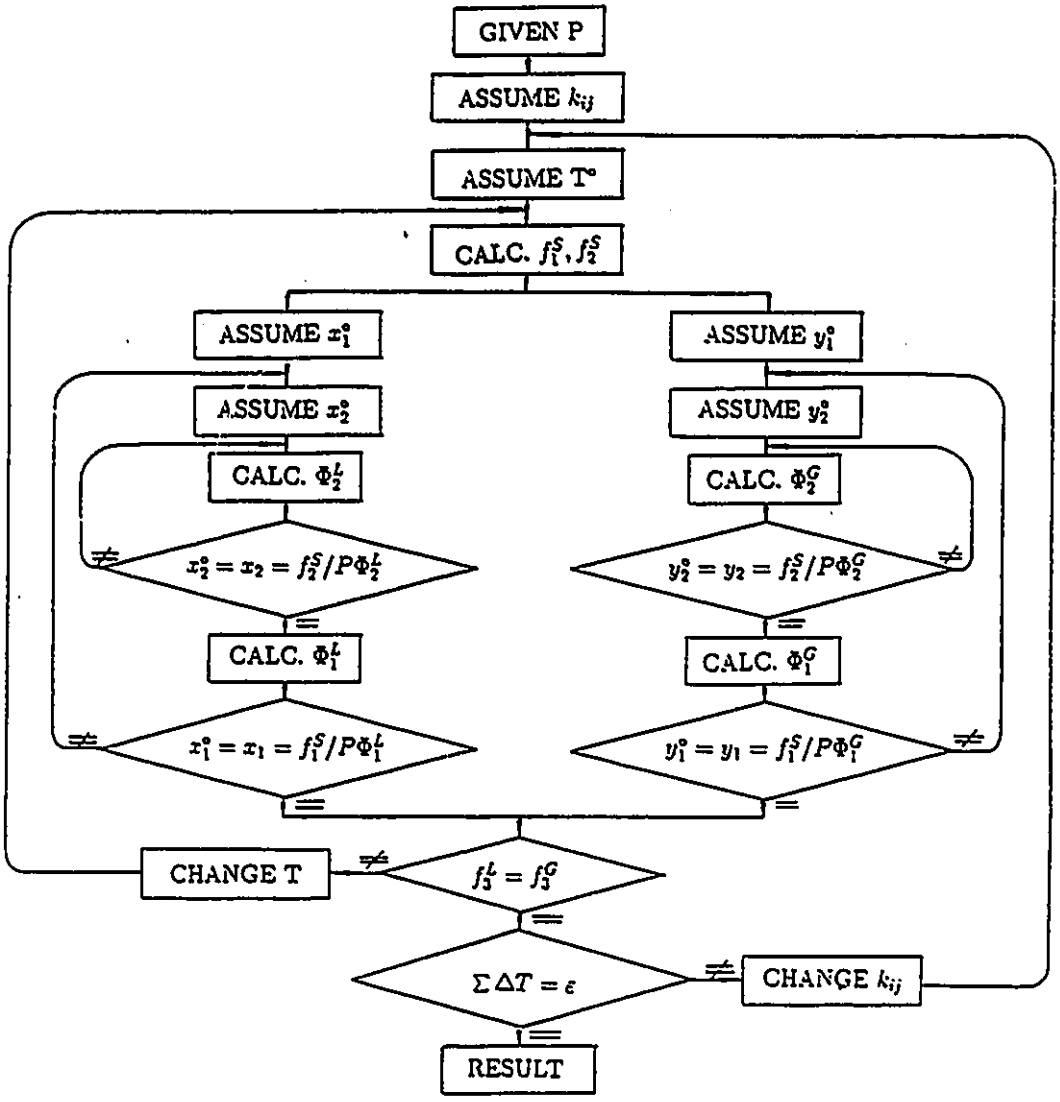

Figure 5.8: Flow Diagram of Computation Procedure Used for Determining the S_1-S_2-L-G Equilibria for Ternary Mixtures.

with k_{12}=0.0092 (see Figure 5.9). The calculation using the PRM equation with the AS or SGR mixing rule did not converge.

Using the same procedure, the calculation of the P-T values of the S_1-S_2-L-G equilibria for the naphthalene-phenanthrene-CO_2 system failed to converge. This is because the representation of the S-L-G equilibria for the binary mixture phenanthrene-CO_2 system using the PRM equation with vdW-1 mixing was unsatisfactory (see Figure 5.6).

5.2 A Combination of Activity-Coefficient Model and Equation-of-State Model for Solid-Liquid-Gas Equilibrium Calculation

In this section, the experiment P-T-x values of the S-L-G three-phase equilibrium data are correlated using a different approach in which a liquid-mixture model is used for calculating the activity coefficient of the heavy component in the liquid phase and the Peng-Robinson equation of state with the vdW-1 mixing rule is used for calculating the fugacity coefficients of both components in the gas phase.

Lemert and Johnston's method [103] in which the same assumptions were made as in the equation-of-state model, was adopted to calculate the S-L-G equilibria for the binary mixtures naphthalene-CO_2 and biphenyl-CO_2. The pressure was chosen as a fixed parameter. The iterative calculation started by assuming a value for temperature, T°. The composition of the heavy component in the gas phase was determined from Eq.(5.7). The composition of the liquid phase was then obtained from the liquid-gas equilibrium condition, Eq.(5.6). In the next step, the regular solution model was used to calculate the activity-coefficient of the heavy component in the liquid phase. The solubility parameters, 9.924 $(cal/ml)^{1/2}$ for naphthalene, 9.891 $(cal/ml)^{1/2}$ for biphenyl and 6.013 $(cal/ml)^{1/2}$ for CO_2 were obtained from

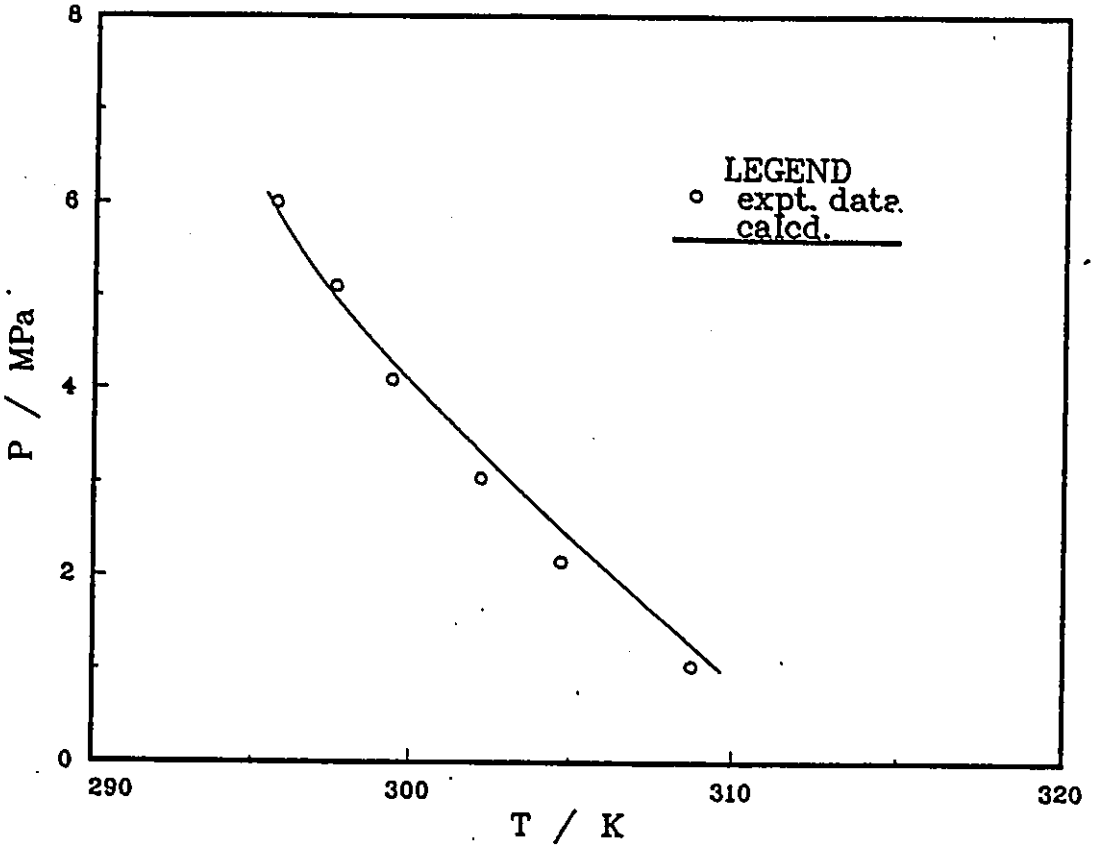

Figure 5.9: Comparison of Calculated and Experimental Results of P-T Projection of S_1-S_2-L-G Equilibria for Naphthalene-Biphenyl-CO_2 Mixture.

the literature [135]. The calculated temperature value was then determined from Eq.(3.22) which can be simplified by making the following assumptions:

1. the difference between the heat capacity of the heavy component in the liquid state and that in the solid state is neglected, i.e., $C_{p1}^{L} - C_{p1}^{S} = 0$;

2. the difference between the molar volume of the heavy component in the liquid state and that in the solid state, $v_1^L - v_1^S$, is independent of pressure.

Eq.(3.22) can then be rewritten as

$$-\ln x_1\gamma_1 = \frac{\Delta H_f}{R}\left(\frac{1}{T} - \frac{1}{T_m}\right) + \frac{(v_1^L - v_1^S)(P - P_1^{sat})}{RT} \tag{5.28}$$

The interaction parameter k_{12} in the vdW-1 mixing rule was found to be 0.107 for the naphthalene-CO_2 mixture and 0.099 for the biphenyl-CO_2 mixture by minimizing the object function expressed by Eq.(5.24).

The results are shown in Figures 5.10 and 5.11. The calculated temperatures on the S-L-G curve agree with the experimental data to within 1.0°C and 0.5°C on the average, and the calculated liquid compositions agree within 0.04 and 0.02 on the average for the naphthalene-CO_2 mixture and the biphenyl-CO_2 mixture, respectively.

5.3 Comparison of the Two Approaches Used in the Representation of S-L-G Equilibria

The Peng-Robinson equation of state with the modified correction factors α expressed in Eqs.(5.13 and 5.14) and the AS and SGR mixing rules represents successfully the P-T-x values of the S-L-G equilibria for the naphthalene-CO_2 mixture. The calculated temperatures agree with the experimental data to within 0.6°C on the average, and the calculated liquid phase compositions agree within 0.02 on the average. The experimental errors in the determination of temperature and mole fraction of the liquid phase composition are ±0.1°C and ±0.005 mole fraction.

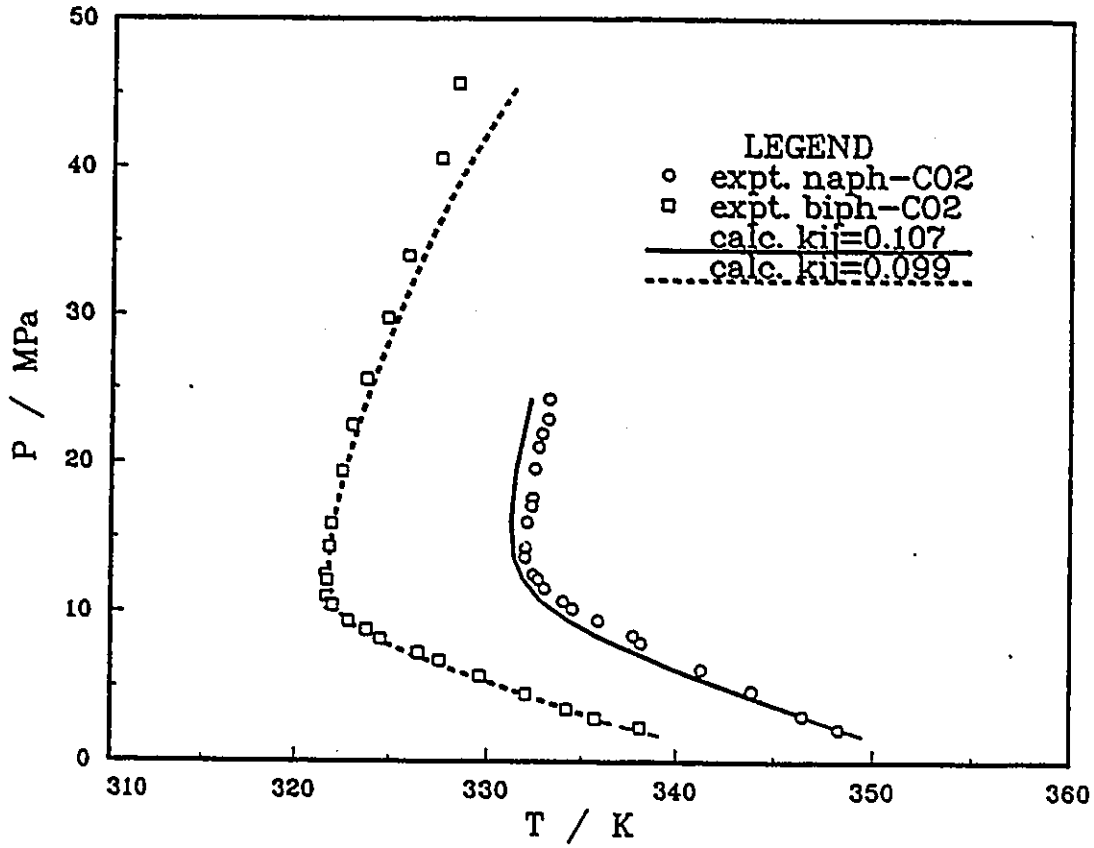

Figure 5.10: Comparison of Calculated and Experimental Results of P-T Values of S-L-G Equilibria for Two Binary Mixtures, Naphthalene-CO_2 and Biphenyl-CO_2 Using the Activity-Coefficient Model.

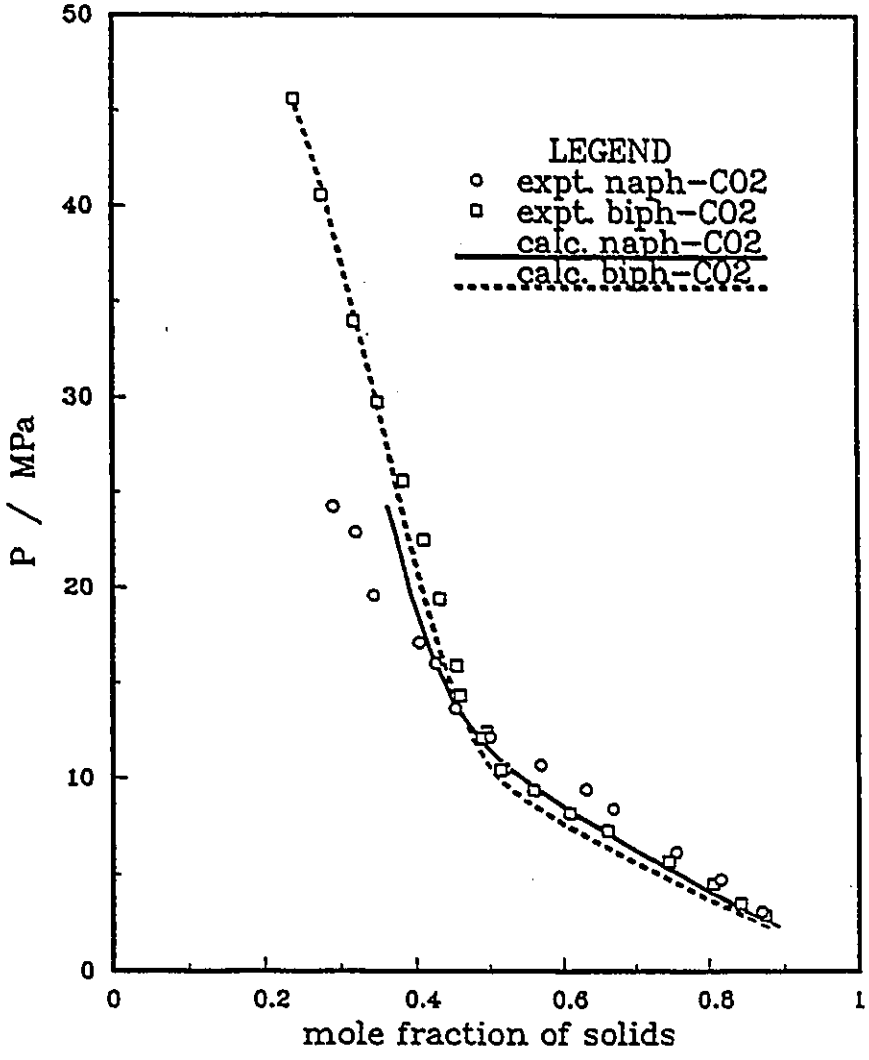

Figure 5.11: Comparison of Calculated and Experimental Results of P-x Values of S-L-G Equilibria for Two Binary Mixtures, Naphthalene-CO_2 and Biphenyl-CO_2 Using the Activity-Coefficient Model.

The calculated results for the biphenyl-CO_2 and the phenanthrene-CO_2 mixtures using the equation-of-state model was not as satisfactory as those for the naphthalene-CO_2 mixture. The good agreement in temperatures or in liquid phase compositions was obtained at the cost of failing in representing the liquid phase compositions or temperatures. The calculated results were very sensitive to the interaction parameters in each mixing rule. While the PRM equation with the AS or SGR mixing rule represents well the S-L-G three-phase equilibria for the binary mixtures consisting of supercritical carbon dioxide and an aromatic compound (naphthalene, biphenyl and phenanthrene), the PRM or PR equation with the vdW-1 mixing rule failed in the representation for such systems.

The activity-coefficient model represented the S-L-G three-phase equilibria for the biphenyl-CO_2 system better than the equation-of-state model did, though the correlation was not satisfactory in the high pressure region (above 40 Mpa). The advantage of the activity-coefficient model is that it needs only one constant k_{ij} and it is easy to achieve convergence in the calculation, i.e., a good initial guess of k_{ij} is not essential to the result. Simple liquid-mixture models, including the regular solution model, are often satisfactory. However, it is difficult to apply this method to the S_1-S_2-L-G four-phase equilibria for the ternary mixtures as well as in the liquid-gas critical region of the binary mixtures. Furthermore, the liquid-mixture model for the calculation of the activity coefficient requires extra parameters, such as the solubility parameter in the regular solution model, which may not be available.

On the contrary, the equation-of-state model needs neither standard states nor the extra parameters for the fugacity and is easily applied to the S_1-S_2-L-G four-phase equilibria for the ternary mixtures as well as to the critical region. The advantage of the equation-of-state model is that it requires only the vapor pressures and the critical properties of the components. However, the equation-of-state model can not represent the multiphase equilibria involving a solid phase if only one constant interaction parameter is employed. Divergence is the main problem when a

poor initial guess for the interaction parameter is chosen. With the AS or SGR mixing rule, the PRM or PR equation failed to converge in representing the S_1-S_2-L-G equilibria for the highly asymmetric ternary systems such as naphthalene-biphenyl-CO_2 and naphthalene-phenanthrene-CO_2.

It appears that these two approaches both are of limited use in correlating and predicting multiphase equilibria involving a solid phase or phases. Fundamentally based thermodynamic models with more insight into the supercritical solvent-solid solute interactions need to be developed in the future.

5.4 Correlation of Solubility Data of Supercritical CO_2 in Liquid Naphthalene and Biphenyl

The solubility data of supercritical CO_2 in the liquids naphthalene and biphenyl were correlated to determine the optimum interaction parameter for the Peng-Robinson [97] equation of state with three different mixing rules, and to assess their abilities to represent the data. The two-parameter van der Waals-type mixing rule (vdW-2), the mixing rules proposed by Adachi-Sugie (AS) [141] and Schwartzentruber et al. (SGR) [142] were chosen for the evaluation.

The two-parameter van-der-Waals-type mixing rule (vdW-2) is defined by:

$$\begin{aligned} a &= \sum_i \sum_j x_i x_j a_{ij} \\ a_{ij} &= (a_i a_j)^{1/2}(1-k_{ij}) \\ b &= \sum_i \sum_j x_i x_j b_{ij} \\ b_{ij} &= \frac{1}{2}(b_i+b_j)(1-l_{ij}) \end{aligned} \tag{5.29}$$

Accordingly, the expression for the fugacity coefficient of component i in the mixture is given by:

$$\ln \Phi_i = \left(\frac{b_i'}{b}-1\right)(z-1)-\ln(z-B)-\frac{A}{2.828B}\left(1+\frac{a_i'}{a}-\frac{b_i'}{b}\right)\ln\left(\frac{z+2.414B}{z-0.414B}\right) \tag{5.30}$$

where

$$A = aP/(RT)^2, \qquad B = bP/RT \tag{5.31}$$

$$a'_i = 2\sum_j x_j a_{ji} \qquad b'_i = 2\sum_j x_j b_{ji} \tag{5.32}$$

The optimum values of the parameters k_{ij}, l_{ij} and m_{ij} were obtained by minimizing the sum of the squares of the differences between the calculated and experimental bubble point pressures. The calculated results are shown in Table 5.2 where ΔP is defined by

$$\Delta P = \frac{1}{n}\sum_{j=1}^{n}\left|\frac{P_j^{cal} - P_j^{exp}}{P_j^{exp}}\right| \times 100 \tag{5.33}$$

Table 5.2 reveals that among the three mixing rules, the SGR mixing rule gives the best fit of the experimental data with the "crossover region" for the biphenyl-CO_2 system predicted at ~36 MPa as shown in Figure 5.12a. The Peng-Robinson equation of state with AS mixing rule yields virtually the same results as that with the vdW-2 mixing rule. The values of k_{ij} and m_{ij} in the AS and SGR mixing rules increase as the temperature decreases, while the l_{ij} values increase with the temperature. A comparison of the calculated results by the Peng-Robinson equation with the SGR mixing rule and the AS mixing rule are shown in Figure 5.12.

5.5 Some Comments on the Correlation of Liquid-Gas Critical Loci

An attempt at correlating the critical-mixture data of the naphthalene-CO_2 and biphenyl-CO_2 mixtures obtained in this study using the Peng-Robinson equation of state was fruitless due to the divergence encountered in the calculations. The correlation and prediction of liquid-gas critical loci is very difficult for highly asymmetric systems where the molecular size, shape and structure as well as the critical conditions for the components differ significantly. The modeling of the phase behavior in the vicinity of the upper critical end point, where the liquid-gas critical curve

Table 5.2: Correlation of the Solubility Data for Two Binary Mixtures, Naphthalene-CO_2 and Biphenyl-CO_2.

T	Max.	No. of	mixing	parameter			dev. in press.
(K)	pressure	data	rule	k_{ij}	l_{ij}	m_{ij}	ΔP
			Biphenyl-CO_2				
343.2	41 Mpa	22	vdW-2	0.0764	-0.0370	-	6.62
			AS	0.1320	0.0395	-	6.45
			SGR	0.1089	0.0260	0.6850	3.59
338.2	44 Mpa	17	vdW-2	0.0785	-0.0336	-	7.72
			AS	0.1249	0.0319	-	6.94
			SGR	0.1029	0.0198	0.7253	4.46
332.2	47 MPa	14	vdW-2	0.0817	-0.0250	-	8.02
			AS	0.1136	0.0212	-	6.79
			SGR	0.0913	0.0138	0.8406	3.74
			Naphthalene-CO_2				
348.2	27 MPa	19	vdW-2	0.0790	-0.0365	-	4.52
			AS	0.1275	0.0346	-	4.15
			SGR	0.1141	0.0263	0.6495	3.68
343.2	27 MPa	13	vdW-2	0.0802	-0.0287	-	5.37
			AS	0.1189	0.0276	-	5.28
			SGR	0.0985	0.0176	0.7479	3.64
338.2	27 MPa	11	vdW-2	0.0830	-0.0097	-	3.23
			AS	0.0954	0.0088	-	3.24
			SGR	0.0877	0.0041	0.7725	3.09

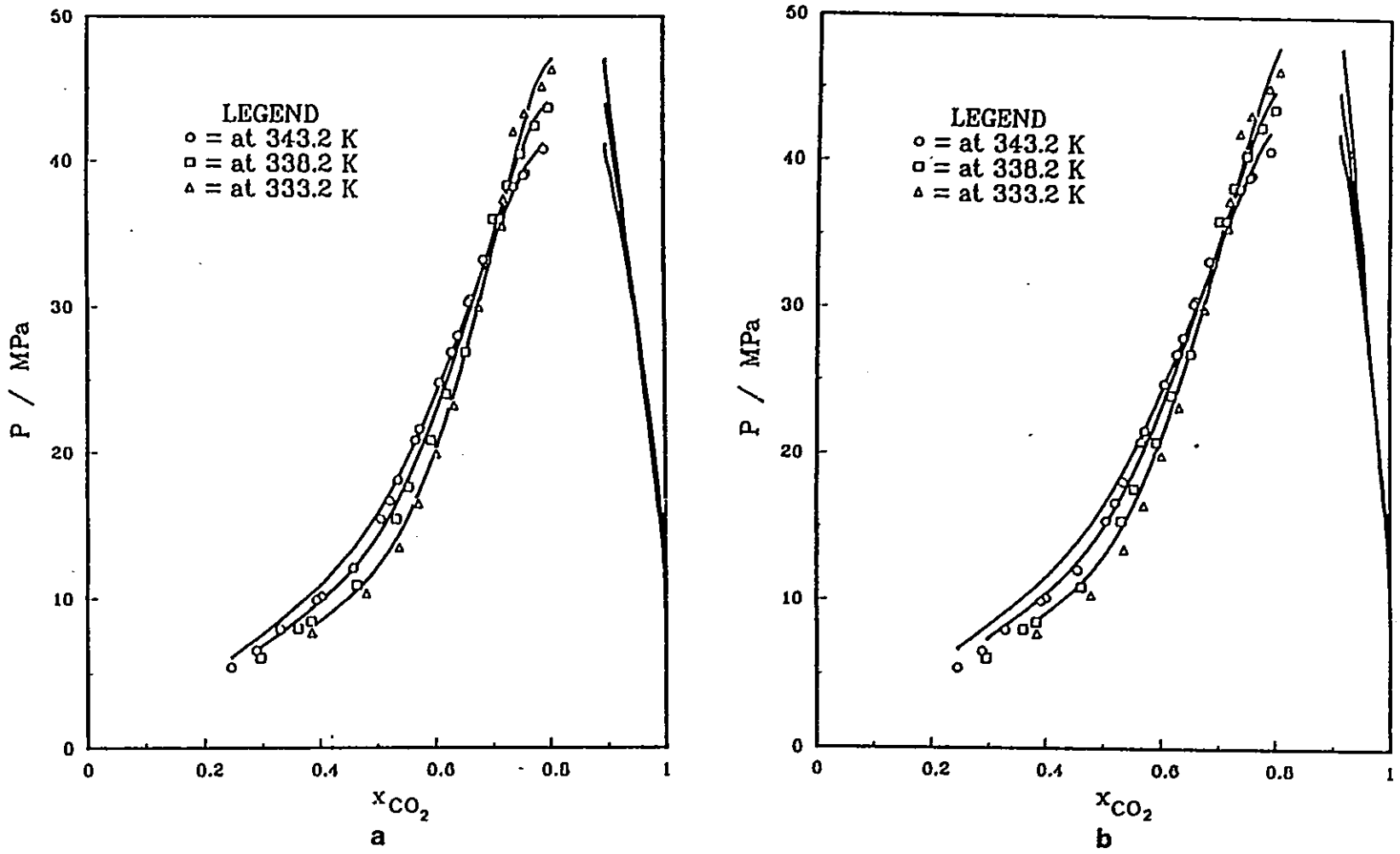

Figure 5.12: Comparison of Calculated Results of the Solubility Data for the Biphenyl-CO_2 Mixture. (a): Results with SGR Mixing Rule; (b): Results with AS Mixing Rule.

intersects the solid-liquid-gas three-phase curve, is extremely hard. The experimental critical-mixture data obtained in this study for both naphthalene-CO_2 and biphenyl-CO_2 systems are very close to their upper critical end points (see Figures 5.13 and 5.14).

The possible solution for overcoming the difficulty may require a more sophisticated model than the simple cubic equation of state. The desired model, such as the statistical thermodynamic model, requires more insight into the supercritical solvent-solid solute interaction, which, in consequence, may require a knowledge of fundamental physico-chemical properties of both solvent and solute, such as intermolecular potential function, collision diameter, and geometric parameters. Such information is, unfortunately, not sufficient or not available in the literature at present.

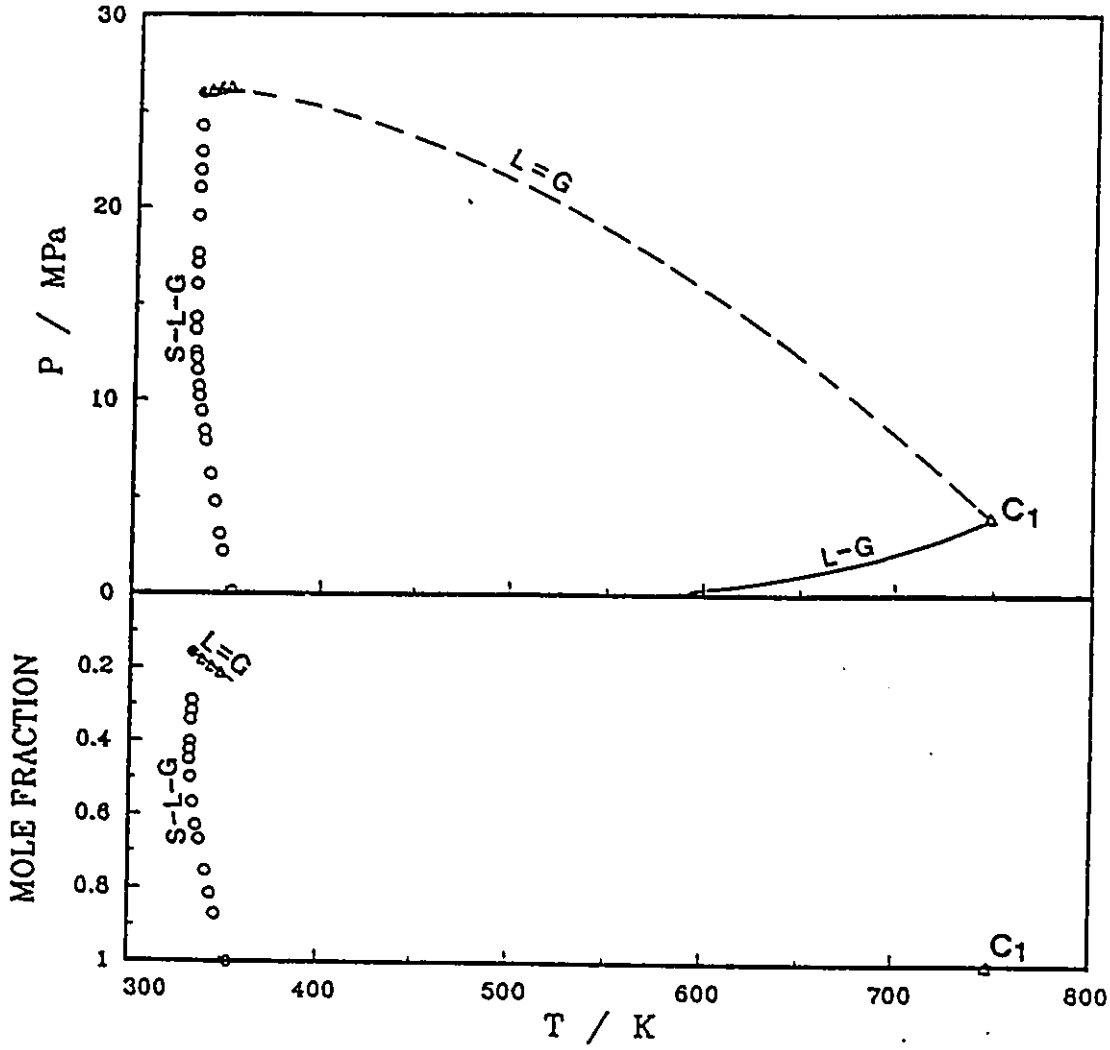

Figure 5.13: Experimental P-T-x Values of S-L-G Equilibria and L=G Critical Loci for the Naphthalene-CO_2 Mixture.

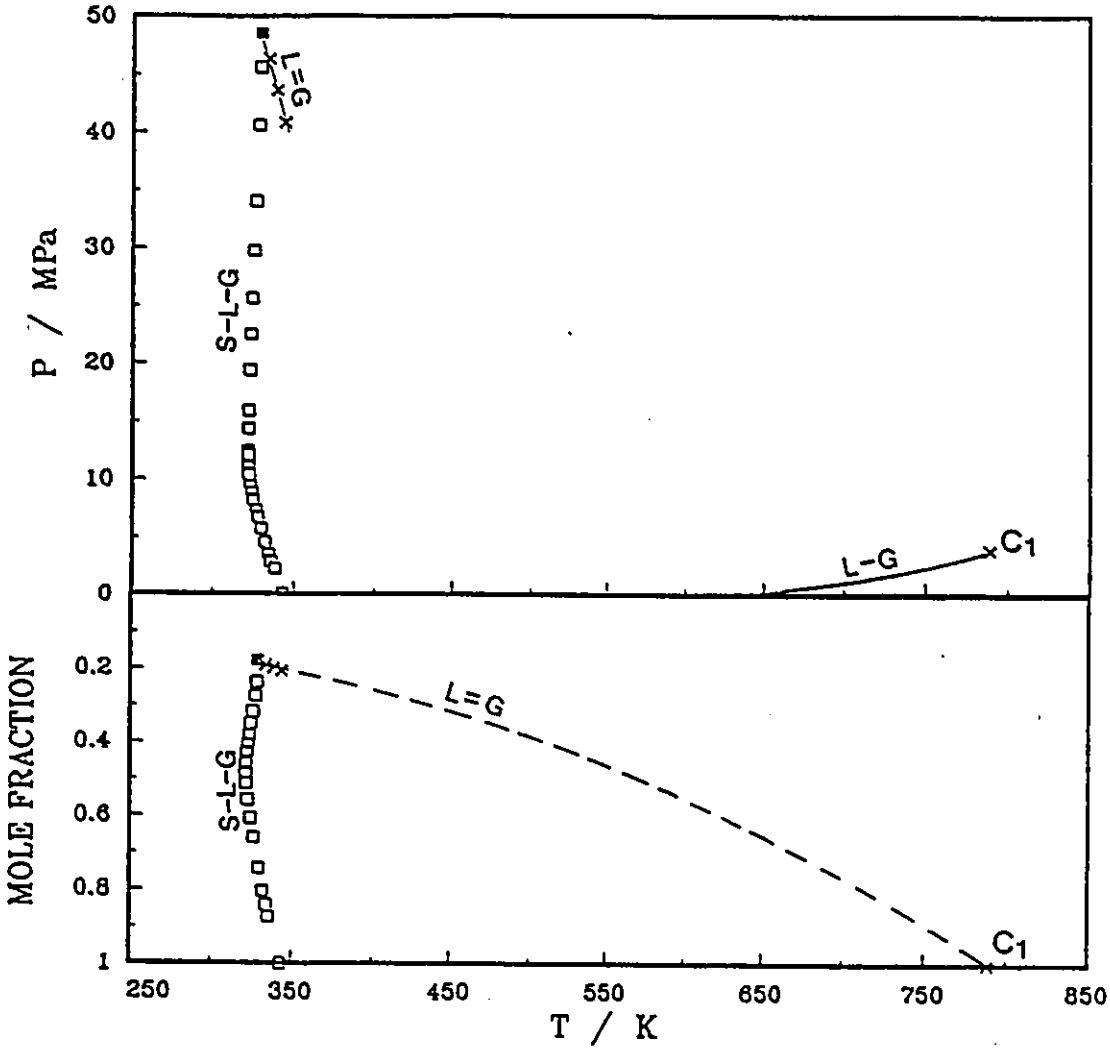

Figure 5.14: Experimental P-T-x Values of S-L-G Equilibria and L=G Critical Loci for the Biphenyl-CO_2 Mixture.

Chapter 6

DISCUSSION OF RESULTS

In this chapter, the experimental results of the "first freezing point" method are compared with those of the "first melting point" method. The advantages of the proposed new technique are pointed out. The freezing point depression of solids under the pressure of a supercritical solvent and the solubility behavior of supercritical mixtures in the vicinity of the critical end points are discussed using the data obtained in this study.

6.1 The Merits of the First Freezing Point Method

For the determination of the three-phase S-L-G equilibria, a new technique called the "first freezing point" method has been developed in this study. This new technique provides a quick and reliable determination of the pressure-temperature-liquid composition (P-T-x) data along the three-phase S-L-G coexistence curves.

Compared with the " first melting point" method [11,65,66], the " first freezing point" method provides more self-consistent results. Figure 6.1 shows the pressure-temperature values of the S-L-G equilibria determined by the "first melting point" method for two binary mixtures, naphthalene-CO_2 and biphenyl-CO_2. Figure 6.2 presents the results obtained from several independent runs in this study using the "first freezing point" method for the same systems. The first formation of the solid

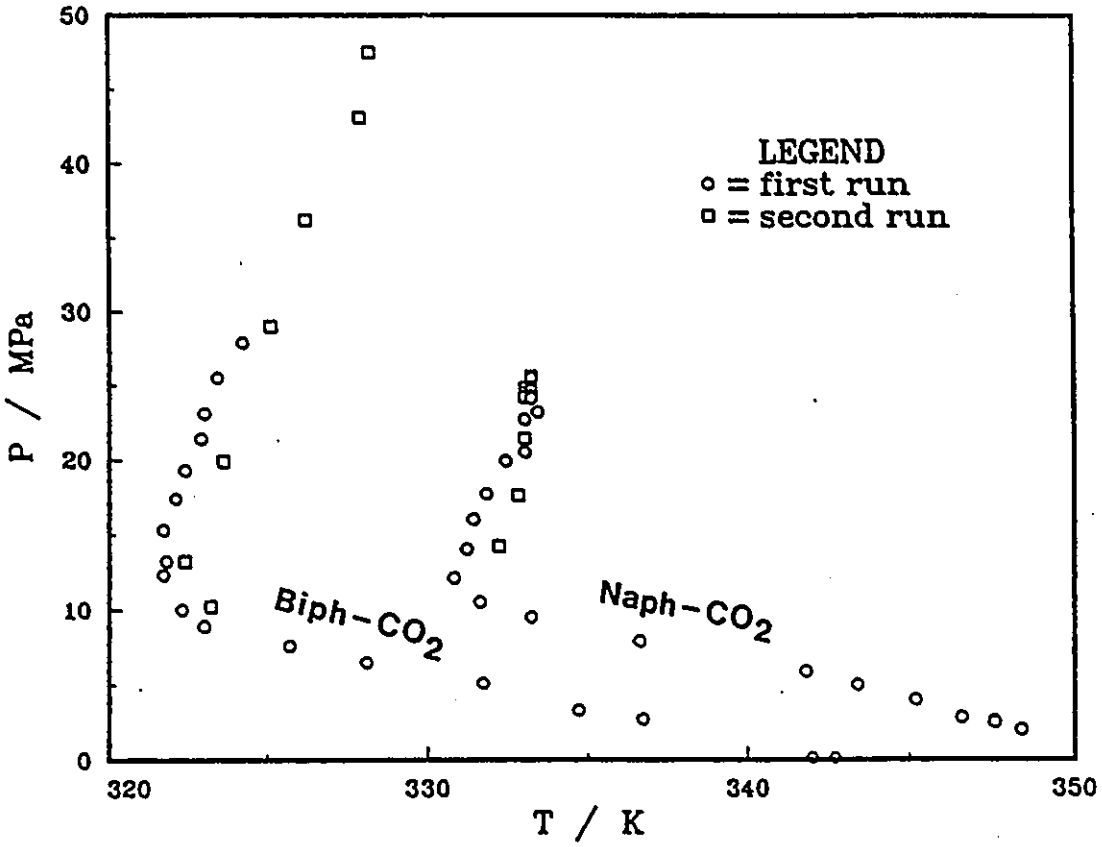

Figure 6.1: Pressure-Temperature Values of the S-L-G Equilibria Determined by the "First Melting Point" Method for the Binary Mixtures Naphthalene-CO_2 and Biphenyl-CO_2 [S4,66].

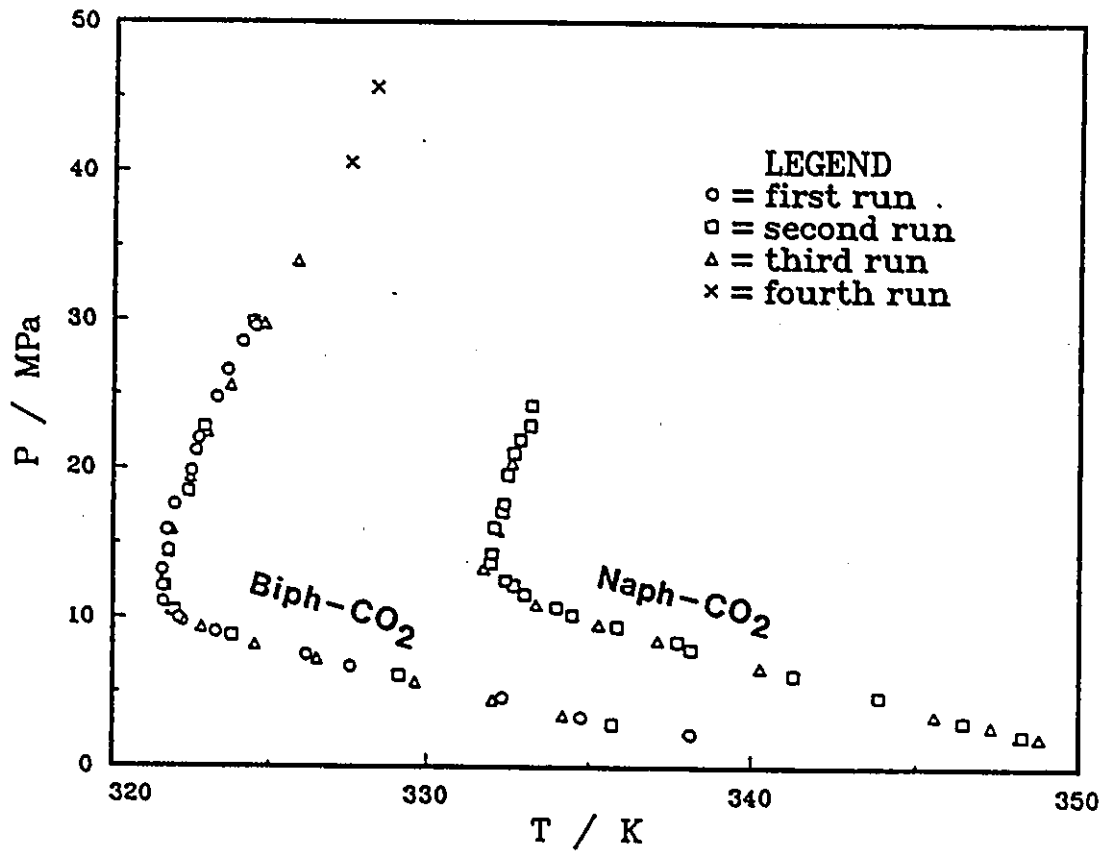

Figure 6.2: Pressure-Temperature Values of the S-L-G Equilibria Obtained from Serveal Independent Runs in This Study Using the "First Freezing Point" Method for the Binary Mixtures Naphthalene-CO_2 and Biphenyl-CO_2.

crystals can be observed precisely in the dual window equilibrium cell. According to the phase rule, the first melting point and the first freezing point of the three-phase S-L-G equilibria are the same since there is only one degree of freedom along the equilibrium line.

At the beginning of this study, the " first melting point" method was adopted in the determination of the S-L-G equilibria. The scattering of the pressure-temperature data was also experienced in our work. It is believed that the uniformity of the liquid composition can not be ensured when the solid begins to melt because of difficulties encountered in agitating the mixture in the cell. The results for the P-T values of the S-L-G equilibria obtained in this work using the "first freezing point" method are in good agreement with those of Prins [11] for the binary mixtures, naphthalene-CO_2 and biphenyl-CO_2 (see Figures 4.2 and 4.3), indicating that the proposed method has its merit. It should be mentioned that all the data points of Prins were obtained from graphical interpolations. As noted recently by Mchugh et al. [100], the first melting point technique leads to spurious results at high pressures.

Compared with the static solubility measurement, the new technique developed in this study provides a much quicker and easier way to determine directly the equilibrium liquid composition. The gas compositions of the three-phase equilibria were not determined in this work. These values are, however, less important than the liquid compositions in the test and development of the thermodynamic models, since the gas phase is virtually supercritical carbon dioxide.

During the course of this study, further effort was made to improve the performance of the first freezing point technique. The experimental set up was modified to reduce the dead space of the equilibrium cell and the time required for the mixture in the cell to reach equilibrium. The magnetic stirrer was replaced by a magnetic pump which recirculated the mixture in the cell when it was in the fluid state. A temperature controlled air bath replaced the water bath to improve the visibility of

the contents in the equilibrium cell. The new experimental set up (the maximum working pressure is 69.0 MPa) is also suitable for further investigation at a higher pressure condition.

To verify the new experimental set up, the S-L-G three-phase equilibria were determined for the systems naphthalene-ethylene and biphenyl-ethylene [137]. The results of the P-T projection of the three-phase curve agreed well with those in the literature [65,75,81,66].

For the binary mixture phenanthrene-carbon dioxide, the experimental P-T values of the three-phase equilibria obtained in this study differ from that reported recently by White and Lira [121] (see Figure 4.8). Their data seem not consistent when the S-L-G three-phase line is extended to the normal freezing point of the pure phenanthrene in the P-T projection. Besides, in our observation both liquid and gas phases existed at pressures above 9 MPa. The phenomenon of the UCEP near 9 MPa and 356 K, as reported by White and Lira, was not observed in this study.

6.2 Freezing Point Depression Under the Pressure of a Supercritical Fluid

The melting curve of a pure solid represents an monovariant two-phase (S-L) equilibrium. In general, the melting temperature of the solid rises, in some cases even steeply, with an increase of pressure, except for some pure substances whose volume decreases on melting. If a supercritical solvent is added to this equilibrium, a three-phase (S-L-G) equilibrium will be established at a variety of pressures. The melting curve of the solid usually bends towards a lower temperature, appearing the so-called "freezing point depression". Under the pressure of the supercritical solvent, this new melting curve is represented by a solid-liquid-gas three-phase coexistence curve and exhibits different shapes depending on the binary systems.

As classified by Lu and Zhang [119], and reported previously in Section 2.1, there are two types of phase behavior: a continuous three-phase S-L-G curve, and two branches of the S-L-G curve intersected by the critical mixture curve at the lower critical end point (LCEP) and the upper critical end point (UCEP). The latter can be further classified into three categories according to the shape of the higher-temperature branch of the S-L-G curve: a negative slope, a negative slope at the beginning and then positive slope, and a positive slope of the S-L-G curve (see section 2.1) in the P-T projection.

The available data indicate that there is a temperature minimum on the S-L-G coexistence curve for binary mixtures of carbon dioxide as the supercritical fluid with naphthalene, biphenyl, m-terphenyl, phenanthrene or octacosane as the slightly volatile component; and that there is a negative slope of the S-L-G curve for binary mixtures of ethylene as the supercritical fluid with naphthalene, biphenyl, hexachloroethane or octacosane as the slightly volatile component [119].

In this section the reason for the freezing point depression of a solid under the pressure of a supercritical fluid, and the different shapes of the S-L-G curves are discussed. The discussion is restricted to the phase behavior of systems composed of one supercritical fluid and one solid component whose triple point is higher than the critical point of the supercritical fluid. For SFE operations, these systems have more interesting phase behavior.

6.2.1 Pressure Effects on the Freezing Point Depression of Solid

The pressure of a supercritical fluid (SCF) has two opposite effects on the freezing point depression of a solid. The increase in hydrostatic pressure causes a rise in freezing point of the solid as long as the volume of the solid increases on melting. On the other hand, the solubility of the gaseous SCF in the liquid phase increases as the pressure increases. Dissolution of the SCF in the liquid phase lowers the

freezing point of the otherwise pure solid. The resultant of these two opposite effects of pressure on the freezing temperature of the solid causes the different shapes of the P-T projection of the S-L-G curves.

As the pressure is elevated from the triple point of the solid, the supercritical solvent starts to dissolve in the liquid phase to form a solution with the slightly volatile component. The S-L-G curve will move initially to lower temperatures as the freezing point is depressed, if the hydrostatic-pressure effect is not strong enough to raise the freezing point of the solid. In the lower pressure range, there exists a linear relationship between pressure and liquid composition (see Figure 4.11, for example). The freezing-point-depression effect due to the dissolution of the supercritical solvent is dominant at this stage. If the pressure is increased further, the dissolution rate of the supercritical solvent slows down, and so does the freezing temperature depression of the solid. However, the hydrostatic-pressure effect is becoming stronger as the pressure is increased, and could finally become the dominant effect. The temperature minimum appears on the P-T projection of the S-L-G curve as a consequence. At $T = T_{min}$, $\frac{dT}{dP} = 0$.

For binary mixtures, such as naphthalene-ethylene and biphenyl-ethylene, the solubility of supercritical ethylene in the liquid phase increases steeply over the entire pressure range from the triple point of the solid to the UCEP [81,137]. Under the operating conditions, the freezing-point-depression effect due to the dissolution of ethylene in the liquid phase plays a more important role than the hydrostatic-pressure effect. Consequently the freezing point depression curve of the solid, or the S-L-G curve has a negative slope in its P-T projection.

Examples of the S-L-G curve with a positive slope in P-T projection are found in the literature for binary gas mixtures at cryogenic conditions, such as hydrogen-carbon dioxide [70] and neon-argon [71]. In the case of the hydrogen-carbon dioxide mixture, hydrogen was the supercritical solvent, while in the case of neon-argon mixture, neither of the components was under supercritical conditions. The hydro-

static pressure effect was the dominant force over the entire pressure range up to 200 MPa for these two binary mixtures.

The phase behavior of binary mixtures consisting of supercritical carbon dioxide and an aromatic compound, studied in this work, belongs to another category. The solubility of CO_2 in the liquid phase increases quickly at the beginning and then reaches a limiting value as the pressure increases. In different pressure ranges, the shape of the S-L-G curve is dominated by either the freezing-point-depression effect due to the dissolution of supercritical carbon dioxide or the hydrostatic-pressure effect. A temperature minimum occurs in the P-T projection of the S-L-G curve as a result of the two opposing effects.

6.2.2 Effect of the Melting Point of Aromatic Compound on the Freezing Point Depression

The aromatic compounds chosen in this study are comprised of either two benzene rings (naphthalene and biphenyl) or three benzene rings (m-terphenyl and phenanthrene). From the limited results obtained in this work, it is found that the freezing point depression is affected by the solubility of supercritical CO_2 in the melted aromatic compound, which is related to its normal melting point.

In the low pressure region (below 10 MPa), the solubility of CO_2 in the liquid phase of each aromatic compound increases rapidly with pressure (see Figure 4.11). The S-L-G three-phase curves, or the freezing point depression curves have almost the same trend towards the lower temperature range (see Figure 4.10). However, as the pressure is increased further, the rate of absorption of CO_2 in the liquid phase become slow. In the cases of m-terphenyl-CO_2 and phenanthrene-CO_2 systems with relatively higher melting temperatures of the solids, the solubilities of CO_2 in the liquid phase are low and quickly reach limiting values with increase of pressure. The curvatures of the freezing point depression curves for these two systems are less than those for the other two systems.

It appears that the lower the melting point of the aromatic compound, the higher the solubility of supercritical CO_2 in the liquid phase, and the more significant the curvature of the freezing point depression curve.

6.2.3 The Slope of the S-L-G Curve at the Triple Point of Solid

The quantitative description of the slope of the S-L-G curve in the vicinity of the triple point of the solid can be obtained from a thermodynamic analysis. For the melted solid-supercritical solvent solution, the temperature as a function of pressure and composition is expressed by

$$dT = \left(\frac{\partial T}{\partial x}\right)_P dx + \left(\frac{\partial T}{\partial P}\right)_x dP \tag{6.1}$$

where x is the mole fraction of the solid in the liquid phase.

In the vicinity of the triple point of the solid, the solubility of the supercritical solvent in the liquid phase is quite small due to the low system pressure. It is safe to assume that the liquid solution obeys the ideal-solution law. Hence,

$$\hat{f}_i = x_i f_i \tag{6.2}$$

where f_i and $\hat{f}_i$ identify the fugacity of pure species i and that of species i in the solution, respectively.

Eq.(6.2) can also be written as

$$\ln \hat{f}_i = \ln x_i + \ln f_i \tag{6.3}$$

Taking the derivatives of both sides of Eq.(6.3) with respect to T at constant P:

$$\left(\frac{\partial \ln \hat{f}_i}{\partial T}\right)_P = \left(\frac{\partial \ln x_i}{\partial T}\right)_P + \left(\frac{\partial \ln f_i}{\partial T}\right)_P \tag{6.4}$$

and using the thermodynamic relationships:

$$\left(\frac{\partial \ln \hat{f}_i}{\partial T}\right)_P = -\frac{\bar{H}_i - H_i^*}{RT^2} \tag{6.5}$$

and

$$\left(\frac{\partial \ln f_i}{\partial T}\right)_P = -\frac{H_i - H_i^*}{RT^2} \tag{6.6}$$

the following expression is found:

$$\frac{1}{x_i}\left(\frac{\partial x_i}{\partial T}\right)_P = \frac{H_i - \bar{H}_i}{RT^2} \tag{6.7}$$

where H_i^* is the molar enthalpy of species i in the ideal gas state; H_i is the molar enthalpy of pure species i at the system temperature and pressure, $H_i = H_i^L$ and $\bar{H}_i$ is the partial molar enthalpy of species i in the ideal solution, $\bar{H}_i = \bar{H}_i^{id} = H_i^S$.

Omitting subscript i, Eq.(6.7) can then be written:

$$\left(\frac{\partial x}{\partial T}\right)_P = \frac{x\Delta H_f}{RT^2} \tag{6.8}$$

where the enthalpy of fusion $\Delta H_f = H^L - H^S$.

Substituting Eq.(6.14) along with the Clapeyron equation

$$\frac{dP}{dT} = \frac{\Delta H_f}{T\,\Delta v_m} \tag{6.9}$$

where Δv_m is the change in volume of the pure solid at melting point T_m, i.e., $\Delta v_m \equiv v^L - v^S$, in the first and second terms of Eq.(6.1), the following expression can be obtained:

$$dT = \frac{RT^2}{x\,\Delta H_f}dx + \frac{T\,\Delta v_m}{\Delta H_f}dP \tag{6.10}$$

Substituting Henry's law

$$dP = kd(1-x) = -kdx \tag{6.11}$$

where k is Henry's coefficient, into the above equation, we obtain:

$$dT = -\frac{RT^2}{kx\,\Delta H_f}dP + \frac{T\,\Delta v_m}{\Delta H_f}dP \tag{6.12}$$

or

$$\frac{dP}{dT} = \frac{kx\,\Delta H_f}{kx\,\Delta v_m T - RT^2} \tag{6.13}$$

At the triple point where T=T_m and x=1, the slope of the S-L-G curve becomes the so-called Ipat'ev's equation [136]:

$$\frac{dP}{dT} = \frac{k \Delta H_f}{k \Delta v_m T_m - R{T_m}^2} \tag{6.14}$$

From the experimental work in this study, a linear relationship between pressure and liquid composition on the S-L-G curve is observed for the binary mixtures, naphthalene-CO_2 and biphenyl-CO_2 up to about 10 MPa, and phenanthrene-CO_2 and m-terphenyl-CO_2 up to about 5 MPa (see Figure 4.11). The corresponding Henry's coefficients are found to be 24.5 MPa for the naphthalene-CO_2 mixture, 21.0 MPa for the biphenyl-CO_2 mixture, 26.0 MPa for the phenanthrene-CO_2 mixture, and 23.0 MPa for the m-terphenyl-CO_2 mixture from the experimental results in this study (see Figure 4.11). With the values of ΔH_f=19.30 kJ/mol, Δv_m=18.7 cm^3/mol and T_m=353.37 K for naphthalene and ΔH_f=18.60 kJ/mol, Δv_m=24.77 cm^3/mol and T_m=342.4 K for biphenyl (see Table 4.17, the value of Δv_m for naphthalene is from [138], and that for biphenyl is estimated from its liquid and solid densities), the slope of the S-L-G curve at the triple point of the solid can be calculated from Eq.(6.14) for the mixture naphthalene-CO_2

$$\frac{dP}{dT} = -0.54 \qquad MPa/K \tag{6.15}$$

and for the mixture biphenyl-CO_2

$$\frac{dP}{dT} = -0.49 \qquad MPa/K \tag{6.16}$$

These results are in good agreement with the values found from the measurements of the P-T projections of the S-L-G curves: -0.53 MPa/K for the naphthalene-CO_2 mixture and -0.43 MPa/K for the biphenyl-CO_2.

6.3 Phase Behavior in the Vicinity of the Critical End Points

The phase behavior of supercritical systems in the vicinities of both the lower critical end point (LCEP) and the upper critical end point (UCEP) is of interest. While the LCEP offers mild solvent power, the UCEP provides greater solubility enhancement. The solubility phenomena near the UCEP are especially important to the supercritical extraction process.

Thermodynamics enable us to predict the dramatic changes of the solubility of a solid in a supercritical fluid phase with small changes of pressure at temperatures close to the LCEP and the UCEP temperatures.

6.3.1 Inflection Point of the Solid-Fluid Equilibrium Line at the Critical End Points

At the LCEP and UCEP temperatures, the solubility of the solid in the fluid phase increases dramatically as the pressure approaches the critical end point pressures, which are depicted by horizontal inflections, as shown in Figures 2.2-2.4. At both LCEP and UCEP, the derivative $\left(\frac{\partial P}{\partial y}\right)_{T_{UCEP}} = \left(\frac{\partial P}{\partial y}\right)_{T_{LCEP}} = 0$. This is demonstrated by thermodynamic analysis in the following section.

At solid-fluid equilibrium, the chemical potential of the solid in each phases must be equal:

$$\mu_1^S(T,P) = \mu_1^F(T,P,y) \tag{6.17}$$

where the pure solid phase is assumed. Subscript 1 represents the solid component and is omitted henceforth.

Isothermal changes of pressure along the equilibrium line lead to:

$$\left(\frac{\partial \mu^S}{\partial P}\right)_T dP = \left(\frac{\partial \mu^F}{\partial P}\right)_{T,y} dP + \left(\frac{\partial \mu^F}{\partial y}\right)_{T,P} dy \tag{6.18}$$

Using the definitions of the molar volume of the pure solid v^S

$$\left(\frac{\partial \mu^S}{\partial P}\right)_T = v^S \tag{6.19}$$

and the partial molar volume of the solid in the gas phase $\bar{v}^F$

$$\left(\frac{\partial \mu^F}{\partial P}\right)_{T,y} = \bar{v}^F \tag{6.20}$$

we then have

$$v^S = \bar{v}^F + \left(\frac{\partial \mu^F}{\partial y}\right)_{T,P} \frac{dy}{dP} \tag{6.21}$$

which can be rewritten as

$$\left(\frac{\partial P}{\partial y}\right)_T = \frac{\left(\frac{\partial \mu^F}{\partial y}\right)_{T,P}}{v^S - \bar{v}^F} \tag{6.22}$$

At the critical point of the mixture, the solid-fluid equilibrium line meets the liquid-gas critical locus where the temperature equals either the LCEP or the UCEP temperature:

$$\left(\frac{\partial \mu^F}{\partial y}\right)_{T,P} = 0 \tag{6.23}$$

The derivatives at both critical end points are then found

$$\left(\frac{\partial P}{\partial y}\right)_{T_{LCEP}} = \left(\frac{\partial P}{\partial y}\right)_{T_{UCEP}} = 0 \tag{6.24}$$

or

$$\left(\frac{\partial y}{\partial P}\right)_{T_{LCEP}} = \left(\frac{\partial y}{\partial P}\right)_{T_{UCEP}} = \frac{v^S - \bar{v}^F}{\left(\frac{\partial \mu^F}{\partial y}\right)_{T,P}} = \infty \tag{6.25}$$

The enhancement of the solubility of a solid by small changes of temperature near the critical end points can also be demonstrated as following.

Taking the derivatives of both sides of Eq.(6.17) with respect to T at constant P:

$$\left(\frac{\partial \mu^S}{\partial T}\right)_P dT = \left(\frac{\partial \mu^F}{\partial T}\right)_{P,y} dT + \left(\frac{\partial \mu^F}{\partial y}\right)_{T,P} dy \tag{6.26}$$

and using the thermodynamic relationships:

$$\left(\frac{\partial \mu^S}{\partial T}\right)_P = -s^S \tag{6.27}$$

and

$$\left(\frac{\partial \mu^F}{\partial T}\right)_{P,y} = \bar{s}^F \tag{6.28}$$

lead to

$$-s^S = -\bar{s}^F + \left(\frac{\partial \mu^F}{\partial y}\right)_{T,P} \frac{dy}{dT} \tag{6.29}$$

Eq.(6.29) can be rewritten as

$$\left(\frac{\partial y}{\partial T}\right)_P = \frac{\bar{s}^F - s^S}{\left(\frac{\partial \mu^F}{\partial y}\right)_{T,P}} \tag{6.30}$$

At the critical end points,

$$\left(\frac{\partial y}{\partial T}\right)_{P_{LCEP}} = \left(\frac{\partial y}{\partial T}\right)_{P_{UCEP}} = \infty \tag{6.31}$$

It is this strong divergence of the solubility with small change of pressure or temperature in the vicinity of the critical end points that provides the opportunity for supercritical extraction processes. Eq.(6.25) and Eq.(6.31) also indicate that it is the criticality that influences the dramatic change of the solubility at the critical end points.

6.3.2 The Solubility Phenomena Near the Critical End Points

At low pressure, one can use the definition of an ideal gas for the chemical potential μ^F of the solid in a supercritical fluid phase:

$$\mu^F = \mu^*(T,P) + RT \ln y \tag{6.32}$$

Taking the derivatives of both sides of Eq.(6.32) with respect to y at constant P and T:

$$\left(\frac{\partial \mu^F}{\partial y}\right)_{T,P} = \frac{RT}{y} \tag{6.33}$$

and substituting it into Eq.(6.22), yields

$$\left(\frac{\partial \ln y}{\partial P}\right)_T = \frac{v^S - \bar{v}^F}{RT} \tag{6.34}$$

At low pressure, the partial molar volume $\bar{v}^F$ is positive and larger than the molar volume of the solid v^S, $\bar{v}^F > v^S$. The difference of $(v^S - \bar{v}^F)$ is negative, indicating that the solubility of the solid in the fluid phase decreases as pressure increases, $\left(\frac{\partial y}{\partial P}\right)_T < 0$. In the low pressure range, the value of $\bar{v}^F$ decreases as pressure increases. The solubility minimum of the solid in the fluid phase occurs when $\bar{v}^F$ finally becomes equal to v^S (see Figure 6.3). From that point onward, the solubility of the solid in the supercritical fluid phase increases as pressure increases, $\left(\frac{\partial y}{\partial P}\right)_T > 0$.

As the pressure increases further, the value of $\bar{v}^F$ becomes negative and large. The value of $\bar{v}^F$ in Figure 6.3 was calculated by Kurnik [140] for the mixture naphthalene-ethylene at temperature T=318 K. In the critical region, the partial molar volume of the slightly volatile solute in the supercritical fluid phase is highly sensitive to temperature and pressure. As the temperature approaches the critical point of the supercritical solvent, $\bar{v}^F$ takes on large negative values with a sharp minimum. The changes of $\bar{v}^F$ value with temperature and pressure were also found experimentally by Wasen and Schneider [139].

In the critical region, Eq.(6.32) no longer holds true. The partial molar volume of the solute in the supercritical fluid phase $\bar{v}^F$ is expressed by:

$$\bar{v}^F = v + (1-y)\left(\frac{\partial v}{\partial y}\right)_{T,P} \tag{6.35}$$

where v is the total molar volume of the mixture in the fluid phase. Substituting Eq.(6.35) and

$$\left(\frac{\partial v}{\partial y}\right)_{T,P} = -\frac{\left(\frac{\partial P}{\partial y}\right)_{T,v}}{\left(\frac{\partial P}{\partial v}\right)_{T,y}} \tag{6.36}$$

into Eq.(6.22), the following expression is obtained

$$\left(\frac{\partial y}{\partial P}\right)_T = \frac{v^S - \left[v - (1-y)\frac{\left(\frac{\partial P}{\partial y}\right)_{T,v}}{\left(\frac{\partial P}{\partial v}\right)_{T,y}}\right]}{\left(\frac{\partial \mu^F}{\partial y}\right)_{T,P}} \tag{6.37}$$

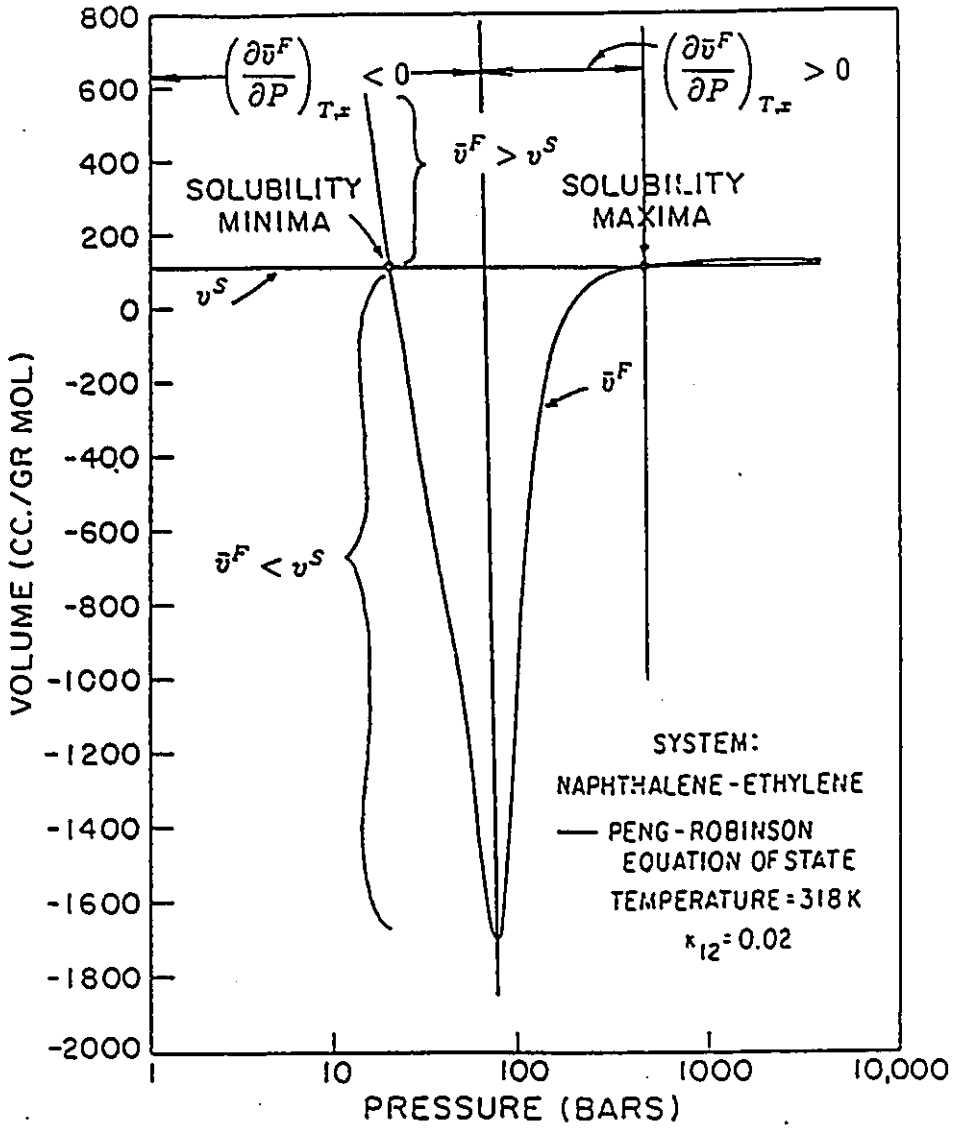

Figure 6.3: Partial Molar Volume of Naphthalene in Supercritical Ethylene [140].

For most of the binary mixtures reported in the literature, the LCEP is found to be very close to the critical point of the supercritical solvent (Table 3.1), where $\left(\frac{\partial P}{\partial v}\right)_T = 0$. Therefore, in the vicinity of the LCEP,

$$\left(\frac{\partial \mu^F}{\partial y}\right)_{T,P} \rightarrow 0, \qquad \left(\frac{\partial P}{\partial v}\right)_{T,y} \rightarrow 0 \tag{6.38}$$

There are two contributions to the divergence in Eq.(6.37) near the LCEP, while only one term $\left(\frac{\partial \mu^F}{\partial y}\right)_{T,P} \rightarrow 0$ near the UCEP. Though the solubility of the solid in the supercritical fluid phase increases greatly near the LCEP, the loading power is rather modest due to the low pressure. In the region near the LCEP, the solubility of the solid is so small that the solid may be considered to be infinitely dilute. In this case, the partial molar volume of the solid in the supercritical fluid phase $\bar{v}^F$ becomes that at infinite dilution $\bar{v}^\infty$. Eq.(6.37) can be expressed near the LCEP by

$$\left(\frac{\partial y}{\partial P}\right)_T = \frac{v^S - \bar{v}^\infty}{\left(\frac{\partial \mu^F}{\partial y}\right)_{T,P}} \tag{6.39}$$

The value of $\bar{v}^\infty$ can be either calculated by an equation of state or measured experimentally [139]. Eq.(6.39) would, therefore, provide some insight into how the solubility of the solid in the supercritical fluid phase changes in the region of the LCEP.

As the pressure increases further, the value of $\bar{v}^F$ will pass the sharp minimum as shown in Figure 6.3. From that point onward, $\left(\frac{\partial \bar{v}^F}{\partial P}\right)_{T,y} > 0$, and the difference of $(v^S - \bar{v}^F)$ becomes smaller as the pressure increases. The solubility of the solid in the supercritical fluid phase will reach its maximum value when $\bar{v}^F$ eventually becomes equal to v^S again at higher pressure. However, the dramatic changes of the solubility appear in the vicinity of the UCEP, where the denominator on the right side of Eq(6.37) approaches zero. Again, it is the criticality which plays the important role in the solubility of the solid in the supercritical fluid phase near the UCEP. Since it is associated with high pressure, the UCEP offers large loading powers which lead to the great solubility enhancement in the critical region.

As the pressure is raised from the critical region of the UCEP, the solubility of the solid in the supercritical fluid phase quickly reaches a limiting value (see Figure 2.2). The pressure at which the solubility reaches its maximum is far beyond the UCEP pressure. For both theoretical and practical purposes, study of phase behavior in the critical region of the UCEP is very important with respect to supercritical fluid extraction.

Chapter 7

CONCLUSIONS

The new contributions to the study of solid-supercritical fluid phase equilibria in this thesis are summarized as follows:

1. A new visual experimental technique, the first freezing point method, was developed for quick and reliable determination of the pressure-temperature projection of the solid-liquid-gas three-phase equilibria for binary and ternary mixtures at supercritical fluid conditions.

Compared with the "first melting point" method in the literature [84,66], the proposed new technique has these advantages:

(1). The pressure-temperature (P-T) projections of the S-L-G equilibria obtained using the "first freezing point" method are more self consistent than those values determined by the "first melting point" method.

(2). The "first freezing point" method allows taking samples from the liquid phase during the determination of the P-T projection of the three-phase S-L-G equilibria. The additional information, the liquid composition of the three-phase S-L-G equilibria, provides a valuable data base for testing and/or developing fundamental thermodynamic models to describe the phase behavior of the mixture at supercritical conditions.

2. The experimental set up for the determination of the multiphase equilibria is also suitable for the measurements of the liquid-gas critical loci of the mixtures

under high pressure. The critical opalescence can be observed.

The UCEPs, where the great solubility enhancement is achieved, were established by means of the intersection method to be 333.4 K, 25.9 MPa and 0.16 mole fraction of naphthalene for naphthalene-carbon dioxide mixture and 328.5 K, 48.5 MPa and 0.18 mole fraction of biphenyl for biphenyl-carbon dioxide mixture.

The experimental results, the pressure-temperature-liquid composition of the solid-liquid-gas three-phase equilibria, and the pressure-temperature-critical composition of the liquid-gas critical loci, obtained in this study also provide the design or process engineers with the information necessary to predict the phase behavior of the carbon dioxide-aromatic compound mixtures at supercritical conditions.

3. A "crossover region" was found in the isothermal solubilities of supercritical carbon dioxide in the liquid biphenyl at a pressure of about 36 MPa. The solubility isotherms converged at that region in the pressure-composition diagram. Below the crossover region pressure, an increase in temperature caused a decrease in solubility of carbon dioxide in the liquid phase, while above that pressure the opposite effect occurred. The explanation for this phenomenon is that at pressures above the crossover region, due to the high density of the supercritical fluid phase, the "escape" of a lighter component, the gas, from the liquid phase into the supercritical fluid phase, is much less sensitive to increases of temperature than at lower pressure.

4. The freezing point depression of a solid and its curve on the pressure-temperature projection is a compromise of two opposite effects: the hydrostatic-pressure effect and the freezing-point depression effect due to the dissolution of the supercritical solvent in the liquid phase.

While the partial molar volume of the solid in the supercritical fluid phase, $\bar{v}^F$ is a key quantity in the pressure dependence of the solubility, it is the criticality which plays the important role in the dramatic change of the solubility at both critical end points.

The solubility maximum of the solid in a supercritical fluid phase appears at a

much higher pressure above the critical region. In practical applications, it is more advantageous to carry out the supercritical fluid extraction process near the UCEP.

5. The addition of a second aromatic compound depresses significantly the freezing point of a solid under the pressure of a supercritical solvent, regardless of whether the triple point of the second compound is higher or lower than that of the first solid. The results of the pressure-temperature projection of the solid 1-solid 2-liquid-gas four-phase equilibria suggest that the assumption that the eutectic composition of the solids does not change with pressure may lead to a not negligible error in measurements.

6. Using the Peng-Robinson equation of state with the modified correction factors α proposed in this study and the AS or SGR mixing rule, the correlations of the S-L-G three-phase equilibria for the solid-supercritical solvent mixture, such as naphthalene-CO_2, biphenyl-CO_2 and phenanthrene-CO_2, and the solubilities of supercritical carbon dioxide in the melted solids, such as naphthalene and biphenyl, were accomplished with satisfactory accuracy.

7. Supercritical chromatograph with the operating conditions found in this study for the ternary mixtures provide a useful tool for the study of the selectivity of the supercritical solvent as well as for the composition analysis of the multicomponent systems at supercritical fluid conditions.

Chapter 8

RECOMMENDATIONS FOR FUTURE STUDIES

1. It appears from this study that the simple cubic equation of state and the activity-coefficient models are of limited use in correlating and predicting either the multiphase equilibria involving a solid phase or phases at supercritical conditions or the liquid-gas critical loci which are close to the UCEP. Fundamentally based thermodynamic models, such as the statistical mechanical models, with more insight into the supercritical solvent-solid solute interactions need to be developed in the future.

2. In the determination of the S_1-S_2-L-G four-phase equilibria, the results of the solid-liquid-gas three-phase curve measurements with different initial loadings of the two solids did not give useful estimates of the eutectic composition under pressure, due to the experimental error. The effort made to obtain the liquid compositions along the four-phase coexistence curve will serve as a useful guide in future study.

3. The binary and ternary mixtures investigated in this study consist of supercritical carbon dioxide and aromatic compounds which contain two or three benzene rings. Future work is required to obtain insight into how different posi-

tions and structures of benzene rings as well as other functional groups would affect the phase behavior of mixtures of this type at supercritical fluid conditions, such as the freezing point depression of the multiphase coexistence curve, and the curvature and temperature minimum of the pressure-temperature projection, etc.

4. The liquid composition analysis by a supercritical chromatograph for the ternary mixtures in this study suggests that the high selectivity of supercritical carbon dioxide is more favorable for naphthalene, which is lower in molecular weight than biphenyl and phenanthrene. The ratio of the two solid (naphthalene-biphenyl and naphthalene-phenanthrene) compositions in the liquid phase remains essentially constant with pressure increases. Further work is needed to study the influence of the "entrainer" on solubilities and selectivities in supercritical systems.

Bibliography

[1] Irani, C.A. and E.W. Funck, *Separations Using Supercritical Gases*, Recent Developments in Separation Science, Vol.3, Part A, pp.171-193, CPC Press, West Palm Beach, Florida,1977.

[2] Williams, D.F., *Extraction with Supercritical Gases*, Chem. Eng. Sci., 36, 1769-1788(1981).

[3] Reid, R.C., *Supercritical Fluid Extraction, a Perspective*, Hougen Lecture Series, 1981.

[4] Randall, L.G., *The present status of Dense (Supercritical) Gas Extraction and Dense Gas Chromatography Impetus for DGC/mc Development*, Sep. Sci. Technol., 17,1-118(1982).

[5] Paulaitis, M.E., V.J. Krukonis, R.T. Kurnik and R.C. Reid, *Supercritical Fluid Extraction*, Review in Chem. Eng., 1, 179-250(1983).

[6] Ely, J.F. and J.K. Baker, *A Review of Supercritical Fluid Extraction*, U.S. Department of Commerce, Malcolm Baldrige, Secretary. National Bureau of Standards, Dec. 1983.

[7] Zosel, K., *Separation with Supercritical Gases: Practical Applications*, Angew, Chem. Int. Ed. Engl., 17, 702-709(1978).

[8] Hannay, J.B. and J. Hogarth, *On the Solubility of Solid in Gases*, Pro. Roy. Soc. (London), 29, 324-326(1879), and ibid., 30, 178(1880).

[9] Hannay, J.B, *On the Solubility of Solid in Gases, 2*, Pro. Roy. Soc. (London), 30, 484-489(1880).

[10] Villard, P., *Solubility of liquids and Solids in Gas*, J. Phys, 5, 455(1896).

[11] Prins, A., *On Critical-End-Point and the System Ethane-Naphthalene*, Acad. Sci. Amsterdam, 17, 1095-1111(1915).

[12] Pilat, S. and M. Godlewicz, U.S. Patent, 2188012 and 2188013 (1936).

[13] Katz, D.L. and F. Kurate, *Retrograde Condensation*, Ind. Eng. Chem., 32, 817-827(1940).

[14] Reamer, H.H., R.H. Olds, B.H. Sage and W.N. Lacey, *Phase Equilibria in Hydrocarbon Systems: Methane-Decane Systems*, Ind. Eng. Chem., 34, 1526(1942).

[15] Diepen, G.A.M. and F.E.C. Scheffer, *On Critical Phenomena of Saturated Solutions in Binary Systems*, J. Am. Chem. Soc., 70, 4081-4085(1948).

[16] Diepen, G.A.M. and F.E.C. Scheffer, *The Solubility of Naphthalene in Supercritical Ethylene*, J. Am. Chem. Soc., 20, 4085-4089(1948).

[17] Zhuze, T.P., Petroleum (London), 23, 298(1960).

[18] Zosel, K., DBP., 20,005,293 (Priority: Feb. 5, 1970).

[19] Gearhart, J.A. and L. Garwin, *ROSE Process Improves Resid Feed*, Hydrocarbon Process, May, 55,125-128(1976).

[20] Williams, D.F. and J.C. Whitehead, U.S. Patent, 3,970,541(1976).

[21] Gangoli, N. and G. Thodos, *Liquid Fuels and Chemical Feedstocks From Coal by Supercritical Gas Extraction*, Ind. Eng. Chem., Prod. Res. Dev., 16, 208(1977).

[22] Adames, R.M., A.H. Knebel and D.E. Rhodes, *Critical Solvent Deashing of Liquefied Coal*, Chem. Engng. Prog., 75(6), 44-48(1979).

[23] Maddocks, R.R., J. Gibson and D.F. Williams, *SCE of Coal*, Chem. Eng. Prog., 25, 49(1979).

[24] Matin, T.G. and D.F. Williams, *Gaseous Solvent Extraction of Oil Shales and Tar Sands*, U.S. Patent, 4,108,760 (1978).

[25] Doscher, T.M. and M. El-Arabi, *Scaled Model Experiments Show How* CO_2 *Might Economically Recover Residual Oil*, Oil and Gas J. 144 (Aug. 1982).

[26] Roselius, W., O. Vitzthum and P. Hubert, *Method for the Production of Caffeine-Free Coffee Extract*, U.S. Patent, 3,843,824 (1974).

[27] Zosel, K., *Process for the Decaffeination of Coffee*, U.S. Patent, 4,247,570 (1981).

[28] Friedrich, J.P., G.R. List and A.J. Heakin, *Petroleum Free Extraction of Oil from Soybeans with Supercritical* CO_2, 72nd Ann. Am. Oil. Chem. Soc. Mtng., New Orleans, May 1981.

[29] Roselius, W., O. Vitzthum and P. Hubert, *Methods of Producing Cocoa Butter*, U.S. Patent, 3,923,847(1975).

[30] Anon. *Extraction Process Benefits Potato Chips, Coffee, Hops*, Food Eng. Intl., Oct. 45-46(1981).

[31] Hubert, P. and O.G. Vitzthum, *Fluid Extraction of Hops, Spices, and Tobacco with Supercritical Gases*, Angew. Chem. Int. Ed. Engl., 17, 710-715(1978).

[32] Calame, J.P. and R.Steiner, *CO_2 Extraction in the Flavor and Perfumery Industries*, Chem. Ind., 399 (June 1982).

[33] Stahl, E. *Extraction of Natural Products with the Means of Supercritical Gases*, Rev. Latinoam. Quim., 11(1), 1(1980).

[34] Vitzthum, O., P. Hubert and W. Sirtl, *Production of Hop Extracts*, U.S. Patent, 4,104,409(1970).

[35] Vollbrecht, R., *Extraction of Hops with Supercritical CO_2* , Chem. and Ind., 397 (June 1982).

[36] Roselius, W., O. Vitzthum and P. Hubert, *Nicotine Removal from Tobacco*, Ger. Offer., 2,043,537 (1972).

[37] Roselius, W., O. Vitzthum and P. Hubert, *Selective Extraction of Nicotine from Tobacco*, Ger. Offer., 2,142,205 (1973).

[38] Yorizane, M., H. Masuoka, S. Ida and T. Ikeda, *High Pressure Vapor-Liquid-liquid Equilibria for the Ethylene-MEK-Water System*, J. Chem. Engng. Japan, 3, 379(1973).

[39] Newsham, D.M.T. and O.P. Stigset, I. Chem. Eng. Symp. Ser., 54, 56(1978).

[40] Texaco. Inc., U.S. Patent, 3,318,805 (1967).

[41] Modell, M., R.D. de Fillipi and V.J. Krukonis, *Regeneration of Activated Carbon with Supercritical Carbon Dioxide*, Paper presented at the ACS Annual Meeting, Miami, FL. 1978.

[42] Modell, M., R.J. Robey, V.J. Krukonis, R.D. de Fillipi and D. Oestereich, *Supercritical Fluid Regeneration of Carbon*, Paper presented at national AIChE Meeting, Boston MA, 1979.

[43] Bangert, L.H., J.L. Lundberg, J.D. Muzzy, G.H. Hoyes, L.H. Olson, and W.D. Freeston Jr, *Advanced Technology Applications in Garment Processing*, Report prepared for the National Science Foundation, National Technical Information Service Report PB, 284,779, Sept. 1977.

[44] Chang, H. and D.G. Marrell, *Solubilities of Methoxy- 1-tetralone and Methyl Nitrobenzoate Isomers and Their Mixtures in Supercritical Carbon Dioxide*, J. Chem. Eng. Data, 30, 74(1985).

[45] Krukonis, V.J. and R.T. Kurnik, *Solubility of the Solid Aromatic Isomers in Carbon Dioxide*, J. Chem. Eng. Data, 30, 247(1985).

[46] Anon. *Supercritical CO_2 Cleans Drill Cuttings*, Chem. Eng. News, Feb. 8, p.30, 1982.

[47] Modell, M., *Processing methods for the Oxidation of Organic in Supercritical Water*, U.S. Patent, 4,338,199 (1982).

[48] Klesper, E., A.W. Corwin and D.A. Turner, *High Pressure Gas Chromatography above Critical Temperatures*, J. Org. Chem., 27, 700-701(1962).

[49] Sie, S.T., W. van Beersum and G.W.A. Rijnders, Sep. Sci., 1, 459(1966).

[50] Wilsch, A., R. Feist and G.M. Schneider, *Capacity Ratios and Diffusion of Low-volatile Organic Compounds in Supercritical Carbon Dioxide from Supercritical Fluid Chromatography (SFC)*, Fluid Phase Equilibria, 10, 299- 306(1983).

[51] Feist, R. and G.M. Schneider, *Determination of Binary Diffusion Coefficients of Benzene, Phenol, Naphthalene and Caffeine in Supercritical CO_2 between 308 and 333 K in the Pressure Range 80 to 160 Bar with Supercritical Fluid Chromatography (SFC)*, Separation Science and Technology, 17, 261-270(1982).

[52] Ehrlich, P. and G.A. Mortimer, *Fundamentals of Free-radical Polymerization of Ethylene*, Adv. Polym. Sci., 7,386(1970).

[53] Ehrlich, P., *Partial Molal Volume Anomaly in Supercritical Mixtures and the Free Radical Ploymerization of Ethylene*, J. Macromol. Sci. Chem. A5, 1259(1971).

[54] Kramer, G.M. and F. Leder, U.S. Patent, 3,880,945, 1975.

[55] Basta, N. and S. McQueen, *Supercritical Fluids: Still Seeking Acceptance*, Chem. Eng., Feb.4, 14-17(1985).

[56] Van Konynenburg, P.H. and R.L. Scott, *Critical Locus and Phase Equilibria in Binary van der Waals Mixture*, Phil. Trans. Roy. Soc., London, A298, 495-540(1980).

[57] Schneider, G.M., *High-Pressure Phase Diagrams and Critical Properties of Fluid Mixtures in Chemical Thermodynamics Vol. 2*, M.L. McGlashan, ed., A Specialist Periodical Report, The Chemical Society, London, 1978, Chap. 4, pp.105-146.

[58] Rowlinson, J.S., "Liquids and Liquid Mixtures", 3rd Ed. Butterworth Scientifi, London, 1982.

[59] McGlashan, M.L., *Phase Equilibria in Fluid Mixtures*, Pure Appl. Chem., 57, 89-103(1985).

[60] Prausnitz, J.M., R.N. Lichtenthaler and E.G. de Azevedo, "Molecular Thermodynamics of Fluid-Phase Equilibria", 2nd Ed., Prentice-Hall Inc., 1986.

[61] Schneider, G.M., *Physicochmical Principles of Extraction with Supercritical Gases*, Angew. Chem. Int. Ed. Engl., 17, 716-727(1978).

[62] Schneider, G.M., *Physicochmical Aspects of Fluid Extraction*, Fluid Phase Equilibria, 10, 141-157(1983).

[63] Rowlinson, J.S. and M.J. Richardson, *The Solubility of Solid in Compressed Gases*, Adv. in Chem. Phys. Vol.2, Edited by I. Prigogine, pp.85-118, 1959.

[64] Donnelly, H.G. and D. L. Katz, *Phase Equilibria in the Carbon Dioxide-Methane System*, Ind. Eng. Chem., 46, 511-517(1954).

[65] Van Gunst, C.A., F.E.C. Scheffer and G.A.M. Diepen, *On Critical Phenomena of Saturated Solutions in Binary Systems 2*, J. Phys. Chem., 57,578-581(1953).

[66] McHugh, M.A. and T.J. Yogan, *Three-Phase Solid-Liquid-Gas Equilibria for Three Carbon Dioxide-Hydrocarbon Solid Systems, Two Ethane-Hydrocarbon Solid Systems, and Two Ethylene-Hydrocarbon Solid Systems*, J. Chem. Eng. Data, 29, 112-115(1984).

[67] McHugh, M.A. and M.E. Paulaitis, *Solid Solubilities of Naphthalene and Biphenyl in Supercritical Carbon Dioxide*, J. Chem. Eng. Data, 25, 326-329(1980).

[68] Cheong, P.L., Dingan Zhang, K. Ohgaki and Benjamin C.-Y. Lu, *High Pressure Phase Equilibria for Binary Systems Involving a Solid Phase*, Fluid Phase Equilibria, 29, 555-562(1986).

[69] McHugh, M.A., A.J. Seckner and T.Y. Yogan, *High Pressure Phase Behavior of Binary Mixtures of Octacosane and Carbon Dioxide*, Ind. Eng. Chem. Fundam., 23, 493-499(1984).

[70] Tsang, C.Y. and W.B. Streett, *Phase Equilibria in the* H_2/CO_2 *System at temperatures from 220 to 290 K Pressures to 172 MPa*, Chem. Eng. Sci., 36, 993-1000(1981).

[71] Streett, W.B. and J.L.E. Hill, *Phase Equilibria in Fluid Mixtures at High Pressures: The Neon-Argon System*, J. Chem. Phys., 54, 5088-5094(1971).

[72] Van Gunst, C.A., F.E.C. Scheffer and G.A.M. Diepen, *On Critical phenomena of Saturated Solutions in Ternary Systems*, J. Phys. Chem., 57,581-583(1953).

[73] Koningsveld, R. and G.A.M. Diepen, *Supercritical Phase Equilibria Involving Solid*, Fluid Phase Equilibria, 10, 159-172(1983).

[74] Koningsveld, R., L.A. Kleintjens and G.A.M. Diepen, *Solubility of Solids in Supercritical Solvents. 1. General Principle*, Ber. Bunsergs. Phys. Chem., 88, 848-855(1984).

[75] Diepen, G.A.M. and F.E.C. Scheffer, *The Solubility of Naphthalene in Supercritical Ethylene*, J. Phys. Chem., 57, 575-577(1953).

[76] Tsekhanskaya, Y.V., M.B. Iomtev and E.V. Mushkina, *Solubility of Naphthalene in Ethylene and Carbon Dioxide under Pressure*, Russian J. of Phys. Chem., 38, 1173-1176(1964).

[77] Barrick, M.W., J.M. Anderson and R.L. Robinson, Jr., *Solubilities of Carbon Dioxide in Naphthalene, Phenanthrene, and Pyrene at Pressures to 10.6 MPa and Temperatures from 373 to 433 K*, J. Chem. Eng. Data, 32, 372-374(1987).

[78] Anderson, J.M., M.W. Barrick and R.L. Robinson, Jr., *Solubilities of Carbon Dioxide in Cyclohexane and trans-Decalin at pressures to 10.7 MPA and Temperatures from 323 to 423 K*, J. Chem. Eng. Data, 31, 172-175(1986).

[79] Zhang, D., Y. Adachi and B. C.-Y. Lu, *Multiphase Equilibria of Ternary System at SFE Conditions*, Proceeding of International Symposium on Supercritical Fluids, Oct. 17-19, 1988, Nice, France, TOME1, 19-26(1988).

[80] Kurnik, R.T. and R.C. Reid, *Solubility of Solid Mixtures in Supercritical Fluid*, Fluid Phase Equilibria, 8, 93-105(1982).

[81] Van Welie, G.S.A. and G.A.M. Diepen, *The P-T-x Space Model of the System Ethylene-Naphthalene*, Rec. Trav. Chin., 80, 659-680(1961).

[82] Van Welie, G.S.A. and G.A.M. Diepen, *The Solubility of Naphthalene in Supercritical Ethane*, J. Phys. Chem., 67, 755-757(1963).

[83] McHugh, M.A. and V.J. Krukonis, "Supercritical Fluid Extraction: Principles and Practice", Butterworths, USA, 1986.

[84] McHugh, M.A., *An Experimental Investigation of the High Pressure Fluid Phase Equilibrium of Highly Asymmetric Binary Mixtures*, Doctoral Dissertation, 1981, University of Delaware.

[85] Andrew, T., Phil. Trans. Roy. Soc., 159, 575(1869).

[86] van der Waals, J.D., Thesis, Leiden, 1873.

[87] Hicks, C.P. and C.L. Young, *The Gas-Liquid Critical Properties of Binary Mixtures*, Chem. Rev., 75, 119-175(1975).

[88] Young, C.L., *Experimental Methods for Studying Phase Behavior of Mixtures at High Temperatures and Pressures*, In "A Specialist Periodical Report Chemical Thermodynamics Vol. 2", Chap. 3, 1978.

[89] Olds, R.H., H.H. Reamer, B.H. Sage and W.N. Lacy, *Phase Equilibria in Hydrocarbon Systems: The n-Butane-Carbon Dioxide System*, Ind. Eng. Chem., 41, 474(1949).

[90] Reamer, H.H. and B.H. Sage, *Phase Equilibria in Hydrocarbon Systems: Volumetric and Phase Behavior of the Propane-n-Decane System*, J. Chem. Eng. Data, 11, 17-24(1966).

[91] Roof, J.G. and J.D. Baron, *Critical Loci of Binary Mixtures of Propane with Methane, Carbon Dioxide and Nitrogen*, J. Chem. Eng. Data, 12, 292-293(1967).

[92] Kay, W.B., *Vapor-Liquid Equilibrium Relations of Binary Systems. The Propane-n-Alkane Systems. n-Butane and n-Pentane*, J. Chem. Eng. Data, 15, 46-52(1970).

[93] Liphard, K.G. and G.M. Schneider, *Phase Equilibria and Critical Phenomena in Fluid Mixtures of Carbon Dioxide + 2,6,10,15,19,23-Hexamethyetetracosane up to 423 K and 100 MPa*, J. Chem Thermodynamics, 7, 805-814(1975).

[94] Thies, M.C. and M.E. Paulaitis, *Vapor-Liquid Equilibrium for 1-Methylnaphthalene-Methanol Mixtures at Elevated Temperatures Pressures*, J. Chem. Eng. Data, 29, 438-440(1984).

[95] Thies, M.C. and M.E. Paulaitis, *Vapor-Liquid Equilibrium for 1-Naphthol/ Methanol and Naphthalene/Methanol Mixtures at Elevated Temperatures and Pressures*, J. Chem. Eng. Data, 31, 23(1986).

[96] Soave, G., *Equilibrium Constants from a Modified Redlich-Kwong Equation of State*, Chem. Eng. Sci., 27, 1197-1203(1972).

[97] Peng, D.-Y. and D.B. Robinson, *A New Two-Constant Equation of State*, Ind. Eng. Chem. Fundam., 15, 59-64(1976).

[98] Peng, D.-Y. and D.B. Robinson, *Calculation of Three-Phase Solid-Liquid-Vapor Equilibrium Using an Equation of state*, in "Equation of State in Engineering and Research", Edited by K.C. Chao and R.L. Robinson, Jr., Advances in Chemistry Series 182, 1979.

[99] Paulaitis, M.E., M.A. McHugh and C.P. Chai, *Solid Solubilities in Supercritical Fluids at Elevated Pressures*, in "Chemical Engineering at Supercritical Fluid Conditions", Edited by M.E. Paulaitis, J.M.L. Penninger, R.D. Gray, Jr. and P. Davidson, Ann Arbor Science, 1983.

[100] McHugh, M.A., J.J. Wattkins, B.T. Doyle and V.J. Krukonis, *High-Pressure Naphthalene-Xenon Phase Behavior*, Ind. Eng. Chem. Res., 27, 1025-1033(1988).

[101] van der Haegen, R.R. Koningveld, L.A. Kleintjens and L. van Opstal, *Solubility of Solids in Supercritical Solvents. IV. Mean-Field Lattice Gas Description for the p-T-x Space Diagram of the System Ethylene-Naphthalene*, Fluid Phase Equilibria, 43, 1-19(1988).

[102] Hildebrand, J.H. and R.L. Scott, "Regular Solutions", 1962.

[103] Lemert, R.M. and K.P. Johnston, *Solid-Liquid-Gas Equilibria in Multicomponent Supercritical Fluid Systems*, Fluid Phase Equilibria, 1989 in print.

[104] Gibbs, J.W., *On the Equilibrium of Heterogeneous Substances, Part I*, Transactions of the Connecticutl Academy, 3, 108(1876), as reprinted in The Scientific Papers of J. Willard Gibbs, Vol. 1, Dover, New York 1961.

[105] Prigogine, I. and R. Defay, "Chemical Thermodynamics", Translated by D.H. Everett, Chapter 16, Longmans Green And Co, 1954.

[106] Hissong, D.W. and W.B. Kay, *The Calculation of the Critical Locus Curve of a Binary Hydrocarbon System*, AIChE J., 16, 580-587(1970).

[107] Huron, M.-J., *Use of the Soave Equation of State and of the Stability Conditions for Calculating the Critical Points of Binary Mixtures*, Chem. Eng. Sci., 31, 837-839(1976).

[108] Huron, M.-J., G.-N. Dufour and J. Vidal, *Vapor-Liquid Equilibrium and Critical Locus Curve Calculations with the Soave Equation for Hydrocarbon Systems with Carbon Dioxide and Hydrogen Sulphide*, Fluid Phase Equilibria, 1, 247-265(1977/78).

[109] Peng, D.-Y. and D.B. Robinson, *A Rigorous Method for Predicting the Critical Properties of Multicomponent Systems from an Equation of State*, AIChE J., 23, 137-144(1977).

[110] Sarashina, E., J. Nohka, Y. Aiai and S. Saito, *Correlation of Critical Loci for Binary Mixtures by the BWR Equation*, J. Chem. Eng. of Japan , 7, 219-222(1974).

[111] Teja, A.S., R. L. Smith and S. J. Sandler, *The Calculation of Critical Points of Fluid Mixtures Effect of Improved Pure Component Critical Point Representation*, Fluid Phase Equilibria, 14, 265-272(1983).

[112] Mainwaring, D.E., R. J. Sadus and G. L. Young, *Prediction of Binary and Ternary Critical Properties Using Deiters' Equation, Hard sphere and Hard Convex Body Equations of State*, Fluid Phase Equilibria, 43, 85-103(1988).

[113] Mainwaring, D.E., R. J. Sadus and G. L. Young, *Deiters' Equation of State and Critical Phenomena*, Chem. Eng. Sci., 43, 459-466(1988).

[114] Deiters, U., *A New Semiempirical Equation of State for Fluids–I, Derivation*, Chem. Eng. Sci., 36, 1139-1146(1981).

[115] Deiters, U., *A New Semiempirical Equation of State for Fluids–II, Application to Pure Substances*, Chem. Eng. Sci., 36, 1147-1151(1981).

[116] Deiters, U., *A New Semiempirical Equation of State for Fluids–II, Application to Phase Equilibria in Binary Mixtures*, Chem. Eng. Sci., 37, 855-861(1982).

[117] Guggenheim, E.A., *The New Equation of State of Longuet-Higgins and Widom*, Mol. Phys., 9, 43-45(1965).

[118] Chou J.F.and J. M. Prausnitz, *A Phenomenological Correction to an Equation of State for the Critical Region*, AIChE. J., 35,1487-1496(1989).

[119] Lu, Benjamin C.-Y. and Dingan Zhang, *Solid-Supercritical Fluid Phase Equilibria*, Pure and Appl. Chem., 61, 1065-1074(1989).

[120] Cheong, P.L., *Phase Behavior of the Naphthalene-Carbon Dioxide System at Supercritical Fluid Conditions*, M.A.Sc. Thesis, 1985, University of Ottawa.

[121] White G.L. and C. T. Lira, *Four Phase (S-S-L-G) Equilibrium of Two Ternary Organic Systems with Carbon Dioxide*, Presented at AIChE Annual Meeting in Washington D. C. Nov. 1988.

[122] Gopal, J.S., G.D. Holder and E. Kosal, *Solubility of Solid and Liquid Mixtures in Supercritical Carbon Dioxide*, Ind. Eng. Chem. Process Des. Dev., 24, 697-701(1985).

[123] Walas, Stanley M., *Phase Equilibrium in Chemical Engineering*, Butterworths Publishers, Boston, 1985.

[124] Schmitt, W.J. and R.C. Reid, *The Solubility of Monofunctional Organic Solids in Chemically Diverse Supercritical Fluids*, J. Chem. Eng. Data, 31, 204-212(1986).

[125] Dobbs, J.M., J.M. Wong and K.P. Johnston, *Non-polar Co-solvents for Solubility Enhancement in Supercritical Fluid Carbon Dioxide*, J. Chem. Eng. Data, 31, 303-308(1986).

[126] Dobbs, J.M. and K.P. Johnston, *Selectivities in Pure and Mixed Supercritical Fluid Solvents*, Ind. Eng. Chem. Res., 26, 1476-1482(1987).

[127] Dobbs, J.M., J.M. Wong, R.J. Laheire and K.P. Johnston, *Modification of Supercritical Fluid Phase Behavior Using Polar Co-solvents*, Ind. Eng. Chem. Res., 26, 56-65(1987).

[128] Walsh, J.M., G.D. Idonomou and M.D. Donohue, *Supercritical Fluid Behavior: The Entrainer Effect*, Fluid Phase Equilibria, 33, 295-314(1987).

[129] Ziger, D.H. and C.A. Eckert, *Correlation and Prediction of Solid-Supercritical Fluid Phase Equilibria*, Ind. Eng. Chem. Process Des. Dev., 22, 582-588(1983).

[130] Haselow, J.S., S.J. Han, R.A. Greenkorn and K.C. Chao, *Equation of State for Supercritical Extraction*, K.C. Chao and R.L. Robinson (Editors), "Equations of State–Theories and Applications", ACS Symposium No. 300, 1986.

[131] Reid, R.C., J.M. Prausnitz and T.K. Sherwood, "The Properties of Gases and Liquids", Third Edition, McGraw-Hill Book Co., New York, 1977.

[132] Osborn, A.G. and D.R. Douslin, *Vapor Pressure and Derived enthalpies of Vaporization for Some Condensed-Ring Hydrocarbons*, J. Chem. Eng. Data. 20, 229-231(1975).

[133] Perry, R.H. and C.H. Chilton (Editors), "Chemical Engineering handbook", 5th ed., McGraw-Hill, New York, 1973.

[134] Bradley, R.S. and T.G. Cleasby, *The Vapor Pressure and Lattice Energy of Some Aromatic Ring Compounds*, J. Chem. Soc., 1690-1692(1953).

[135] Henley, E.J. and J.D. Seader, "Equilibrium-stage Separation Operations in Chemical Engineering," John Wiley and Sons, New York, N.Y., 1981.

[136] Ipat'ev, V.V. et al, J. Phys. Chem. U.S.S.R., 22, 833(1948).

[137] Cheung, A.S.F., *Phase Behavior of Two Binary System Containing Ethylene at Supercritical Fluid Conditions*, M.As. Thesis, 1988, University of Ottawa, Canada.

[138] De Swaan Arons, J., and G.A.M. Diepen, *Thermodynamic Study of Melting Equilibria under Pressure of a Supercritical Gas*, Rec. Trav. Chin., 82, 249-257(1963).

[139] Van Wasen, U. and G.M. Schneider, *Partial Molar Volumes of Naphthalene and Fluorine at Infinite Dilution in Carbon Dioxide near Its Critical Point*, J. Phys. Chem., 84, 229-230(1980).

[140] Kurnik, R.T., *Supercritical Fluid Extraction: A Study of Binary and Multicomponent Solid Fluid Equilibria*, Doctoral Dissertation, 1981, Massachusetts Institute of Technology.

[141] Adachi, Y. and H. Sugie, *A New Mixing Rule—Modified Conventional Mixing Rule*, Fluid Phase Equilibria, 28, 103-118(1986).

[142] Schwartzentruber, J., F. Galivel-Solastiouk and H. Renon, *Representation of the Vapor-Liquid Equilibrium of the Ternary System Carbon Dioxide-Propane-Methanol and Its Binaries with a Cubic Equation of State: A New Mixing Rule*, Fluid Phase Equilibria, 38, 217-226(1987).

[143] Schmitt, W.J. and R.C. Reid, *The Use of Entrainers in Modifying the Solubility of Phenanthrene and Benzoic Acid in Supercritical Carbon Dioxide and Ethane*, Fluid Phase Equilibria, 32, 77-99(1986).

[144] Peter, S. and G. Brunner, *The Separation of Nonvolatile Substance by Means of Compressed Gases in Countercurrent Processes*, Angew. Chem. Int. Ed. Eng., 17, 746-750(1978).

[145] Brunner, G., *Selectivity of Supercritical Compounds and Entrainer with Respect to Model Substances*, Fluid Phase Equilibria, 10, 289-298(1983).

Appendix A

Calibration of the Supercritical Fluid Chromatograph (SFC)

The SFC was calibrated for the determination of the solid contents in the equilibrium liquid phase of the two ternary mixtures, naphthalene-biphenyl-CO_2 and naphthalene-phenanthrene-CO_2. o-Terphenyl was used as an internal standard for both cases. In each case, the calibration solutions were prepared using approximately 0.3~0.4 grams of the solid mixture, naphthalene(1), biphenyl(2) and o-terphenyl(3), or naphthalene(1), phenanthrene(2) and o-terphenyl(3), weighed with a Mettler H20 microbalance, and dissolved in 100 ml of acetone in a volumetric beaker. The accuracy of the weighing was ± 0.0001 gram.

The concentration of the internal standard was kept approximately constant in each of the calibration solutions while the mole ratios of the determined solids, naphthalene, or biphenyl, or phenanthrene and the internal standard, n_1/n_3 and n_2/n_3 varied from 0.5 to 6.0. The peak area ratios of the determined solid (1) or solid (2) and the internal standard were defined as AR_1 or AR_2, respectively, which were determined for each sample using the same analytical column– 200 mm in length and 4.6 mm in diameter, packed with Hypersil ODS 5 μm particles. The mole ratio, as a function of the area ratio, was then determined by a linear least-

square analysis using the following equation to fit the data:

$$\frac{n_1}{n_3} = intercept + slope(\bar{AR}_1) \tag{A.1}$$

$$\frac{n_2}{n_3} = intercept + slope(\bar{AR}_2) \tag{A.2}$$

where $\bar{AR}_1$ and $\bar{AR}_2$ are the averaged area ratios.

Tables A.1–A.4 give the calibration results of the SFC for the two ternary mixtures. These data were fitted by Eq.(A.1) or Eq.(A.2). The obtained intercepts, slopes and linear correlation coefficients (LCC) are listed in Table A.5.

Table A.1: Calibration Results of Naphthalene for the Naphthalene-Biphenyl-CO_2 System.

no. of moles ($*10^3$)		$\frac{n_1}{n_3}$			Standard Dev.
naph(1)	o-ter(3)		AR_1	$\overline{AR}_1$	of $\overline{AR}_1$
0.7075	0.3260	2.1702	0.6083		
			0.6022		
			0.6190		
			0.6297	0.6148	0.010
1.4224	0.4236	3.3579	0.9570		
			0.9491		
			0.9611		
			0.9553	0.9556	0.004
1.5139	0.3927	3.8551	1.1165		
			1.0450		
			1.0646		
			1.0253		
			1.1196	1.0742	0.038
1.6447	0.3524	4.6671	1.3649		
			1.3208		
			1.3784		
			1.3101	1.3436	0.029
2.1427	0.3301	6.4911	1.9573		
			1.9512		
			1.9212		
			1.9402	1.9425	0.014

Table A.2: Calibration Results of Biphenyl for the Naphthalene-Biphenyl-CO_2 System.

no. of moles ($*10^3$)		n_2			Standard Dev.
biph(2)	o-ter(3)	n_3	AR_2	$\overline{AR}_2$	of $\overline{AR}_2$
0.4341	0.3260	1.3316	1.8707		
			1.8949		
			1.8938		
			1.8671	1.8816	0.013
0.8733	0.4236	2.0616	4.9488		
			5.0833		
			5.2062		
			5.1529	5.0978	0.096
1.0420	0.3927	2.6534	6.8504		
			6.5756		
			6.6359		
			6.8425		
			6.3575	6.6524	0.184
1.1818	0.3524	3.3536	8.6206		
			8.2254		
			8.6205		
			8.3311	8.4494	0.175
1.3774	0.3301	4.1727	10.0793		
			10.0723		
			9.9035		
			10.0433	10.0246	0.071

Table A.3 Calibration Results of Naphthalene for the Naphthalene-Phenanthrene-CO_2 System.

no. of moles ($*10^3$)		$\frac{n_1}{n_3}$			Standard Dev.
naph(1)	o-ter(3)		AR_1	$\overline{AR}_1$	of $\overline{AR}_1$
0.2340	0.4545	0.5148	0.3886		
			0.3907		
			0.4105		
			0.3896	0.3948	0.009
0.4924	0.4362	1.1288	0.8084		
			0.8239		
			0.7903		
			0.8130	0.8089	0.012
0.5698	0.4326	1.3172	0.9149		
			0.9145		
			0.9076		
			0.8694	0.9016	0.019
0.6927	0.3939	1.7586	1.2493		
			1.2766		
			1.2537		
			1.2280	1.2519	0.017
1.9123	0.7044	2.7148	1.8817		
			1.9149		
			2.0654		
			2.0460	1.9770	0.080

Table A.4 Calibration Results of Phenanthrene for the Naphthalene-Phenanthrene-CO_2 System.

no. of moles ($*10^3$)		$\frac{n_2}{n_3}$			Standard Dev.
phen(2)	o-ter(3)		AR_2	$\overline{AR}_2$	of $\overline{AR}_2$
0.2192	0.4545	0.4823	0.8059		
			0.8142		
			0.8244		
			0.8054	0.8125	0.008
0.4215	0.4362	0.9663	1.7419		
			1.7697		
			1.7321		
			1.7118	1.7389	0.021
0.5299	0.4326	1.2249	2.4129		
			2.4518		
			2.2517		
			2.2986	2.3538	0.081
0.6383	0.3939	1.6205	3.3995		
			3.3751		
			3.4061		
			3.3832	3.3910	0.012

Table A.5: The Values of Intercepts, Slopes and Linear Correlation Coefficients (LCC) for Two Ternary Systems.

	naphthalene-biphenyl-CO_2		naphthalene-phenanthrene-CO_2	
	naphthalene(1)	biphenyl(2)	naphthalene(1)	phenanthrene(2)
intercept	0.2717±0.1197	0.4916±0.2425	0.0158±0.0466	0.1625±0.0593
slope	3.2345±0.0945	0.3462±0.0346	1.3788±0.0391	0.4392±0.0261
LLC	0.9987	0.9854	0.9988	0.9965

Appendix B

Calibration of Pressure Transducers

The Data Instrument pressure transducers (model AB/HP, Serial No. A06342 and 13429, max. 69.0 MPa; model SA, Serial No. 13585, max. 34.5 MPa) were calibrated with a dead weight pressure tester (Testing Instrument Co.). These calibrations were done every 5~6 months during the measurements. The calibration curves for the three transducers are shown in Figures B.1-B.3. In the figures, the reading up curve (in solid line) was used when the pressure was increased and the reading down curve (in dash line) was used when the pressure was decreased.

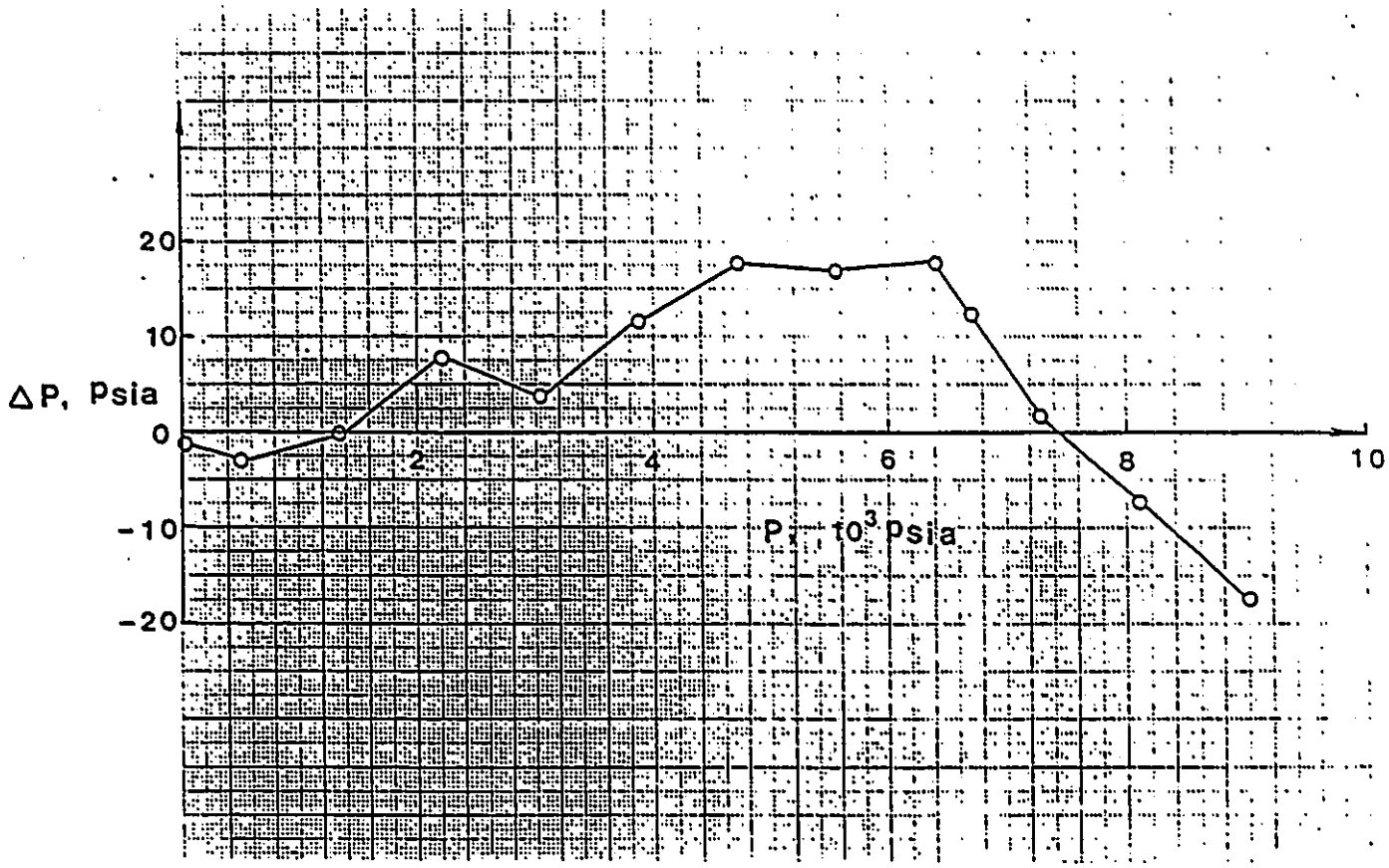

Figure B.1: Calibration Curve of Pressure Transducer for Model AB/HP Serial No. A06342.

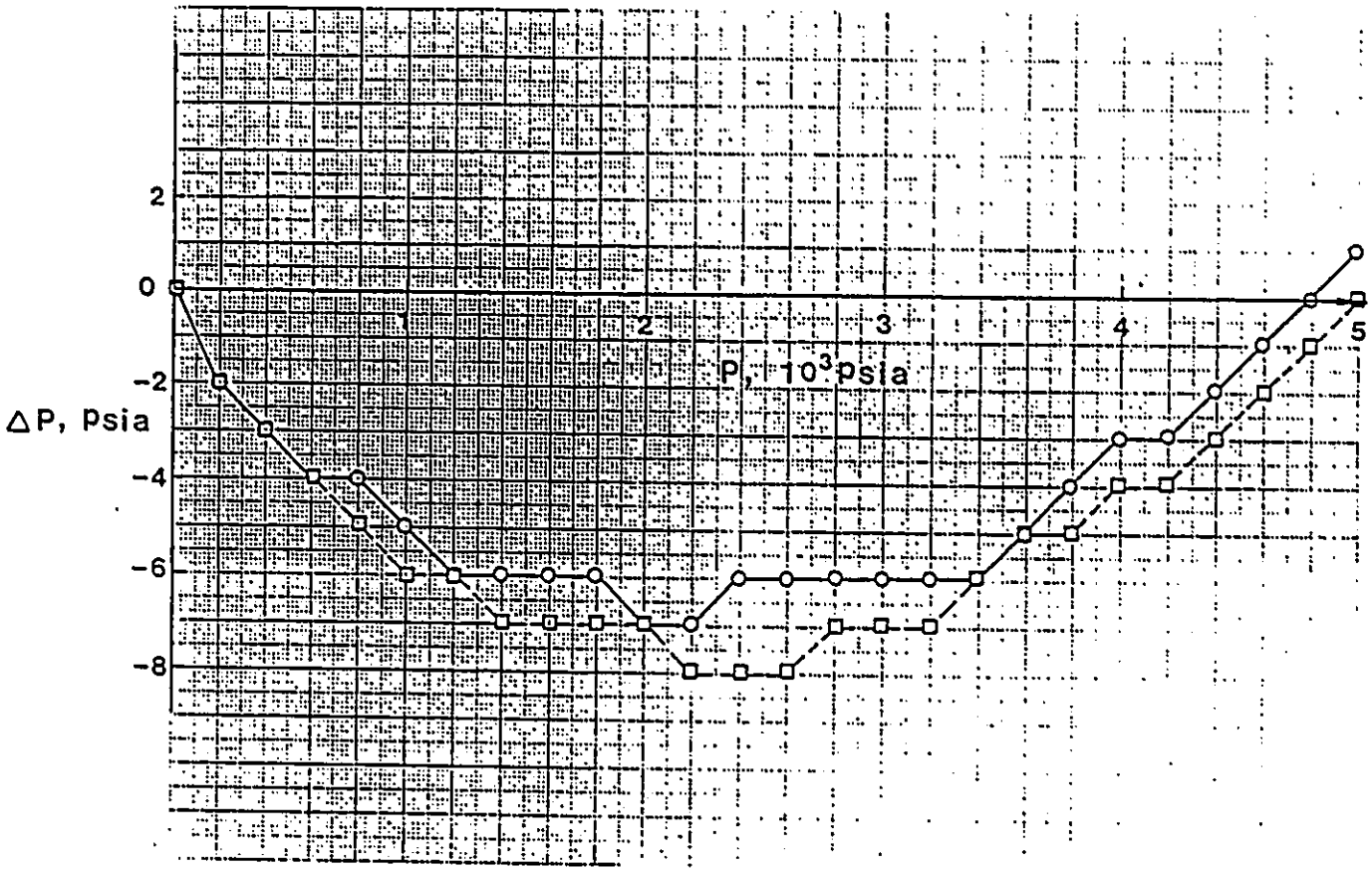

Figure B.2: Calibration Curves of Pressure Transducer for Model AB/HP Serial No. 13429.

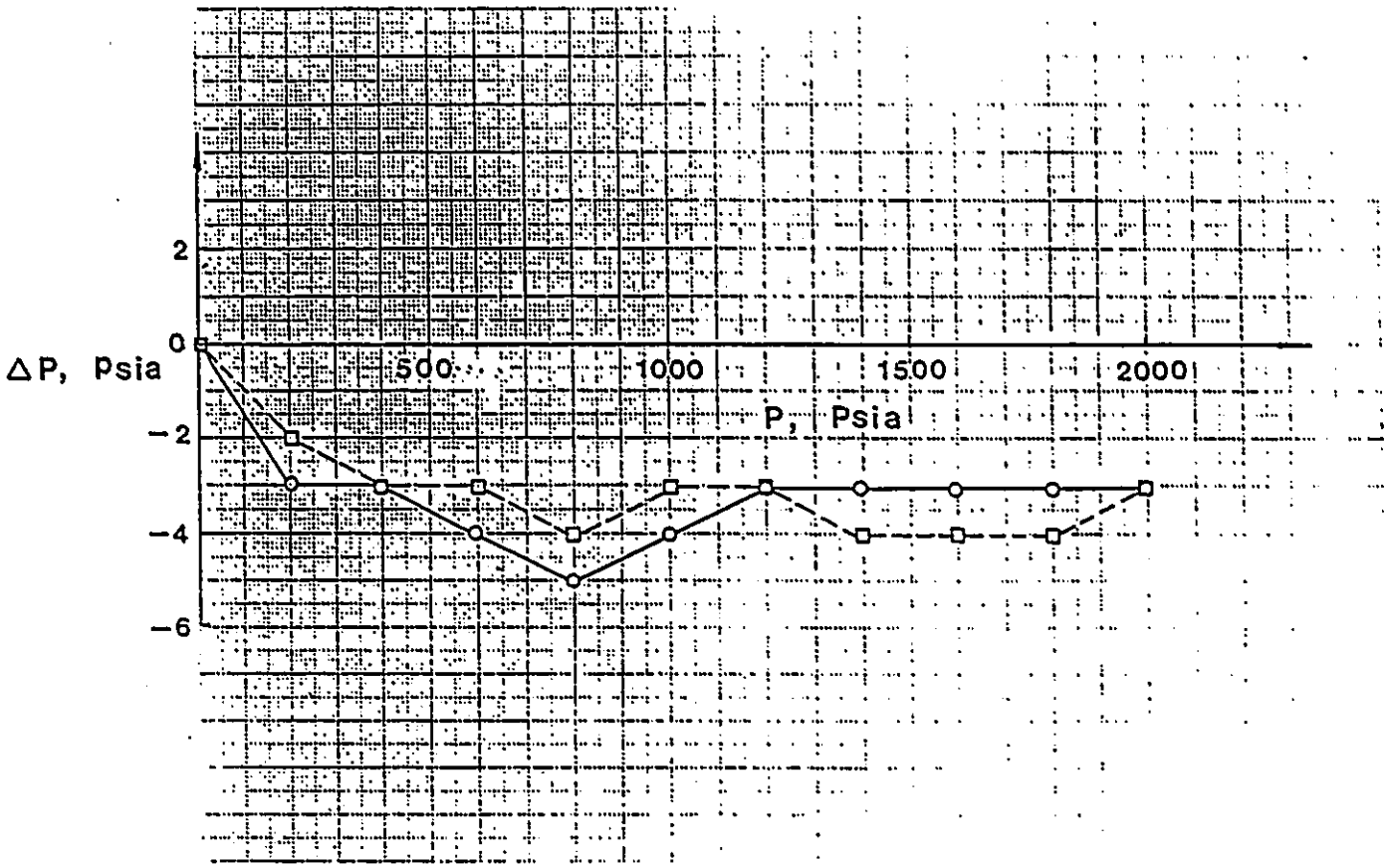

Figure B.3: Calibration Curves of Pressure Transducer for Model SA Serial No. 13585.

Appendix C

Calibration of Quartz Thermometer and Thermocouples

The quartz thermometer (model 2801 A) with sensor (Serial No. 1431-20) and three thermocouples in the air bath were calibrated at the triple point of pure water (0.010 °C) with a platinum resistance thermometer (Serial No. 1775701, calibrated using 1968 IPTS scale, Leeds and Northrup). The resistance at the triple point of water, R_t, was found to be 25.59398 Ω at a bridge temperature of 24.8 °C. The resistance of the thermometer, R_0, at 0°C was found to be 25.59296 Ω using the following equation:

$$\frac{R_t}{R_0} = 1 + At + Bt^2 \qquad \text{(C.1)}$$

where A = 3.98654×10^{-3}, B = -5.985×10^{-7}, and t is in °C. The resistance thermometer was then used to calibrate the quartz thermometer as well as the thermocouples in the air bath using Eq.(C.1). The results obtained for the quartz thermometer are shown in Table C.1. The thermocouples in the air bath were calibrated twice during the measurements. The results are shown in Figures C.1 and C.2.

Table C.1: Calibration Results of the Quartz Thermometer.

Reading temp., t_R °C	Estimated temp., t_E (using Eq.C.1), °C	$\Delta t = t_E - t_R$ °C
-0.0453	0.010*	0.0553
19.065	19.042	-0.023
39.962	39.920	-0.042
50.122	50.054	-0.068
60.261	60.151	-0.110
69.782	69.653	-0.129
80.016	79.490	-0.526

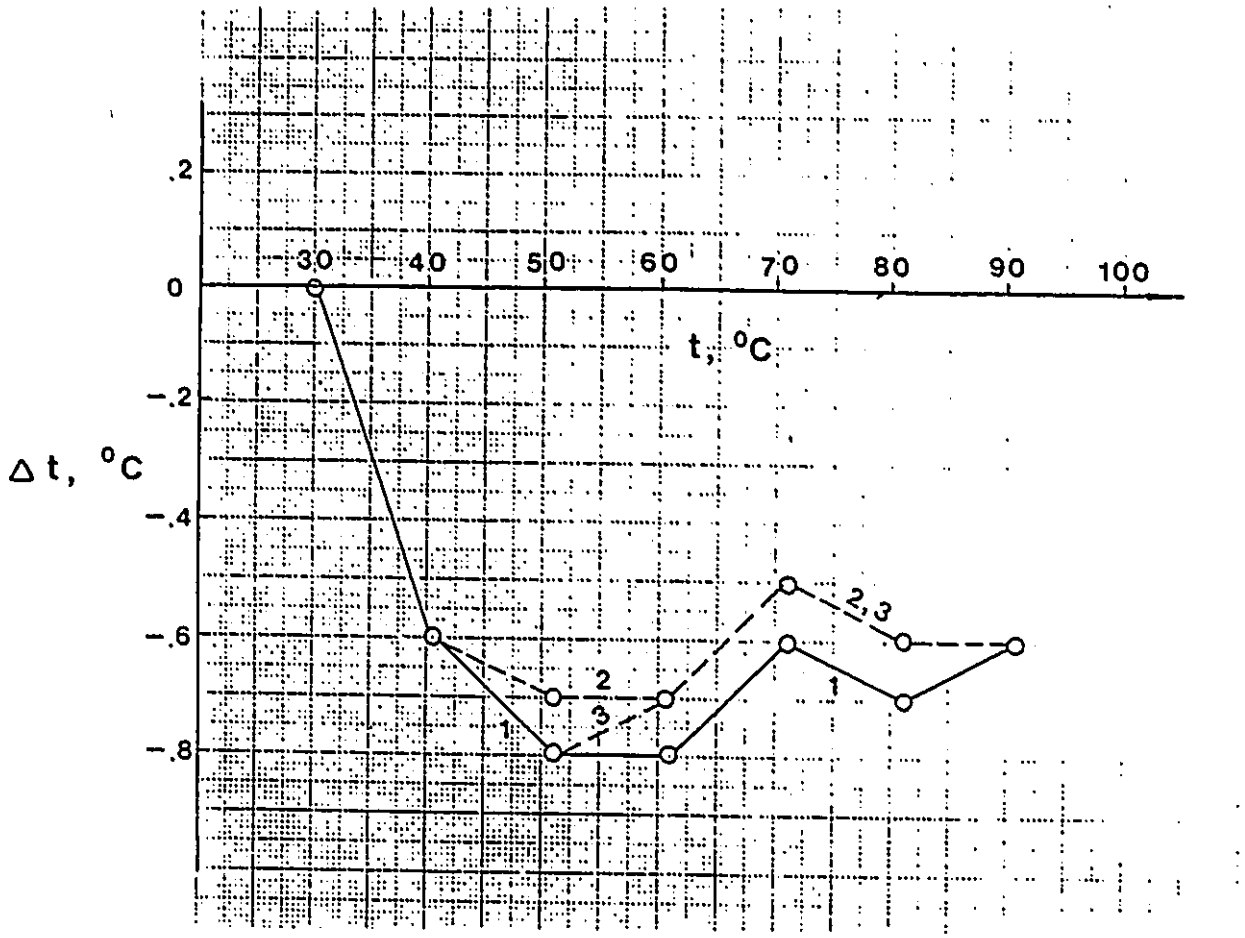

Figure C.1: Calibration Curves I of the Thermocouples in the Air Bath.

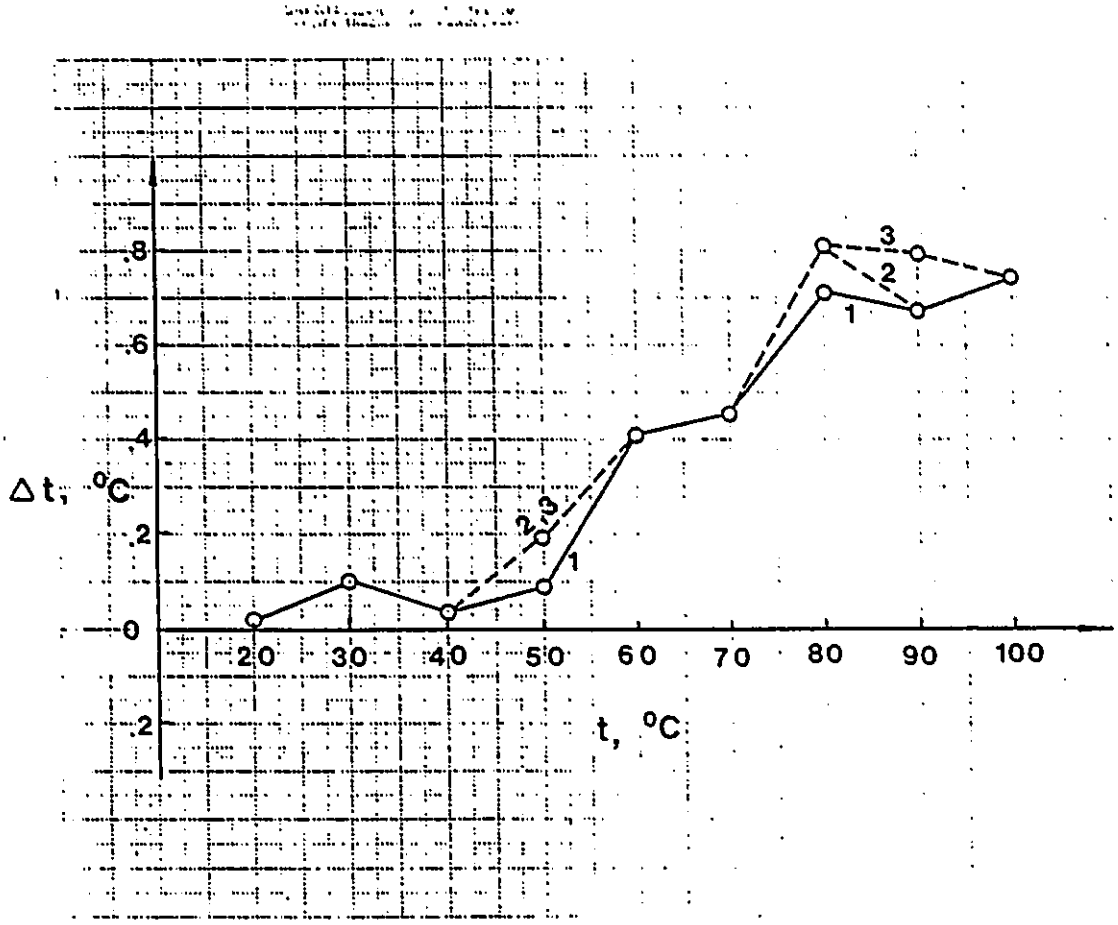

Figure C.2: Calibration Curves II of the Thermocouples in the Air Bath.

Appendix D

Determination of the P-n_{CO2} Relationship in the Sample Loop for P-T-x Measurement

The pressure-number of moles of CO_2 relationship in the sample loop for the P-T-x measurement was determined by the following procedure. A sampler was evacuated before charging with carbon dioxide, the amount of which was determined by weighing. The sample loop volume was confined by the loop from valve 5 to valve 10 including cylinder L placed in a water bath (see Figure 4.6) and was evacuated by the vacuum pump P. The sampler was then connected with valve 9 and expanded through it into the sample loop. The increase in pressure of the pressure gauge (Heise, Newtown Conn.) was then recorded. The relationship between the pressure change and the number of moles of carbon dioxide was obtained by expanding different amounts of carbon dioxide into the sample loop. The results obtained are listed in Table D.1. The pressure increases after expansion were converted into values at 298.15 K using the ideal gas law. The average of the values (n_{CO2}/P) was found to be 1.275×10^{-3} mole/psia at 298.15 K with a standard deviation = 0.025×10^{-3}.

Table D.1: Determination of P-n_{CO_2} Relationship in the Sample Loop for the P-T-x Measurement.

weight of vacuum sampler (g)	weight of sampler with CO_2 (g)	no. of moles of CO_2 (mole)	ΔP after expansion (psia)	water bath temperature (°C)	n_{CO_2} / ΔP (mole/psia)
132.96537	133.44935	0.01100	8.70	23.30	1.264
132.96565	133.34865	0.00870	6.85	23.30	1.270
132.96528	133.28272	0.00721	5.68	22.50	1.269
132.96510	133.22090	0.00581	4.58	25.16	1.269
132.96526	133.10628	0.00320	2.52	25.87	1.270
132.96525	133.01491	0.00113	0.85	26.24	1.329

Appendix E

Computer Programs for the Calculation of the S-L-G Three-Phase Equilibria

In this section, the computer programs for calculating the S-L-G three-phase equilibria for binary mixtures using both the equation-of-state model and the combination of the activity-coefficient model and the equation-of-state model are presented.

```
C   ****************************************************************
C   *          THE CORRELATION OF SLG 3-PHASE EQUILIBRIA           *
C   *                 USING SRK OR PR EOS                          *
C   *                   PRESSURE IS FIXED                          *
C   *                ASSUME PURE SOLID PHASE                       *
C   *                   PRODUCED  IN JULY 1987                     *
C   *                   MODIFIED IN OCT. 1988                      *
C   ****************************************************************
C       MIXING RULES:
C              JMIX = 1   VDW-1 MIXING RULE
C                   = 2   SGR MIXING RILE
C                   = 3   ADACI-SUGIE MIXING RULE
C       EQUATIONS OF STATE:
C              JEOS = 1   SRK EOS
C                     2   PR  EOS
      IMPLICIT DOUBLE PRECISION (A-H,O-Z)
      PARAMETER(KK=1)
      COMMON/BRO1/ TC(3),PC(3),OM(3),AC(3),SM(3),B(3),A(3),R,ND
      COMMON/BRO2/ PE(50),TE(50),TCAL(50),XE(50),XC(50),YC(50)
      COMMON/BRO3/ DEVT(50),DEVX(50),AVGT,AVGX,SKIJ,SKJI
      COMMON/BRO4/ PSS(50),FIV(3),FIL(3),SVL,SVV,VS
      COMMON/BRO5/ AP(3),BP(3),A2P(3),A3P(3),JMIX,JEOS,A12
      COMMON/BRO6/ FS(50),SFS(50),XK(50)
      COMMON/BRO7/ SFV(50),SFL(50),SMVL(50),SMVV(50),REF(50)
      COMMON/BRO8/ ANTA,ANTB,ANTC
      REAL*8 COEF(KK),XKL(KK),H(KK*(KK+1)/2),G(KK),WOR(3*KK)
      DIMENSION TITLE(15)
       CHARACTER OPT*20
       EXTERNAL FUN
C-------------------------------------------------------C
            JMIX = 1
            JEOS = 2
C-------------------------------------------------------C
      READ(5,900) TITLE
      WRITE(6,910) TITLE
      READ(5,*) ND
      WRITE(6,'(21HNUMBER OF DATA POINTS,I3)') ND
      R=82.05
      DO 10 I = 1, 2
      READ(5,*) TC(I),PC(I),OM(I)
      IF (JEOS .EQ. 2) GO TO 80
C
C*********** FOR SRK EOS ***************************
      AC(I)=0.42747*R**2*TC(I)**2/PC(I)
      B(I)=0.08664*R*TC(I)/PC(I)
      SM(I)=0.48000+1.57400*OM(I)-0.17600*OM(I)**2
      GO TO 10
C
C*********** FOR PR EOS ****************************
   80 AC(I)=0.45724*R**2*TC(I)**2/PC(I)
      B(I)=0.07780*R*TC(I)/PC(I)
      SM(I)=0.37464+1.54226*OM(I)-0.26992*OM(I)**2
C***************************************************
10    CONTINUE
      WRITE(6,920)
```

```
      WRITE(6,925) (TC(I),PC(I),OM(I),AC(I),B(I),SM(I),I=1,2)
      READ(5,*) ANTA, ANTB, ANTC, VS
      DO 20 J=1, ND
      READ(5,*) TE(J), PE(J), XE(J)
C     TE(J)=TE(J)+273.15
20    PE(J)=PE(J)*9.869
      WRITE(6,940)
      DO 21 J=1, ND
21    WRITE(6,930)  TE(J), PE(J)/9.869, XE(J)
      WRITE(6,960)
      WRITE(6,930) ANTA, ANTB, ANTC, VS
      WRITE(7,*) 'OPT?'
      READ(7,*) OPT
      READ(7,*) XKL
      IF(OPT.EQ.'OPT') THEN
         CALL ZXMIN(FUN,KK,5,350,3,XKL,H,G,F,WOR,IEE)
      ELSE
         CALL FUN(KK,XKL,F)
      ENDIF
            WRITE(6,931)
            DO 90 J=1,ND
90          WRITE(6,933) J,SFS(J),SFV(J),SFL(J),REF(J)
            WRITE(6,934)
            DO 91 J=1,ND
C           WM=128.174*XE(J)+44.01*(1.-XE(J))
C           WM=154.212*XE(J)+44.01*(1.-XE(J))
            WM=178.234*XE(J)+44.01*(1.-XE(J))
91          WRITE(6,932) J,WM/SMVL(J),44.01/SMVV(J)
      AVGT = 0
      AVGX = 0
      DO 70 J = 1, ND
      AVGT = AVGT+DABS(DEVT(J))/TE(J)
70    AVGX = AVGX+DABS(DEVX(J))/XE(J)
      AVGT = AVGT*100./FLOAT(ND)
      AVGX = AVGX*100./FLOAT(ND)
      WRITE(6,975) AVGT, AVGX
      WRITE(6,980)
      DO 40 J = 1, ND
40    WRITE(6,930) PE(J)/9.869, TE(J), TCAL(J), DEVT(J)
      WRITE(6,1000)
      DO 50 J = 1, ND
50    WRITE(6,930) PE(J)/9.869, XE(J), XC(J), DEVX(J), YC(J)
      WRITE(6,1200) XKL
      WRITE(6,1400) (TCAL(J),PE(J)/9.869, J=1,ND)
      WRITE(6,1300) (XC(J),PE(J)/9.869, J=1,ND)
  900 FORMAT(18A4)
  910 FORMAT(1H ,///,5X,18A4)
  920 FORMAT(1H ,/,5X,'TC(K)',9X,'PC(ATM)',6X,'OM',6X,'AC',14X,'B',
     &  11X,'SM')
  925 FORMAT(6F12.3)
  930 FORMAT(7F10.4)
  931 FORMAT(1H ,/,11X,'FS(P/ATM)',4X,'FV(ATM)',6X,'FL(ATM)',6X,'DEV%')
  932 FORMAT(I6,3X,F12.4,5X,F12.4)
  933 FORMAT(I6,3X,F10.6,3X,F10.6,3X,F10.6,3X,F10.6)
  934 FORMAT(1H ,/,15X,'ROL(G/CC)',8X,'ROV(G/CC)')
```

```
  940 FORMAT(1H ,/,4X,'TE(K)',5X,'PE(MPA)',4X,'XE')
  960 FORMAT(1H ,/,5X,'ANTA',5X,'ANTB',6X,'ANTC',6X,'VS')
  975 FORMAT(1H ,15X,'AVGT% =',F10.4,3X,'AVGX% =',F10.4)
  980 FORMAT(1H ,/,5X,'PE(MPA)',2X,'TE(K)',3X,'TCAL(K)',7X,'DEVT')
 1000 FORMAT(1H ,/,5X,'PE(MPA)',4X,'XE',7X,'XC',7X,'DEVX',7X,'YC')
 1200 FORMAT(1H ,/,5X,'KIJ= ',F10.5,5X,'LJI= ',F10.5,5X,'MIJ=',F10.5)
 1300 FORMAT(F7.4,F12.4)
 1400 FORMAT(F7.2,F12.4)
      END

      SUBROUTINE FUN(NX,XKL,FF)
      IMPLICIT REAL*8(A-H,O-Z)
      REAL*8 COEF(3),XKL(NX)
      COMMON/BRO1/ TC(3),PC(3),OM(3),AC(3),SM(3),B(3),A(3),R,ND
      COMMON/BRO2/ PE(50),TE(50),TCAL(50),XE(50),XC(50),YC(50)
      COMMON/BRO3/ DEVT(50),DEVX(50),AVGT,AVGX,SKIJ,SKJI
      COMMON/BRO4/ PSS(50),FIV(3),FIL(3),SVL,SVV,VS
      COMMON/BRO5/ AP(3),BP(3),A2P(3),A3P(3),JMIX,JEOS,A12
      COMMON/BRO6/ FS(50),SFS(50),XK(50)
      COMMON/BRO7/ SFV(50),SFL(50),SMVL(50),SMVV(50),REF(50)
      COMMON/BRO8/ ANTA,ANTB,ANTC
      COEF(1)=XKL(1)
C     COEF(2)=XKL(2)
C     COEF(3)=XKL(3)
C
      NPA=1
C
      DO 26 J=1,ND
C
      PSS(J)=ANTA-ANTB/(TE(J)+ANTC)
      PSS(J)=10.0**PSS(J)
      PSS(J)=PSS(J)*0.9869
      FS(J)=PSS(J)*DEXP(VS*(PE(J)-PSS(J))/R/TE(J))
C       WRITE(7,*) 'FS',FS(J)
C
      T2=TE(J)
C
C  MODIFIED PR EOS
C
C     FOR NATPHTHALENE(1)
C
C     COEF(1)=.99408-.0022965*TE(J)-.13305E-5*TE(J)**2
C     COEF(1)=.085674+.52836E-3*PE(J)/9.869-.19837/PE(J)*9.869
C     COEF(1)=.098295+.75746E-4*PE(J)/9.869-.27039/PE(J)*9.869
C VDW-1 MR
C     COEF(1)=.250019-0.0115886*PE(J)/9.869
C    &       +.248859E-3*(PE(J)/9.869)**2-.320266/PE(J)*9.869
C
C AS MR
C     COEF(1)=-0.128012+0.0151917*PE(J)/9.869
C    &       -0.279714E-3*(PE(J)/9.869)**2+1.26703/PE(J)*9.869
C
C     COEF(2)=0.203321-0.610237E-2*PE(J)/9.869
C    &       +0.740631E-4*(PE(J)/9.869)**2-1.70624/PE(J)*9.869
C
```

```
C     FOR BIPHENYL(1)
C
C     COEF(1)=.280471-0.0137134*PE(J)/9.869
C    &      +.179159E-3*(PE(J)/9.869)**2-.547051/PE(J)*9.869
C     COEF(1)=.446852-0.0114899*PE(J)/9.869
C    &      +.122218E-3*(PE(J)/9.869)**2-.499911/PE(J)*9.869
C
C     FOR PHENANTHRENE(1)
C
C     COEF(1)=.258298+.951569E-4*PE(J)/9.869-1.00407/PE(J)*9.869
C     COEF(1)=.201194+0.549345E-2*PE(J)/9.869
C    &      -.144939E-3*(PE(J)/9.869)**2-.841285/PE(J)*9.869
C     COEF(1)=3.72237-2.83193*PE(J)/9.869-1.08883/PE(J)*9.869
C     COEF(1)=-14.4699+22.5435*PE(J)/9.869
C    &      -11.7132*(PE(J)/9.869)**2+3.22810/PE(J)*9.869
C
C  ORIGINAL PR
C
C     FOR NATPHTHALENE(1)
C
C     COEF(1)=.12597+.31108E-3*PE(J)/9.869-.25298/PE(J)*9.869
C        WRITE(7,*) 'COEF',COEF(J)
  102 IT=0
 5    IT=IT+1
      IF(IT.GT.100) STOP 'NO CONVERGENCE'
      CALL TEMP(NPA,J,T2,COEF,RET2)
       IF(IT.EQ.1) THEN
      T1=T2*1.01
      IT=IT+1
      CALL TEMP(NPA,J,T1,COEF,RET1)
      ENDIF
      TCAL(J)=(T2*RET1-T1*RET2)/(RET1-RET2)
C     TCAL(J)=(T2*RET2*.5+.5*T1*RET2-T2*RET1)/(RET2-RET1)
C     TCAL(J)=(T2*RET1-T1*RET2)/(RET1-RET2)*.5+(T1+T2)*.25
C     TCAL(J)=((T2*RET1-T1*RET2)/(RET1-RET2)-T2)*.1+T2*.9
      IF(DABS(RET2).GT.1.D-5) THEN
      T1=T2
      RET1=RET2
      T2=TCAL(J)
      GOTO 5
      ENDIF
   50 CONTINUE
      RE=DABS(FS(J)-FIV(1)*YC(J))/FS(J)
      REF(J)=RE*100.
      DEVT(J)=TE(J)-TCAL(J)
      DEVX(J)=XE(J)-XC(J)
      SFV(J)=FIV(1)*YC(J)
      SFL(J)=FIL(1)*XC(J)
      SFS(J)=FS(J)
      SMVL(J)=SVL
C     WRITE(7,*) J
26    SMVV(J)=SVV
      FF=0.
      DO 80 J=1,ND
      FF=FF+((XC(J)-XE(J))/XE(J))**2
```

```
      FF=FF+(((TCAL(J)-TE(J))/TE(J))**2)/0.005
   80 CONTINUE
C     WRITE(7,'(3HK12,F9.5)') COEF(1)
      WRITE(7,'(5H X F ,4G15.5)') XKL,FF
      RETURN
      END
C
      SUBROUTINE TEMP(NPA,J,T,COEF,RET)
      IMPLICIT REAL*8(A-H,O-Z)
      COMMON/BRO1/ TC(3),PC(3),OM(3),AC(3),SM(3),B(3),A(3),R,ND
      COMMON/BRO2/ PE(50),TE(50),TCAL(50),XE(50),XC(50),YC(50)
      COMMON/BRO3/ DEVT(50),DEVX(50),AVGT,AVGX,SKIJ,SKJI
      COMMON/BRO4/ PSS(50),FIV(3),FIL(3),SVL,SVV,VS
      COMMON/BRO5/ AP(3),BP(3),A2P(3),A3P(3),JMIX,JEOS,A12
      COMMON/BRO6/ FS(50),SFS(50),XK(50)
      COMMON/BRO7/ SFV(50),SFL(50),SMVL(50),SMVV(50),REF(50)
      COMMON/BRO8/ ANTA,ANTB,ANTC
      DIMENSION COEF(NPA)
C**   PSS(J)=ANTA-ANTB/(T+ANTC)
C     PSS(J)=10.0**PSS(J)
C     PSS(J)=PSS(J)*0.9869
C      WRITE(7,*) 'T',T
C     FS(J)=PSS(J)*DEXP(VS*(PE(J)-PSS(J))/R/T)
C-----------------------------------------------------------------
      XA=XE(J)
      YA=1.E-4
      NXY=0
11    DAK1 = YA/XA
      DAK2 = (1.-YA)/(1.-XA)
       X0=XA
       Y0=YA
C
C *** LIQUID PHASE ******************************
      CALL CONST(NPA,J,T,XA,COEF,AT,BT)
      CALL VOLUME(J,T,AT,BT,VL,VV,ZL,ZV)
      CALL FUG(J,T,XA,AT,BT,ZL,FIL)
         SVL=VL
         XC(J)=XA
C
C *** VAPOR  PHASE ******************************
      CALL CONST(NPA,J,T,YA,COEF,AT,BT)
      CALL VOLUME(J,T,AT,BT,VL,VV,ZL,ZV)
      CALL FUG(J,T,YA,AT,BT,ZV,FIV)
C        WRITE(6,990) YA,AT,BT,VL,VV
         SVV=VV
         YC(J)=YA
      DAKC1 =FIL(1)/FIV(1)
      RE1 = DABS(DAK1-DAKC1)
      DAKC2 =FIL(2)/FIV(2)
      RE2 = DABS(DAK2-DAKC2)
      IF (RE1 .LT. 2.0D-3 .AND. RE2 .LT. 2.0D-3) GO TO 51
      NXY=NXY+1
      IF (NXY .GT. 100) STOP 'NO CONVERGENCE IN XY LOOP'
      XA = (DAKC2-1.)/(DAKC2-DAKC1)
       XA=(XA+X0)*.5
```

```
      IF (XA .LT. 0.0) XA=X0*1.2
      IF (XA .GT. 1.0) XA=X0*0.8
      YA = DAKC1*XA
      IF (YA.GT..50) YA=.5
      GO TO 11
   51 RET=(FS(J)-FIV(1)*YA)/FS(J)
C     WRITE(7,'(4HK12=,2G13.5,3HX Y,2G13.5)') DAKC1,DAKC2,XA,YA
      RETURN
      END
C
      SUBROUTINE CONST(NPA,J,T,X,COEF,AT,BT)
      IMPLICIT REAL*8(A-H,O-Z)
      COMMON/BRO1/ TC(3),PC(3),OM(3),AC(3),SM(3),B(3),A(3),R,ND
      COMMON/BRO2/ PE(50),TE(50),TCAL(50),XE(50),XC(50),YC(50)
      COMMON/BRO3/ DEVT(50),DEVX(50),AVGT,AVGX,SKIJ,SKJI
      COMMON/BRO4/ PSS(50),FIV(3),FIL(3),SVL,SVV,VS
      COMMON/BRO5/ AP(3),BP(3),A2P(3),A3P(3),JMIX,JEOS,A12
      COMMON/BRO6/ FS(50),SFS(50),XK(50)
      COMMON/BRO7/ SFV(50),SFL(50),SMVL(50),SMVV(50),REF(50)
      REAL*8 COEF(NPA), ALFA(3)
C** MODIFIED PR EOS ***************************
C
C * FOR NAPHTHALENE(1)
C     ALFA(1)=1.+1.125363*(1.-(T/TC(1))**.5)-.1791811*(1.-T/TC(1))
C    &   -.002358876*(1.-(T/TC(1))**2)
C
C * FOR BIPHENYL(1)
C     ALFA(1)=1.-13.05755*(1.-(T/TC(1))**.5)+16.13556*(1.-T/TC(1))
C    &   -5.367846*(1.-(T/TC(1))**2)
C       WRITE(7,*) 'MPR AL ',J, ALFA(1)
C
C * FOR PHENANTHRENE(1)
      ALFA(1)=1.+4.272634*(1.-(T/TC(1))**.5)-2.097627*(1.-T/TC(1))
     &   +0.04738668*(1.-(T/TC(1))**2)
C
      ALFA(1)=ALFA(1)**2
      ALFA(2)=1.0*EXP(0.5856143*(1.-(T/TC(2))))
C   ORIGINAL PR EOS
      DO 10 I=1,2
C     ALFA(I)=(1.0+SM(I)*(1.0-(T/TC(I))**0.5))**2
      A(I)=AC(I)*ALFA(I)
   10 CONTINUE
C       WRITE(7,*) 'PR AL ',J, ALFA(1)
C       WRITE(7,*) 'AL MPR ',ALFA(1),ALFA(2)
C     ALFA(1)=(1.0+SM(1)*(1.0-(T/TC(1))**0.5))**2
C     ALFA(2)=(1.0+SM(2)*(1.0-(T/TC(2))**0.5))**2
C       WRITE(7,*) 'AL PR ',ALFA(1),ALFA(2)
      X2=1.-X
      GOTO(15,20,22),JMIX
C********* VDW-1 MIXING RULE ***********************************
   15 A12=(A(1)*A(2))**0.5*(1.-COEF(1))
      AT=X**2*A(1)+X2**2*A(2)+2.*X*X2*A12
      BT=X*B(1)+X2*B(2)
      GO TO 30
C********* VDW-2 MIXING RULE ***********************************
```

```
C  20 A12=(A(1)*A(2))**0.5*(1.-COEF(1))
C     B12=(B(1)+B(2))/2.*(1.-COEF(2))
C     AT=X**2*A(1)+X2**2*A(2)+2.*X*X2*A12
C     BT=X**2*B(1)+X2**2*B(2)+2.*X*X2*B12
C     AP(1)=2.*(X*A(1)+X2*A12)
C     AP(2)=2.*(X*A12+X2*A(2))
C     BP(1)=2.*(X*B(1)+X2*B12)
C     BP(2)=2.*(X*B12+X2*B(2))
C     WRITE(7,'(5HCOEF=,2G15.5)') COEF
C*****************************************************************
C************** SGR MIXING RULE ******************************
   20 CMIJ=COEF(3)
      CMJI=1.-COEF(3)
      A12=(A(1)*A(2))**0.5*(1.-COEF(1)-COEF(2)*
     &    (CMIJ*X-CMJI*X2)/(CMIJ*X+CMJI*X2))
      AT=X**2*A(1)+X2**2*A(2)+2.*X*X2*A12
      BT=X*B(1)+X2*B(2)
      AP(1)=2.*(X*A(1)+X2*A12-2.*X*X2**2*(A(1)*A(2))**.5
     &      *COEF(2)*CMIJ*CMJI/(CMIJ*X+CMJI*X2)**2)
      AP(2)=2.*(X*A12+X2*A(2)+2.*X2*X**2*(A(1)*A(2))**.5
     &      *COEF(2)*CMIJ*CMJI/(CMIJ*X+CMJI*X2)**2)
      GO TO 30
C************** ADACHI-SUGEI MIXING RULE ***************************
   22 A12=(A(1)*A(2))**0.5*(1.-COEF(1)-COEF(2)*(X-X2))
      AT=X**2*A(1)+X2**2*A(2)+2.*X*X2*A12
      BT=X*B(1)+X2*B(2)
      AP(1)=2.*(X*A(1)+X2*A12-2.*X*X2**2*COEF(2)*(A(1)*A(2))**.5)
      AP(2)=2.*(X*A12+X2*A(2)+2.*X2*X**2*COEF(2)*(A(1)*A(2))**.5)
   30 RETURN
      END

      SUBROUTINE VOLUME(J,T,AT,BT,VL,VV,ZL,ZV)
      IMPLICIT REAL*8(A-H,O-Z)
      COMMON/BR01/ TC(3),PC(3),OM(3),AC(3),SM(3),B(3),A(3),R,ND
      COMMON/BR02/ PE(50),TE(50),TCAL(50),XE(50),XC(50),YC(50)
      COMMON/BR03/ DEVT(50),DEVX(50),AVGT,AVGX,SKIJ,SKJI
      COMMON/BR04/ PSS(50),FIV(3),FIL(3),SVL,SVV,VS
      COMMON/BR05/ AP(3),BP(3),A2P(3),A3P(3),JMIX,JEOS,A12
      COMMON/BR06/ FS(50),SFS(50),XK(50)
      COMMON/BR07/ SFV(50),SFL(50),SMVL(50),SMVV(50),REF(50)
      DIMENSION AA(3),X(3)
      RA=AT*PE(J)/(R*T)**2
      RB=BT*PE(J)/(R*T)
      GOTO(5,20) JEOS
C******** FOR SRK EOS ********
 5    AA(1)=-1.0
      AA(2)=RA-RB-RB**2
      AA(3)=-RA*RB
      GO TO 10
C******* FOR PR EOS **********
   20 AA(1)=RB-1.0
      AA(2)=RA-3*RB**2-2*RB
      AA(3)=-(RA*RB-RB**2-RB**3)
C*****************************
   10 CONTINUE
```

```
      CALL TRTON(AA,X,N)
      ZL=X(1)
      ZV=X(3)
      VL=ZL*R*T/PE(J)
      VV=ZV*R*T/PE(J)
      RETURN
      END
C
      SUBROUTINE FUG(J,T,X,AT,BT,Z,F)
      IMPLICIT REAL*8(A-H,O-Z)
      COMMON/BRO1/ TC(3),PC(3),OM(3),AC(3),SM(3),B(3),A(3),R,ND
      COMMON/BRO2/ PE(50),TE(50),TCAL(50),XE(50),XC(50),YC(50)
      COMMON/BRO3/ DEVT(50),DEVX(50),AVGT,AVGX,SKIJ,SKJI
      COMMON/BRO4/ PSS(50),FIV(3),FIL(3),SVL,SVV,VS
      COMMON/BRO5/ AP(3),BP(3),A2P(3),A3P(3),JMIX,JEOS,A12
      COMMON/BRO6/ FS(50),SFS(50),XK(50)
      COMMON/BRO7/ SFV(50),SFL(50),SMVL(50),SMVV(50),REF(50)
      REAL*8 FAI(3), F(3)
      X2=1.-X
      RA=AT*PE(J)/(R*T)**2
      RB=BT*PE(J)/(R*T)
      GOTO(5,60),JEOS
5     GOTO(21,20,22),JMIX
C
C************ SRK VDW-1 MIXING RULE ***********************************
21    FAI(1)=B(1)/BT*(Z-1.0)-DLOG(Z-RB)-RA/RB*(2.*(X*A(1)+X2*A12)/AT
     &  -B(1)/BT)*DLOG(1.0+RB/Z)
      FAI(2)=B(2)/BT*(Z-1.0)-DLOG(Z-RB)-RA/RB*(2.*(X2*A(2)+X*A12)/AT
     &  -B(2)/BT)*DLOG(1.0+RB/Z)
      GO TO 30
C************ SRK VDW-2 MIXING RULE ***********************************
   20 FAI(I)=(BP(I)/BT-1.)*(Z-1.0)-DLOG(Z-RB)-RA/RB*(1.+AP(I)/AT
     &  -BP(I)/BT)*DLOG(1.0+RB/Z)
      GO TO 30
C
C****************** SRK P-REID MIXING RULE ****************************
   22 FAI(I)=-DLOG(Z-RB)+B(I)/BT*(Z-1.)-RA/RB*((AP(I)-A2P(I)+A3P(I))
     & /AT-B(I)/BT)*DLOG(1.0+RB/Z)
      GO TO 30
C**********************************************************************
C
  60   GOTO(45,70,77),JMIX
C
C************ PR VDW-1 MIXING RULE ************************************
45    FAI(1)=B(1)/BT*(Z-1.0)-DLOG(Z-RB)-RA/RB*(2.*(X*A(1)+X2*A12)/AT
     &  -B(1)/BT)/2.82843*DLOG((Z+2.41421*RB)/(Z-0.41421*RB))
      FAI(2)=B(2)/BT*(Z-1.0)-DLOG(Z-RB)-RA/RB*(2.*(X2*A(2)+X*A12)/AT
     &  -B(2)/BT)/2.82843*DLOG((Z+2.41421*RB)/(Z-0.41421*RB))
      GO TO 30
C************ PR VDW-2 MIXING RULE ************************************
C  70 FAI(1)=(BP(1)/BT-1.)*(Z-1.0)-DLOG(Z-RB)-RA/RB*(1.+AP(1)/AT
C     &  -BP(1)/BT)/2.82843*DLOG((Z+2.41421*RB)/(Z-0.41421*RB))
C      FAI(2)=(BP(2)/BT-1.)*(Z-1.0)-DLOG(Z-RB)-RA/RB*(1.+AP(2)/AT
C     &  -BP(2)/BT)/2.82843*DLOG((Z+2.41421*RB)/(Z-0.41421*RB))
C      GO TO 30
```

```
C*********************************************************************
C***************** PR SGR MIXING RULE ************************
   70 FAI(1)=-DLOG(Z-RB)+B(1)/BT*(Z-1.)-RA/RB*(AP(1)/AT
     & -B(1)/BT)/2.82843*DLOG((Z+2.41421*RB)/(Z-0.41421*RB))
      FAI(2)=-DLOG(Z-RB)+B(2)/BT*(Z-1.)-RA/RB*(AP(2)/AT
     & -B(2)/BT)/2.82843*DLOG((Z+2.41421*RB)/(Z-0.41421*RB))
      GO TO 30
C***************** PR ADACHI-SUGEI MIXING RULE ***********************
   77 FAI(1)=-DLOG(Z-RB)+B(1)/BT*(Z-1.)-RA/RB*(AP(1)/AT
     & -B(1)/BT)/2.82843*DLOG((Z+2.41421*RB)/(Z-0.41421*RB))
      FAI(2)=-DLOG(Z-RB)+B(2)/BT*(Z-1.)-RA/RB*(AP(2)/AT
     & -B(2)/BT)/2.82843*DLOG((Z+2.41421*RB)/(Z-0.41421*RB))
C*********************************************************************
   30 CONTINUE
      DO 10 I=1, 2
10    F(I)=PE(J)*DEXP(FAI(I))
      RETURN
      END
C
      SUBROUTINE TRTON(A,X,N)
      IMPLICIT REAL*8(A-H,O-Z)
      REAL*8 A(3),X(3)
      CALL TRNLQ(A,X,N)
      IF( N .NE. 1 ) GO TO 10
      X(2)=X(1)
      X(3)=X(1)
      RETURN
   10 XM=X(1)
      IF( X(2) .GT. X(1) ) GO TO 11
      X(1)=X(2)
      X(2)=XM
   11 XM=X(1)
      IF( X(3) .GT. X(1) ) GO TO 12
      X(1)=X(3)
      X(3)=XM
   12 XM=X(3)
      IF( X(3) .GT. X(2) ) GO TO 13
      X(3)=X(2)
      X(2)=XM
   13 RETURN
      END
C
C
      SUBROUTINE TRNLQ(A,X,N)
      IMPLICIT REAL*8(A-H,O-Z)
      REAL*8 A(3),X(3)
      PAI=3.141592653589
      E=(3.*A(2)-A(1)*A(1))/9.
      F=(2.*A(1)**3-9.*A(1)*A(2)+27.*A(3))/27.
      D=F*F+4.*E*E*E
      IF( D ) 1,2,2
    2 F1=(-F+ DSQRT(D))/2.
      F2=(-F- DSQRT(D))/2.
      X(1)=-A(1)/3.
      IF( F1 .NE. 0. ) X(1)=X(1)+F1/ DABS(F1)**(2./3.)
```

```
      IF( F2 .NE. 0. ) X(1)=X(1)+F2/ DABS(F2)**(2./3.)
      N=1
      GO TO 10
    1 R= DSQRT(-E*E*E)
      COR=-F/2./R
      THETA=DARCOS(COR)
      XX=2.*R**(1./3.)
      XY=-A(1)/3.
      X(1)=XX* DCOS(THETA/3.)+XY
      X(2)=XX* DCOS((THETA+2.*PAI)/3.)+XY
      X(3)=XX* DCOS((THETA+4.*PAI)/3.)+XY
      N=3
   10 RETURN
      END
```

```
C   ****************************************************************
C   *          THE CORRELATION OF SLG 3-PHASE EQUILIBRIA           *
C   *                  USING SRK OR PR EOS                         *
C   *                   PRESSURE IS FIXED                          *
C   *                ASSUME PURE SOLID PHASE                       *
C   *            EQUATION OF STATE FOR VAPOR PHASE                 *
C   *        GAMA MODEL---REGULAR SOLUTION FOR LIQUID PHASE        *
C   *                  PRODUCED  IN NOV. 1989                      *
C   ****************************************************************
C       MIXING RULES:
C              JMIX = 1   CONVENTIONAL MIXING RULE (VDW-1)
C                   = 2   CONVENTIONAL MIXING RULE (VDW-2)
C                   = 3   ADACHI-SUGEI MIXING RULE
C       EQUATIONS OF STATE:
C              JEOS = 1   SRK EOS
C                     2   PR  EOS
      IMPLICIT DOUBLE PRECISION (A-H,O-Z)
      PARAMETER(KK=1)
      COMMON/BRO1/ TC(3),PC(3),OM(3),AC(3),SM(3),B(3),A(3),R,ND
      COMMON/BRO2/ PE(50),TE(50),TCAL(50),XE(50),XC(50),YC(50)
      COMMON/BRO3/ DEVT(50),DEVX(50),AVGT,AVGX,SKIJ,SKJI
      COMMON/BRO4/ PSS(50),FIV(3),FIL(3),SVL,SVV,VS
      COMMON/BRO5/ AP(3),BP(3),A2P(3),A3P(3),JMIX,JEOS,A12
      COMMON/BRO6/ FS(50),SFS(50),XK(50)
      COMMON/BRO7/ SFV(50),SFL(50),SMVL(50),SMVV(50),REF(50)
      COMMON/BRO8/ ANTA,ANTB,ANTC
      COMMON/BRO9/ GAMA(50),X2C(50),Y2C(50)
      REAL*8 COEF(2),XKL(KK),H(KK*(KK+1)/2),G(KK),WOR(3*KK)
      DIMENSION TITLE(15)
       CHARACTER OPT*20
       EXTERNAL FUN
C-------------------------------------------------------C
            JMIX = 1
            JEOS = 2
C-------------------------------------------------------C
      READ(5,900) TITLE
      WRITE(6,910) TITLE
      READ(5,*) ND
      WRITE(6,'(21HNUMBER OF DATA POINTS,I3)') ND
      R=82.05
      DO 10 I = 1, 2
      READ(5,*) TC(I),PC(I),OM(I)
      IF (JEOS .EQ. 2) GO TO 80
C
C*********** FOR SRK EOS ***************************
      AC(I)=0.42747*R**2*TC(I)**2/PC(I)
      B(I)=0.08664*R*TC(I)/PC(I)
      SM(I)=0.48000+1.57400*OM(I)-0.17600*OM(I)**2
      GO TO 10
C
C*********** FOR PR EOS ****************************
   80 AC(I)=0.45724*R**2*TC(I)**2/PC(I)
      B(I)=0.07780*R*TC(I)/PC(I)
      SM(I)=0.37464+1.54226*OM(I)-0.26992*OM(I)**2
C***************************************************
```

```
10    CONTINUE
      WRITE(6,920)
      WRITE(6,925) (TC(I),PC(I),OM(I),AC(I),B(I),SM(I),I=1,2)
      READ(5,*) ANTA, ANTB, ANTC, VS
      DO 20 J=1, ND
      READ(5,*) TE(J),PE(J),XE(J),XK(J)
C     TE(J)=TE(J)+273.15
20    PE(J)=PE(J)*9.869
      WRITE(6,940)
      DO 21 J=1, ND
21    WRITE(6,930)  TE(J), PE(J)/9.869, XE(J)
      WRITE(6,960)
      WRITE(6,930) ANTA, ANTB, ANTC, VS
      WRITE(7,*) 'OPT?'
      READ(7,*) OPT
      READ(7,*) XKL
      IF(OPT.EQ.'OPT') THEN
         CALL ZXMIN(FUN,KK,5,350,3,XKL,H,G,F,WOR,IEE)
      ELSE
         CALL FUN(KK,XKL,F)
      ENDIF
            WRITE(6,931)
            DO 90 J=1,ND
90          WRITE(6,933) J,SFS(J),SFV(J),SFL(J),REF(J)
            WRITE(6,934)
            DO 91 J=1,ND
            WM=128.174*XE(J)+44.01*(1.-XE(J))
C           WM=154.212*XE(J)+44.01*(1.-XE(J))
C           WM=178.234*XE(J)+44.01*(1.-XE(J))
91          WRITE(6,932) J,WM/SMVL(J),44.01/SMVV(J)
      AVGT = 0
      AVGX = 0
      DO 70 J = 1, ND
      AVGT = AVGT+DABS(DEVT(J))/TE(J)
70    AVGX = AVGX+DABS(DEVX(J))/XE(J)
      AVGT = AVGT*100./FLOAT(ND)
      AVGX = AVGX*100./FLOAT(ND)
      WRITE(6,975) AVGT, AVGX
      WRITE(6,980)
      DO 40 J = 1, ND
40    WRITE(6,930) PE(J)/9.869, TE(J), TCAL(J), DEVT(J)
      WRITE(6,1000)
      DO 50 J = 1, ND
50    WRITE(6,930) PE(J)/9.869, XE(J), XC(J), DEVX(J), YC(J)
      WRITE(6,1200) XKL
      WRITE(6,1400) (TCAL(J),PE(J)/9.869, J=1,ND)
      WRITE(6,1300) (XC(J),PE(J)/9.869, J=1,ND)
  900 FORMAT(18A4)
  910 FORMAT(1H ,///,5X,18A4)
  920 FORMAT(1H ,/,5X,'TC(K)',9X,'PC(ATM)',6X,'OM',6X,'AC',14X,'B',
     &  11X,'SM')
  925 FORMAT(6F12.3)
  930 FORMAT(7F10.4)
  931 FORMAT(1H ,/,11X,'FS(P/ATM)',4X,'FV(ATM)',6X,'FL(ATM)',6X,'DEV%')
  932 FORMAT(I6,3X,F12.4,5X,F12.4)
```

```
  933 FORMAT(I6,3X,F10.6,3X,F10.6,3X,F10.6,3X,F10.6)
  934 FORMAT(1H ,/,15X,'ROL(G/CC)',8X,'ROV(G/CC)')
  940 FORMAT(1H ,/,4X,'TE(K)',5X,'PE(MPA)',4X,'XE')
  960 FORMAT(1H ,/,5X,'ANTA',5X,'ANTB',6X,'ANTC',6X,'VS')
  975 FORMAT(1H ,15X,'AVGT% =',F10.4,3X,'AVGX% =',F10.4)
  980 FORMAT(1H ,/,5X,'PE(MPA)',2X,'TE(K)',3X,'TCAL(K)',7X,'DEVT')
 1000 FORMAT(1H ,/,5X,'PE(MPA)',4X,'XE',7X,'XC',7X,'DEVX',7X,'YC')
 1200 FORMAT(1H ,/,5X,'KIJ= ',F10.5,5X,'LJI= ',F10.5)
 1300 FORMAT(F7.4,F12.4)
 1400 FORMAT(F7.2,F12.4)
      END

      SUBROUTINE FUN(NX,XKL,FF)
      IMPLICIT REAL*8(A-H,O-Z)
      REAL*8 COEF(2),XKL(NX)
      COMMON/BRO1/ TC(3),PC(3),OM(3),AC(3),SM(3),B(3),A(3),R,ND
      COMMON/BRO2/ PE(50),TE(50),TCAL(50),XE(50),XC(50),YC(50)
      COMMON/BRO3/ DEVT(50),DEVX(50),AVGT,AVGX,SKIJ,SKJI
      COMMON/BRO4/ PSS(50),FIV(3),FIL(3),SVL,SVV,VS
      COMMON/BRO5/ AP(3),BP(3),A2P(3),A3P(3),JMIX,JEOS,A12
      COMMON/BRO6/ FS(50),SFS(50),XK(50)
      COMMON/BRO7/ SFV(50),SFL(50),SMVL(50),SMVV(50),REF(50)
      COMMON/BRO8/ ANTA,ANTB,ANTC
      COMMON/BRO9/ GAMA(50),X2C(50),Y2C(50)
      COEF(1)=XKL(1)
      COEF(2)=XKL(2)
C     COEF(2)=0.1
C
      NPA=1
C
      DO 26 J=1,ND
C
      PSS(J)=ANTA-ANTB/(TE(J)+ANTC)
      PSS(J)=10.0**PSS(J)
      PSS(J)=PSS(J)*0.9869
      FS(J)=PSS(J)*DEXP(VS*(PE(J)-PSS(J))/R/TE(J))
C
      T1=TE(J)
    5 CALL TEMP(NPA,J,T1,COEF)
      RET=TCAL(J)-T1
      IF (ABS(RET).GT.1.D-1) THEN
      T1=TCAL(J)
      GO TO 5
      END IF
C
      RE=DABS(FS(J)-FIV(1)*YC(J))/FS(J)
      REF(J)=RE*100.
      DEVT(J)=TE(J)-TCAL(J)
      DEVX(J)=XE(J)-XC(J)
      SFV(J)=FIV(1)*YC(J)
      SFL(J)=FIL(1)*XC(J)
      SFS(J)=FS(J)
      SMVL(J)=SVL
   26 SMVV(J)=SVV
      FF=0.
```

```
      DO 80 J=1,ND
C     FF=FF+((XC(J)-XE(J))/XE(J))**2
C     FF=FF+(((TCAL(J)-TE(J))/TE(J))**2)/0.005
   80 FF=FF+(((TCAL(J)-TE(J))/TE(J))**2)
      DO 81 J=ND-4,ND
   81 FF=FF+((XC(J)-XE(J))/XE(J))**2
C     WRITE(7,'(3HK12,F9.5)') COEF(1)
      WRITE(7,'(5H X F ,4G15.5)') XKL,FF
      RETURN
      END
C
      SUBROUTINE TEMP(NPA,J,T,COEF)
      IMPLICIT REAL*8(A-H,O-Z)
      COMMON/BR01/ TC(3),PC(3),OM(3),AC(3),SM(3),B(3),A(3),R,ND
      COMMON/BR02/ PE(50),TE(50),TCAL(50),XE(50),XC(50),YC(50)
      COMMON/BR03/ DEVT(50),DEVX(50),AVGT,AVGX,SKIJ,SKJI
      COMMON/BR04/ PSS(50),FIV(3),FIL(3),SVL,SVV,VS
      COMMON/BR05/ AP(3),BP(3),A2P(3),A3P(3),JMIX,JEOS,A12
      COMMON/BR06/ FS(50),SFS(50),XK(50)
      COMMON/BR07/ SFV(50),SFL(50),SMVL(50),SMVV(50),REF(50)
      COMMON/BR08/ ANTA,ANTB,ANTC
      COMMON/BR09/ GAMA(50),X2C(50),Y2C(50)
      DIMENSION COEF(NPA)
C**   PSS(J)=ANTA-ANTB/(T+ANTC)
C     PSS(J)=10.0**PSS(J)
C     PSS(J)=PSS(J)*0.9869
C      WRITE(7,*) 'T',T
C     FS(J)=PSS(J)*DEXP(VS*(PE(J)-PSS(J))/R/T)
C-----------------------------------------------------------------
      XA=XE(J)
      YA=1.E-3
      NY=0
      NX=0
C
C *** VAPOR  PHASE ****************************
   11 CALL CONST(NPA,J,T,YA,COEF,AT,BT)
      CALL VOLUME(J,T,AT,BT,VL,VV,ZL,ZV)
      CALL FUG(J,T,YA,AT,BT,ZV,FIV)
C        WRITE(6,990) YA,AT,BT,VL,VV
         SVV=VV
      YC(J)=FS(J)/FIV(1)
      Y2C(J)=1.-YC(J)
      REY=YC(J)-YA
      IF (ABS(REY).LT.1.D-3) GO TO 22
      NY=NY+1
      IF (NY .GT. 100) STOP 'NO CONVERGENCE IN Y LOOP'.
      YA=YC(J)
      GO TO 11
C
C *** LIQUID PHASE ****************************
   22 CALL CONST(NPA,J,T,XA,COEF,AT,BT)
      CALL VOLUME(J,T,AT,BT,VL,VV,ZL,ZV)
      CALL FUG(J,T,XA,AT,BT,ZL,FIL)
         SVL=VL
      X2C(J)=Y2C(J)*FIV(2)/FIL(2)
```

```
      XC(J)=1.-X2C(J)
      REX=XC(J)-XA
      IF (ABS(REX).LT.1.D-3) GO TO 33
      NX=NX+1
      IF (NX .GT. 100) STOP 'NO CONVERGENCE IN X LOOP'
      XA=XC(J)
      GO TO 22
   33 CONTINUE
C******** CALC. GAMA USING REGULAR SOLUTION MODEL *************
C        RTLN(GAMA1)=V1L*PHI2**2*(SOPR1-SOPR2)**2
C          SOPR1,SOPR2----SOLY PARAMETER, (CAL/CM3)**.5
C          V1L,V2L--------MOLAR VOLUME IN LIQUID STATE, CM3/MOL
C          PHI2-----------FRACTION OF MOLAR VOLUME 2
C          R--------------1.987 CAL/MOL/K
C        TM-------------MELTING POINT OF COMP. 1, K
C        DH-------------HEAT OF FUSION, J/MOL
C*************************************************************
C******* FOR NAPH-CO2
      SOPR1=9.924
      SOPR2=6.013
      V1L=132.0
      V2L=44.0
      TM=353.5
      DH=19300.
C****** FOR BIPH-CO2
C     SOPR1=9.891
C     SOPR2=6.013
C     V1L=155.8
C     V2L=44.0
C     TM=342.7
C     DH=18600.
C
      PHI2=X2C(J)*V2L/(X2C(J)*V2L+XC(J)*V1L)
      GAMA(J)=V1L*PHI2**2*(SOPR1-SOPR2)**2/1.987/T
      GAMA(J)=DEXP(GAMA(J))
C
      TCAL(J)=1/TM-8.314/DH*(DLOG(XC(J)*GAMA(J))+(V1L-VS)*(PE(J)-PSS(J))
     &        /T/R)
      TCAL(J)=1/TCAL(J)
      RETURN
      END
C
      SUBROUTINE CONST(NPA,J,T,X,COEF,AT,BT)
      IMPLICIT REAL*8(A-H,O-Z)
      COMMON/BR01/ TC(3),PC(3),OM(3),AC(3),SM(3),B(3),A(3),R,ND
      COMMON/BR02/ PE(50),TE(50),TCAL(50),XE(50),XC(50),YC(50)
      COMMON/BR03/ DEVT(50),DEVX(50),AVGT,AVGX,SKIJ,SKJI
      COMMON/BR04/ PSS(50),FIV(3),FIL(3),SVL,SVV,VS
      COMMON/BR05/ AP(3),BP(3),A2P(3),A3P(3),JMIX,JEOS,A12
      COMMON/BR06/ FS(50),SFS(50),XK(50)
      COMMON/BR07/ SFV(50),SFL(50),SMVL(50),SMVV(50),REF(50)
      COMMON/BR09/ GAMA(50),X2C(50),Y2C(50)
      REAL*8 COEF(NPA), ALFA(3)
      DO 10 I=1,2
      ALFA(I)=(1.0+SM(I)*(1.0-(T/TC(I))**0.5))**2
```

```
      A(I)=AC(I)*ALFA(I)
   10 CONTINUE
      X2=1.-X
      GOTO(15,20,22),JMIX
C********* VDW-1 MIXING RULE ************************************
   15 A12=(A(1)*A(2))**0.5*(1.-COEF(1))
      AT=X**2*A(1)+X2**2*A(2)+2.*X*X2*A12
      BT=X*B(1)+X2*B(2)
      GO TO 30
C********* VDW-2 MIXING RULE ************************************
   20 A12=(A(1)*A(2))**0.5*(1.-COEF(1))
      B12=(B(1)+B(2))/2.*(1.-COEF(2))
      AT=X**2*A(1)+X2**2*A(2)+2.*X*X2*A12
      BT=X**2*B(1)+X2**2*B(2)+2.*X*X2*B12
      AP(1)=2.*(X*A(1)+X2*A12)
      AP(2)=2.*(X*A12+X2*A(2))
      BP(1)=2.*(X*B(1)+X2*B12)
      BP(2)=2.*(X*B12+X2*B(2))
C     WRITE(7,'(5HCOEF=,2G15.5)') COEF
      GO TO 30
C************** ADACHI-SUGEI MIXING RULE ****************************
   22 A12=(A(1)*A(2))**0.5*(1.-COEF(1)-COEF(2)*(X-X2))
      AT=X**2*A(1)+X2**2*A(2)+2.*X*X2*A12
      BT=X*B(1)+X2*B(2)
      AP(1)=2.*(X*A(1)+X2*A12-2.*X*X2**2*COEF(2)*(A(1)*A(2))**.5)
      AP(2)=2.*(X*A12+X2*A(2)+2.*X2*X**2*COEF(2)*(A(1)*A(2))**.5)
   30 RETURN
      END

      SUBROUTINE VOLUME(J,T,AT,BT,VL,VV,ZL,ZV)
      IMPLICIT REAL*8(A-H,O-Z)
      COMMON/BRO1/ TC(3),PC(3),OM(3),AC(3),SM(3),B(3),A(3),R,ND
      COMMON/BRO2/ PE(50),TE(50),TCAL(50),XE(50),XC(50),YC(50)
      COMMON/BRO3/ DEVT(50),DEVX(50),AVGT,AVGX,SKIJ,SKJI
      COMMON/BRO4/ PSS(50),FIV(3),FIL(3),SVL,SVV,VS
      COMMON/BRO5/ AP(3),BP(3),A2P(3),A3P(3),JMIX,JEOS,A12
      COMMON/BRO6/ FS(50),SFS(50),XK(50)
      COMMON/BRO7/ SFV(50),SFL(50),SMVL(50),SMVV(50),REF(50)
      COMMON/BRO9/ GAMA(50),X2C(50),Y2C(50)
      DIMENSION AA(3),X(3)
      RA=AT*PE(J)/(R*T)**2
      RB=BT*PE(J)/(R*T)
      GOTO(5,20) JEOS
C******** FOR SRK EOS ********
    5 AA(1)=-1.0
      AA(2)=RA-RB-RB**2
      AA(3)=-RA*RB
      GO TO 10
C******* FOR PR EOS **********
   20 AA(1)=RB-1.0
      AA(2)=RA-3*RB**2-2*RB
      AA(3)=-(RA*RB-RB**2-RB**3)
C*****************************
   10 CONTINUE
      CALL TRTON(AA,X,N)
```

```
      ZL=X(1)
      ZV=X(3)
      VL=ZL*R*T/PE(J)
      VV=ZV*R*T/PE(J)
      RETURN
      END
C
      SUBROUTINE FUG(J,T,X,AT,BT,Z,F)
      IMPLICIT REAL*8(A-H,O-Z)
      COMMON/BRO1/ TC(3),PC(3),OM(3),AC(3),SM(3),B(3),A(3),R,ND
      COMMON/BRO2/ PE(50),TE(50),TCAL(50),XE(50),XC(50),YC(50)
      COMMON/BRO3/ DEVT(50),DEVX(50),AVGT,AVGX,SKIJ,SKJI
      COMMON/BRO4/ PSS(50),FIV(3),FIL(3),SVL,SVV,VS
      COMMON/BRO5/ AP(3),BP(3),A2P(3),A3P(3),JMIX,JEOS,A12
      COMMON/BRO6/ FS(50),SFS(50),XK(50)
      COMMON/BRO7/ SFV(50),SFL(50),SMVL(50),SMVV(50),REF(50)
      COMMON/BRO9/ GAMA(50),X2C(50),Y2C(50)
      REAL*8 FAI(3), F(3)
      X2=1.-X
      RA=AT*PE(J)/(R*T)**2
      RB=BT*PE(J)/(R*T)
      GOTO(5,60),JEOS
5     GOTO(21,20,22),JMIX
C
C************ SRK VDW-1 MIXING RULE ***********************************
21    FAI(1)=B(1)/BT*(Z-1.0)-DLOG(Z-RB)-RA/RB*(2.*(X*A(1)+X2*A12)/AT
     &  -B(1)/BT)*DLOG(1.0+RB/Z)
      FAI(2)=B(2)/BT*(Z-1.0)-DLOG(Z-RB)-RA/RB*(2.*(X2*A(2)+X*A12)/AT
     &  -B(2)/BT)*DLOG(1.0+RB/Z)
      GO TO 30
C************ SRK VDW-2 MIXING RULE ***********************************
   20 FAI(I)=(BP(I)/BT-1.)*(Z-1.0)-DLOG(Z-RB)-RA/RB*(1.+AP(I)/AT
     &  -BP(I)/BT)*DLOG(1.0+RB/Z)
      GO TO 30
C
C****************** SRK P-REID MIXING RULE ***************************
   22 FAI(I)=-DLOG(Z-RB)+B(I)/BT*(Z-1.)-RA/RB*((AP(I)-A2P(I)+A3P(I))
     & /AT-B(I)/BT)*DLOG(1.0+RB/Z)
      GO TO 30
C*********************************************************************
C
  60   GOTO(45,70,77),JMIX
C
C************ PR VDW-1 MIXING RULE ************************************
45    FAI(1)=B(1)/BT*(Z-1.0)-DLOG(Z-RB)-RA/RB*(2.*(X*A(1)+X2*A12)/AT
     &  -B(1)/BT)/2.82843*DLOG((Z+2.41421*RB)/(Z-0.41421*RB))
      FAI(2)=B(2)/BT*(Z-1.0)-DLOG(Z-RB)-RA/RB*(2.*(X2*A(2)+X*A12)/AT
     &  -B(2)/BT)/2.82843*DLOG((Z+2.41421*RB)/(Z-0.41421*RB))
      GO TO 30
C************ PR VDW-2 MIXING RULE ************************************
   70 FAI(1)=(BP(1)/BT-1.)*(Z-1.0)-DLOG(Z-RB)-RA/RB*(1.+AP(1)/AT
     &  -BP(1)/BT)/2.82843*DLOG((Z+2.41421*RB)/(Z-0.41421*RB))
      FAI(2)=(BP(2)/BT-1.)*(Z-1.0)-DLOG(Z-RB)-RA/RB*(1.+AP(2)/AT
     &  -BP(2)/BT)/2.82843*DLOG((Z+2.41421*RB)/(Z-0.41421*RB))
      GO TO 30
```

```
C***************** PR ADACHI-SUGEI MIXING RULE ***********************
   77 FAI(1)=-DLOG(Z-RB)+B(1)/BT*(Z-1.)-RA/RB*(AP(1)/AT
     & -B(1)/BT)/2.82843*DLOG((Z+2.41421*RB)/(Z-0.41421*RB))
      FAI(2)=-DLOG(Z-RB)+B(2)/BT*(Z-1.)-RA/RB*(AP(2)/AT
     & -B(2)/BT)/2.82843*DLOG((Z+2.41421*RB)/(Z-0.41421*RB))
C*************************************************************************
   30 CONTINUE
      DO 10 I=1, 2
10    F(I)=PE(J)*DEXP(FAI(I))
      RETURN
      END
C
      SUBROUTINE TRTON(A,X,N)
      IMPLICIT REAL*8(A-H,O-Z)
      REAL*8 A(3),X(3)
      CALL TRNLQ(A,X,N)
      IF( N .NE. 1 ) GO TO 10
      X(2)=X(1)
      X(3)=X(1)
      RETURN
   10 XM=X(1)
      IF( X(2) .GT. X(1) ) GO TO 11
      X(1)=X(2)
      X(2)=XM
   11 XM=X(1)
      IF( X(3) .GT. X(1) ) GO TO 12
      X(1)=X(3)
      X(3)=XM
   12 XM=X(3)
      IF( X(3) .GT. X(2) ) GO TO 13
      X(3)=X(2)
      X(2)=XM
   13 RETURN
      END
C
C
      SUBROUTINE TRNLQ(A,X,N)
      IMPLICIT REAL*8(A-H,O-Z)
      REAL*8 A(3),X(3)
      PAI=3.141592653589
      E=(3.*A(2)-A(1)*A(1))/9.
      F=(2.*A(1)**3-9.*A(1)*A(2)+27.*A(3))/27.
      D=F*F+4.*E*E*E
      IF( D ) 1,2,2
    2 F1=(-F+ DSQRT(D))/2.
      F2=(-F- DSQRT(D))/2.
      X(1)=-A(1)/3.
      IF( F1 .NE. 0. ) X(1)=X(1)+F1/ DABS(F1)**(2./3.)
      IF( F2 .NE. 0. ) X(1)=X(1)+F2/ DABS(F2)**(2./3.)
      N=1
      GO TO 10
    1 R= DSQRT(-E*E*E)
      COR=-F/2./R
      THETA=DARCOS(COR)
      XX=2.*R**(1./3.)
      XY=-A(1)/3.
      X(1)=XX* DCOS(THETA/3.)+XY
      X(2)=XX* DCOS((THETA+2.*PAI)/3.)+XY
      X(3)=XX* DCOS((THETA+4.*PAI)/3.)+XY
      N=3
   10 RETURN
      END
```

Appendix F

Computer Program for the Calculation of the Solubility of Supercritical CO_2 in the Liquid Phase of the Aromatic Compound

In this section, the computer program for calculating the solubility of supercritical CO_2 in the liquid phase of the aromatic compound is presented.

```
C   ***************************************************************
C   *          THE CORRELATION OF V-L 2-PHASE EQUILIBRIA           *
C   *                 USING SRK OR PR EOS                          *
C   *              BUBBLE POINT METHOD (T,X——P,Y)                  *
C   *                 VLE—— MARCH, 89                              *
C   ***************************************************************
C       MIXING RULES:
C              JMIX = 1   RENON MIXING RULE
C                   = 2   CONVENTIONAL MIXING RULE (VDW-2)
C                   = 3   ADACHI-SUGIE MIXING RULE
C       EQUATIONS OF STATE:
C              JEOS = 1   SRK EOS
C                     2   PR  EOS
      IMPLICIT DOUBLE PRECISION (A-H,O-Z)
      PARAMETER(KK=3)
      COMMON/BRO1/ TC(3),PC(3),OM(3),AC(3),SM(3),B(3),A(3),R,ND
      COMMON/BRO2/ TE(50),PE(50),PCAL(50),XE(50),YE(50),YC(50)
      COMMON/BRO3/ DEVP(50),DEVY(50),AVGP,AVGY
      COMMON/BRO4/ FV(3),FL(3),SVL,SVV
      COMMON/BRO5/ AP(3),BP(3),A2P(3),A3P(3),JMIX,JEOS,A12
      COMMON/BRO7/ SFV(50),SFL(50),SMVL(50),SMVV(50),REF(50)
      REAL*8 COEF(KK),XKL(KK),H(KK*(KK+1)/2),G(KK),WOR(3*KK)
      DIMENSION TITLE(15)
       CHARACTER OPT*20
       EXTERNAL FUN
C-------------------------------------------------------C
            JMIX = 1
            JEOS = 2
C-------------------------------------------------------C
      READ(5,900) TITLE
      WRITE(6,910) TITLE
      READ(5,*) ND
      R=82.05
      DO 10 I = 1, 2
      READ(5,*) TC(I),PC(I),OM(I)
      IF (JEOS .EQ. 2) GO TO 80
C
C************ FOR SRK EOS ***************************
      AC(I)=0.42747*R**2*TC(I)**2/PC(I)
      B(I)=0.08664*R*TC(I)/PC(I)
      SM(I)=0.48000+1.57400*OM(I)-0.17600*OM(I)**2
      GO TO 10
C
C************ FOR PR EOS ****************************
   80 AC(I)=0.45724*R**2*TC(I)**2/PC(I)
      B(I)=0.07780*R*TC(I)/PC(I)
      SM(I)=0.37464+1.54226*OM(I)-0.26992*OM(I)**2
C***************************************************
10    CONTINUE
      WRITE(6,920)
      WRITE(6,925) (TC(I),PC(I),OM(I),AC(I),B(I),SM(I),I=1,2)
      WRITE(6,'(21HNUMBER OF DATA POINTS,I3)') ND
      DO 20 J=1, ND
      READ(5,*) TE(J), PE(J), XE(J), YE(J)
      XE(J)=1.0-XE(J)
```

```
      TE(J)=TE(J)+273.15
20    PE(J)=PE(J)*9.869
      WRITE(6,940)
      DO 21 J=1, ND
21    WRITE(6,930)  TE(J)-273.15, PE(J)/9.869, XE(J)
      WRITE(7,*) 'OPT?'
      READ(7,*) OPT
      READ(7,*) XKL
      IF(OPT.EQ.'OPT') THEN
         CALL ZXMIN(FUN,KK,5,350,3,XKL,H,G,F,WOR,IEE)
      ELSE
         CALL FUN(KK,XKL,F)
      ENDIF
            WRITE(6,931)
            DO 90 J=1,ND
90          WRITE(6,933) J,SFV(J),SFL(J),REF(J)
            WRITE(6,934)
            DO 91 J=1,ND
            WM=154.212*XE(J)+44.01*(1.-XE(J))
91          WRITE(6,932) J,WM/SMVL(J),44.01/SMVV(J)
      AVGP = 0
      AVGY = 0
      DO 70 J = 1, ND
C     AVGY = AVGY+DABS(DEVY(J))/YE(J)
70    AVGP = AVGP+DABS(DEVP(J))/PE(J)
      AVGP = AVGP*100./FLOAT(ND)
C       AVGY = AVGY*100./FLOAT(ND)
      WRITE(6,975) AVGP, AVGY
      WRITE(6,980)
      DO 40 J = 1, ND
40    WRITE(6,930) TE(J)-273.15, PE(J)/9.869, PCAL(J)/9.869,
     &     DEVP(J)/9.869
      WRITE(6,1000)
      DO 50 J = 1, ND
50    WRITE(6,930) TE(J)-273.15, YE(J), YC(J), DEVY(J)
      WRITE(6,1200) XKL
      WRITE(6,1300) (1.-XE(J),PCAL(J)/9.869, J=1,ND)
      WRITE(6,1300) (1.-YC(J),PCAL(J)/9.869, J=1,ND)
  900 FORMAT(18A4)
  910 FORMAT(1H ,///,5X,18A4)
  920 FORMAT(1H ,/,5X,'TC(K)',9X,'PC(ATM)',6X,'OM',6X,'AC',14X,'B',
     & 11X,'SM')
  925 FORMAT(6F12.3)
  930 FORMAT(7F10.4)
  932 FORMAT(I6,3X,F12.4,5X,F12.4)
  933 FORMAT(I6,3X,F10.6,3X,F10.6,3X,F10.6,3X,F10.6)
  931 FORMAT(1H ,/,11X,'FV(P/ATM)',4X,'FL(ATM)',6X,'DEVX')
  934 FORMAT(1H ,/,15X,'ROL(G/CC)',8X,'ROV(G/CC)')
  940 FORMAT(1H ,/,4X,'TE(C)',4X,'PE(MPA)',6X,'XE')
  975 FORMAT(1H ,15X,'AVGP% =',F10.4,3X,'AVGY% =',F10.4)
  980 FORMAT(1H ,/,5X,'TE(C)',4X,'PE(MPA)',3X,'PCAL(MPA)',2X,'DEVP')
 1000 FORMAT(1H ,/,5X,'TE(C)',7X,'YE',7X,'YC',6X,'DEVY')
 1200 FORMAT(1H ,/,5X,'KIJ= ',F10.5,5X,'LIJ= ',F10.5,5X,'MIJ= ',F10.5)
 1300 FORMAT(F7.4, F12.4)
      END
```

```
C
      SUBROUTINE FUN(NX,XKL,FF)
      IMPLICIT REAL*8(A-H,O-Z)
      REAL*8 COEF(3),XKL(NX)
      COMMON/BRO1/ TC(3),PC(3),OM(3),AC(3),SM(3),B(3),A(3),R,ND
      COMMON/BRO2/ TE(50),PE(50),PCAL(50),XE(50),YE(50),YC(50)
      COMMON/BRO3/ DEVP(50),DEVY(50),AVGP,AVGY
      COMMON/BRO4/ FV(3),FL(3),SVL,SVV
      COMMON/BRO5/ AP(3),BP(3),A2P(3),AJP(3),JMIX,JEOS,A12
      COMMON/BRO7/ SFV(50),SFL(50),SMVL(50),SMVV(50),REF(50)
      COEF(1)=XKL(1)
      COEF(2)=XKL(2)
      COEF(3)=XKL(3)
      NPA=3
      DO 26 J=1,ND
      P2=PE(J)
      IT=0
 5    IT=IT+1
      IF(IT.GT.100) STOP 'NO CONVERGENCE'
      CALL PRES(NPA,J,P2,COEF,RET2)
       IF(IT.EQ.1) THEN
      P1=P2*0.98
      IT=IT+1
      CALL PRES(NPA,J,P1,COEF,RET1)
      ENDIF
C       WRITE(7,*)P2,RET2
C       WRITE(7,*)P1,RET1
      PCAL(J)=(P2*RET1-P1*RET2)/(RET1-RET2)
C     PCAL(J)=(P2*RET2*.5+.5*P1*RET2-P2*RET1)/(RET2-RET1)
      IF(DABS(RET2).GT.1.D-5) THEN
      P1=P2
      RET1=RET2
      P2=PCAL(J)
      GOTO 5
      ENDIF
   50 CONTINUE
      DEVP(J)=PE(J)-PCAL(J)
      DEVY(J)=YE(J)-YC(J)
      SFV(J)=FV(1)*YC(J)
      SFL(J)=FL(1)*XE(J)
      RE=DABS(SFV(J)-SFL(J))/SFL(J)
      REF(J)=RE*100.
      SMVL(J)=SVL
26    SMVV(J)=SVV
      FF=0.
      DO 80 J=1,ND
C     FF=FF+((YC(J)-YE(J))/YE(J))**2
      FF=FF+(((PCAL(J)-PE(J))/PE(J))**2)
   80 CONTINUE
C     DO 90 J=ND-5,ND
C  90 FF=FF+(((PCAL(J)-PE(J))/PE(J))**2)*50.
      WRITE(7,'(5H X F ,4G15.5)') XKL,FF
      RETURN
      END
C
```

```
      SUBROUTINE PRES(NPA,J,P,COEF,RET)
      IMPLICIT REAL*8(A-H,O-Z)
      COMMON/BRO1/ TC(3),PC(3),OM(3),AC(3),SM(3),B(3),A(3),R,ND
      COMMON/BRO2/ TE(50),PE(50),PCAL(50),XE(50),YE(50),YC(50)
      COMMON/BRO3/ DEVP(50),DEVY(50),AVGP,AVGY
      COMMON/BRO4/ FV(3),FL(3),SVL,SVV
      COMMON/BRO5/ AP(3),BP(3),A2P(3),A3P(3),JMIX,JEOS,A12
      COMMON/BRO7/ SFV(50),SFL(50),SMVL(50),SMVV(50),REF(50)
      DIMENSION COEF(NPA)
C-----------------------------------------------------------
      XA=XE(J)
C     WRITE(7,*) J,TE(J)
      YA=1.E-4
      NXY=0
11     XO=XA
       YO=YA
C
C *** LIQUID PHASE ********************************
      CALL CONST(NPA,J,P,XA,COEF,AT,BT)
      CALL VOLUME(J,P,AT,BT,VL,VV,ZL,ZV)
      CALL FUG(J,P,XA,AT,BT,ZL,FL)
         SVL=VL
C
C *** VAPOR  PHASE ********************************
      CALL CONST(NPA,J,P,YA,COEF,AT,BT)
      CALL VOLUME(J,P,AT,BT,VL,VV,ZL,ZV)
      CALL FUG(J,P,YA,AT,BT,ZV,FV)
C        WRITE(6,990) YA,AT,BT,VL,VV
         SVV=VV
         YC(J)=XE(J)*(FL(1)/FV(1))
C            WRITE(7,*) YC(J)
         YC2=(1.-XE(J))*(FL(2)/FV(2))
      RE= DABS(YC(J)-YA)
      IF (RE .LT. 1.0D-3) GO TO 51
      NXY=NXY+1
C        WRITE(7,*) NXY
C        WRITE(7,*) YA,YC(J)
      IF (NXY .GT. 100) STOP 'NO CONVERGENCE IN XY LOOP'
        SUMY=YC(J)+YC2
        YC(J)=YC(J)/SUMY
        YC2=YC2/SUMY
      YA = YC(J)
      IF (YA. GT. 0.1) YA=0.1
      GO TO 11
   51 RET=1.-YC(J)-YC2
      RETURN
      END
C
      SUBROUTINE CONST(NPA,J,P,X,COEF,AT,BT)
      IMPLICIT REAL*8(A-H,O-Z)
      COMMON/BRO1/ TC(3),PC(3),OM(3),AC(3),SM(3),B(3),A(3),R,ND
      COMMON/BRO2/ TE(50),PE(50),PCAL(50),XE(50),YE(50),YC(50)
      COMMON/BRO3/ DEVP(50),DEVY(50),AVGP,AVGY
      COMMON/BRO4/ FV(3),FL(3),SVL,SVV
      COMMON/BRO5/ AP(3),BP(3),A2P(3),A3P(3),JMIX,JEOS,A12
```

```
      COMMON/BRO7/ SFV(50),SFL(50),SMVL(50),SMVV(50),REF(50)
      REAL*8 COEF(NPA),ALFA(3)
C      WRITE(7,'(3H K3,3G15.5)') COEF
C   MODIFIED PR EOS
      ALFA(1)=1.+1.125363*(1.-(TE(J)/TC(1))**.5)
     &   -0.1791811*(1.-TE(J)/TC(1))
     &   -0.002358876*(1.-(TE(J)/TC(1))**2)
      ALFA(1)=ALFA(1)**2
      ALFA(2)=1.0*EXP(0.5856143*(1.-(TE(J)/TC(2))))
C   ORIGINAL PR EOS
      DO 10 I=1,2
      ALFA(I)=(1.0+SM(I)*(1.0-(TE(J)/TC(I))**0.5))**2
      A(I)=AC(I)*ALFA(I)
   10 CONTINUE
      X2=1.-X
      GOTO(15,20,22),JMIX
C********* VDW-1 MIXING RULE ***********************************
C 15  A12=(A(1)*A(2))**0.5*(1.-COEF(1))
C     AT=X**2*A(1)+X2**2*A(2)+2.*X*X2*A12
C     BT=X*B(1)+X2*B(2)
C     GO TO 30
C************** RENON MIXING RULE ****************************
   15 CMIJ=COEF(3)
      CMJI=1.-COEF(3)
      A12=(A(1)*A(2))**0.5*(1.-COEF(1)-COEF(2)*
     &    (CMIJ*X-CMJI*X2)/(CMIJ*X+CMJI*X2))
      AT=X**2*A(1)+X2**2*A(2)+2.*X*X2*A12
      BT=X*B(1)+X2*B(2)
      AP(1)=2.*(X*A(1)+X2*A12-2.*X*X2**2*(A(1)*A(2))**.5
     &      *COEF(2)*CMIJ*CMJI/(CMIJ*X+CMJI*X2)**2)
      AP(2)=2.*(X*A12+X2*A(2)+2.*X2*X**2*(A(1)*A(2))**.5
     &      *COEF(2)*CMIJ*CMJI/(CMIJ*X+CMJI*X2)**2)
      GO TO 30
C********* VDW-2 MIXING RULE ***********************************
   20 A12=(A(1)*A(2))**0.5*(1.-COEF(1))
      B12=(B(1)+B(2))/2.*(1.-COEF(2))
      AT=X**2*A(1)+X2**2*A(2)+2.*X*X2*A12
      BT=X**2*B(1)+X2**2*B(2)+2.*X*X2*B12
      AP(1)=2.*(X*A(1)+X2*A12)
      AP(2)=2.*(X*A12+X2*A(2))
      BP(1)=2.*(X*B(1)+X2*B12)
      BP(2)=2.*(X*B12+X2*B(2))
C     WRITE(7,'(5HCOEF=,2G15.5)') COEF
      GO TO 30
C************** ADACHI-SUGEI MIXING RULE ***************************
   22 A12=(A(1)*A(2))**0.5*(1.-COEF(1)-COEF(2)*(X-X2))
      AT=X**2*A(1)+X2**2*A(2)+2.*X*X2*A12
      BT=X*B(1)+X2*B(2)
      AP(1)=2.*(X*A(1)+X2*A12-2.*X*X2**2*COEF(2)*(A(1)*A(2))**.5)
      AP(2)=2.*(X*A12+X2*A(2)+2.*X2*X**2*COEF(2)*(A(1)*A(2))**.5)
   30 RETURN
      END
C
      SUBROUTINE VOLUME(J,P,AT,BT,VL,VV,ZL,ZV)
      IMPLICIT REAL*8(A-H,O-Z)
```

```
      COMMON/BRO1/ TC(3),PC(3),OM(3),AC(3),SM(3),B(3),A(3),R,ND
      COMMON/BRO2/ TE(50),PE(50),PCAL(50),XE(50),YE(50),YC(50)
      COMMON/BRO3/ DEVP(50),DEVY(50),AVGP,AVGY
      COMMON/BRO4/ FV(3),FL(3),SVL,SVV
      COMMON/BRO5/ AP(3),BP(3),A2P(3),A3P(3),JMIX,JEOS,A12
      COMMON/BRO7/ SFV(50),SFL(50),SMVL(50),SMVV(50),REF(50)
      DIMENSION AA(3),X(3)
      RA=AT*P/(R*TE(J))**2
      RB=BT*P/(R*TE(J))
      GOTO(5,20) JEOS
C******** FOR SRK EOS ********
 5    AA(1)=-1.0
      AA(2)=RA-RB-RB**2
      AA(3)=-RA*RB
      GO TO 10
C******* FOR.PR EOS **********
   20 AA(1)=RB-1.0
      AA(2)=RA-3*RB**2-2*RB
      AA(3)=-(RA*RB-RB**2-RB**3)
C*****************************
   10 CONTINUE
      CALL TRTON(AA,X,N)
      ZL=X(1)
      ZV=X(3)
      VL=ZL*R*TE(J)/P
      VV=ZV*R*TE(J)/P
      RETURN
      END
C
      SUBROUTINE FUG(J,P,X,AT,BT,Z,F)
      IMPLICIT REAL*8(A-H,O-Z)
      COMMON/BRO1/ TC(3),PC(3),OM(3),AC(3),SM(3),B(3),A(3),R,ND
      COMMON/BRO2/ TE(50),PE(50),PCAL(50),XE(50),YE(50),YC(50)
      COMMON/BRO3/ DEVP(50),DEVY(50),AVGP,AVGY
      COMMON/BRO4/ FV(3),FL(3),SVL,SVV
      COMMON/BRO5/ AP(3),BP(3),A2P(3),A3P(3),JMIX,JEOS,A12
      COMMON/BRO7/ SFV(50),SFL(50),SMVL(50),SMVV(50),REF(50)
      REAL*8 FAI(3), F(3)
      X2=1.-X
      RA=AT*P/(R*TE(J))**2
      RB=BT*P/(R*TE(J))
      GOTO(5,60),JEOS
5     GOTO(21,20,22),JMIX
C
C*********** SRK VDW-1 MIXING RULE **********************************
21    FAI(1)=B(1)/BT*(Z-1.0)-DLOG(Z-RB)-RA/RB*(2.*(X*A(1)+X2*A12)/AT
     &  -B(1)/BT)*DLOG(1.0+RB/Z)
      FAI(2)=B(2)/BT*(Z-1.0)-DLOG(Z-RB)-RA/RB*(2.*(X2*A(2)+X*A12)/AT
     &  -B(2)/BT)*DLOG(1.0+RB/Z)
      GO TO 30
C*********** SRK VDW-2 MIXING RULE **********************************
   20 FAI(I)=(BP(I)/BT-1.)*(Z-1.0)-DLOG(Z-RB)-RA/RB*(1.+AP(I)/AT
     &  -BP(I)/BT)*DLOG(1.0+RB/Z)
      GO TO 30
C
```

```
C***************** SRK P-REID MIXING RULE ***************************
   22 FAI(I)=-DLOG(Z-RB)+B(I)/BT*(Z-1.)-RA/RB*((AP(I)-A2P(I)+A3P(I))
     & /AT-B(I)/BT)*DLOG(1.0+RB/Z)
      GO TO 30
C*****************************************************************
C
  60   GOTO(45,70,77),JMIX
C
C************ PR VDW-1 MIXING RULE ***********************************
C  45 FAI(1)=B(1)/BT*(Z-1.0)-DLOG(Z-RB)-RA/RB*(2.*(X*A(1)+X2*A12)/AT
C     &  -B(1)/BT)/2.82843*DLOG((Z+2.41421*RB)/(Z-0.41421*RB))
C      FAI(2)=B(2)/BT*(Z-1.0)-DLOG(Z-RB)-RA/RB*(2.*(X2*A(2)+X*A12)/AT
C     &  -B(2)/BT)/2.82843*DLOG((Z+2.41421*RB)/(Z-0.41421*RB))
C      GO TO 30
C****************** PR RENON MIXING RULE ***************************
   45 FAI(1)=-DLOG(Z-RB)+B(1)/BT*(Z-1.)-RA/RB*(AP(1)/AT
     & -B(1)/BT)/2.82843*DLOG((Z+2.41421*RB)/(Z-0.41421*RB))
      FAI(2)=-DLOG(Z-RB)+B(2)/BT*(Z-1.)-RA/RB*(AP(2)/AT
     & -B(2)/BT)/2.82843*DLOG((Z+2.41421*RB)/(Z-0.41421*RB))
      GO TO 30
C************ PR VDW-2 MIXING RULE ***********************************
   70 FAI(1)=(BP(1)/BT-1.)*(Z-1.0)-DLOG(Z-RB)-RA/RB*(1.+AP(1)/AT
     &  -BP(1)/BT)/2.82843*DLOG((Z+2.41421*RB)/(Z-0.41421*RB))
      FAI(2)=(BP(2)/BT-1.)*(Z-1.0)-DLOG(Z-RB)-RA/RB*(1.+AP(2)/AT
     &  -BP(2)/BT)/2.82843*DLOG((Z+2.41421*RB)/(Z-0.41421*RB))
      GO TO 30
C****************** PR ADACHI-SUGEI MIXING RULE ***********************
   77 FAI(1)=-DLOG(Z-RB)+B(1)/BT*(Z-1.)-RA/RB*(AP(1)/AT
     & -B(1)/BT)/2.82843*DLOG((Z+2.41421*RB)/(Z-0.41421*RB))
      FAI(2)=-DLOG(Z-RB)+B(2)/BT*(Z-1.)-RA/RB*(AP(2)/AT
     & -B(2)/BT)/2.82843*DLOG((Z+2.41421*RB)/(Z-0.41421*RB))
C*****************************************************************
   30 CONTINUE
      DO 10 I=1, 2
10    F(I)=P*DEXP(FAI(I))
      RETURN
      END
C
      SUBROUTINE TRTON(A,X,N)
      IMPLICIT REAL*8(A-H,O-Z)
      REAL*8 A(3),X(3)
      CALL TRNLQ(A,X,N)
      IF( N .NE. 1 ) GO TO 10
      X(2)=X(1)
      X(3)=X(1)
      RETURN
   10 XM=X(1)
      IF( X(2) .GT. X(1) ) GO TO 11
      X(1)=X(2)
      X(2)=XM
   11 XM=X(1)
      IF( X(3) .GT. X(1) ) GO TO 12
      X(1)=X(3)
      X(3)=XM
   12 XM=X(3)
```

```
      IF( X(3) .GT. X(2) ) GO TO 13
      X(3)=X(2)
      X(2)=XM
   13 RETURN
      END
C
C
      SUBROUTINE TRNLQ(A,X,N)
      IMPLICIT REAL*8(A-H,O-Z)
      REAL*8 A(3),X(3)
      PAI=3.141592653589
      E=(3.*A(2)-A(1)*A(1))/9.
      F=(2.*A(1)**3-9.*A(1)*A(2)+27.*A(3))/27.
      D=F*F+4.*E*E*E
      IF( D ) 1,2,2
    2 F1=(-F+ DSQRT(D))/2.
      F2=(-F- DSQRT(D))/2.
      X(1)=-A(1)/3.
      IF( F1 .NE. 0. ) X(1)=X(1)+F1/ DABS(F1)**(2./3.)
      IF( F2 .NE. 0. ) X(1)=X(1)+F2/ DABS(F2)**(2./3.)
      N=1
      GO TO 10
    1 R= DSQRT(-E*E*E)
      COR=-F/2./R
      THETA=DARCOS(COR)
      XX=2.*R**(1./3.)
      XY=-A(1)/3.
      X(1)=XX* DCOS(THETA/3.)+XY
      X(2)=XX* DCOS((THETA+2.*PAI)/3.)+XY
      X(3)=XX* DCOS((THETA+4.*PAI)/3.)+XY
      N=3
   10 RETURN
      END
```